

**Descaling of Petroleum Production Tubing utilising
Aerated High Pressure Flat Fan Water Sprays**

Abubakar Jibrin ABBAS
(B.Eng., M.Sc.)

Descaling of Petroleum Production Tubing utilising Aerated
High Pressure Flat Fan Water Sprays

Abubakar Jibrin ABBAS

School of Computing, Science and Engineering,
College of Science and Technology,
University of Salford, Manchester, UK

Submitted in Partial Fulfilment of the Requirements of the
Degree of Doctor of Philosophy, November, 2014

Contents

List of Tables	vi
List of Figures.....	vii
Acknowledgements	xv
Declaration.....	xvii
Confidentiality Notice	xviii
List of Publications.....	xix
Conversion Table.....	xxi
Nomenclature	xxii
Abstract.....	xxiv
Chapter 1.....	1
Introduction	1
1.1 Preamble	1
1.2 Scales in Oil production	1
1.3 Research problem statement.....	2
1.4 Research contributions	4
1.5 Research Aim	4
1.6 Research Objectives.....	5
1.7 Structure of the Research Thesis	5
Chapter 2.....	8
Scale Formation in Oil and Gas Production	8
2.1 Overview.....	8
2.2 Scale Formation in Oil and Gas Production.....	9
2.3 Industrial Scale Problems	10
2.4 Sources and Types of Mineral Scale in Oil Production	12
2.4.1 Chemistry of scale formation	12
2.4.2 Oilfield Scale Types	16
2.5 Scale Prevention and Treatment	25
2.5.1 Wire line operations	25
2.5.2 Chemical Scale Dissolver.....	25
2.5.3 Mechanical Treatment Methods	29
2.5.4 Jetting Techniques	30
2.6 Summary	36

Chapter 3	37
Spray Jet Break-Up, Cavitation and Erosion.....	37
3.1 Spray Jet Break up	37
3.1.1 Primary Spray break-up.....	40
3.1.2 Secondary Spray break-up.....	41
3.2 Spray Droplet Break up Models	42
3.2.1 The Classic WAVE model	42
3.2.2 Spray Characterisations	43
3.2.3 Spray Pattern	45
3.2.4 Spray Characterisations	50
3.3 Spray Jet Cleaning	57
3.4 Cavitation Water	60
3.4.1 Classes of cavitation	62
3.5 Cavitation in Spray Nozzles	65
3.6 Cavitation erosion	67
3.6.1 Spherical bubble in water	67
3.7 Cavitation Erosion and Mitigations.....	68
3.7.1 Cavitation damage control in dams	68
3.7.2 Pressure Wave front in aerated flows	71
3.8 Summary	74
Chapter 4.....	75
Experimental Set up and Procedure.....	75
4.1 Overview.....	75
4.2 Entrained-air Measurements and Spray Characterizations.....	77
4.2.1 Experimental set up	77
4.2.2 Experimental apparatus	78
4.2.3 Experimental procedure.....	80
4.2.4 Accuracy and Errors in Hot-Wire Anemometry.....	81
4.3 Spray Characterization	82
4.3.1 Experimental set up using PDA	82
4.3.2 Spray Characterization and Measurement grid	84
4.3.3 PDA Experimental procedure.....	85
4.3.4 Accuracy and error analysis	87
4.4 Impact Pressure Measurement.....	93
4.4.1 Experimental set up	93
4.4.2 Experimental procedure.....	94
4.4.2 Accuracy and error analysis	94

4.5 Cavitation measurements	95
4.5.1 Experimental set up	95
4.5.1 Experimental procedure.....	96
4.5.2 Source of error in cavitation measurement.....	96
4.6 Scale Removal Set-up	97
4.6.1 Experimental set up	97
4.6.2 Pressure Chamber Design, Construction and Set up	98
4.6.3 Soft scale samples preparations.....	104
4.7 Summary	111
Chapter 5.....	112
Results and Discussions.....	112
5.1 Overview	112
5.2 Entrained-Air Velocities Measurement and the High Pressure Water Sprays (Phase-I)	113
5.2.2 Spray Characterizations Measurement using PDA	118
5.3 Cavitation Measurements (Phase–II).....	134
5.3.1 Overview of cavitation in multi-phase flows	134
5.4 Scale Removal (Phase –III)	137
5.4.1 Overview	137
5.4.2 Non-aerated scale removal trials	138
5.4.3 Aerated scale removal	145
5.4.4 Comparison of non-aerated and aerated chamber scale removal	150
5.4.5 Comparison with current commercial scale removal techniques	154
5.5 Summary	162
Chapter 6.....	163
Spray Jet Breakup and Cavitation’s Modelling using CFD-Fluent.....	163
6.1 Overview	163
6.2 Principle of Spray and Cavitation Flow Models in CFD.....	163
6.3 Nozzle Selection for Erosion and Impact performance	164
6.3.1 Turbulent models.....	164
6.3.2 Geometry and Meshing	165
6.3.3 Boundary Conditions.....	168
6.3.4 Criteria for Convergence	169
6.3.5 Model Equations and Boundary Conditions.....	169
6.4 Entrained-air velocities measurements and Spray characterisation (Phase-I).....	170
6.4.1 Entrained-air Velocities.....	170
6.4.2 Spray characterisations	178

6.5 Cavitation measurements (Phase-II)	195
6.5.1 Bubble generation.....	195
6.5.2 Turbulent Kinetic energy.....	199
6.5.3 Droplet momentum.....	201
6.5.4 Flat fan operating conditions	203
6.5.5 Cavitation in Flat fan nozzles	205
6.5.6 Aeration effect on cavitation length in Flat fan (Entrained-air medium).....	208
6.6 Scale removal using measurement using CFD (Phase-III)	211
6.6.1 Scale removal set up	211
6.6.2 Comparison of aerated and non-aerated scale removal	215
6.7 Summary	218
Chapter 7.....	219
Conclusion and Recommendations	219
7.1 Conclusions	219
7.2 Recommendations	221
REFERENCES	222
APPENDICES	233
Appendix A: Chamber Design.....	233
A1:Aerated chamber top section	233
A2: Aerated chamber internals	234
A3: Aerated chamber (scale section).....	235
Appendix B: Atomizer Header Design	236
Appendix C: Overlap spray header design	237
Appendix D: Overlapping Spray Pattern	238
Appendix E: Flat fan Atomizer Chart.....	239
Appendix F: CFD Graphics	240
F1: Density profile in flat fan atomizer(1bar)	240
F2:Turbulent kinetic energy profile in solid stream atomizer	241
F3: Velocity vectors in flat fan atomizer	242
F4: Velocity profile in flat fan atomizer	243
F5: Pressure profile in flat fan atomizer	244
Appendix G: Calculations for commercial descaling	245
Appendix H: List of Publications	246

List of Tables

	Page
Table 3.1 Mean diameter and their applications	55
Table 4.1 Clear acrylic tube vendor's specifications	87
Table 4.2 Clear acrylic tube vendor's specifications	105
Table 5.1 Scale removal efficiency comparison	157
Table 5.2 <i>Khuff</i> field descaling parameters	159
Table 5.3 Descaling conditions of EW 873	162
Table 5.4 <i>Khuff</i> field descaling data	163
Table 5.5 Atomizer characteristics comparison	163
Table 5.6 Scale removed comparison	164
Table 6.1 Boundary conditions	174
Table 6.2 Criteria for convergence	174

List of Figures

Figure 2.1 Scale formation along production tubing	9
Figure 2.2 Oil production assembly profiles	11
Figure 2.3 Precipitation of CaCO ₃ in bulk	17
Figure 2.4 Barium sulphate scale inside production tubing	21
Figure 2.5 Typical SrSO ₄ Scale Depositions	23
Figure 2.6 Scale in Production Tubing	24
Figure 2.7 EDTA action on scale dissolution	26
Figure 2.8 Dependency on scale solubility with Temperature	27
Figure 2.9 Dependency on scale solubility with Temperature	28
Figure 2.10 Cross section of mechanical atomizers	30
Figure 2.11: Performance of a water jetting tool	32
Figure 3.1 Sheet disintegration break-up	38
Figure 3.2 Forces acting along spray jet	39
Figure 3.3 Break-up length behaviour of liquid jet	39
Figure 3.4 Liquid atomisation mechanisms	40
Figure 3.5 Classification of atomisers	44
Figure 3.6 Full Cone Pattern	46
Figure 3.7 Spill Return	47
Figure 3.8 Hollow Cone Atomiser spray	47
Figure 3.9 Flat Spray Pattern	48
Figure 3.10 Flat Spray Atomiser	49
Figure 3.11 Typical particle drop size distribution	51
Figure 3.12 Typical Drop size bars for number and volume	52
Figure 3.13 Typical particle drop size frequency distribution curves	52
Figure 3.14 Typical particle shape of cumulative drop size	53
Figure 3.15 Spray angle	55

Figure 3.16 Spray cleaning set up	56
Figure 3.17 Scale sample from a Production Tubing	57
Figure 3.18 Schlumberger Jetting Technique	58
Figure 3.19 Phase change diagram	60
Figure 3.20 Oxygen solubility in water at different temperature and pressure	62
Figure 3.21 Pressure cycle in cavitation	62
Figure 3.22 Classification of cavitation	63
Figure 3.23 Cavitation regimes along Francis turbine	63
Figure 3.24 Light emitted by a trapped cavitation bubble	64
Figure 3.25 Typical flows through a nozzle	65
Figure 3.26 Typical spherical bubble in a bulk liquid	68
Figure 3.27 Flow pattern in aerated spill way	69
Figure 3.28 Aeration chamber	70
Figure 3.29 Experimental aerated chamber	71
Figure 3.30 Pressure wave front with and without aeration	72
Figure 3.31 Aerated flow at low 1.6% air concentration	72
Figure 4.1 Experiment and simulation validation stages	76
Figure 4.2 Entrained-air set up	77
Figure 4.3 Hot Wire cross section	78
Figure 4.4 Entrained-air velocities measurement grid	80
Figure 4.5 PDA set up	82
Figure 4.6 PDA Experimental set up cross section	83
Figure 4.7 PDA aerated chamber	84
Figure 4.8 Measurement Grid	85
Figure 4.9 Measuring volume	87
Figure 4.10 Doppler signal burst at measuring volume	87
Figure 4.11 Doppler signal from different source	88

Figure 4.12 Light scattering models	89
Figure 4.13 Ellipsoidal nature of droplets	90
Figure 4.14 Burst validation	90
Figure 4.15 Slit effect in suppression scattered light	91
Figure 4.16 Gaussian beam imperfections	92
Figure 4.17 Impact pressure measurement set up	93
Figure 4.18 Load cell set up	93
Figure 4.19 Impact force probe Calibration	95
Figure 4.20 Cavitation experimental set up	96
Figure 4.21 Descaling chamber set-up	97
Figure 4.22 Design of the chamber	98
Figure 4.23 Interior section	99
Figure 4.24 Scale holder details	99
Figure 4.25 Atomizer plenum design	100
Figure 4.26 View of metallic cover	102
Figure 4.27 Assembled views of metallic cover	103
Figure 4.28 Scale sample assembly(without chamber)	104
Figure 4.29 Scale holder	105
Figure 4.30 Wax scale preparation(a) empty holder (b) hot-filled wax	105
Figure 4.31 Prepared wax scale samples (a) after cooling (b) prepared samples	106
Figure 4.32 Scale samples (a) Hard (b) Medium	106
Figure 4.33 Chamber assembly	107
Figure 4.34 Canon Eos Kiss F	109
Figure 5.1 Entrained-air measurement grids	113
Figure 5.2 Entrained-air velocities at various downstream positions	115
Figure 5.3 Entrained air velocities at various injection pressures	117

Figure 5.4 Spray droplets and velocities grid	119
Figure 5.5 SMD across the spray width	120
Figure 5.6 Typical measurement positions using PDA	121
Figure 5.7 SMD at the centre and edge of spray	122
Figure 5.8 SMD at (a) negative edge, (b) centre, (c) positive edge	123
Figure 5.9 Droplet mean velocities at various stand-of distances	125
Figure 5.10 Droplet means velocities at various injection pressure	126
Figure 5.11 Droplet mean velocities at centre and spray edges	127
Figure 5.12 Droplet momentums at various injection pressure	129
Figure 5.13 Droplet momentums at various positions	130
Figure 5.14 Impact pressure grid	131
Figure 5.15 Impact pressure distribution proposes by <i>Bendig</i>	132
Figure 5.16 Impact pressure distributions at (a) 4.8, (b) 6.0 and (c) 10MPa	133
Figure 5.17 Cavitation region measurement positions	135
Figure 5.18 Cavitation bubble suppression with increasing aeration	136
Figure 5.19 Experimental scale samples	138
Figure 5.20 Non-aerated scale removal set-up	139
Figure 5.21 Comparison of scale removed	140
Figure 5.22 soft scales mass removed (non-aerated)	141
Figure 5.23 Medium scale removed (non-aerated)	141
Figure 5.24 Hard scale removed (non-aerated)	141
Figure 5.25 Soft scale samples after trials at various injection pressures	142
Figure 5.26 Medium scales after trials at various injection pressure	143
Figure 5.27 Hard scale removed (non-aerated)	144
Figure 5.28 Soft scale removal (aerated)	146
Figure 5.29 Medium scale removal (aerated)	146

Figure 5.30 Hard scale removal (aerated)	146
Figure 5.31 Soft scale samples after trials at various injection pressures (aerated)	147
Figure 5.32 Medium scales after trials at various injection pressures (aerated)	148
Figure 5.33 Hard scale removed (aerated)	149
Figure 5.34 Soft scale removal comparisons	151
Figure 5.35 Medium scale removal comparisons	151
Figure 5.36 Hard scale removal comparisons	151
Figure 5.37 Aerated versus Non-aerated erosion at various pressures	152
Figure 5.38 Comparison between laboratory and commercial pressure scale removal	154
Figure 5.39 Khuff productivity performances	155
Figure 5.40 Scale samples removed (a) from Al-Khuff field (b) SRG Lab	156
Figure 5.41 Khuff scale profile	156
Figure 5.42 EW 873 Field location map	157
Figure 5.43 Atomizer assembly used for the EW 873 descaling	157
Figure 5.44 Scale deposition cross section in EW 873	158
Figure 5.45 Comparison with the commercial technologies	161
Figure 6.1 Geometry development (a) laboratory chamber(b) model development in 3D	165
Figure 6.2 Flat-fan nozzle assemblies	166
Figure 6.3 Chamber meshed model in 3D	167
Figure 6.4 Exploded view of the Meshed domains for the flat fan nozzle in 2D	168
Figure 6.5 Entrained-air profiles (a) with, and (b) without the sprays	172
Figure 6.6 Entrained-air velocities at various stand-off distances	173
Figure 6.7 Entrained-air velocities at various spray injection pressure	174
Figure 6.8 Comparisons of Entrained-air velocities between experimental and CFD	175
Figure 6.9 Comparisons of Entrained-air velocities between experimental and CFD	178
Figure 6.10 Comparisons of Entrained-air velocities between HWA and CFD at 50mm	178

Figure 6.11 SMD profile using CFD	179
Figure 6.12 SMD at various downstream positions	180
Figure 6.13 SMD at various pressures	181
Figure 6.14 SMD comparisons between PDA and CFD at 4.8MPa	182
Figure 6.15 SMD comparisons between PDA and CFD at 6.0MPa	183
Figure 6.16 SMD comparisons between PDA and CFD at 10MPa	184
Figure 6.17 Droplet mean velocities	185
Figure 6.18 Droplet mean velocities at various downstream stand-off distances	186
Figure 6.19 Droplet mean velocities at (a) 4.8MPa (b) 6.0MPa (c) 10MPa	187
Figure 6.20 Droplet mean velocities comparison between PDA and CFX at 4.8MPa	188
Figure 6.21 Droplet mean velocities comparison between PDA and CFX at 6.0MPa	189
Figure 6.22 Droplet mean velocities comparison between PDA and CFX at 10MPa	190
Figure 6.23 Spray jet image and models	192
Figure 6.24 Negative centre plane pressure profiles at different spray injection pressure	193
Figure 6.25 Negative plane pressures at centre-edge cross section	194
Figure 6.26 Fluent model nozzles(a) Flat-fan nozzle (b) solid stream nozzle	195
Figure 6.27 Experimental model nozzles(a) Flat-fan nozzle (b) solid stream nozzle	195
Figure 6.28 Cavitation bubble generation as a measure of density	196
Figure 6.29 Cavitation bubbles regions (a) Solid stream (b) Flat-fan atomizer	197
Figure 6.30 Cavitation bubble length validation	198
Figure 6.31 Density vector velocities	199
Figure 6.32 Turbulent kinetic energy comparisons	200
Figure 6.33 Fluent turbulent kinetic energy (a) solid stream (b) Flat-fan atomizer	201
Figure 6.34 Velocities distribution in different nozzles	202
Figure 6.35 Velocities' profiles for (a) solid stream and (b) Flat-fan nozzles	203
Figure 6.36 Pressure profile for Flat-fan nozzle in different medium	204
Figure 6.37 CFD pressure profiles for Flat-fan nozzle in different medium plane	205
Figure 6.38 Density at ambient condition in different medium	206

Figure 6.39 CFD Images of cavitation in Flat-fan atomizer in different medium	207
Figure 6.40 Aeration effect on cavitation	208
Figure 6.41 Aeration effect on turbulent kinetic energy	209
Figure 6.42 Aeration effect on droplet velocities	209
Figure 6.43 Aeration effect on pressure	210
Figure 6.44 Erosion prediction using CFD	211
Figure 6.45 Erosion plane	212
Figure 5.46 Experimental momentum impact variations	212
Figure 5.47 Simulated momentum impact variations	213
Figure 6.48 CaCO ₃ comparison	214
Figure 6.49 CaSO ₄ comparison	215
Figure 6.50 CaO comparison	216
Figure 6.51 Gypsum (CaSO ₄ .2H ₂ O) comparisons	216
Figure 6.52 Experimental versus CFD simulation erosion	217
Figure 6.53 CaSO ₄ comparison	217

Acknowledgements

I wish to acknowledge few individuals who's supported and helped me through this journey of successful completion of this life-long dream. To my parents, my pillars, you raised me up to become what I am. You are truly the best parent that anyone could hope for. May ALLAH give you a long-live to be with you and continue to get your blessings.

To my supervisor Professor G.G. Nasr for his tremendous efforts in ensuring that I remained committed, focused and imaginative in my thinking, sayings and even writing. You both acted as a father, guardian, and even a friend at some occasions. Your humility has given me courage to be close to you and learnt so much from your vast of knowledge and character.

To my lecturers and staffs Dr. G.C.Enyi, Dr. Denver James, Mr. Ali Kadir, Dr. Burby, N.E. Connor, and Dr. Amir Nourian, Dr. Musa Abuhesa, Mr Alan Mappin and his twin brother Mr Michael Mappin for their committed guidance, stimulation and courage and support. This team has given me all I wanted to stay happy and indeed attain success. To the Petroleum Technology Development Fund (PTDF) for my sponsorship to study both M.Sc and PhD, I pray this scheme is sustained to benefit others. To the management of Ahmadu Bello University (ABU), Zaria for their efforts in capacity building schemes. To Alh Tanimu Ahmed, my guardian, who always make sure he does anything possible to help me succeed. To Muhammad Maude for your support and guidance in my career development.

To my brothers, Alh Muntari, Malam Aminu, Malam Bashir, Auwalu, Aliyu, your support has been very helpful, and to my late brother Malam Abdullahi for being there for me throughout our childhood life and up to his last days, I pray for your departed soul to rest in Jannatul Firdaus. To my sisters, Saadatu, Hauwau, Khadija, Aisha, Amina, Hassana, Hussaina, Sabira for your unending sisterly support.

To my wife Ummulkhairi for your linguistic and moral support, thanks for the courage, support and patience through this journey. You made my heart glows when returning home. To my daughter Aisha for being the most memorable part of this journey, your

smiles, having meals with me has been a good way of forgetting the academic stresses. To my cousins, Khadija, Aliyu, Hafsah, Yusuf for your support.

To Dr.I.A Muhammad for your uncountable support that make this study successful. To my academic father, Prof. Idris Bugaje for words of courage, support and constant contact to make sure I am doing well. To my mentor, late Engr. A.I.V. Ukaegbu for your fatherly support and courage to pursue this study to this level, I always remember you for being my prayer time keeper in the office.

To Alh M.B Umar for his continuous support to move forward. To my industrial mother, Engr Nike Fashokun, for her continuous concern and enquiries about my progress. To my inspirational guardians, the family of Alhaji Abba Abubakar Rafindadi for their committed support, prayers and ensuring that I am always doing my things right. To my late elderly colleague Mahmoud Nasir, for being the first on-call in all my academic and industrial endeavours. May ALLAH(SWT) light his grave and reward him with Jannatil Firdausi.

To my friends Sabbar, Hassan, Abubakar, Faruq, Muhammad, Hassan, Abdulkadir, Hayatu and all others whose names were not mentioned for their commitment, solidarity and being there always for me.

Space will not permit me to enumerate the people in my life who made this task possible, by Allah's will. ALLAH, the almighty knows you all.

Declaration

I, Abubakar Abbas Jibrin, declare that this dissertation report is my original work, and has not been submitted elsewhere for any award. Any section, part or phrasing that has been used or copied from other literature or documents copied has been clearly referenced at the point of use as well as in the reference section of the thesis work.

.....

Signature

.....

Date

.....

Approved by

Prof G.G.Nasr
(Supervisor)

.....

Confidentiality Notice

THIS DOCUMENT AND THE INFORMATION IN IT ARE PROVIDED IN CONFIDENCE, FOR THE SOLE PURPOSE OF THESIS, AND IS CURRENTLY WAITING FOR APPROVAL FOR COMMERCIALISATION, NOT BE DISCLOSED TO ANY THIRD PARTY OR USED FOR ANY OTHER PURPOSE WITHOUT THE EXPRESS WRITTEN PERMISSION OF THE AUTHOR. JOURNAL PUBLICATIONS MADE FROM THIS RESEARCH ARE YET TO BE PUBLISHED AND WILL BE RELEASED WHEN THE CONTRACTUAL FORMALITIES ARE COMPLETED

List of Publications

1. A.J.Abbas & G.G.Nasr(2014) Descaling Oil Wells using Water Sprays and Entrained-air, *Society of Petroleum Engineers Journal*(To be submitted)
2. Abbas, A.J., Burby, M., & Nasr, G.G. (2014) Predicting Spray Break-up region using Entrained-Air for Oil Production Tubing, *Sprays and Atomization Journal*(To be submitted)
3. Abbas, A.J., Yahaya, A.A.,& Nasr, G.G., (2013) Comparative Design review of West African Gas Pipelines Hydraulics between Hysys simulation and theoretical models, Pipeline Technology Conference, Ostend, Belgium.
4. Abbas, A.J., Nasr, G.G., Burby, M.L., & Nourian, A., (2013) Entrained Air around a high pressure flat fan spray. 25th Annual Conference on Liquid Atomization and Spray Systems, Pittsburgh, PA, USA.
5. Abbas, A.J., Nasr, G.G., A.Nourian, & Enyi, G.C.,(2013) Scale formation mechanism and removal using high pressure water spray jets, 25th European Conference on Liquid Atomization and Spray Systems, Chania, Greece.
6. A.J.Abbas, G.G.Nasr, A.Nourian, & G.C.Enyi, (2014) Characterization of Flat-fan Nozzle for Descaling Oil and Gas Production Tubing, 26th Annual Conference on Liquid Atomization and Spray Systems, Portland, OR, USA. May, 2014
7. A.J.Abbas, G.G.Nasr, A.Nourian, & M.Burby, (2014) Predicting Flat-fan Spray Break-up using Entrained-air, 26th Annual Conference on Liquid Atomization and Spray Systems, Portland, OR, USA.
8. G.C.Enyi, A.J.Abbas, G.G.Nasr, & M.Burby, (2013)Emission Reduction in GTL Facility using Spray Technique, 25th Annual Conference on Liquid Atomization and Spray Systems, Pittsburgh, PA, USA.

9. Nuhu, M.,Mujadid, M.M, Hamisu, A.A, Abbas, A.J.,Babangida, D.,Tsunatu, D.,Aminu, Y.Z., Mustapha, Y.,Ahmed, I., & Onukak, I.E., (2013) Optimum design parameter determination of biogas digester using human faeces as feedstock. *Journal of Chemical Engineering and Material Science* 4(3) DOI: 10.5897/JCEMS13.0156

Conversion Table

Parameter	SI	Other Conversion Factors
Pressure	101.325kPa	1atm
		1.01325ar
		0.101325Mpa
		101325Pa
		14.7psi
Flow	$1\text{m}^3/\text{s}$	$35.32\text{ft}^3/\text{s}$
		219.96gal(UK)/s
		1000liter/s
		543439BOPD
Length	1m	1000mm
		0.001km
		3.28ft
		39.37in
Temperature	0°C	32°F
		273.15K
		492R

Nomenclature

σ	Surface tension, kg/ s ²
Π	3.14
D^2	droplet diameter
U	velocity, m/s
ρ	liquid density, kg/ m ³
t	Time [sec]
C_w	Specific capacity of water(J/kgK)
E	Thermal energy stored(J)
E	Voltage across the hot wire (V)
F	Force
H	Heat transferred to the surrounding (J)
l/min	Litres per minute
δ_i	Middle diameter of droplet sizes in range (m)
f_D	Doppler frequency
T	Temperature (°C)
T_{wall}	Temperature at the wall(K)
T_{air}	Temperature of air(K)
h	Overall heat transfer coefficient(W/m ² °C)
R	Radius
Re	Reynolds number (= $\rho_L U_o d_o / \mu_L$)
D	Droplet diameter (μm)
χ	Downstream distance (mm)
P	Pressure (MPa)
I	Current (A)
R	Resistance (Ω)
O	Orifice diameter (mm)
Q	Liquid volume flow rate (l/min)
Q_{conv}	Heat transferred by convection(J)
ν_i	Liquid viscosity
θ	Angle of spray (degrees)

λ	Wavelength (m)
μ	Dynamic viscosity (Ns/m ²)
d	Droplet
G	Gas (air)
L	Liquid (water)
M	Mass
D ₃₀	Volume mean diameter (μm)
D ₂₀	Surface mean diameter (μm)
D ₃₂	Sauter Mean Diameter (SMD) (μm)
PDA	Phase Doppler Anemometry
LDA	Laser Doppler Anemometry
RR	Rosin Rammler
W	Power Generated(J/s)
Nu	Nusselt Number
Gr	Grashof Number
h	Coefficient of heat transfer(W/m ² °C)
R	Resistance(Ohms)
CFD	Computational Fluid Dynamics
W	Power generated by the Joule's heating(W)
A	Surface area(m ²)
A, B	Constants
n	Constant

Abstract

Recent attempts to utilise solid particles in combination with high pressure water sprays has caused environmental and safety concern, in cleaning mineral and organic scale inside the Oil and Gas Production Tubing. To increase cleaning performance only high pressure aerated water sprays at high impact force instead should be used. Multi-nationals petroleum companies are facing immense challenges in removing the scale due to the decrease in cavitation bubbles along the production tubing when high pressure water sprays are applied. This has also resulted in high maintenance costs and low productivity of the 'wells' with multi billions pounds financial losses per annum. Currently scales are removed using either aggressive chemicals (acids), complete replacement of the tubing, or solid-liquid sprays which are both expensive and causes environmental concern. This research demonstrated that the application of air-water combination (aerated sprays) are the solution in complete removal of various scales in the production tubing without the use of solid particles and the cavitation bubbles.

This novel experimental technique of scale removal utilised air concentration (or aeration) in combination with high pressure flat fan sprays, of up to 10 MPa, at low flow rate (up to 12 l/min) with high impact pressure of approximately 0.15 MPa, in removing scale along production tubing using a simulated aeration chamber. It was found that varying air concentration from 3 to 12%, within the emulated chamber, improved scale erosion up to 28% higher than non-aerated technique. This enabled the mass of the scale to be removed at the 'stand-off distance' of 25 mm relative to scale samples, irrespective of cavitation bubble length suppression which is normally about 2 mm away from the atomiser orifice exit, compared to non-aerated techniques (solids and water). Scale erosion was found to be 12.80g, 7.31 g, and 65.80 g at aerated conditions compared to non-aerated provision which found to be 9.88g, 6.33g and 5.31 g, at the required liquid pressure 10 MPa, for the hard, medium and soft scale samples that are typically found in oil production tubing.

Prior to scale removal trials sprays were characterised qualitatively and quantitatively under the ambient conditions as well as inside the aerated simulated chamber. Air velocities were found to be approximately 18m/s towards the water spray centre which then decays to 3 m/s towards the spray periphery under ambient conditions using hot wire anemometer. Moreover, the flat fan sprays were also characterised utilising Phase Doppler Anemometry (PDA). It was found that the high pressure water liquid droplet velocities were in the range of 75 to 117 m/s with droplet diameters of 55 to 81 μm (SMD) at flow rates of 7.6 to 11.3 l/min at various stand-off distances of 25, 50 and 75mm, providing an impact pressure of 0.05, 0.10 and 0.15 MPa respectively.

Qualitatively cavitation bubble length was also estimated using high resolution imaging techniques which were found to be between 1 to 2 mm from the atomiser exit orifice under submerged conditions, at the stand-off distance ≤ 25 mm where the scale is normally removed. Beyond this range (1-2 mm) where the cavitation bubbles are not present, that are normally the benefactors to scale removal process, requires air concentration up to

12%. This ensures that a complete removal of the mass of corresponding scales to be achieved with varying chemical scale compositions. The air concentration is the ratio of total mass of air within the simulated chamber to mass of the liquid sprays impacting directly onto the scale samples.

The results of the experimental trials were used to validate the available CFD fluent models with regards to spray dynamics, aerated air (velocities), cavitation bubble generations and scale erosion (removal). The sensitivity analysis using the CFD modelling gave close comparison with those obtained through experimental trials. Spray droplets size and their velocities were found to be within $\pm 10\%$ compared to those obtained via experimental findings. The aerated air velocities were also compared with the data generated from CFD which were found to be approximately $\pm 9\%$. Furthermore, the cavitation bubble generation and the mass of the scale removed were found to vary within $\pm 5\%$ and $\pm 7\%$ respectively, when compared to the CFD data.

Finding emerged that the spray droplets especially at the centre undergoes acceleration after primary breakup, which due to higher velocities resulting from the acceleration has left the entrained-air particles behind, which is characterise with substantially low-pressure region, giving rise to utilisation of the air-water interaction model. This could be another approach in further understanding the break regions within the high pressure liquid sprays.

Chapter 1

Introduction

1.1 Preamble

Among oil and gas production challenges, scale formation along production tubing is regarded as the difficult production challenges among upstream operations, with prominent reported areas such as the largest oilfield in the world, Al Ghawar in Saudi Arabia [1], Gulf of Mexico, North Sea and Canada among others, with high tendency to scale formation as a result of gradual or sudden accumulation of mineral salts, which reduces flow cross sectional area. This causes high pressure drop along the tubing which reduce the production rate to the barest minimum if no urgent measure is taken, yearly, this results in millions of dollar production lost. Therefore, continuous energy demand by the global community may suffer sufficient drawback of supply if such issues are not timely addressed. Scale removal has continued to attract production enhancement with several cases of revenue increase resulting after the operation [2]. A case study of CaCO_3 removed scale well in Indonesian *Duri* field, built revenue by USD3.6 million within 90 days and a payback period of 18 days [3]. While the effect of scale can be instantaneous, with a case of North Sea *Miller* field, where scale growth within 24 hours and halted production of 30,000 Barrels of Oil Per Day (BOPD) to zero [4]. However, cost implication of avoiding or removing scale runs into millions of dollars per year, and the consequences of not attending to it cost even more. Indeed, gas production wells have recently been reported scaling problems in the Middle East, consisting predominantly Fe_7S_8 [1], causing deposits along the production tubing with decreasing production and access difficulty. Other mineral scale types have also been a subject of concern as the chemistries of formation and chemical contents of the reservoir fluid plays an important role.

1.2 Scales in Oil production

With most of the reservoir formation made up of different salt types from origin, it become practically clear that oil and gas, and scale resulting salts are naturally formed together in the same reservoir environment, and therefore can never be isolated but rather, identifying the optimum approach to minimizing their negative effects such as nucleation along perforations,

valves, production tubing, casing, pumps and other down hole completion equipment is the primary target. Indeed, different type of oil and gas reservoir are characterised with different salts types as well as different fluids content, though, in most cases, the salts are associated with the formation water as dissolved components at reservoir conditions. Consequently, production processes which derive the oil and gas to the surface due to naturally driven mechanism of pressure difference, results in substantial change of flowing properties, such as temperature and pressure. These sometimes favour the formation of scales before reaching the surface; which are not easily manipulated based on their manner of natural occurrence.

There has been continual development in routine control and monitoring mechanism, of the flow along the production tubing, which can now easily be manipulated to achieve certain production targets. Indeed, artificially induced reservoirs, which suffers decline in production are now agitated to achieve increased production rate using water injection (mostly sea water containing ions such as sulphates and carbonates ions etc.), these however may again suffer water incompatibility problems with the produced water, resulting in the precipitation of $BaSO_4$, $MgSO_4$ or $CaSO_4$ types of scales. This simply confirm that scale problems in production may not be found at early production days but rather with age of production in some wells.

Therefore, a need to improve sustainability of processes leading to mitigation and control of these scales cannot be overemphasized, despite the current chemical, mechanical as well as the jetting techniques for scale removal, recent development in the oil and gas multi-national companies have shown wider acceptance of using high pressure water sprays (jetting) [5],[6] as a more promising technology for scale removal [1],[7],[8],[9]. However, most of the current jetting techniques include a *sterling beads*(solid particles) along with the water jets [10],[11],[12] which possess environmental concern of adding solids to the surface equipment's while removing mineral scale, increasing the pump sophistication due to changes in density of the injecting water all in an effort to compensate cavitation erosion decrease due to increasing depth. This requires alternative re-think and an opportunity for further research.

1.3 Research problem statement

Application of high pressure water spray jet in the removal of mineral scale deposits along production tubing has been adopted by several multi-national companies such Schlumberger, Shell and Saudi Aramco in their various production fields in most cases, characterized by

decrease in production rates [10],[11],[12], which successfully removes scale at ambient conditions at desired rate, however, the efficiency of the water jet has been reported to undergo substantial decrease whenever the jet moves down the production tubing [11] due to increase in ambient pressure at depth, causing lesser amount of the scale removing efficiency, which is attributed to the suppression of cavitation.

The cavitation is a process in which liquid undergoes change in phase to vapour upon decrease in pressure across the jetting atomizer equals to the vapour pressure of water, leading to low erosion with less or no cavitation, has been viewed as the drawback of using water jets alone. Consequently, solid particles (sterling beads) were sought to compensate for the low performance. However, using a pump to deliver water mixed with solid suspension is well known to require sophisticated pump design to deliver higher density suspension of solid and liquid. The possible material damage that may affect the impeller off the pump, and possibility of causing solid deposits along the production tubing itself and other down hole equipment compelled necessary research work to investigate the possibility of enhancing the jetting technique performance without necessarily adding the sterling beads. Although, several attempts were made in the past to identified the basic factors affecting the cavitating jet performance in the field of multi-phase flow for applications relating to hydraulic machinery, drilling operations and mining, so far, the problem of diminishing cavitation tendency with increasing depth require further research input and hence to crown it all, enhancing the performance of the water spray jet using solid-free water jet along petroleum production is liable to making key input both to the sustainability of using environmentally friendly process and also cost-effective descaling technique. These has led to the development of an integral idea of utilising an aerated chamber designed and developed in Spray Research Group (SRG) laboratory to simulate petroleum production containing flat fan nozzles suitable for high pressure cleaning [13][14] in order to answer vital research questions which remained unanswered. These questions are:

- Does an air concentration in aerated chamber led to the suppression of cavitation in Flat-fan sprays?
- What is the relationship between cavitation bubble length and the air concentration in aerated chambers in Flat fan sprays?
- Does the air concentration in the aerated chamber enhance the erosion performance?
- Does the application of aerated chambers bring sustainability in the oil production as well as the environment?

Increasing global energy demand and consequent increase in oil prices is the driving force for optimizing production operations as well as designing new technologies for achieving energy security around the globe. Production rate from oil and gas wells may be hampered by several operational challenges; one of the most common is scale build up around the production tubing, pumps, perforations, valves, casing or down hole completion equipment, resulting in reduced production rate to even zero sometimes.

Several attempts are in practice for scale removal, among them are the mechanical techniques which uses an impinging mechanical forces for vibrating and loosening the scales from the production tube, however degradation or deteriorating effect on the tubing itself has been a major setback. Other technique involves using acids for dissolving the scales, and indeed, corrosion nature of acids and its environmental hazards to personnel and the tubing itself cannot be neglected.

1.4 Research contributions

- Enhancing the erosional performance in descaling oil wells through aeration techniques utilising high pressure flat fan atomizers.
- Providing for the first time, quantitative and qualitative knowledge data base with respect to the entrained-air behaviour in relation to cavitation bubble generation, stand-off distance (the distance from the atomiser to the scale target) for bubble collapse and erosion mechanism in removing scale in oil and gas production.

1.5 Research Aim

- To study the mechanism of scale erosion attributed to high pressure, high impact aerated flat fan atomizers.
- To establish scale erosion performance in relation to cavitation erosion at realistic ‘well’ depth in the simulated aerated chamber, and
- To validate experimental data using CFD models

1.6 Research Objectives

The cardinal objective of this research work is to utilise aerated chamber for the removal of mineral scale along oil production tubing using high pressure flat fan nozzles with the following specific goals:

- To investigate the parametric effects of spray dynamics (i.e. droplet velocity, size, and flow rate) in relation to impact pressure, air concentration, cavitation and erosion.
- To measure the mass of scale eroded at varying air concentration using aerated chamber.
- To develop corresponding CFD models for the validation of experimental results obtained in spray characterisation, cavitation, and scale erosion.

1.7 Structure of the Research Thesis

The thesis is arranged in chapter forms, with each chapter providing the set of information and actions performed as contained in the research work as follows:

Chapter 1: Introduction

The chapter introduces the concept of scale formation along production tubing as a major oil and gas production problem, and then provide a brief description of the existing technologies for treating scale formation, their advantages and disadvantages of such methods. Developing a research approach to enhancing the performance high pressure water sprays using simulated aerated chamber. Research contributions, aims and objectives are also provided.

Chapter 2: Scale formation and removal in oil and gas production

The chapter provides the fundamentals of scales formation including its chemistries and factors favouring the formation of the scale, with typical examples of case studies in different oil and gas fields across the globe, as well as cost implications and investments in tackling the problem. The chapter then provides the different types of scales and their formations, as well as detailed descriptions of the technologies involved in their removal with emphasis to challenges, success and way forward.

Chapter 3: Spray cleaning using high pressure water jets

This chapter selected the use of high pressure water sprays as the most sustainable approach to scale removal, with emphasis on the disadvantage of using solid particles along water jets. Subsequent solution of aerated high pressure sprays was selected to replace the currently used solid and water combination for environmental sustainability and safeguarding the integrity of the production tubing. Flow behaviour and characterisation of spray systems is provided with emphasis on high pressure atomizer applicable for cleaning purposes. Fundamental parameters such as droplet velocities, droplet sizes, impact forces and their effects on the entrained air were to be described. Various attempts by researchers and companies explained based on their atomizer types and operating conditions with arguments on the effect of cavitation phenomena and how it occurs along the water jets with detailed description of the effect of the surrounding air onto the jets and the walls of the surroundings.

Chapter 4: Experimental set up

The chapter covers the detailed experimental set up, description and design involved based on the previous chapter(s) and set up sketches, drawings, fabrication and assemblies of the various test rigs, with each set up interdependencies and necessity explained. The chapter covers the following experimental test conducted: Entrained air velocities measurement around a flat-fan atomizer at various pressures axially and radially; Phase Doppler Anemometry (PDA) for the characterization of the flat-fan nozzle at the same pressure entrained-air velocities were measured as intended in this experiments with the choice and operating conditions explained; the impact force measurement test rig conducted for the force distribution along the flat fan width; and the design of the high pressure air chamber for the descale test involving the ambient and pressurized chamber.

Chapter 5: Results and Discussion

The chapter discusses the results obtained from the various tests conducted in Chapter 4, with emphasis to the relevance of the results and findings made from it. Comparison was made to recent applications in the industries with emphasis on how the current research findings can lead to more environmentally friendly descaling operations in oil and gas processes.

Chapter 6: Spray Jet Break up, Cavitation and Erosion using Computational Fluid Dynamics

The chapter discusses the applications and relevance of CFD modelling in the analysis of the spray jet behaviour including the various models involved, domain and benefit of CFD simulation to the subject area in which experimental findings were bound to be limited.

Chapter 7: Conclusions and Future Works

The chapter provides conclusions of the findings made from the research and benefits of the findings by establishing the knowledge data base for the oil and gas industry applications. Research gaps were also identified which could potentially be in the area of spray cleaning.

Chapter 2

Scale Formation in Oil and Gas Production

2.1 Overview

Formation of mineral scale deposit along oil and gas production tubing due to interactions of ions originating principally from incompatible water source occurring usually in wells adopting water injection method [15] has continue to be a challenge to the petroleum production experts. Considering the necessity to maintain the production rate as well as water injection [16] to achieve economic benefits from the hydrocarbon wells, scale formation are managed throughout the life of such wells in terms of its chemistries of scale formation. The engineering principles for the fields as well as completion systems adopted in the specific well. Scale usually result due to interactions of ions in incompatible water, ordinarily two set of water said to be incompatible upon generating a precipitation on reacting chemically with each other, other scales may be formed due to outgassing, during production enhancement using sea water.

However, the major factor attributed to scale precipitation is primarily temperature or pressure variation(or fluctuation), PH shifting, outgassing and water incompatibility, although, several produced water that have attained oversaturation with specified condition and scale-prone did not form scale [11]. It is therefore necessary to highlight that scale formation requires a necessary growth from its solution with the formation of less stable atoms. Further growth to form clusters from the atoms is caused by fluctuation in ionic equilibrium. Sea water is known to contain substantial amount of such ions as SO_4^{2-} , with low concentration of Ca^{2+} , Ba^{2+} , or Sr^{2+} are frequently used by offshore production companies for the water re-injection, on the other hand, formation water from production wells contains more Ca^{2+} , Ba^{2+} , or Sr^{2+} than the SO_4^{2-} , whenever disposal water mixes with injection sea water, insoluble clusters may result.

Oil and gas production is mostly accompanied with produced water, which due to flow behaviour loses pressure and temperature along the production tubing, resulting in the release of gases such as CO_2 and subsequent PH shift (increase) of the produced water and calcium carbonate precipitation[11].Flow restriction caused by mineral scale can be a main source of formation damage[17],[18].

2.2 Scale Formation in Oil and Gas Production

Scale formation along production of oil and gas has water as a major factor, reservoirs most often contains waters, which as a general solvent can be rich in salts as a scale components, usually rich in various cations, as deep subsurface water derived salts components as a result of contacts with minerals found in sedimentary regime; water found in carbonates or calcite-cemented sandstones reservoirs are rich in Ca^{2+} , and Mg^{2+} , also sandstones contains Ba^{2+} and Sr^{2+} cations, though composition of dissolved minerals may vary mineral diagenesis and other alterations along the reservoir, a typical quoted total dissolved solids up to 400 mg/L in some reservoirs [11]. Unavoidable use of sea water with high concentrations of ions such as SO_4^{2-} as a by-product of marine life and water evaporation; for production enhancement and pressure maintenance especially in offshore located wells, commingling with produced water associated with minerals from sedimentary rocks causing precipitation of scale which reduces the surface area of flow as shown in Fig. 2.1. causing adverse decrease in production as well as injection rates leading to costly downtime for removal [16], thus, becoming a serious challenge to the supply chain.

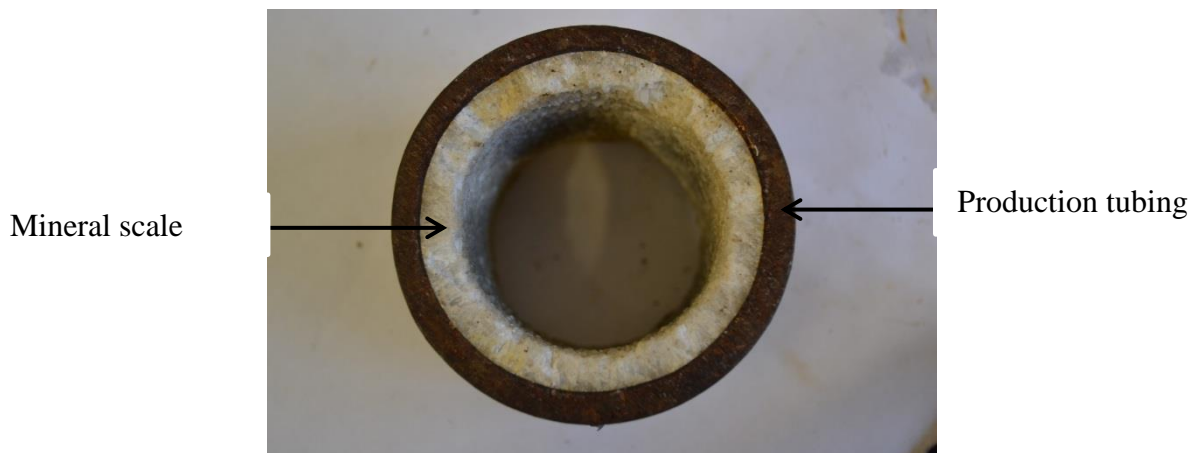


Figure 2.1 Scale formation along production tubing

However, [19] propose three mechanisms for the formation of mineral scale in oilfield as

- Reduction in solubility due to decrease in pressure or temperature increase,
- Precipitation due to mixing of incompatible water(usually formation water carries Ca^{2+} , Ba^{2+} and the sea water rich in SO_4^{2-} resulting in BaSO_4), and
- Evaporation of Brine leading to increased concentration above the solubility range.

Consequences of scale formation may lead to well productivity damage in terms of permeability depreciation, and hence plug production tubing and other sub-surface equipment

which may eventually lead to safety hazard[20],[21]. However, it becomes necessary to access such production problems to enable their remediation.

2.3 Industrial Scale Problems

Several cases of reports from industrial experts has continue to show prevalence of scale formation during production with the Iranian carbonate scale offshore field under water injection [21], the *Gyda* field located in the north-eastern around the Norwegian continental shelf of the North Sea[19], *Miano* gas field located about 350 km north of Karachi, Pakistan, which exhibited sudden production decline associated with water influx, gas permeability decline and flow decrease along the production tubing due to carbonate deposit [22].Scale of Iron was also reported in the world largest oil field *Al-Ghawar*, spanning 225 km in length with 30km width, its FeS scale present in this gas field was known to depend on mineralogy of the formation, the gas type produced, the produced water, practices of completion as well as gas flowing conditions [1], the *Alba* field located in the UK continental shelf [23], upper Zakum field in Abu-Dhabi, accounted as the 4th largest identified in the world [2] other fields reported include Siri field where Sulphate and carbonate scale were found [24], with several others unaccounted for in this research, could cause a drastic decrease in productivity such as that found in Miller field of North Sea with a production from 30,000bopd to Zero within 24 hours [11]. The formation of scale is one of the most challenging issues that have to be dealt with in oilfields on a day to day basis. However certain engineers have been able to tackle the problem head on and this might be because those engineers have an opportunity to see physically or actually inspect scale samples or the fact that most scale deposits are located outside the well are visible oil bearing formations. Scale formation builds up gradually and eventually would result in the blockage of production tubing from the reservoir to the surface. Results gathered from field data shows that scales tend to occur during and after water injection operations not only inside the inner surface of facilities, but also form the well-head down to the bottom of the well-bore and even to the reservoir in the order as (i) Injector well-bore, (ii) Near the injection well-bottom hole, (iii) Within the reservoir, (iv) At the skin of the producer well, (v) In the producer wellbore and finally, (vi) At the surface facilities.

Scale formed in in the injection well pipe is usually produced as injected water from the surface brings dissolved minerals, like seawater does. A temperature change along the injection well causes the precipitation of the minerals. Scale formed in the reservoir and bottom hole is more as a result of the mixing of two incompatible waters rather than

temperature changes. The scale that is formed in the skin of well production is because a well shutdown gets filled with water and then reacts with water from the reservoir to form scale.

Temperature changes as the flow goes up a production tubing is the main cause of scale formation in the tubing, but a variation in pressure resulting in liquid and gas phase compositional changes is another reason. A pressure change results in change in pH of water due to the liberation of CO₂ from the water [25].

The formation of scales can occur in many parts along water paths from the water injector well through a production well until surface equipment as shown in Fig. 2.2 indicating the several surface and subsurface valves liable to be affected by scale formation.

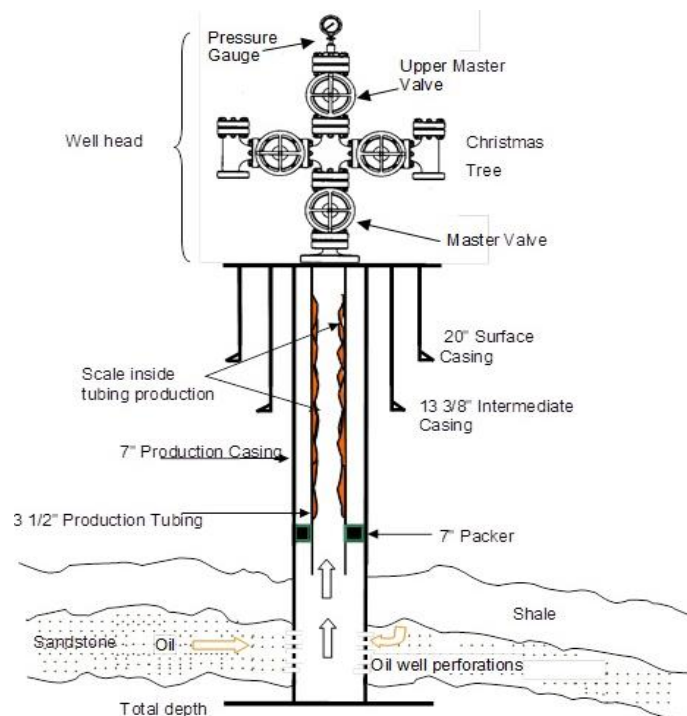


Figure 2.2 Oil production assembly profile [26]

Due to the changes that take place with the temperature and pressure in oil and gas reservoirs during production, it is possible to have organic scales like paraffin waxes and asphaltenes being deposited outside the crude oil plugging the formation in the process. The solidification of CaCO₃ and BaSO₄ may also take place to block the paths of flow.

Scales are formed by the development of unstable clusters of atoms known as seed crystals in a process termed homogenous nucleation. The clustering of these atoms is usually triggered

by fluctuations in the equilibrium concentrations of the ions in solutions that are supersaturated. These atoms grow by ions being adsorbed onto imperfect surfaces of the crystals extending the crystal size in the process. It can be shown that large crystals favour continuing crystal growth, and there is the likelihood of small crystal seeds disintegrating. Therefore, for a large enough degree of super-saturation, seed crystal formation would encourage an increase in scale growth. This means therefore that the seed crystals act as a catalyst for the formation of scale.

Unfortunately, water-flooding operations have been designed without a proper knowledge of the level of damage due in formation and wellbore that is caused by the deposition of scale and hence no proper scale risk assessments were carried out. In contrast, each scale type differ in its chemistry of formation as well as its mitigation methods, which then necessitate understanding the formation process of the various types prior to outlining its cleaning or inhibition options.

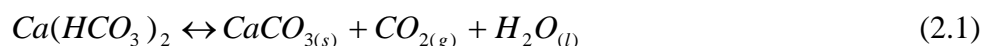
2.4 Sources and Types of Mineral Scale in Oil Production

2.4.1 Chemistry of scale formation

Scale precipitation occurs due to mixing of brine which are incompatible or changes in the physical conditions include temperature, pressure, or pH [27]. The precipitation of solids from brines that are present in production flow systems and reservoir results in the formation of mineral crystalline deposits known as oilfield scales. Variation in the ionic products and composition, pressure, temperature as well as PH of the brine are the key driving force for the precipitation of these mineral scales [28].

The factors variation as classified and cited by[28] are into three main methods:

- (a) Pressure or temperature decrease which leads to the decrease in the ionic solubility of the salt (this leading mostly to the precipitation of the carbonate scales like CaCO_3)



- (b) Mixing of two incompatible brines such as a mixture of sea water which is rich in sulphate compounds with formation water which is rich in cations like barium,

calcium and strontium leads to the precipitation of sulphate scales such as barium sulphate($BaSO_4$)



- (c) Evaporation of brine which results in an increase in salt concentration above the limit of solubility resulting in salt precipitation (this occurs mainly in High Pressure/High Temperature gas wells as a result of the mixture of dry gas streams with low rate brine stream leading to the dehydration and precipitation of sodium chloride NaCl).

Scale formation builds up gradually and eventually would result in the blockage of production tubing from the reservoir to the surface. Results gathered from field data shows that scales tend to occur during and after water injection operations not only inside the inner surface of facilities, but also from the well-head down to the bottom of the well-bore and even to the reservoir. Scale formed in the injection well pipe usually occurs as injected water from the surface brings dissolved minerals, like seawater does. A temperature change along the injection well causes the precipitation of the minerals. Scale formed in the reservoir and bottom hole is more as a result of the mixing of two incompatible waters rather than temperature changes [29]. The scale that is formed in the skin of well production is because a well shutdown gets filled with water and then reacts with water from the reservoir to form scale.

Temperature changes as the flow goes up a production tubing is the main cause of scale formation in the tubing, but a variation in pressure resulting in liquid and gas phase compositional changes is another reason. A pressure change results in change in pH of water due to the liberation of CO_2 from the water [30]

The formation of scales can occur in many parts along water paths from the water injector well through a production well to the surface equipment. Due to the changes that take place with the temperature and pressure in oil and gas reservoirs during production, it is possible to have organic scales like paraffin waxes and asphaltenes being deposited outside the crude oil plugging the formation in the process. The precipitation of calcium carbonate and barium sulphate may also take place to block the paths of flow.

Scales are formed by the development of unstable clusters of atoms known as seed crystals in a process termed homogenous nucleation [31]. The clustering of these atoms is usually triggered by fluctuations of the equilibrium concentrations of the ions in solutions that are supersaturated. These atoms grow by ions being adsorbed onto imperfect surfaces of the crystals extending the crystal size in the process. It can be shown that large crystals favour continuing crystal growth, and there is the likelihood of small crystal seeds disintegrating. Therefore, for a large enough degree of super-saturation, seed crystal formation would encourage an increase in scale growth. This means therefore that the seed crystals act as a catalyst for the formation of scale.

Sometimes, possibilities exist of non-scale formation despite the produced waters that are oversaturated and scale prone with. The driving force resulting in scale formation could be change in pressure, temperature, or pH shift, out-gassing or contact between incompatible waters, for scale to form it must grow out of solution. Firstly, a fluid that is saturated forms unstable clusters of atoms in a process known as homogeneous nucleation. A local fluctuation in the equilibrium ionic concentration in supersaturated solutions causes atoms to cluster forming seed crystals [11]. These seed crystals become larger as ions are adsorbed onto defects on the surface of the crystals thereby extending the size of the crystal. The seed crystal grows by energy that is driven by a decrease in surface free energy of the crystal. This free energy experiences a decrease rapidly as radius increases after a critical radius might have been exceeded. The implication of this is that large crystals are favourable to continuous growth while smaller seed crystals may dissolve again. Therefore, given a degree of saturation that is large enough, seed crystal formation will result in the growth of scale deposits. The seed crystals act as catalyst for scale formation.

Also, crystal growth is likely to be initiated on a pre-existing fluid-boundary surface [32], in a process referred to as Heterogeneous nucleation. Heterogeneous nucleation sites include defects on the pipe surface such as roughness or perforations in liners or joint seams in production tubing or pipelines. Scale deposition can also be catalysed by high degree of turbulence. The accumulation of scale occurs at the bubble point pressure of the flow system [31]. This gives a clear understanding of the reason why scale is deposited rapidly on downhole completion equipment

The existence of solid particles along the production tubing's, pipelines, or even surface facilities has been a great source of flow assurance concern to the oil production operations,

with the solid types classified into two broad classes as organic, comprising of asphaltenes, wax and soaps and the inorganic containing mineral salts such as CaCO_3 and BaSO_4 generally termed as scales [33]. Although emphasis will be given to the scale as the harder solid type threatening production, which its precipitation occurs anytime there is the interaction of ions of incompatible salts, or changes in the physical conditions such as Temperature, PH or pressure [27]. The precipitation of salts from brines that is present in production flow systems and reservoir results in the formation of inorganic crystalline deposits known as oilfield scales. Changes in the ionic composition, pH, pressure and temperature of the brine are the driving force for the precipitation of these scales.

The scale precipitated in most oilfields has water as the basic reason why they are formed. This is so because scale will only be formed if water is produced from the well. Water is generally a very good solvent and hence can carry with it large amounts of minerals that can cause scaling. When natural waters come in contact with mineral phases in natural environments, certain mineral components are dissolved and carried by these waters. This results in formation of complex fluids which are rich in ions, some of which are close to the limits of saturation for certain mineral phases. Seawater for example is rich in ions that are by-products of marine life and water evaporation, while the water in the ground and near surface are chemically different from those associated with oil and gas wells. As sedimentary minerals are altered, deep subsurface water becomes enriched with ions. For example, carbonate and calcite-cemented sandstone reservoirs have a high concentration of divalent calcium (Ca^{2+}) as well as magnesium (Mg^{2+}) cations, while sandstone formations contain barium sulphate (Ba^{2+}) and Strontium (Sr^{2+}) cations.

The total dissolved solids can be as high as 400g/L (3.34ppg)[11], but the exact composition would depend on the diagenesis of the mineral and other alterations that occurred as reservoir fluids flowed and mixed over time.

When the natural state of any fluid is altered such that solubility limits for components are exceeded, scale formation begins. The solubility's of these minerals have a dependence on temperature and pressure that is rather complex, so an increase in temperature will result in an increase in water solubility of a mineral. That is to say that more ions are dissolved at higher temperatures. A decrease in pressure on the other hand tends to result in a decrease in mineral solubility's and as such a rule of thumb has been developed that states that solubility of most minerals decreases by a factor of two for every pressure decrease of 7000 psi

(48MPa)[11]. Calcium carbonate is one of the minerals that does not conform to this rule and tends to show an increasing solubility in water as temperature reduces [11]

Scale is deposited in subsurface and surface oil and gas production equipment and this is a serious challenge that affects water injection systems of oilfields. Scale plugs the oil-production matrix or fractures and perforated intervals blocking oil and gas production in the process. It could also cause the blockage of production lines, equipment and impair the flow of fluids. The effects would include failure of production equipment, emergency shutdowns, increase in maintenance cost of equipment and a huge decrease in the production efficiency. Equipment failure would also result in safety concern. Scale can also be deposited from water type as a result of the super-saturation with scale forming salts due to changes in the physical conditions which the water exists. When two incompatible waters mix together and reach super-saturation point, scale can also be deposited [28].

2.4.2 Oilfield Scale Types

The Oilfield scale that are commonly encountered in the oil and gas operations are numerous considering the variety of combinations of ions possibly found around the field itself or injected as part of the production enhancement techniques. These scales include sulphate compounds such as calcium sulphate (anhydrite, gypsum), barium sulphate (barite), and strontium sulphate (celestite) as well as calcium carbonate. Other scale types reported include compounds of iron such as iron oxides, iron carbonate and iron sulphides[28][34].Among the scale types, commonest ones are provided in the next section.

2.4.2.1 Calcium Carbonate Scale

Calcium carbonate popularly known as calcite scale is found frequently in oilfield operations due to wide availability of limestone regions [35]. Other crystalline forms of calcium carbonate include Aragonite and Vaterite but calcite which shows the greatest stability in terms of strength especially for oilfield scenarios and as a result is the most common type of calcium carbonate scale that is encountered during production operations. Calcium carbonate scales are deposited as a result of the precipitation of calcium carbonate as demonstrated by the Eq. 2.3



It is also possible to have calcium carbonate scale formed as a result of the combination of bicarbonate ions and calcium, and this is the primary reason why calcium carbonate scales are deposited in oilfield operations. Small amount of ions from bicarbonate dissociate at the pH values corresponding to most injection wells to form H^+ and CO_3^{2-} [24], which is shown in Fig. 2.3 after precipitation [35]

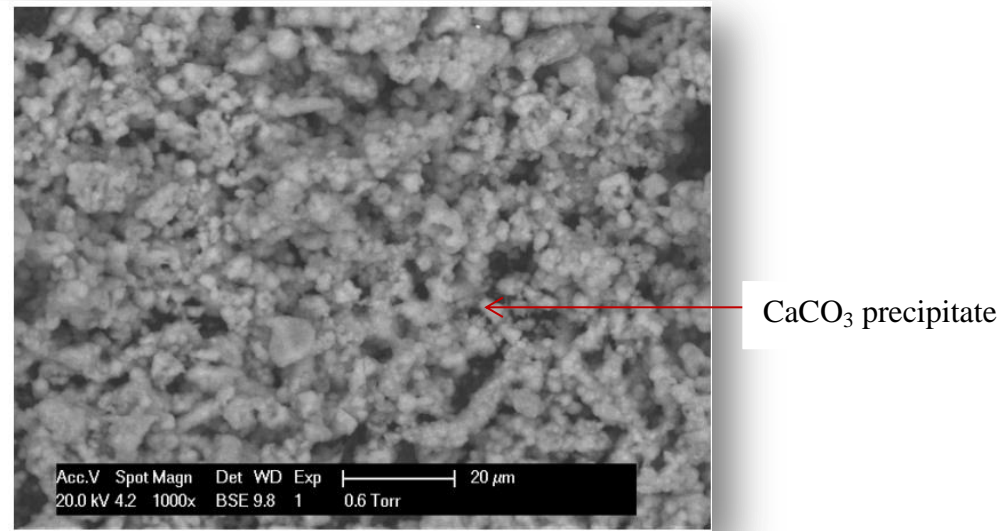
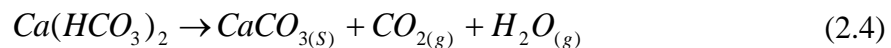


Figure 2.3 Precipitation of $CaCO_3$ in bulk [35]

Calcium carbonate scale is deposited on majority of subsurface as well as surface production, causing facilities in oilfields to have an operational problems in the process. The initial dissolution of carbonate-scale-forming component is as a result of the super-saturation of the formation water with calcium carbonate due to a pressure drop during production.

According to [19], when the connate or aquifer water transitting through the bubble point, leading to the evolution of carbon dioxide, carbonate scale is formed. The evolution of carbon dioxide results in a decline in the solubility with respect to the carbonate, and a precipitate with divalent ions such as iron and calcium is formed as outlined by the Eq 2.4

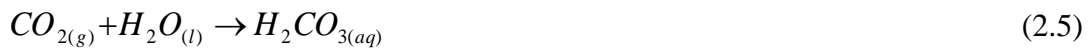


Before an oil reservoir is produced, different fluids (oil, brine and gas in some cases) coexist under a set of thermodynamic conditions. These include Temperature, Pressure, Amount and Volume. If the correct values of three out of these four variables are known, then the other variable can be calculated along with other thermodynamic parameters and equilibrium.

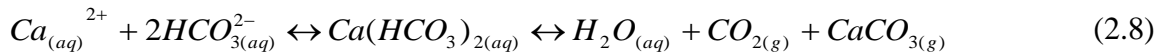
Calcium carbonate precipitation stems from CO₂ and Ca²⁺ ions dissolved in brine during the production process of the fluids in the field. On the other hand, under static or non-flowing conditions (reservoir conditions), it can be assumed that the entire fluid system is in thermodynamic equilibrium. CaCO₃ precipitation caused due to the loss of CO₂ from formation water produced in the pre-seawater breakthrough period can be observed. It is not difficult to control CaCO₃ scale precipitation by the use of scale inhibitors or acid removal, although precipitation of the salt could have been done prior to water injection, however, being water injection process is usually performed in offshore injections where feasibility of crystallization can be difficult considering the large quantity of salty water from sea water utilised; and the weight and space requirement for such operations resulting in huge financial implications. A continuous pressure drop leads to degassing of the carbon dioxide resulting in an elevation of the pH in the produced water and calcium carbonate precipitation [28].

The solubility of calcium carbonate depends on various factors and these include:

- (i) Effect of carbon dioxide partial pressure – carbonate scales do not require just the effect of temperature, pressure, as well as water composition for their prediction. Knowledge of the chemical reactions between brine and CO₂ in the gas phase is very important. Many reservoirs are made up of carbonate mineral cements as well as carbon dioxide and as a result, the formation water is saturated with calcium carbonate at reservoir conditions which could have temperatures as high as 200°C and pressure up to 30Mpa. CO₂ coming in contact with water dissolving to form carbonic acid as illustrated by the Eq. 2.5



The equation above shows that acid carbon dioxide comes in contact with water dissolving to form carbonic acid and this acid is ionised to form H⁺ and CO₃²⁻ ion. It can be seen that the second ionisation constant of the carbonic acid is much smaller than the first ionisation constant and hence bicarbonate ions greatly outnumber the carbonate ions that are present. Calcium carbonate in the dissolved state is believed to exist as calcium ions and bicarbonate ions. The precipitation of calcium carbonate can therefore be expressed in Eq 2.8



By increasing the carbon dioxide concentration, more calcium bicarbonate is formed. A decrease in the carbon dioxide content in this system in equilibrium will result in the formation of calcium carbonate. Based on this, it can be deduced that the calcium carbonate's solubility is mainly affected by the CO₂ content of the water[36].

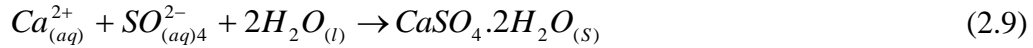
2.4.2.2 Calcium Sulphate (CaSO₄)

Calcium sulphate scales are crystalline deposits that are attracted to many surfaces. They contain principally ions of calcium and sulphate and may also contain traces of many other ions, when they are deposited from complex poly-metallic solutions. Calcium sulphate scales are co-precipitated with strontium sulphates and can form solid solutions together. Also, it may contain trace amounts of rust, silt or wax if precipitated from oilfield fluids [28]. Calcium sulphate occurs regularly as one of three different phases. The most common phase is Gypsum which forms at relatively low temperatures. At temperatures above 100°C, anhydrite (CaSO₄) is formed which is the stable phase. However, at temperatures above 100°C hemihydrate is formed particularly in laminar systems and in high-ionic product brines [37].

A pressure drop is the cause of deposition for gypsum or anhydrite in downhole conditions. This also has a greater effect than temperature as cited in. Depending on ionic strength or temperature, these compounds may be stable and have decreasing solubilities as temperature increases [24]. Calcium sulphate is one of the major scales in the oil and gas industry which cause severe flow problems as well as formation damage issues. The most difficult oilfield scale to remove is gypsum. This is due to its low solubility in water at 25°C. Increase in temperatures, causes more insolubility in water as low as 1.69 kg in 1 m³ of water at 90°C. Other factors that affect the solubility of gypsum include the solution pH value and pressure. Generally, calcium sulphate scale is more soluble at low pH values and high pressures [38].

The precipitation of calcium sulphate scale has been reported in many publications to occur during operations in different oilfields such as water injection. The chemical incompatibility of two mixing fluids is the main reason for calcium sulphate scale formation. For instance, when injected seawater which is high in sulphate ions is mixed with formation water with characteristic high calcium ions, then calcium sulphate scale would be precipitated whenever its solubility limit is exceeded.

Also, it was observed that the acidizing treatment of limestone/dolomite in Dagan and Kangan formations could result in calcium sulphate formation. This was attributed to a rise in pH value of the solution. At the initial stage, calcium sulphate scale is soluble in life acid solutions, but as the solution's pH level increases, it is re-precipitated. Calcium sulphate or gypsum scaling can be expressed by the Eq. 2.9:



According to [19] cited by [28], cases where water injection (seawater, aquifer, river or produced water) is used for maintenance and sweep, the mixing of brines that are incompatible could lead to sulphate scale formation when the injection water contains sulphate ions.

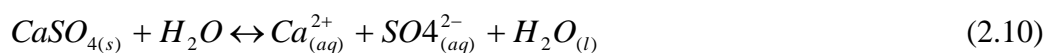
Solubility and precipitation of Calcium Sulphate

The factors that could affect the precipitation of scale include super saturation, temperature, pressure, ionic strength, evaporation, agitation, contact time and *pH*.

- Effect of Temperature and Pressure

The solubility of gypsum increases with temperature up to 40°C and then decreases with temperature. Also, anhydrite is less soluble than gypsum so as a result, anhydrite is the preferred form of calcium sulphate scale in hotter and deeper wells. It is difficult to predict what form of calcium sulphate would be precipitated from solution under a given set of conditions. At temperatures above 40°C, anhydrite will be precipitated ahead of gypsum. This is the case because it has a lower solubility. Gypsum on the other hand may be found at temperatures up to 100°C at temperatures above 100°C, anhydrite would be precipitated directly from solution, but in time gypsum can be dehydrated to form anhydrite [21]

Investigation made by [35] restates that the solubility of calcium sulphate in water increases with pressure. This is because when scale is dissolved in water as shown ionically in Eq. 2.10, a decrease occurs in the total volume of the system.



A drop in pressure could result in calcium scale formation in production wells and near the wellbore, this can create scale deposit both in the formation as well as the piping.

- Effect of Ionic Strength

Calcium sulphate solubility is greatly affected by ions concentration.

2.4.2.3 Barium Sulphate Scale (BaSO₄)

Barium sulphate scale could have various sources and compositions and can also be formed by different factors which include i) Changes in temperature, (ii) Changes in pressure, (iii) Changes in salinity, (iv) Changes in pH, (v) Mixing of two or more waters of different composition. Barium sulphate scale shown in Fig. 2.4, is responsible for problems in oilfields such as, (i) Clogging of valves, flow lines and other surface installations which require expensive cleaning treatment as well as inhibitor injection continuously inside the production completions, (ii) Drop in oil production due to restrictions that are formed in the production tubing, which leads to loss of millions of dollars in production, (iii) Health and safety concerns as a result of radioactive waste disposal.

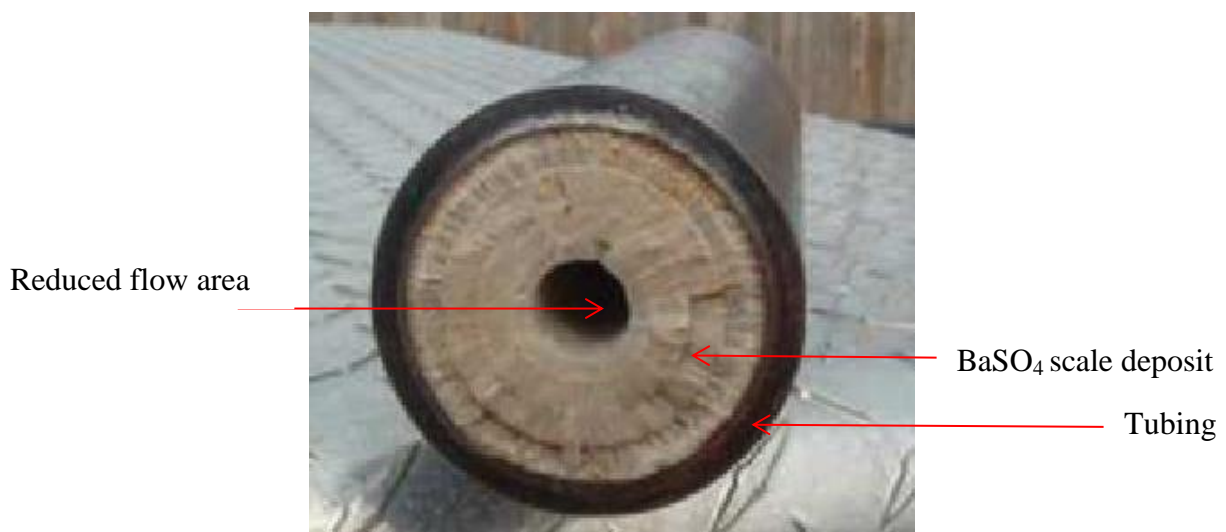


Figure 2.4 Barium sulphate scale inside production tubing [39]

Barium scale is formed mainly because of the mixing of seawater used as injection water, and formation water. Seawater which is frequently used for injection into reservoirs during secondary or enhanced recovery water flooding operations is rich in ions that are by-products of water evaporation and marine life. Typically, seawater is rich in SO₄²⁻ anions having concentrations above 2000mg/L (about 0.02ppg). On the other hand, ground water and water

in near-surface environments are often dilute and different chemically from deep subsurface water associated with gas and oil.

The alteration of sedimentary minerals results in the enrichment of deep subsurface waters with ions. Barium (Ba^{2+}) and strontium (Sr^{2+}) cations are contained in sandstone formations. Barium sulphate scales begin to precipitate when the state of any natural fluid is perturbed until the solubility limit for one or more of the components is exceeded. Barium sulphate formation is based on the Eq. 2.11 indicating the sources of the ionic constituent components:



Barium sulphate solubility increases by a factor of two for temperature ranging between 25 to 100°C and decreases by the same magnitude when temperature is nearly 200°C [40]. Barium sulphate scale is the most insoluble that can be precipitated from oilfield waters. This results in the formation of hard scale which is extremely difficult to remove. At surface conditions, its solubility is less than that of calcium sulphate by a thousand times. It is easy to predict as its precipitation depends on; salt content, temperature or pressure drop. The treatment of barium sulphate scales should focus on prevention mainly through the use of scale-control chemicals as removal by conventional methods is very difficult [28]. Seawater is used often during work overs or formation flooding and it contains a significant amount of barium ions. The mixing of the seawater and formation waters is a common cause of barium sulphate scale formation and represents a risk of subsequent formation and wellbore damage caused by the barium sulphate deposition. The treatment of $BaSO_4$ scale must be focused particularly on prevention by the use of scale-control chemicals. The severity of scaling is determined by the rate of scaling and efficiency of the chemical inhibitors.

2.4.2.5 Strontium Sulphate Scale ($SrSO_4$)

Strontium sulphate scales until very recently appeared in oil fields in the presence of Barium sulphate scale. Several production wells around the world have observed the precipitation of almost pure strontium sulphate scale. It is formed primarily as a result of the comingling of waters, producing water that is supersaturated with $SrSO_4$. Strontium sulphate scale behaves like barium sulphate scale only differing by the fact that barium sulphate is more soluble under the same conditions. They are also often precipitated along with barium sulphate scales. The solubility of strontium sulphate scales play important roles in various disciplines

cutting across many disciplines in science and engineering. An example is the formation of strontium scale in oil and/or geothermal fields as shown in Fig. 2.5, which are accompanied frequently by other sulphate or alkaline earth metals [28].

Investigation conducted for the scale formation attributed to water injection processes [41] as a result of mixing of incompatible water sand thermodynamic conditions. Results showed that at ambient conditions, strontium sulphate scale was formed and verified by the use of software modelling. A study for the formation of barium and strontium sulphate scales at 70°C in a porous media under the influence of flow in static bulk solutions was carried out. The results showed that (Ba, Sr)SO₄ solid-solution scale precipitated in porous media was initiated from heterogeneous nucleation followed by rapid scaling, ion precipitation and crystal growth. Less strontium sulphate scale was precipitated as compared to barium sulphate [42].

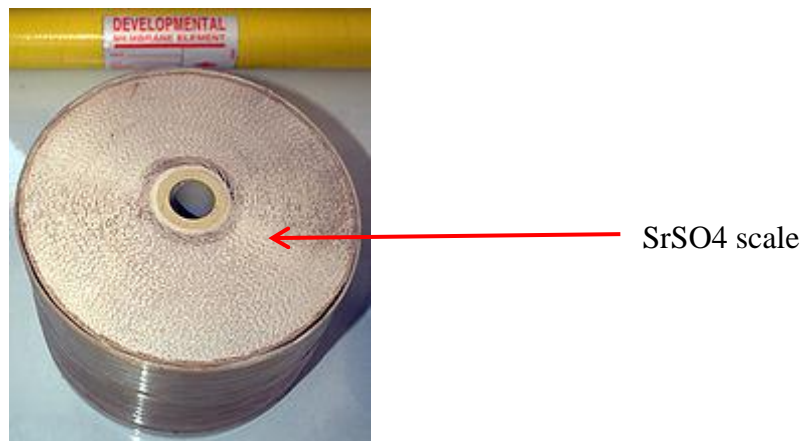


Figure 2.5 Typical SrSO₄ Scale Depositions [43]

Strontium sulphate scale (SrSO₄) is the predominant scale type found in UZ field. It was discovered that Strontium sulphate scale is deposited gradually when the concentration of sea water is between 20 -80% in produced fluid. The saturation index gives an indication of how many times over the solubility level the scale is, and gives an idea of the kinetic driving force behind the deposition especially during removal shown in Fig. 2.6. A value greater than unity one shows that the super-saturation of the mineral in that particular brine and likely to deposit scale. The greater the value, the more rapidly the scale is likely to be deposited [2]. Fluid boundary surfaces that are pre-existing also tend to initiate the growth of crystals.

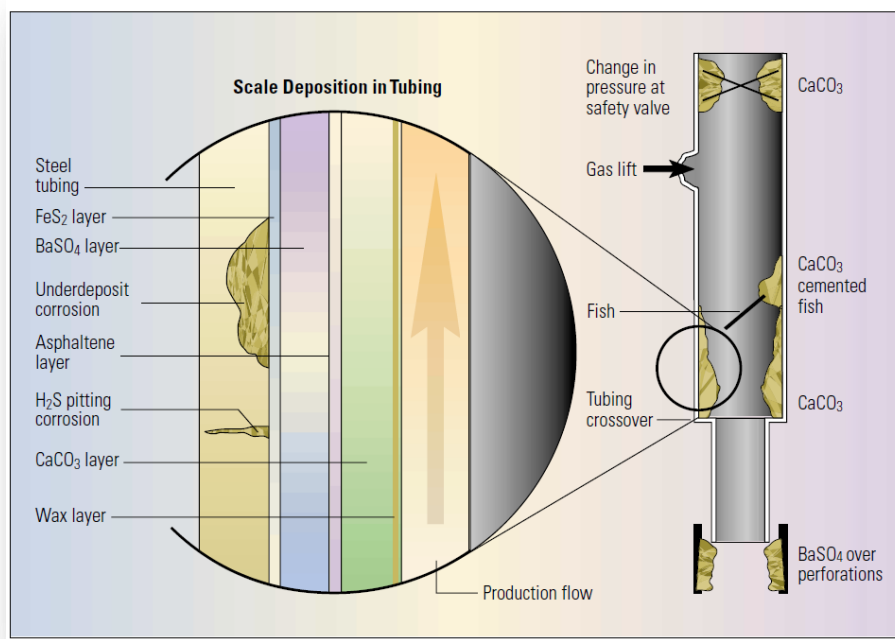


Figure 2.6 Scale in Production Tubing [3]

The work done by [44] cited by [45] reported that scale begins to form when the limit of solubility of one or more of the components has been exceeded. Minerals solubility has been shown to have a dependence on temperature and pressure that is complex. The change in temperature and pressure, outgassing, shift in pH, or the contact of incompatible waters causes the precipitation of minerals. Evidence of the existence of scale can be seen as scale samples or X-ray evidence from core analysis, chemical modelling, as well as wellhead parameter all give an indication of scale accumulation when there is a rapid increase in pressure reading cited by [45].

The most reliable technique for analytically determining the composition of scale deposits is X-ray diffraction and Energy Dispersive Spectroscopy (EDS). These tools are used together to rapidly determine the percentage mineral composition of scale. A thorough chemical analysis apart from revealing the composition of a scale deposit, can also give indications of problems related to scale inhibitor choice [46]. Compatibility tests were carried out by [47] to see two different mechanisms of scale formation, one mechanism as a result of the interaction of different water, and the other because of thermodynamic changes. The test was conducted with mixing waters at different temperatures and ambient pressure, followed by mixing of the

waters at reservoir pressure and temperature. Calcium and Sulphate ions changes were observed and are indicative of the formation of calcium sulphate in all proportions of mixing except their own waters of formation and injection. Although it was observed that scale was formed by the tests conducted, shortcomings of the research include the impossibility of determining the type of calcium sulphate either anhydrite or gypsum formed. Also, changes were observed in the sulphate ions.

2.5 Scale Prevention and Treatment

2.5.1 Wire line operations

Maintaining a consistent production drop along the pipe is the most efficient way of producing oil and gas. Prevention would be the best approach to tackling the issue of scale, and chemical inhibition is the method that is preferred for maintaining well productivity. Thousands of scale inhibitors exist together with dilution for different areas of usage, from domestic boilers to oil production rigs. Majority among ingredients block the enlargement of scale crystals by “poisoning” the scale nuclei growth [11]. Inhibitors are usually evaluated on the basis of performance, thermal stability, calcium tolerance, effect of pH and dissolved iron on inhibition and the availability of an analytical method that is reliable for determining the concentration of an inhibitor. Several test methods maybe necessary in order to accurately determine the suitability of an inhibitor to handle the task at hand.

A field test will most definitely be the best option to check inhibitor suitability. However, the candidate inhibitors must first be subjected to laboratory test. The result of the laboratory test would give an indication of the best inhibitor to be used in the field. The laboratory tests should aim at reproducing as many conditions of the field that are practically possible [48].

2.5.2 Chemical Scale Dissolver

Chemical methods of scale removal are often the cheapest and first approach particularly when the sale is not easily accessible or formed where common mechanical methods of removal would be too expensive or ineffective if deployed. Hydrochloric acid is in most cases the first choice employed in the treatment of calcium carbonate scale and although the acid reaction may hide some of the problems, the spent solutions of acid for scale removal are initiators for the recurrence of scale deposits [2], [45]. Sulphate scale is very difficult to treat

chemically as they have a low solubility in acids. Chemical methods can be used in the treatment of strong chelating agents in the formation matrix; that is compounds that lock up the metallic ions of the scale within their closed ring structure thereby breaking up acid resistant scale.

Chemical treatment methods can be controlled by knowledge of how well the chemicals used can access the scale surface. Therefore, the surface-to-volume ratio or the surface-to-mass ratio is an important parameter in the efficiency of the removal process. For this reason, the deposition of scale in the production tubing shows a small surface area for a large total deposited mass and as a result, chemical systems reactivity is too slow to make chemical treatment a good removal technique [3]. The challenge posed by the use of hydrochloric acid in the treatment of calcium carbonate scale which resulted in the recurrence of scale deposits was remedied by the introduction of chemicals that can chelate calcium carbonate as these had the ability to halt the reprecipitation cycle. Ethylenediaminetetraacetic acid (EDTA) shown in Fig. 2.7, became the favourite candidate to be used for improved methods of chemical removal and is still used today in various forms. Treatment methods using EDTA are more expensive and slower in comparison with hydrochloric acid but are very effective on scale deposits that require chemical removal techniques [11].

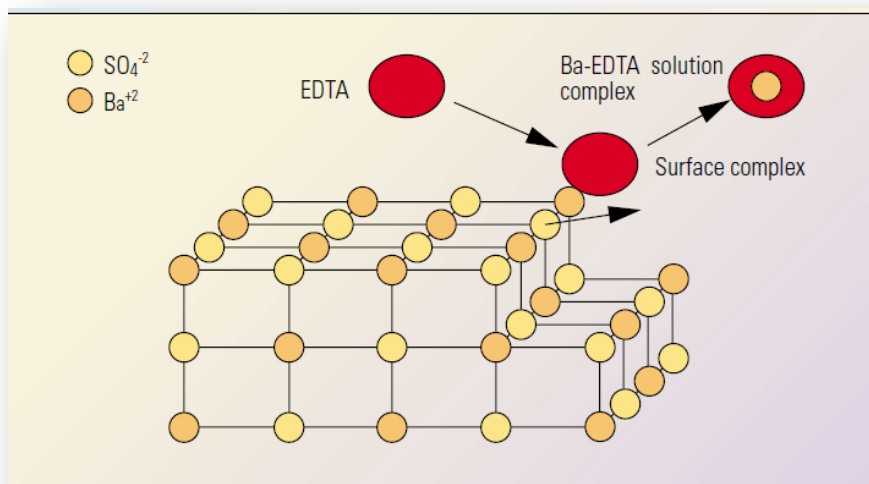


Figure 2.7 EDTA action on scale dissolution [11]

The limiting amount of solute that can be dissolved in a solvent under a given set of physical conditions is referred to as Solubility. Ions present in aqueous solutions are the chemical

species of interest. A combination of these ions could lead to the formation of compounds that have a low solubility. As soon as the solubility of these compounds is exceeded, they are precipitated from the solution in form of solids. If on the other hand, a large amount of solute is maintained in contact with a small amount of solvent, a reverse process which is equally very important is reached due to continuous dissolution. The return of species that have been dissolved to undissolved state is known as precipitation. The rate of dissolution and precipitation is the same, and the composition of dissolved solute in a solvent of known amount is constant with time. This is so because the process is one of dynamic equilibrium and solutions in a state of equilibrium are said to be saturated solutions. The solubility of any solute in a given solvent is referred to as the concentration of a saturated solution.

If a solution contains solute composition that is less than what is required for saturation, it is said to be an unsaturated solution, a solution on the other hand that has its concentration higher than a saturated solution as a result of certain factors such as changes in concentration of other species or temperature etc. is said to be *supersaturated*. An increase in concentration or temperature of a solvent would lead to an increase, decrease or constant solubility depending on the type of system involved. The formation of scale begins when any natural fluids state is disturbed such that the limit of solubility for more than one component is exceeded. There is however a complicated dependence of mineral solubility on temperature and pressure. So typically, a temperature increase would tend to increase the water solubility of a mineral. Greater amounts of ions are dissolved as the temperature and pressure gets higher as shown in Fig. 2.8.

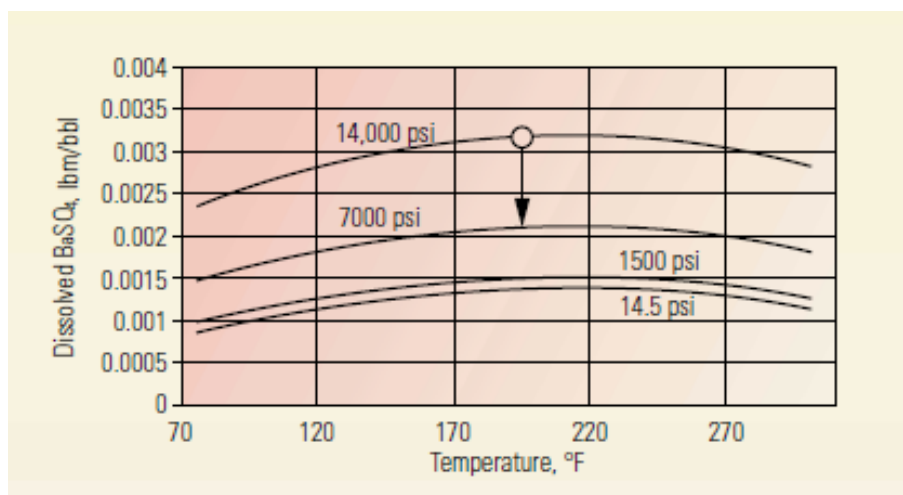


Figure 2.8 Dependency on scale solubility on pressure and temperature[11]

On the other hand, a decrease in pressure would tend to decrease solubility. Also, not all the minerals conform to the typical temperature trend; calcium carbonate for instance shows a trend of increasing solubility in water as temperature decreases shown in Fig. 2.9. Barium sulphate solubility increases by a factor of two for temperature ranges between 25°C and 100°C and decreases by the same magnitude as the temperature approaches 200°C. This trend mainly is influenced due to the brine salinity background [11].

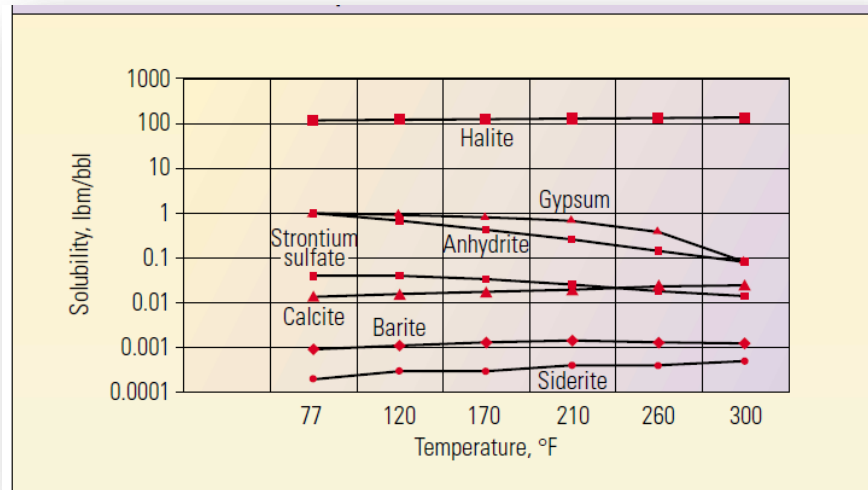


Figure 2.9 Dependency on scale solubility with Temperature [11]

The solubility of carbonate minerals increases as the acidity of the fluids is increased and there is sufficiently supplied acidity from CO_2 and H_2S at high pressure. As a consequence of this, formations waters that are in contact with both carbonate rocks and acid gases could become rich in dissolved carbonate minerals. There is a complex irregular dependency on the composition of brine, pressure and temperature of the gas above the liquid phase. This gas pressure effect is in orders of magnitude greater than the effect that would normally be expected as a result of pressure on solubility of a mineral. In general, a fall in pressure results in CO_2 leaving the water phase thereby causing a pH rise which in turn would result in the formation of calcite scale.

Ions are present in aqueous solution and are made up of different chemical species. A combination of these ions results in the formation of compounds that have various water solubility. The capacity of water to maintain those compounds in solution is limited, and once and once their solubility's are exceeded, then the water becomes supersaturated leading to a

precipitation of the compounds as solids. Solid materials maybe precipitated from solution if either (i) The water contains ions that are capable of scale forming compounds of limited solubility, or (ii) change in physical conditions or water composition occurs and hence lowering the solubility [28].

2.5.3 Mechanical Treatment Methods

There is a wide range of mechanical tools that can be employed in the removal of scale deposits in the wellbore, production tubing and at the sand face. The mechanical methods like the chemical techniques have a limited range of application and so the method selected would depend on the scale deposit and the well. Although the mechanical methods of scale are varied, they are still considered the most successful options in scale removal especially in tubing's [45]. The earliest scale removal technique involved the use of explosive outgrowth to rattle the pipes and break off any brittle scale. The downside to the use of explosives was that although they provided great energy impact that helped to remove scale, they damaged the tubing and cement in the process. Scales formed in the tubing are usually very thick and too strong for the safe use of explosives for removal and have very low porosity and hence chemical treatment would be ineffective in a reasonable time frame. Therefore for deposits such as these removal techniques to be employed are those for drilling rock and milling steel. This has led to the development of impact bits and milling technology run on coiled tubing inside tubular and these use a range of milling configurations and chipping bits. A hydraulic motor or a hammer-type impact tool supplies the downhole power source. The motors are powered fluids, stator as well as the rotor combinations that turn the bit. Their power is dependent on the fluid supply rate as well as the motor size [11].

Other mechanical methods include the use of abrasive slurries, sterling beads abrasives, scale blasting technique typically shown in Fig. 2.10 etc. [45].

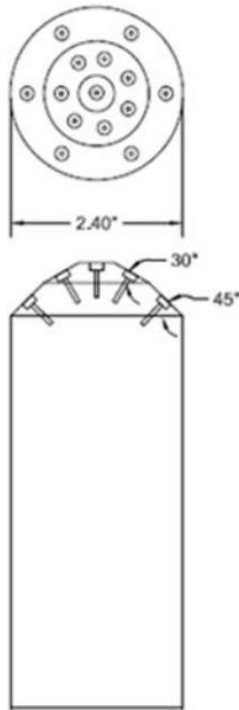


Figure 2.10 Cross section of mechanical atomizers [49]

Oilfield systems require the use of chemicals other than scale inhibitors; therefore scale inhibitors must be compatible with other production chemicals used in the system such as paraffin inhibitors, biocides, corrosion inhibitors and surfactants. The compatibility of scale inhibitors with oilfield chemicals such as corrosion inhibitors, biocides and surfactants is very important. This is because inhibitors are mostly anionic and could react with cationic amine derivatives such as amine fatty acid salts, diamines and quaternary ammonium chlorides [36]. According to [28], a range of good scale inhibitor performance should be efficient at 5-15 ppm in clean water. Another reason for this is that inhibitors are adsorbed onto solid surfaces in water and therefore reduce the amount available for scale formation inhibition.

2.5.4 Jetting Techniques

The chemical nature of mineral scale characterised with strong ionic bonds among the salts ions and the crystal lattices is bound to require an energetic approach to be removed, enabling the mechanical approach to scale removal to have been reported substantial success in its operations [11],[49],[50]. There is a wide range of mechanical tools that can be employed in the removal of scale deposits in the wellbore, production tubing and at the sand face, coupled

with variability in the nature of scale types found in different locations, lead to variability in the selection of different tools suitable for a particular well. The mechanical methods similar to other techniques such as the chemical techniques suffer limitations in the generality of application and hence the method adopted would depend on the scale deposit types, chemical nature and the well itself. Among the earliest techniques involved the use of explosives breaking the scale layers; however, secondary effects including the destruction of the tubing make it a non-viable option. An additional disadvantage of explosives was that although it enable provision of substantial energy upon impact that removes the scale, they damage the tubing and cement in the process. Scales formed in the tubing are usually very thick and too strong for the safe use of explosives for removal and have very low porosity and hence chemical treatment would be ineffective in a reasonable time frame. Therefore for deposits such as these removal techniques to be employed are those for drilling rock and milling steel. This has led to the development of impact bits and milling technology run on coiled tubing inside tubular and these use a range of milling configurations and chipping bits. A hydraulic motor or a hammer-type impact tool supplies the downhole power source. The motors are powered fluids, stator and rotor combinations that turn the bit. Their power is dependent on the fluid supply rate and motor size [11]. Other mechanical methods include the use of abrasive slurries, sterling beads abrasives, scale blasting technique etc. [45].

This method involves applications that employ high pressure jetting technology used together with coiled tubing for removing scale deposits in production tubing. Water is the most convenient fluid used in fluid jetting for scale removal. Water jets have been in use for several decades with patents dating back to the 1940's. However, due to the challenges of high ambient pressure, confined space for operation, submergence and remoteness of the toll from the pump, equipment development for downhole operations has been really slow.

Water jets break down scale deposits by four main mechanisms. However, only three of these mechanisms are necessary in downhole applications as shown in Fig. 2.11. These mechanisms include:

- (a) Erosion: this describes the erosive power possessed by the jet itself. It is a very significant factor even under submerged ambient conditions.
- (b) Abrasion: the action of an abrasive material or solid may be important irrespective of whether they are carried downhole with water or entrained from debris in the wellbore or tubing.

- (c) Stress Cycling: this refers to fine surface cracks that are usually found in downhole scale due to the impingement of water jet, thereby inducing a stress pattern around the jet.
- (d) Cavitation: this is a destructive mechanism on the surface of the scale deposit, but is usually hampered by high ambient pressures downhole.

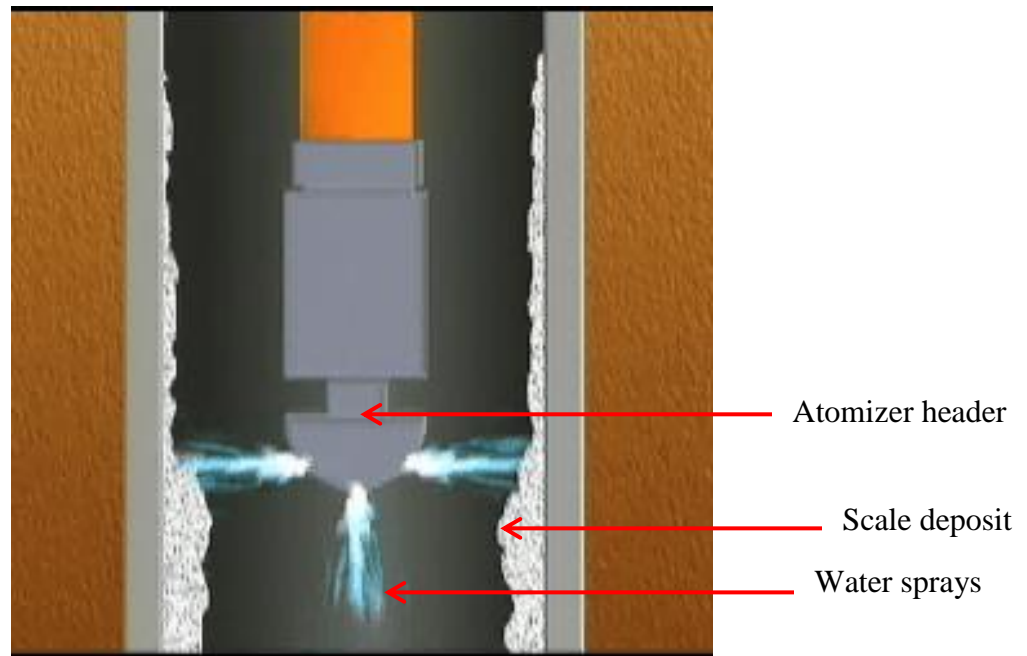


Figure 2.11: Performance of a water jetting tool [51]

Water jetting is effective on soft scale like halite, but it is less effective on medium to hard scale like calcite and barium sulphate. At surface conditions, water jetting removes scale by cavitation. This involves the formation of small bubbles in the fluid jet stream. A large pressure release as the fluid passes through the jet nozzle causes the formation of these bubbles. On impact with the scale, the bubbles collapse causing erosion of the scale deposit. Coats carried out water jetting scale removal process that involved alternating between a jetting tool and a vibrating impact drill to expedite the removal process. It was also stated that utilizing the jetting tool and impact drill for removal achieved scale clean up from 13,000 to 13200 feet and hydrochloric acid was used as a final clean up step. Although they claim that this procedure led to improved production and low cost of work carried out, the use of impact tools would damage the integrity of the tubing, and also hydrochloric acid used could develop corrosion issues and environmental concerns.

The Research done by [10] Stated that a new system of jetting was developed which demonstrated ability to clean the toughest scales from production tubing even up to the full

ID without damaging the wellbore. The system used dissolvers at a rate of penetration that is acceptable by currently used systems. Pure liquid jetting systems were ineffective on the scale where use of acids was inappropriate, and sand abrasive systems could damage the tubing. A careful evaluation of material properties of the scale, substrate tubing steel and abrasive particles led to selectively eroding of brittle scale from the tubing without wearing out the steel.

The system comprised of a suite of jetting tools with abrasives and was supported by a computer software package for the optimization of tool design with respect to head size, nozzle size, flow rates and pressure to maximise the penetration of the tool. The formulation of the jetting fluid was done with *sterling beads* with an aqueous solution of polymer for suspension and cleanout. The tubing was cleaned at a penetration rate of 30 to 60 ft/hr initially and was controlled by setting 1000 to 2000lb_f and allowing it to drill off. Results showed on physical examination of the tubing that no scale deposit was left. There was however a little damage to the plastic coating that lined the production tubing although the steel itself was undamaged. The use of sterling beads as part of the jetting fluid system would result in damage to equipment at the surface like valves and chokes and other downhole equipment as well.

According to [52], a high pressure water spray technique was proposed in the removal of scale using minimum supply of water. The approach was experimental and involved the volume of scale removed test undertaken under atmospheric conditions using a simulated down-hole production tube of an oil and gas well. High pressure water atomisers (greater than 7 MPa) with high impact force (greater than 10 MPa) and a spray size of between 350µm to 2000µm were used. Comparisons were made using one and two atomisers respectively. Results showed that two atomisers used together removed more scale than the one, although increased volume of water used may caused flooding in the well, single atomizer could have been carefully used to ensure precision prior to using multiple atomizers. Indeed, the problem with this approach however is that the test were carried at atmospheric conditions and does not adequately represent real oil/gas well condition, and therefore pressurized system could have potential benefits.

A coiled tubing abrasive jetting technique was described by [50] as employed by Petrobras in one of their oil fields due to the problem of barium sulphate scaling. The method employed a special abrasive material developed by Schlumberger's research centre in conjunction with

jetting technology for hard scale removal. A software package was used for support and helped with selection of tools and process optimization. The actual scale cleanout operation was done by use of the following products;

- i. Xantham Gum gel of concentration 30 lbs/1000gal;
- ii. Abrasive particles of 3% concentration by weight
- iii. Bactericides and anti-foam products used together with the brine to mix the gel.

The rate for cleanout was between 12 and 15 m/h for depth between 2546 and 3087m. The pump rates were between 1.5 and 1.7bpm with a circulation pressure of about 3500- 4000 psi.

Three jetting tools were used each having an operational life of about 12 hours. The treated well showed an increase in oil production of 1025% with a pay-out time for intervention of 19 days, although some of the scale types can build –up within 24 hours to block production to zero[11], other types may take longer times to build-up . While these numbers look impressive, abrasive materials used for jetting would pose a problem to surface equipment like valves and pumps and would cause considerable damage to them. Also, cyclone separators would be impacted and very large ones would be required.

A non-rotating high pressure jetting technique to remove scale from production tubing was employed in the Namorado field wells in Brazil. There was no positive outcome obtained for this method because of the hardness of Barium sulphate scale encountered in the oil wells. An abrasive jetting system was then employed to clean the tubing. It was reported that scale removal was successful, although a few problems were observed. Finally, a two-step treatment using a Positive Displacement Motors (PDM) and a bit for removing the scale mechanically was followed by treatment using a Pulse-rotating jetting tool.

The process involved three stages;

- i. A dummy run with wireline equipment for pre-,
- ii. Running a downhole motor and mill in hole, and
- iii. Running a pulse-rotating jetting tool with a “drifting scrapper” in hole.

During the downhole motor job, brine was pumped at low rates continually until the scale was tagged, and to help carry the barium sulphate scale deposits to the surface, viscous pills of Xantham gum were used comingled with nitrogen and also with gas lift.

It was reported that the well was revitalized with production up to former levels[40]. Both methods used have drawbacks with the abrasive jetting system leaving scale sediments and

abrasive agents that caused damage to separation processes. The second approach raises environmental concerns which have to do with the treatment of the Xantham fluid gum that was employed to carry barium sulphate scale particles to the surface.

Abrasive jetting has been touted by many as the solution to scale removal problems. A tool has been developed by a service company that does not use sand or normal fluid such as water. It employs specialized particles that are less effective than sand, but more effective than fluids such as water. The tool has been optimized such that it removes scale up to a certain radius in a well without damage to the tubing. This tool is configured such that it can also be employed as fluid jet. It has been effective in several different wells where it has been used[53].The limitation of this tool is that it poses a significant challenge in downhole applications as it could cause accidental damage to downhole equipment

Recent PhD research conducted by [26] considers the use of overlapping flat fan sprays for descaling operations, which provided an increased energy of impact required for the descaling of the scale samples, however, considerations in this study intend to minimize the water volume getting into the oil well by adopting single flat fan nozzle, indeed, an improved technique of subjecting the scale surface with an additional impact using aeration was adopted. Details of the impact explored due to aeration are discussed in Section 3.6.

2.6 Summary

The chapter consider the concepts and mechanism of scale formation across oil production tubing which causes production losses and the efforts applied to removal scale in oil and gas productions as follows:

- The mineral and other hydrocarbon scale deposits have been regarded as the most difficult oil production problems encountered.
- Among the types of scale in the oil industry, Barium Sulphate and Iron sulphide are among the hardest type.
- While chemical methods were discouraged for removing scales, high pressure spray jetting has continued to gain wider acceptance.
- Different type of oilfield may suffer different scale types, with a various chemical characteristics leading to possible different approach to removal.

Chapter 3

Spray Jet Break-Up, Cavitation and Erosion

3.1 Spray Jet Break up

This chapter introduces the concept of High pressure liquid spray break-up, characterisation, cavitation, impact as well as erosion especially as it attracted applications in cleaning industrial materials, cutting as well as coating upon targets surfaces. Particular emphasis is provided to High pressure nozzles such as Flat fan, considering its suitability in cleaning oil production scales as chosen in this investigation based on the performance characterisation shown in characterisation(Section 5.1,5.2. and 5.3) and successful applications in other descaling purposes across metal industry [54].The concept of spray as a process of dispersing a high momentum liquid to droplets has been an interesting research area with wide applications in process industries such as chemical, mechanical, aerospace, medicine, agriculture, metallurgy [55],[56],[57],[58]–[64]. However, complex dynamic nature of spray systems arises from variability with operating conditions, atomizer type and ambient conditions [13], which made it necessary to understand how each spray types are developed. Spray research has been improving since 19th century, when Lord Rayleigh investigated an infinite liquid column while exhibit break up, his findings indicated surface tension force to be the main cause of the instability [65]. Indeed, he also verified the size of the droplet being twice the diameter of the jet for a liquid column break up at low velocities arising from destructive symmetric disturbance.

Among the various experimental works conducted, emphasis was given to planar liquid jets for their simplistic behaviour [66] indicated in Fig.3.1. These sheets are used widely for purposes related to impact of the impinging sheet on the solid surface. A common practice has been the use of fan nozzle such that the spray properties are dictated mounted orifice [67]. While studying a fan-spray nozzle, a network of unconnected threads formed, this was caused by perforation in the sheets [68].

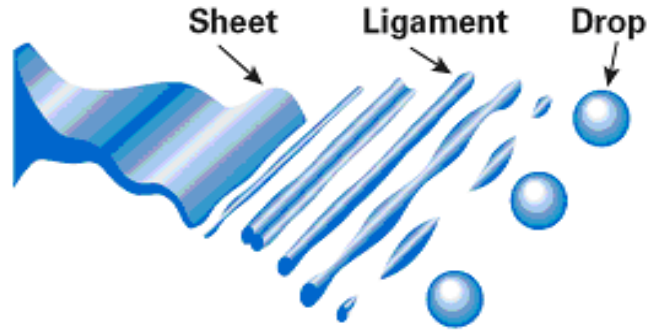


Figure 3.1 Sheet disintegration break up proposed by [66]

While several properties of spray jet do exist, the initial concern has been the break up length, which has been defined as the distance from the nozzle exit to point of disintegration of the continuous part of the liquid jet [69]. This region signifies the primary break-up. However, the generated droplets undergoes break-up as it passes through a surrounding air, due to relative velocity effect between the liquid and the surrounding air, a non-uniform pressure gradient become more experienced by the droplets and subsequent deformation is established which leads to further break-up. Although dimensionless numbers such as Weber numbers are used to characterise the momentum of the jet as it exit the nozzle shown in Eq. 3.1, low Weber number characterise low flow rate, which the emerging jet has insufficient momentum to form continuous jet while it passes through an ambient air surrounding, leading to form dripping shapes are formed [70], which increase in flow rate beyond a certain value enable the formation of the continuous jet.

$$We_a = \frac{\rho_a U_{rel}^2 d}{\sigma} \quad (3.1)$$

The interaction between aerodynamic, gravitational, capillary and inertial forces results in generating a disturbance, which consequently cause the break-up shown in Fig. 3.2. However, movement of the spray further ahead, results in the formation of secondary break-up, due to substantial interplay between the forces mentioned earlier. Each of the break-up region is known to controlled certain spray characterisation, as primary break-up determines the length of the liquid jet approaching or hitting a target, or in combustion process determines the amount of liquid impacting on the piston, as consequently affecting the combustion efficiency; secondary break-up determines the population and size of droplets formed, which in-turn measure the quality of the atomization and evaporation in fuel engines.

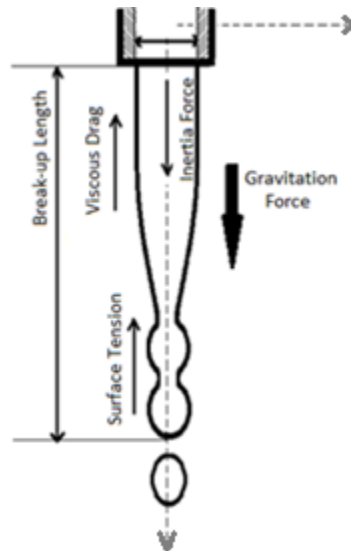


Figure 3.2 Forces acting along spray jet [70]

Several research works verify reduction in break-up length with increasing injection velocities until a constant value is reached. Other findings indicated a range of 20-30mm diesel spray break-up at inlet pressure of 20MPa [71]. Although some authors confirm the break-up length depends inversely on the ambient pressure, but still believe more to depend complicatedly on injection pressure, break-up processes and momentum changes contribute non-linearly to the break-up length as shown in Fig. 3.3

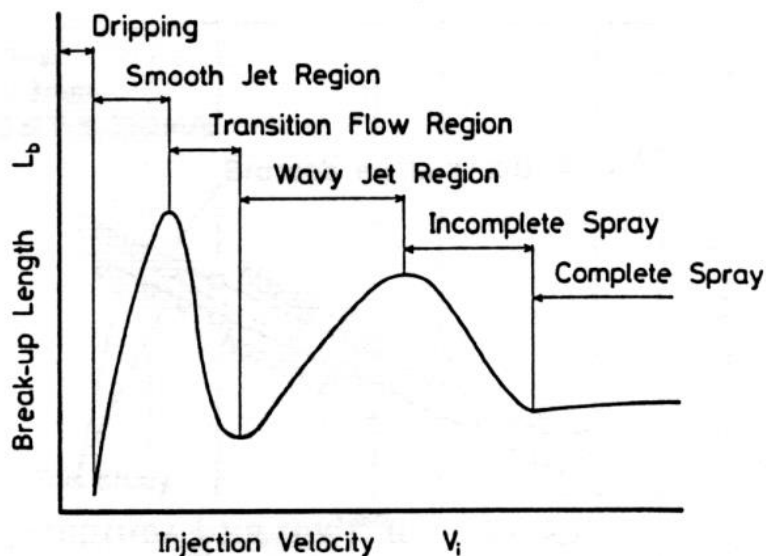


Figure 3.3 Break-up length behaviour of liquid jet [71]

The two phases of atomization are shown in Fig. 3.4, with the each region characterised by varying aerodynamic interplay of forces.

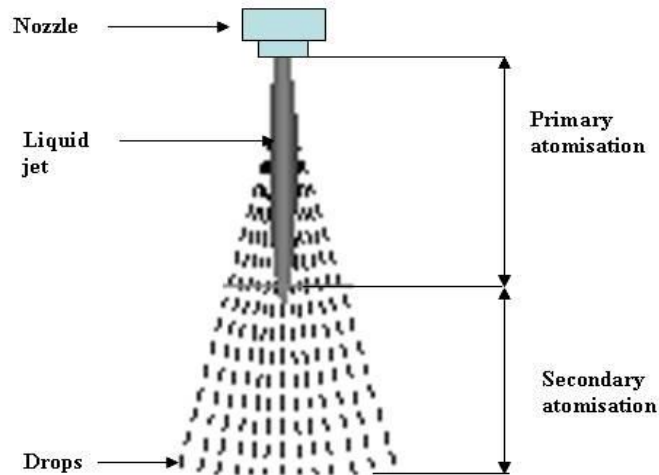


Figure 3.4 Liquid atomisation mechanisms [72]

The main objective of atomisation is often to produce small droplets, a definition of “good atomisation” has been considered. Dombrowski and Munda [75] described the condition for good atomisation as the “most effective way of utilizing the energy imparted to the liquid has a large specific surface before it commences to break down into drops. By careful atomiser design a coherent jet of water can be produced that has sufficient force and with a small enough footprint to ensure high impact pressure at the surface of the tank wall.

3.1.1 Primary Spray break-up

Whenever liquid leaves nozzle exit, a sudden appearance of smooth jet is observed, as the liquid moves further away, a gradual disturbance in the jet is noticed, which increases downstream until the amplitude of the disturbance equals the jet radius, at which droplets begin to pinch off from the liquid jet [70], therefore, primary break-up was considered to be as a results of the instability experienced by the jet surface, leading to the pinch off of the droplets [76], indeed, turbulent oscillations of the liquid and hydrodynamic cavitation within the nozzle has been identified as the controlling mechanism [71]. The mechanism of break up is certainly unknown at higher velocity. The jet break up at a short distance from the discharge is a chaotic behaviour and the result is a conical spray with a wide range of droplet size, and an average droplet diameter much smaller than the jet diameter. The atomisation regime is usually divided in two stages, a primary atomisation which occur near the atomiser

exit, and a secondary atomisation which occurs further downstream and reduces the droplets size. The factors affecting the primary atomisation are: inertial effect, turbulence, changes in velocity profile, surface tension, and cavitation.

3.1.2 Secondary Spray break-up

Continuous movement of the detached droplets from the liquid sheet across the surrounding air undergoes further break-up to smaller droplets, a process known as Secondary break-up or droplet break-up. A droplet generated from the primary atomisation may be unstable and break into smaller droplets depending on the competition at the surface, between external aerodynamic forces, and internal forces due to surface tension and viscosity. The distribution of the force over the droplet varies with time as the droplet shape changes. So if either the internal and external forces are in equilibrium, or the external forces can be compensated by droplet shape change, the droplet remains stable. However if the external forces are larger, the droplet deforms up to break in small droplets. The size where the droplet is stable, is known as critical droplet size, the break up time of any droplet larger than the critical size, increase with decreasing the droplet size. For the factors affecting the secondary atomisation instead, additionally to all the previous factors, the aerodynamic interaction plays a major influence factor.

Despite the rich literature experimental and theoretical validations performed, its detailed mechanism remain unclear, consequently, qualitative description of the behaviour of drop break-up process still have disconnections and uncertainties. The non-uniform pressure and shear stress on the surfaces of the droplets caused by the relative motion of the droplet across the surrounding air, causing deformation, which when overcomes the surface tension leads to disintegration of the droplets, which the newly formed droplets sometimes undergo further break-up until the droplet diameter formed has acquire the minimum required surface tension to overcome the external forces. Although, break-up behaviour is known to be complex and depend on injection velocities, turbulence and cavitation effects. However, it is believed that aerodynamic stripping of the smaller droplets from the heavier droplets as proposed by *Kelvin-Helmholtz instability* or better on the disintegration of heavier droplets to finer ones due to the effects of normal stress as proposed *Rayleigh-Taylor instability*. Various dimensionless numbers generated can be used to relate the various forces of interplay as mentioned in Section 3.1. Findings made it further clear that region of break-up undergoes

transition based on the dimensionless groups for the surrounding air the *Ohnesorge number* Oh , their mathematical expressions can be written in Eq. 3.2:

$$Oh = \frac{\mu_l}{\sqrt{\rho_a d \sigma}} \quad (3.2)$$

With ρ_a as the density of the air surrounding the spray, U_{rel} as the relative velocity between the liquid droplets and the surrounding air, d , the droplet diameter, σ surface tension, and μ_l the liquid molecular viscosity. Several studies have shown the dependence of upstream conditions, nozzle geometry and fluid type to determine the break up as well as cavitation possibilities.

3.2 Spray Droplet Break up Models

Describing the pattern and manner spray break-up generates droplets after exiting the nozzle in both the primary and the secondary region requires fundamental models to ascertain the complex behaviour of the fluid interaction and energy changes. Although a Computational Fluid Dynamics (CFD) has been used to model the complex behaviour using the *Lagrangian* approach. Analysis of the atomisation may involve one or both of the WAVE model approach, Stochastic and Taylor Analogy Break-up (TAB) models which have been incorporated in the CFD code with their boundaries and region of interaction clearly defined as below.

3.2.1 The Classic WAVE model

The sudden instability experienced by liquid jet which passed through a nozzle, and subsequent disintegration of the liquid sheets at low and high Weber Number, has been of great relevance in atomisation applications, which includes coating, drug delivery, electronic cooling, emission control, cleaning [52] Liquid jet break up downstream of an orifice leading to interrupted flow characterise various interacting forces and patterns, which research has continue to follow to the unending journey as its dynamics is still requires more efforts to unveil. Research has shown aerodynamic instability as the major cause of break up, while a mathematical model developed by Kelvin Helmholtz indicated the generated waves which break sheets into ligaments and subsequent varicose forces results the formation of droplets [77].

Recent efforts to use high pressure spray jet for the removal of scales in the oil and gas industry necessitate the characterization of the velocity profile around the spray nozzle, with a view of finding the optimum conditions necessary for the spray impact to overcome the scale in the reservoir tubing. The velocity droplet distribution just around the spray nozzle has suffered a serious limitation in standard measurement methods, varying from a decreased Signal-to-Noise Ratio (SNR) using Particle Image Velocimetry (PIV) as well as lower validation rate when using Phase Doppler Anemometry(PDA) as a consequence of high density liquid ligament characterised with big non-spherical molecules [78]. However, the general quality of a flashing spray are estimated based on droplet size distribution, jet spray angle, velocity distribution and length of penetration either for atmospheric flashing or partial vacuum conditions. Efforts were then made to develop an efficient correlations for the flashing liquid jet at the high density region near the nozzle.

3.2.2 Spray Characterisations

The atomisation process is when a volume of liquid is breaking up into multiplicity of small drops. This process is one in which a liquid jet or sheet is disintegrated by the kinetic energy of the liquid itself, or by exposure to high-velocity air or gas, or as a result of mechanical energy of atomization results in a wide spectrum of drop sizes.

There are many ways to produce spray. In order to minimize drop size, most of these essentially need a high relative velocity between the liquid and the surrounding gas as possible [74]. In order to accurately assess and understand drop size data, all the key variables such as atomiser type, pressure, capacity, liquid properties and spray angle have to be taken into consideration. Atomisers can be broadly classified according to their geometry and applications. The following are the types of atomiser and their application in industry. Fig. 3.5 shows the general classification of atomizers according to the method of utilising input energy for atomization [79],[80].

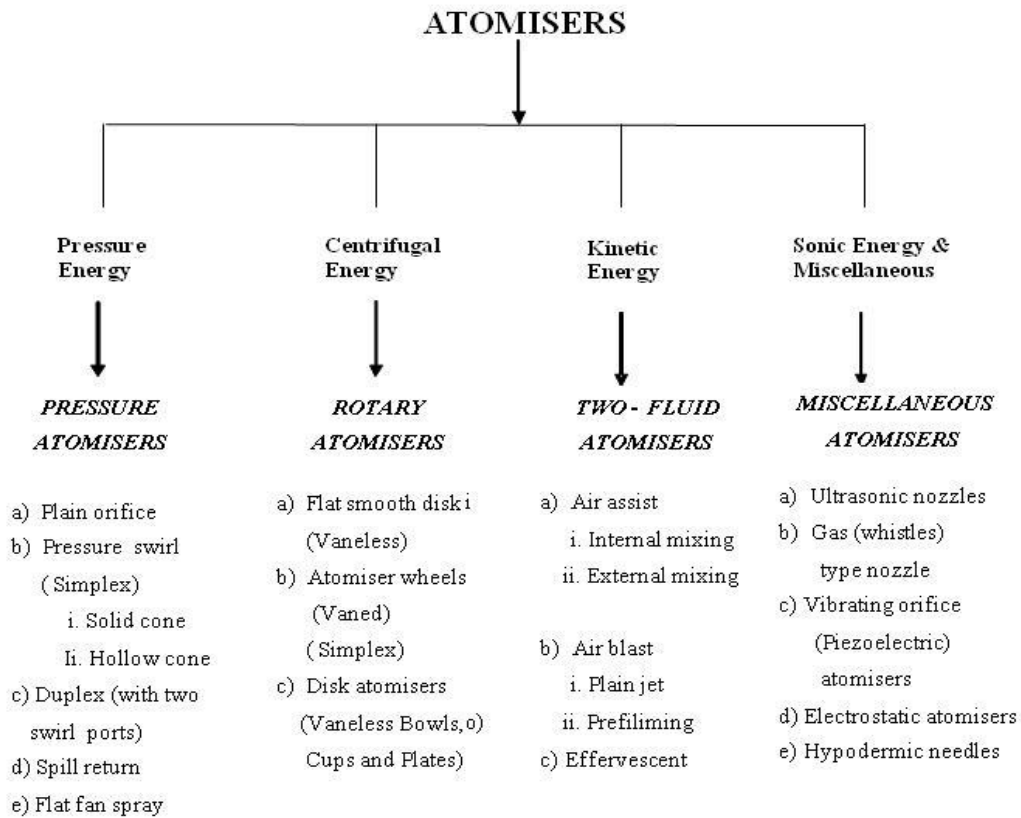


Figure 3.5 Classification of atomisers [79],[80]

3.2.2.1 Pressure Jet Atomiser

The pressure jet atomizer uses a simple orifice and is used more commonly in fuel injection applications, particularly in diesel engine. Its small orifice (usually less than 0.3mm) and high pressure (usually greater than 100MPa) are needed to produce a fine spray ($D_{32} < 200\mu\text{m}$).

3.2.2.2 Pressure Swirl Atomiser

Pressure swirl atomizers have been widely utilised in gas turbine engines, furnaces, agricultural related sprays, and petrol direct injection automotive engines. Works also done by [75] and others have speculated that the drop sizes may be correlated with the wavelengths that grow on the surface of the sheet. To analyse this kind of atomiser, combination of theoretical and empirical information is required to provide approximate equations for discharge coefficient and spray angle [82].

3.2.2.3 Solid and Hollow Cone Pressure Atomiser

These type of atomisers are less used than the others, but it is employed when a wide spray with high impact and uniform coverage (typically between 30° and 100° total angle). Usually a thin exit sheet at the swirl atomiser exit does not occur; the drop sizes are always more than for a hollow cone swirl atomiser of the same capacity [83].

3.2.2.4 Impact-Type Pressure Atomiser

These form another category of pressure atomiser, and also exhibit a wide range of designs. Generally the liquid is impacted upon a shaped surface as it's emerges from an orifice and a flat spray pattern is produced. These atomisers are likely to be used when a flat spray pattern is required. However, the orifice size must be relatively large, to minimise the chance of blockage. These types of atomisers are used in safety systems where a spray must reliably operate, e.g. for cooling or removal of gases[64].

3.2.3 Spray Pattern

Usually a minimum pressure of about 0.07 MPa is required to generate a well-developed spray but this pressure needs to be increased where there is a restrictive passage ways through the atomiser [83]. There are basically a number of different types of spray patterns that can be achieved in a variety of ways as mentioned earlier. Which are:

- Full Cone;
- Flat Jet spray; and
- Hollow cone.

3.2.3.1 Full Cone Pattern

Typical applications of full cone sprays includes spray cooling such as continuous casting, gas conditioning and scrubbing, process cooling etc. Due to variability in the number of process requirements, full cone atomisers have emerged into a range of specialised types, where full pattern similar to a full cone, is obtained via different techniques as shown in Fig. 3.6.

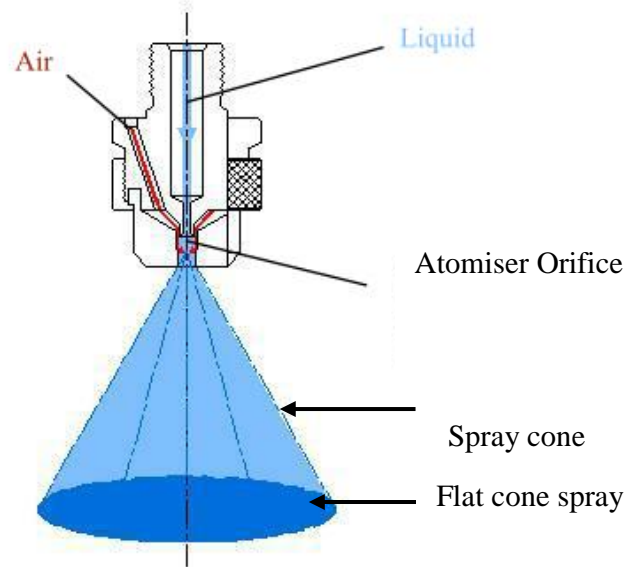


Figure 3.6 Full Cone Pattern [84]

3.2.3.2 Spill Return Atomiser

These atomisers use a special shaped vane placed at the atomiser inlet, this imparts a rotational action to liquid through the atomiser. By virtue of this rotational movement, water exiting the atomiser orifice appears in the shape of full cone. The cone angle is dependent of both the exit speed and the internal design of the atomiser. This varies from 15° to 120° , as shown in Fig. 3.7 for a spill return [85]. Standard Full Cone atomisers can also be produced as square full cone atomisers, where the square shape of the spray with a pyramidal form is designed by a special outlet orifice.

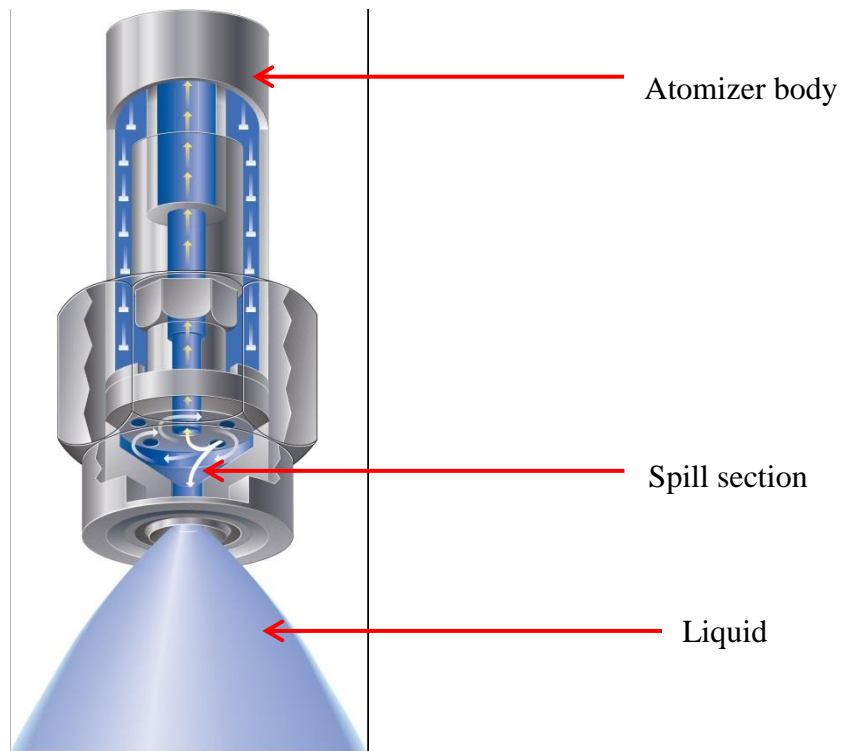


Figure 3.7 Spill Return [85]

3.2.3.3 Hollow Cone (Atomiser)

Hollow type cone spray atomisers produce atomized liquid flow, with a spray patterns characterised by a ring-shaped, the impact area where liquid is occupied on the outer edge of the spray patternation. Two designs of hollow cone atomiser are available: axial and tangential. Fig.3.7 shows a hollow Cone Atomiser spray.

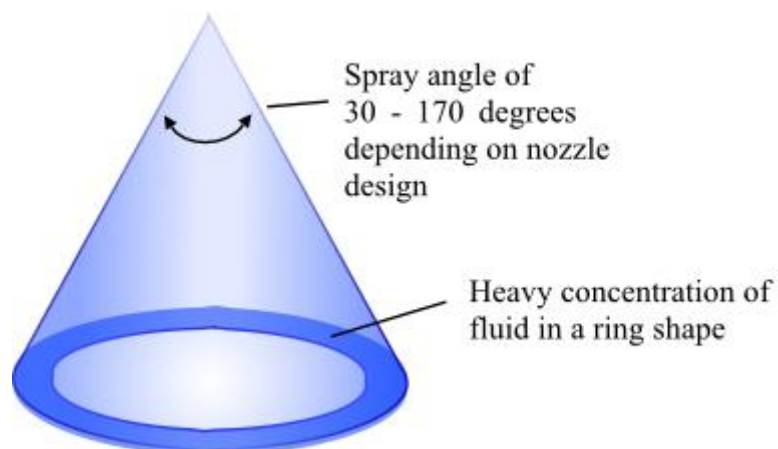


Figure 3.8 Hollow Cone Atomiser spray [86]

3.2.3.4 Flat Fan (Atomiser)

A well-chosen de-scaling atomiser is an indispensable component of the spray system and makes it possible to apply the water in a well-defined shape; and with a high velocity on the surface of the scale deposit in the oil well production tubing in order to remove the scale. It is the flat fan atomiser that is being considered in this thesis. This atomiser, manufactured by Lechler [54] is one of the companies that specialises in Spray Technology for industrial applications. Several technical properties have to be taken into account for producing and selecting an atomiser. A flat fan spray atomiser has technical features such as sharply defined and linear spray pattern. Lecher flat fan atomisers produce a liquid distribution and provide a consistent, uniform coverage over the impact area, as shown in Fig. 3.9

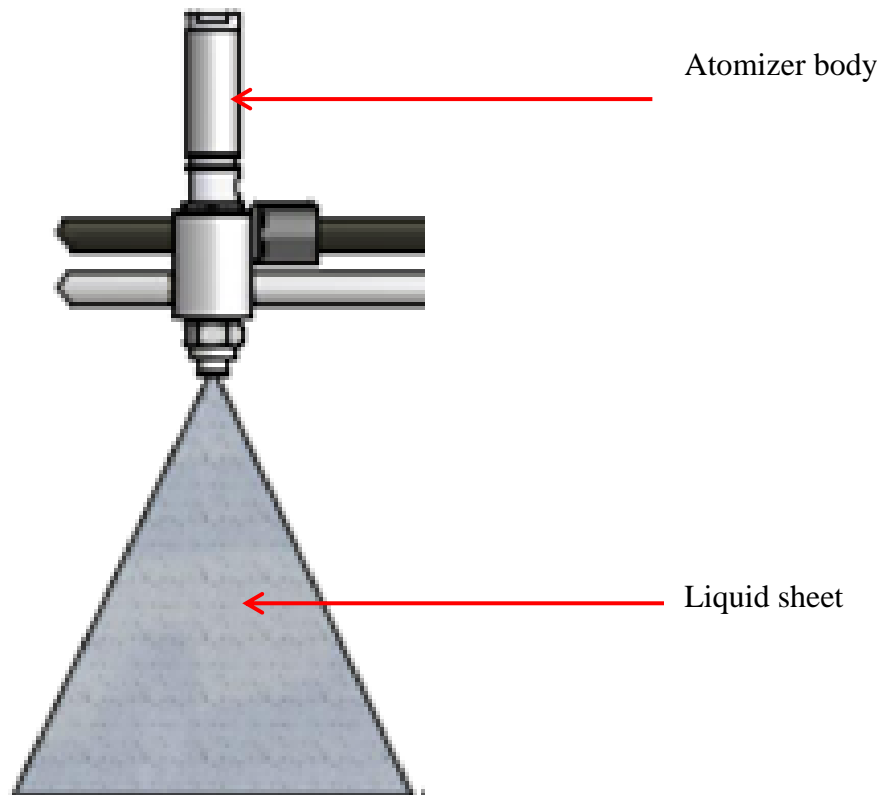


Figure 3.9 Flat Spray Pattern [87]

Fig. 3.10 shows the flat spray atomiser used in this investigation, which was produced by Lechler, enable to deliver high impact even at low flow rate as shown in Appendix E.

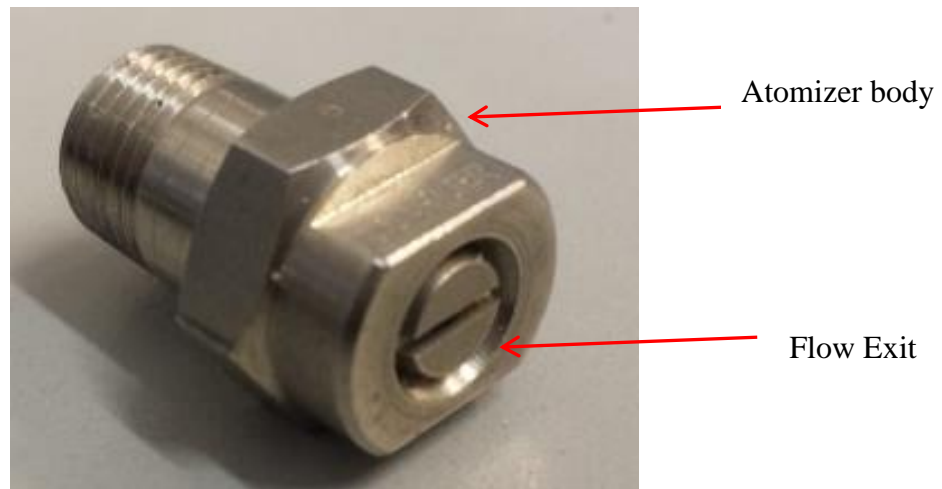


Figure 3.10 Flat Spray Atomiser

This design produces a uniform spray and impact distribution across the entire pattern width. According to Lechler [13] for flat fan spray atomiser to give a consistent and uniform coverage, for a given spray width, the overlapping of the sprays could be around 1/3 or 1/4 of the width of the spray. This is to avoid interference of the spray, particularly when the atomiser orifice offset by 5° to 15° to the pipe axis. The proper selection of spray parameters allows the de-scaling process to be optimized, to achieve improved scale removal at lower energy cost. This has turned hydraulic scale removal from being a simple question of high pressure to a developing science.

3.2.3.5 Rotary Atomiser

Rotary atomiser uses centrifugal force applied to the liquid in order to fling a thin film from a rotating cup, disk or “Bell”. The fundamentals of the technique are well known [83] and the technique has two major potential advantages : (a) the possibility of producing very narrow droplet size distributions, and (b) the additional flexibility of the use of mechanical forces to pre-film the liquid rather than rely on small orifices. Advantage (a) occurs for relatively low flow rates because it requires the atomiser to operate in the direct droplet or ligament regimes of break-up at the rim of the cup or disk. At higher flow rates a continuous sheet forms at the rim and the size distribution width is similar to that for pressure jet atomisation. However, this high through put mode of operation can be combined with an annular air jet at right angles to the sheet to give a pre-filming atomiser known as a pre-filming, air-blast rotary fine cup. Generally, an increase in rotational speed and decrease in liquid flow rate improves atomisation quality. New development have made it possible to handle flow rates up to

40kg/s at high wheel periphery speed that yield very fine atomisation (SMD below 20 microns).

3.2.3.6 Ultrasonic Atomiser

Ultrasonic atomiser is less common when compared with the aforementioned techniques but it is particularly suited to producing low flow rate (<0.2 l/min) sprays with very low kinetic energy and relatively narrow size distributions. The size distribution width is typically between that of a rotary atomiser in the direct drop regime, and a pressure swirl atomiser.

3.2.3.7 Electrostatic Atomisation

This is another niche market technique. True electrostatic atomisers inject charge into the liquid sheets such that the charge at the surface sheet of liquid acts against forces of surface tension and hence causes break-up. This is rarely used in practical devices but it is used actively, being explored in many application areas including liquid atomisation. The last two of these advantages apply to what are often referred to as electrostatic atomisers, but which atomize by a discharge or direct injection of charge.

3.2.4 Spray Characterisations

Sprays can be classified as: narrow angle (angle less than 30°), medium angle (angle between 30° and 70°), and wide angle (greater than 70°). Patterning is referred to as the shape of the spray boundary and the distribution droplets inside the boundary. Depending on the distribution max flux (controlled by the atomiser orifice), it can be: hollow cone, full cone spray or flat cone spray. The aforementioned terms can be defined as:

- **Dispersion:** the degree of dispersion can be defined as the ratio of the volume of the spray to the actual volume of the liquid contained within the spray.
- **Penetration:** The penetration can be defined as the maximum distance downstream of the atomiser to the tip of the atomiser. [88].
- **Patterning:** is a measure of volume per unit area covered by the liquid both radially and circumferentially to determine the distribution of liquid within a

spray and also refer to the shape of the sprays boundary and the distribution of droplets inside the boundary.

- **Spray angle:** The cone angle is considered as the angle formed by two straight lines originated from the discharge orifice.

3.2.4.1 Drop Size

Drop size refers to the actual size of the particular drops that comprise an atomiser's spray pattern. The importance of drop size and its applications in spray systems have increased considerably over the years. Each spray pattern provides a range of drop sizes and this range is known as the drop size distribution. Factors that affect drop size are liquid properties, atomiser capacity, spray pressure and spray angle.

3.2.4.2 Drop Size Distribution (DSD)

An important element when selecting an atomiser for a specific application is drop size. Drop size distribution is an important and valuable parameter of the atomisation process in addition to droplet mean diameter. It may have a particular shape for example, (narrow, wide, few large drops or few small drops) for best possible operations. Fig. 3.11, in which $\Delta D = 5\mu\text{m}$.

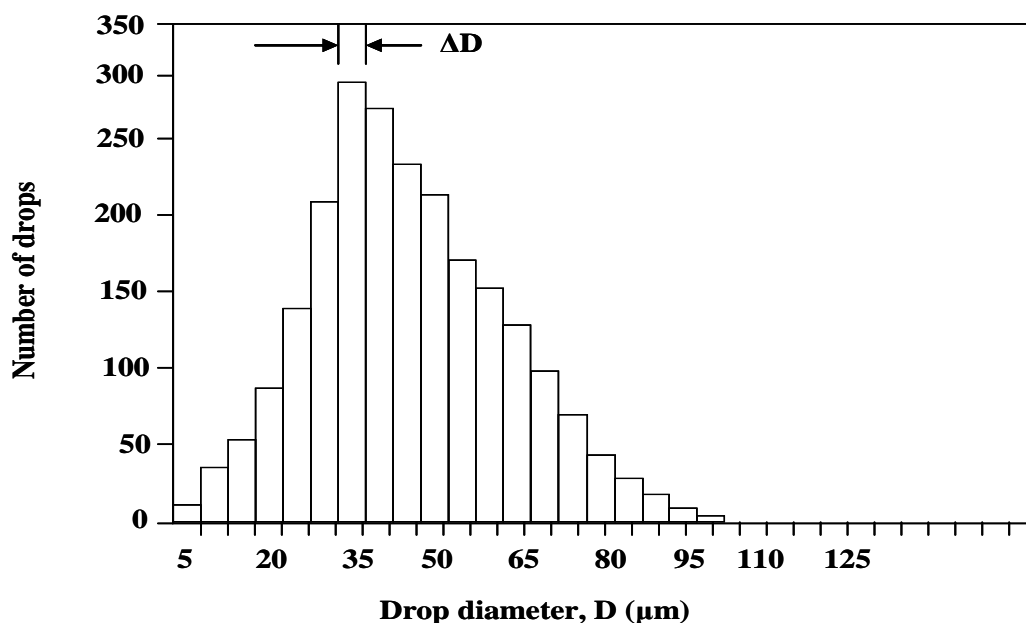


Figure 3.11 Typical drop size distribution[83]

If the spray volume corresponding a given range of drop size mostly between $(D-\Delta D)/2$ and $(D+\Delta D)/2$, is plotted as a function of drop size, as shown in Fig. 3.12, the resulting distribution is skewed to the right due to the larger drops weighing effect.

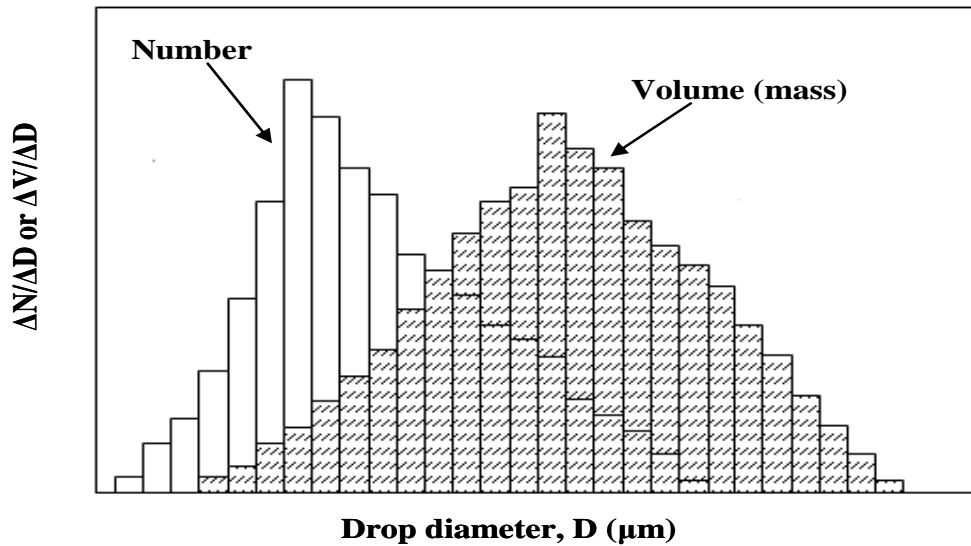


Figure 3.12 Drop size bars based on number and volume [74]

By making (ΔD) , a continuous size distribution (number as well as volume) curve, usually referred to as frequency distribution curve for the spray, can be obtained. A typical of such distribution is shown in Fig. 3.13 and 3.14.

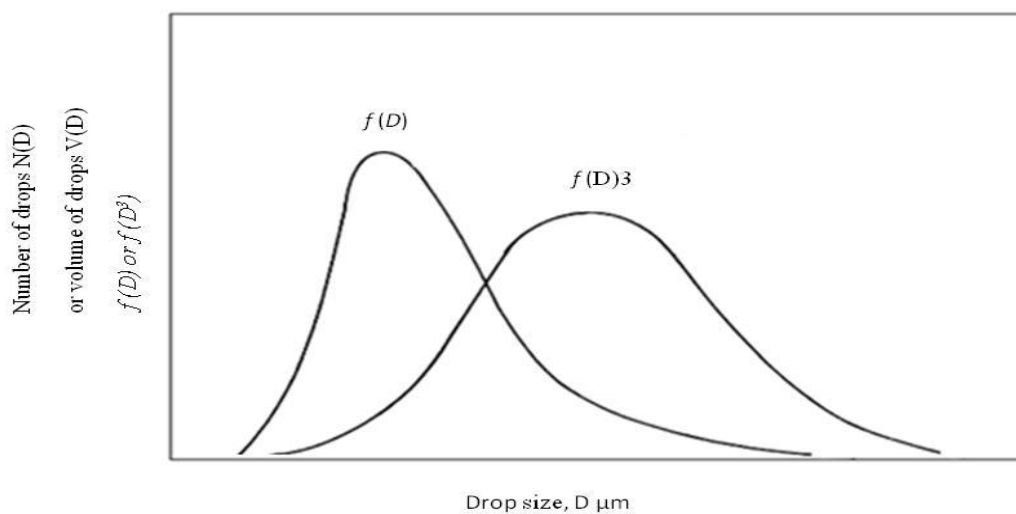


Figure 3.13 Typical drop size frequency distribution curves (number and volume)

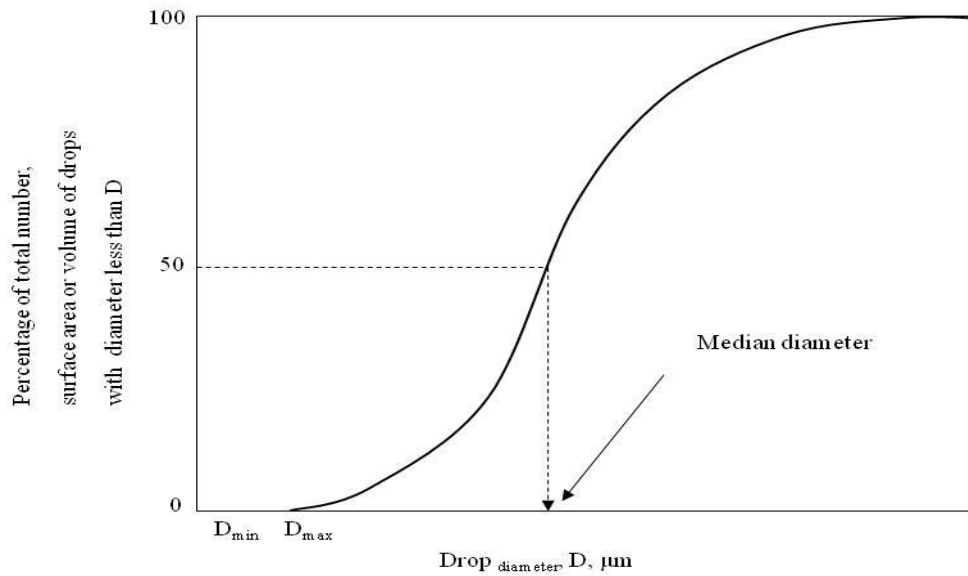


Figure 3.14 Typical shape of cumulative drop size

3.2.4.3 Characterisation of Droplet Sizes

A mean diameter can be used to describe the quality of spray by representing the original set with uniform drops. The way that the mean drop size is calculated depends upon the application for which the data is being used. Table 3.1 indicate the manner in which the mean diameters are defined from the measured droplets sizes, where (N) is the number of drops in size class (i) and (D_i) is the middle diameter of size class parameters such as Sauter mean diameter (D_{32}) should only be used when there is a clear reason for so doing for example when vaporization rate of the spray is of interest [74]. In this study the Sauter Mean Diameter was used.

Table 3.1 Mean diameter and their applications[83]

a	b	Name of mean diameter	Symbol	Expression	Application
1	0	Length or arithmetic diameter (AMD)	d_{10}	$\frac{\sum N_i d_i}{\sum N_i}$	Comparisons
2	0	Surface area	d_{20}^2	$\left(\frac{\sum N_i d_i^2}{\sum N_i} \right)^{\frac{1}{2}}$	Surface area controlling
3	0	Volume	d_{30}^3	$\left(\frac{\sum N_i d_i^3}{\sum N_i} \right)^{\frac{1}{3}}$	Volume controlling
2	1	Surface area-length	d_{21}	$\frac{\sum N_i d_i^2}{\sum N_i d_i}$	Absorption
3	1	Volume-length	d_{31}^2	$\left(\frac{\sum N_i d_i^3}{\sum N_i d_i} \right)^{\frac{1}{2}}$	Evaporation
3	2	Sauter Mean Diameter (SMD)	d_{32}	$\frac{\sum N_i d_i^3}{\sum N_i d_i^2}$	Vaporisation
4	3	De Brouckere	d_{43}	$\frac{\sum N_i d_i^4}{\sum N_i d_i^3}$	Combustion equilibrium

3.2.4.4 Spray Angle

The spray angle can be defined as the angle formed between two straight lines originating from the injector tip to the outer spray periphery [74]. An increase in spray angle will reduce the spray drop size distribution and vice versa. Fig. 3.15 shows the effect. Normally, all capacity chart used by manufacturers are based on the theoretical spray width.

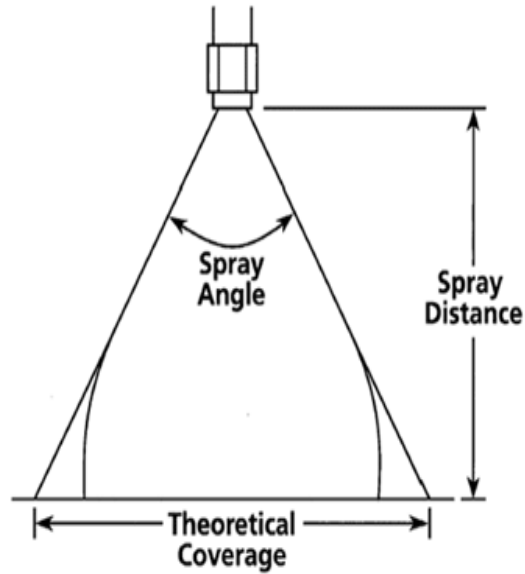


Figure 3.15 Spray angle [89]

3.2.4.5 Spray Impact Pressure

Considerations for the measurement of Spray Impact Pressure(SIP) has been an important parameter especially for high pressure cleaning applications [54], with nozzles characterised with lower spray angle being more effective. Models can be generated based on the Newton's 2nd law of motion in order to ascertain the Impact expected at target surfaces.

Consider a spray jet with an angle θ , placed a distance h , away from the surface as shown in Fig. 3.16, the momentum of the water sprays is transformed into an impact force along the target surface area to generate pressure, and hence:

$$F = ma \tag{3.3}$$

Where F , is the force (N), m , mass (kg), and a , acceleration due to gravity considering a vertical component of the flow to be the resultant force.

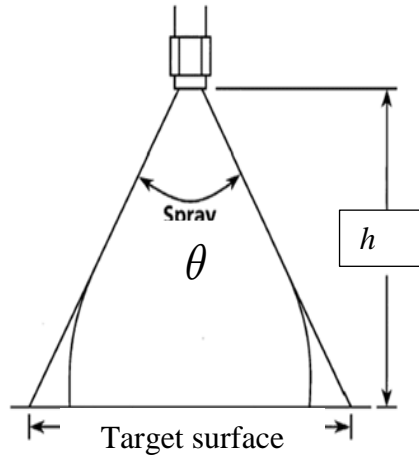


Figure 3.16 Spray cleaning set up

This component Force, F can be re-write in the form of a momentum through replacing the acceleration as velocity gradient, which using the Bernoulli's equation, has been transformed into pressure and density [54] derived in Eq. 3.4 and 3.5.

$$F = \frac{d}{dt} (m \times v) = v \frac{dm}{dt} + m \frac{dv}{dt} = m \frac{dv}{dt} = m \times v \quad ,$$

Where \dot{m} is the mass flow rate and, \dot{v} is the velocity gradient considering $\frac{dm}{dt} = 0$ at constant flow rate. Substituting mass and density in terms of

$$\rho = \frac{m}{v}, \text{ and } \Delta p = \frac{1}{2} \rho v^2$$

$$F = \dot{V} \sqrt{2p\rho} \tag{3.4}$$

And hence, the Impact pressure being,

$$P_{\text{impact}} = \frac{F}{A} = \frac{v \sqrt{2p\rho}}{2dh(\tan \frac{\theta}{2})} \tag{3.5}$$

Since Area impacted by the spray, $A = 2dh(\tan \frac{\theta}{2})$

Where d , is the spray thickness, and h , the downstream distance from the nozzle to the surface of contact to be cleaned. The next section utilised the impact pressure for scale cleaning.

3.3 Spray Jet Cleaning

Utilising a high pressure abrasive water jet has been one of the successful method in scale cleaning across many companies such as Schlumberger [10], North Sea for Philips Petroleum Company, Norway [5], One of the major problems facing the oil industry today is that of the mineral growth occurring in hydrocarbon producing wellbores. Many wells already have production scales but the scale blockage problems are growing as the breakthrough of the injected water is becoming more common and the scale itself becoming more tenacious. Fig. 3.17 shows the scale sample in production tubing.

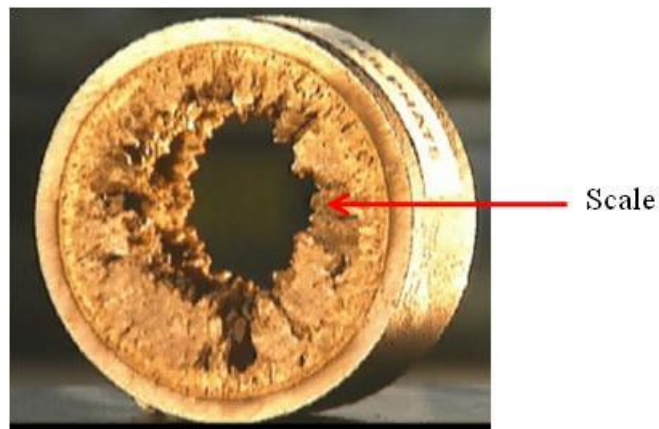


Figure 3.17 Scale sample from a Production Tubing

The primary effects of minerals scale growth in the production tubing is to lower production rate through increasing the surface roughness and hence reducing the flowing area. The pressure drop therefore goes up and production goes down. If the mineral growths increase, the access to lower section of the well becomes often impossible and ultimately the growth in the tubing itself will block them completely. As the reservoir becomes depleted and water break through occurs, the water, which is often high in dissolve minerals, enters the well and starts to flow up through the pipe. As it raises a combination of cooling and drop in pressure saturates the liquid. The salt, which has been dissolved come out of solution and scaling on the tubing, begins to develop along the flow through a production tuning.

A more severe situation arises in the case of breakthrough of injected seawater, which is often high in sulphate salts, and its mixing with formation water containing a high percentage of other salts can result in Barium or strontium sulphates being deposited.

Scientists and Engineers from Schlumberger Research Centre in Cambridge, UK, have been developing a new abrasive Jetting Technique to clean both tubing and well bore equipment without damage to wellbore equipment's. In order to test the Jetting technique under realistic conditions a full-scale test facility was built in Cambridge, this Jet Cutting Rig (JCR) is powered by 750 kW pump and can simulate jetting with backpressure of up to 5000 psi and realistic nozzle drops achievable in coil tubing operations. Fig. 3.18 shows the schematic of Schlumberger Jetting Technique.

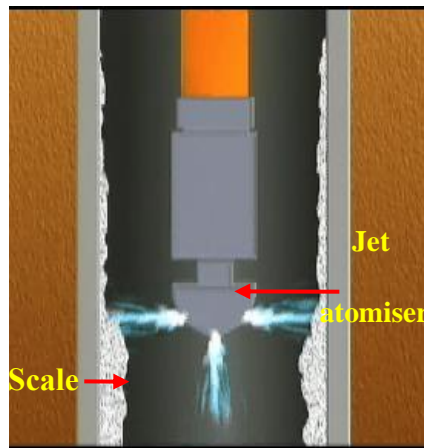


Figure 3.18 Schlumberger Jetting Technique[90]

The task is to undertake a depth study of jetting performance. The most critical finding is that the performance of the jet on the down hole condition is significantly different from that of the surface. In surface conditions without back pressure, small bubbles form on the jet and collapse on the target with large erosive effect. This process is known as Cavitation. At down hole pressure, however the formation of these bubbles as well as the erosive effects is suppressed. Typically, the jet is four times more erosive close to the surface than in down hole condition. In order words a jetting scale removal may work effectively in a shallow wells but under realistic down hole conditions. The performance may be impaired considerably. Tests on scale tubing recovered from a producing well show that a pure water jet without dissolvers is almost totally ineffective.

Adding a small concentration of sand to the system changes the characteristic and performance of the jetting system. A sand abrasive jet will remove the scale from the tubing but it will also cut the tubing steel running the risk of puncturing the production tubing and destroying the integrity of the well. To devise a safe jetting system to remove the scale but retain the integrity of the tubing steel, a details study of the interaction between the abrasive particles, the target scale and the tubing steel was made and since the behaviour of the individual particle is critical, we built the particle impact tester to study the collusion and high speed particle impacts. In the erosion of ductile materials such as tubing steel, the shape of the particle is critical. For example, a sharp sand particle will plunge on the surface and shave away the steel posing high level of damage.

However, a hard spherical particle impacting on the surface will still deform the surface but will leave a spherical crater but will cause much less damages. In the case of scale and other brittle materials, the abrasive shape is not important, as the surface is removed not by the powering action of the abrasive but by the impact process, which causes nucleate networks of fractures through the materials. The use of spherical particles is not the total solution.

A repeated impact of multiple particles resulted to high levels of particles from the surface and levels the erosion of the tubing steel which is less than those of the sand but still reliable in terms of the tubing integrity. Another key property is the fracture toughness. If the abrasive is too weak or the surface too strong, then the impacting particles will shatter into fine dust, causing no damage to the scale. The result of the scientific study was to design the right abrasive materials that will cause damage to the scale without damaging the tubing surface. This material is sterling beads(stony beams). The performance of these abrasive on production tubing is to remove the scale and leave the tubing in clean and undamaged condition. The development of this technology has enabled a new generation of tools to be developed for cleaning tubing.

Pre-quality success can only be gauged by the performance in a scaled well. One of our clients used the strong beams system to remove Tricalcium Carbonate scales when all other systems have failed completely and 2000 tons of Carbide mills were destroyed in days. Trials of using the stony beam system worked to a large extent, as it cleaned a 25 ft of tubing at between 30 to 90 ft/lb, although risk the mechanical integrity of the tubing [91][1], as well as the environmental concern, the scale in the section treated with stony beam has completely removed.

The Schlumberger study although has produced an interesting results but the study lacks the evaluating the possibility of either enhancing the cavitation for erosion benefit or developing other environmentally friendly options, instead, an abrasive jetting was proposed which beside its environmental consequence is also liable to damage of the production tubing especially where it has been used for several years. The subsequent section discusses cavitation and its erosional tendencies, which was the baseline for using solid particles to enhance erosion, where cavitation subsides.

3.4 Cavitation Water

The process in which water undergoes phase transitions due to pressure drop from liquid to vapour often called *flashing*, and hence pressure recovery of the vapour phase to liquid is considered *cavitation* shown in Fig. 3.19. The fluid transition occurring between different phases of liquid into two distinctive processes, either by changing the temperature thereby causing *boiling*, or lowering the pressure at constant Temperature called *cavitations*.

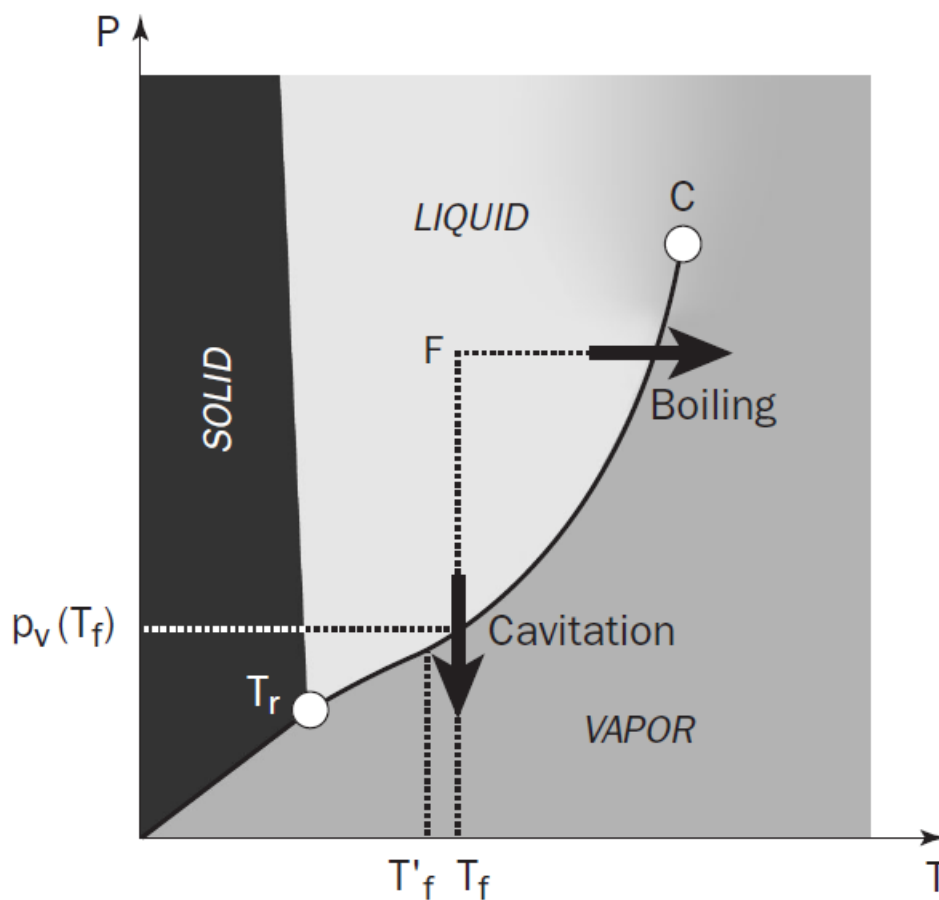


Figure 3.19 Phase change diagram [92]

The occurrence of cavitation relates to pressure drop along fluid has been used widely in the industry for various applications, although it has been remarkably known due to its negative effects of causing wear and tear along pump impellers, control valves etc, the variety of measurement of such rate are computed based on a dimensionless group.

The flow of fluid such as water through a restriction causes a drop in the pressure of the flow, although geometry of each atomiser determines the level of pressure fluctuations achieved. Although the expansion of the cavitation bubble can be achieved either through acoustic, optic, particle or hydrodynamics[93], indeed the geometry system i.e. nozzle design is responsible for the hydrodynamic cavitation due to pressure variation along the nozzle, acoustic cavitation is resulted from sound waves in a liquid due to pressure fluctuation. Cavitation phenomena is known to exist due to drastic drop in fluid pressure approaches the saturated vapour pressure, as a results, air solubility decreases, thereby causing an air filled bubble cavities generation, as the pressure drops further closer to saturated vapour pressure of water, boiling of water causes phase change even at room temperature, thereby water vapour cavities are filled with the water vapours. Subsequent pressure rise resulting in higher solubility of air in water for example in oxygen as shown in Fig. 3.20, the cavities then undergoes diminishes gradually due to the solubility, in systems where rapid pressure change are obtained, such cavities results in violent collapse causing pressure shock.

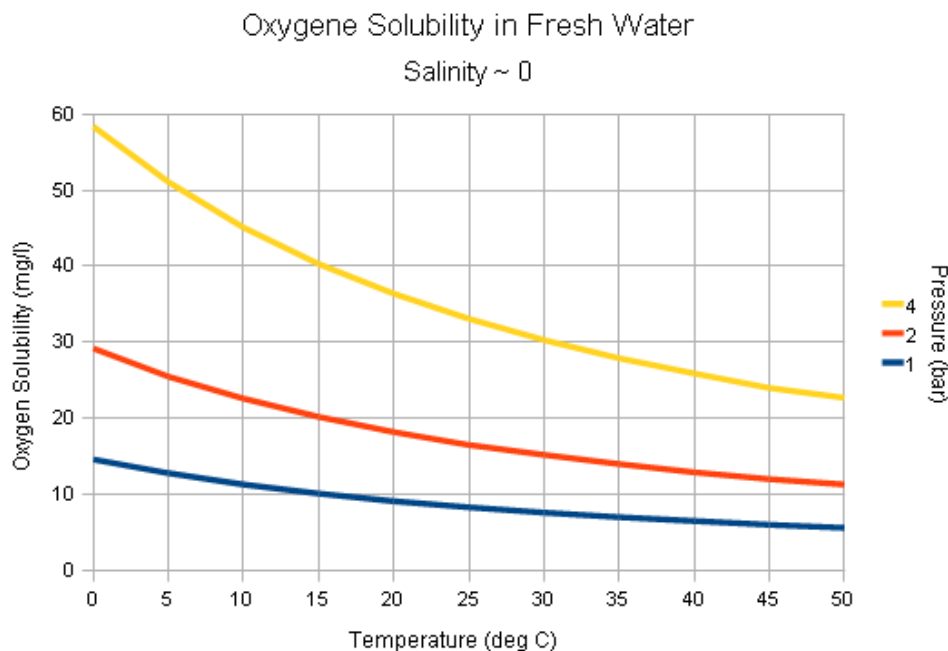


Figure 3.20 Oxygen solubility in water at different temperature and pressure[94]

The process of cavitation hence follows a routine pattern around a pressure curve as shown in Fig. 3.21, with aeration and evaporation causing cavity growth due to pressure drop, and dissolution of air and condensation leading to cavity collapse at higher pressure.

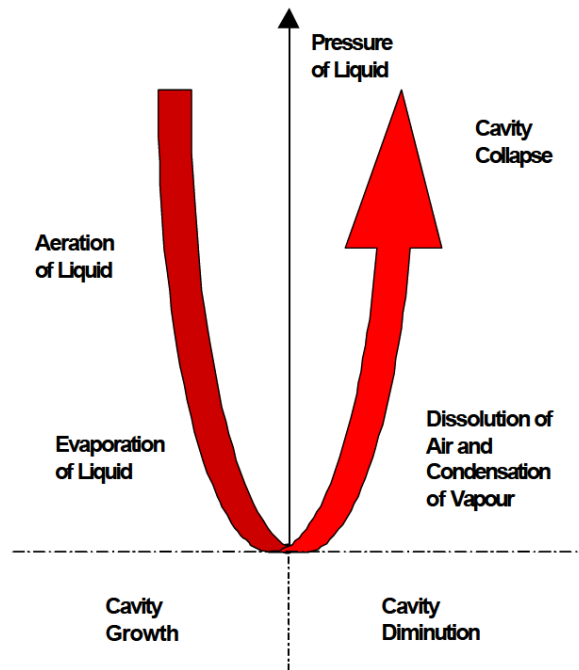


Figure 3.21 Pressure cycle in cavitation[95]

3.4.1 Classes of cavitation

The cavitation phenomena has been known to be caused by pressure variation along liquid systems, although there are variety of forces resulting into the pressure variation, and therefore the cavitation can hence be classified based on those forces. There are four broad classes of cavitation such as; hydrodynamic, acoustic, optical as well as particle shown in Fig. 3.22.

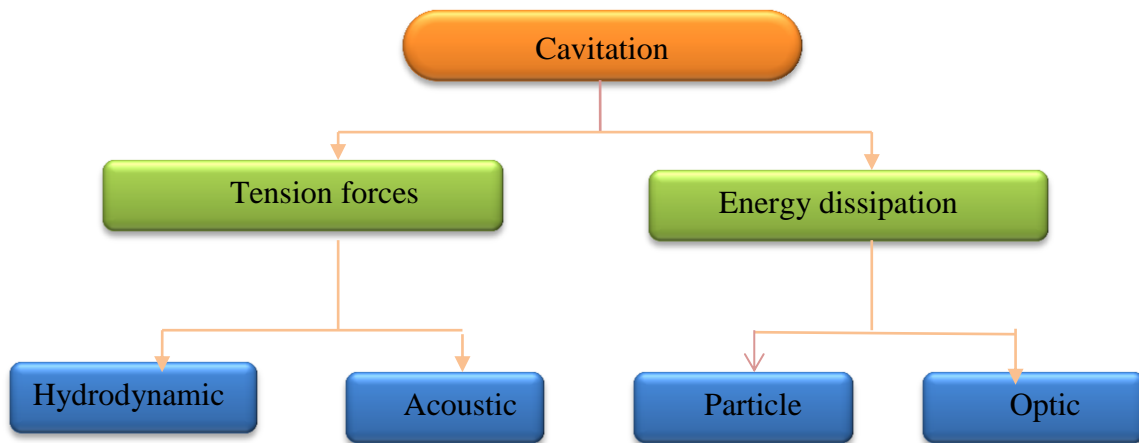


Figure 3.22 Classification of cavitation [96]

3.4.1.1 Hydrodynamic cavitation

The hydrodynamic cavitation occurs due to drop in pressure along a flowing fluid to the saturated vapour pressure of water. This is usually encountered in hydraulic machinery such as turbine, impellers, hydrofoils, nozzles as shown in Fig. 3.22. Most often hydrodynamic cavitation occurrence causes erosion on material surface resulting in severe damage.

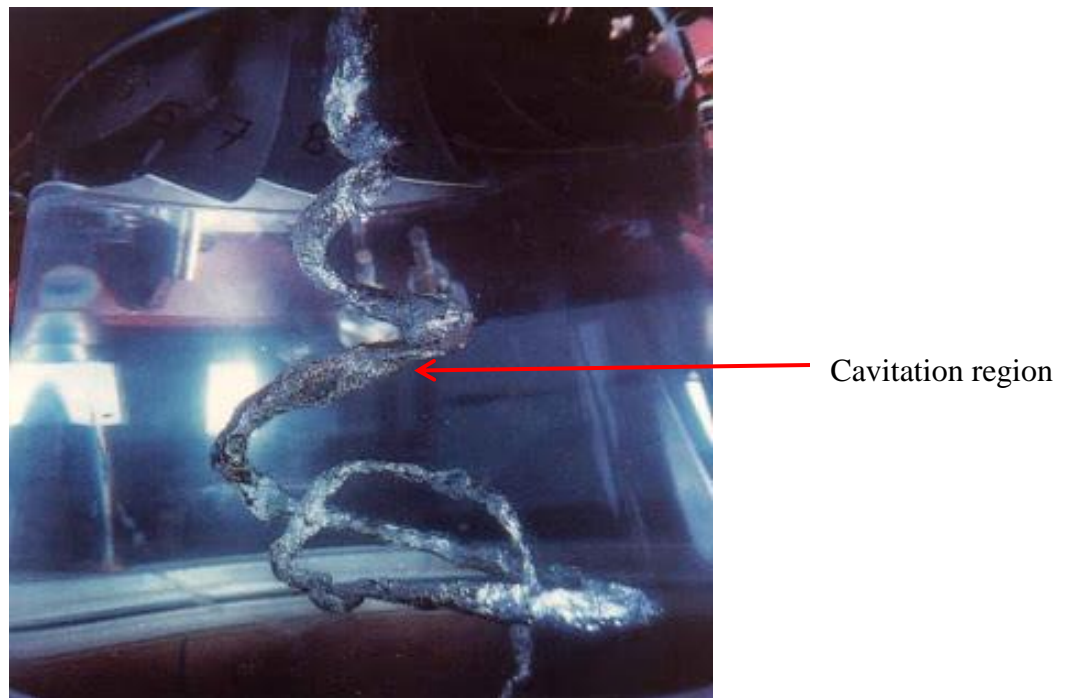


Figure 3.23 Cavitation regimes along Francis turbine[97]

Hydrodynamic cavitation has been among the major concern in industries due to degradation in materials caused by the cavitation erosion.

3.4.1.2 Acoustic cavitation

Cavitation occurrence due to pressure shock caused by acoustic waves, which in turn proceeds along nucleation, growth and subsequent collapse of the bubbles. The application of this type of cavitation has been widely reported in the field of sonochemistry, sonoluminescence as well as sonoporation. The noble art of crushing kidney stones (lithotripsy) as well as transfer of genes and the treatment of cancer [98]. The light emitted is typically shown in Fig. 3.24.

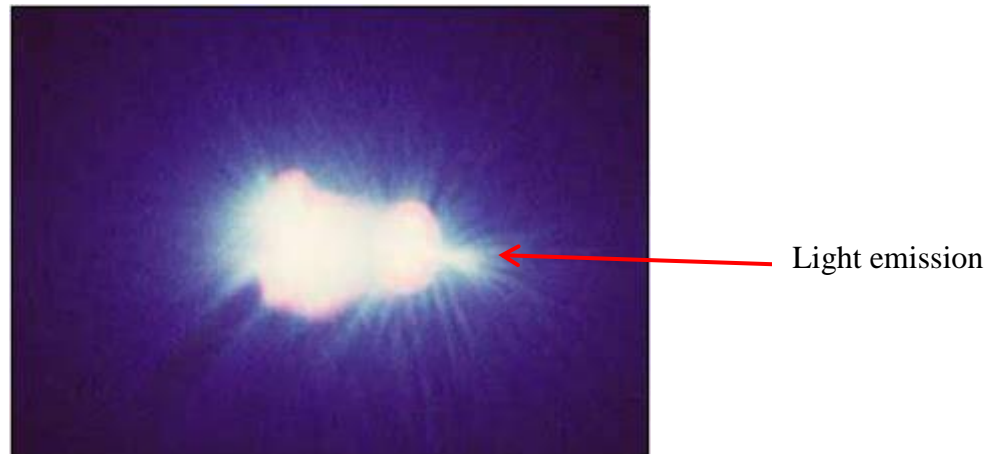


Figure 3.24 Light emitted by a trapped cavitation bubble [98]

3.4.1.3 Optic cavitation

Optic cavitation is generated through a medium radiated by high-intensity beam of laser. Usually extreme conditions caused the liquid medium break down resulting in the cavitation bubble.

3.4.1.4 Particle cavitation

The passage of high energy protons or neutrinos along a medium causes ionisation and subsequent energy transfer which results in heating and tiny bubbles are formed called particle cavitation.

3.5 Cavitation in Spray Nozzles

Flow through nozzles is characterised by fluid flow rate obtained in terms of pressure difference, nozzle geometry and size, as well as flowing fluid properties such as viscosities, surface tensions etc. Cavitation occurrence at exit flow, is due to sufficient increase in pressure difference across orifice, causing the boundary layer tending to separate from the wall of the orifice wall as a results of sudden change in cross sectional area of flow and direction[99], hence cavitation emerges whenever the sharp edge of the orifice, leading to flow detaching from the wall of the orifice[95], which generates a hole called *vena contracta* consequently causing a recirculation region between the wall of the hole and the *vena contracta*. The illustration of the flow behaviour is shown in Fig. 3.25 indicating an inlet flow passing through an orifice, increasing flow across the *vena contracta* causes higher velocity in the downstream section.

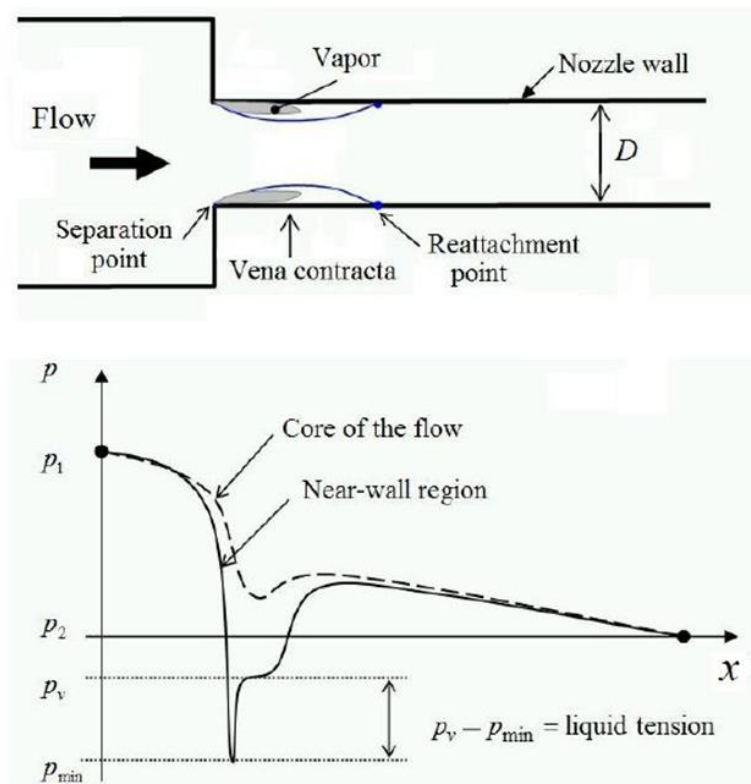


Figure 3.25 Typical flows through a nozzle[100]

Thereby causing increased dynamic pressure and decreased static pressure head resulting such pressure decreased reaching the saturated vapour pressure P_v , which usually occurs in the *core of the flow* as shown in Fig. 3.24. Cavitation then emerges. Cavitation bubbles travels along the water flows downstream but subsequently collapses as pressure appreciates. Lowering the downstream pressure extends the cavitation bubble length [95]. The acceleration of the water causes resulting in pressure depression, which cavitation results as long as the static pressure reaches the saturated vapour pressure of water. It is evident that the downstream pressure plays an important role into the length of the cavitation bubbles, as lower downstream pressure extends the cavitation growth further downstream, while sudden pressure recovery at the downstream causes cavity implosion and violent behaviour of cavitation shock waves [95]. In addition to mentioned studies, several others have prove that the higher injection in terms of flow rates leading to low pressure below critical values especially at the *vena contracta* forms vapour cavities [71], this considers to be hydrodynamic cavitation has been known to improve spray jet breakup[101]. It is evident that when cavitation extent is high, decreasing the downstream pressure do not necessarily increase flow rate as a results of phenomena called *choking*. While trying to perform detail investigation on the cavitation flows along nozzle, researchers have showed experimentally the two(2) dimensional numbers as the most significant dimensionless group as Reynolds number and Cavitation number, which the cavitation number, σ expressed in Eq. 3.6

$$\sigma = \frac{P_{\infty} - P_v}{0.5\rho v_{\infty}^2} \quad (3.6)$$

Where σ is the cavitation number, P_{∞} pressure of the fluid, ρ_w density, P_v saturated vapour pressure and velocity of the flow, and the Reynolds number R_e as described in Eq. 3.7

$$R_e = \frac{\rho_w U d}{\mu_w} \quad (3.7)$$

Where ρ_w is the density of water, velocity of water, U , diameter, d , and viscosity of water as μ_w .

3.6 Cavitation erosion

The severe action of causing mechanical degradation of material as results of violent collapse of cavitation bubbles is termed *cavitation erosion*. Cavitation erosion has been proved to be form near the solid surface [95]. Numerous researches has proven the mechanism of cavitation; although the transition of bubble growth, collapse as well as transition of the bubbles leading to cavitation erosion is still not well understood in the literature. To understand the relationship between cavitation generation, collapse and erosion, this section will highlight the various mathematical models and experiments conducted together with simulations in order to understand the transition between cavitation bubbles and quantitatively ascertain the erosion extent.

3.6.1 Spherical bubble in water

There are two possible classes of approach in which a spherical bubble collapse may lead to cavitation erosion, regarded as *symmetric* collapse in which it occurs in the bulk liquid, this results in the release of shock waves which is transferred to the surrounding liquid; on the other side *asymmetric* collapse of bubbles occurs when the bubble is in partial or complete contact with solid boundary, with the collapse causing disturbance greatly to the side ways of the solid boundary, making the fluid to penetrate through the cavity and hence a microjet is formed [95]. Rayleigh-Plesset equation will now be used to describe the behaviour of the cavity collapse for both the symmetric and asymmetric case.

3.6.1.1 Rayleigh-Plesset model

Considering a spherical bubble cavity with radius $R(t)$ as dependant on time t , in a bulk infinite liquid at constant temperature. Taken a portion of the liquid in contact with the bubble, the forces acting upon the bubble cavity includes the pressure of the inner bubble P_b , the stress due to viscous forces, τ_r , the stress normal to the surface, σ_r , as well as the surface tension, σ , [102] shown in Fig. 3.26, as long as there is an equilibrium with no mass flow into or out of the bubble, the force balance behaves as in Eq. 3.8:

$$P_b + \sigma_r - 2\tau_r - \frac{2\sigma}{R} = 0 \quad (3.8)$$

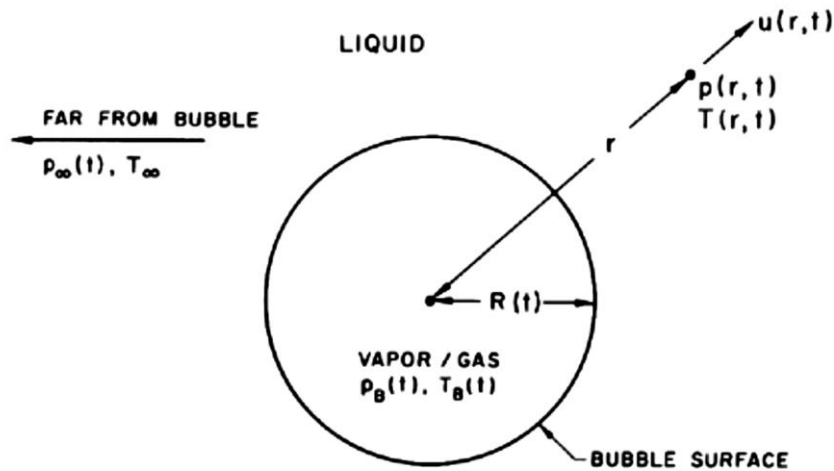


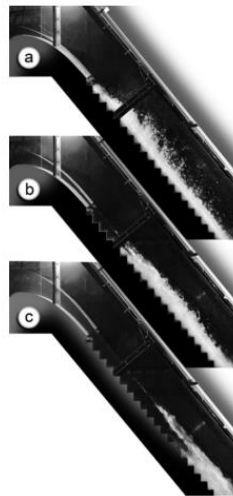
Figure 3.26 Typical spherical bubble in a bulk liquid[102]

3.7 Cavitation Erosion and Mitigations

3.7.1 Cavitation damage control in dams

Cavitation damage has been a source of concern especially in hydraulic machinery [103], spillway tunnels, spillway dams, and chute spillways with high gradient structure [104], these are typically dams discharging water at the velocity range of 20-50 m/s [105]. Although water velocities of up to 140 m/s are obtainable with the 10 MPa inlet pressure across the Flat fan nozzle, which may give higher cavitation chances compared to the water dams with considerably lower velocities investigated, using the dam spill ways characteristic height of up to 300m, exposing additional likelihood of air-entrainment, cavitation, fluctuation-vibrations as well as energy dissipation in such high dams. As a results of the combined high flow velocities, cavities are often generated due to under pressure and high-pressure, leading to cavitation erosion along the concrete, which was prevented successfully using aerators supplying high air concentration in the cavitation regions shown in Fig. 3.26, and thereby economically and effectively combating the cavitation-erosion [104]. Although, aerators caused weakening effect on the dam walls[104].

Originally, [106] reported Peterka to have investigated experimentally the application of aeration in cavitation control, with his findings leading to reduce cavitation erosion with as small as 0.4% air concentration, flow pattern in aerated spill ways shown in Fig. 3.27 can be mitigated from erosion through increasing the air concentration from (a) 1.0%, through (b) 1.7%, and then (c) 3.1%. Further increase in the air concentration to 7.4% completely eliminated the cavitation erosion, this was noticed as the bursting and hammer-beating was eliminated completely[107]. Subsequent expansions into this technique were developed further investigated by other researchers with air concentration of 1-2% at near wall of the surface.



(a) 1.0, (b) 1.7, (c) 3.1% air

Figure 3.27 Flow pattern in aerated spill way [108]

Perhaps, despite the numerous disadvantages of cavitation, its inherent ability to cause erosion have attracted wider applications in submerged cleaning using cavitation water jets [10],[109][109][61],[62],[⁶⁰[60],[108], while a spray-air interaction was also chosen for this investigation as higher impact force unto the surface were noticed (see Section 6.3). Previous researchers developed models suitable for understanding the water-air interaction especially for high flow velocities. Consideration were made to the material balances of both the water and air mixture into the chamber an empty chamber shown in Fig. 3.28 with an approximate length of 1m and a radius of 0.10m.

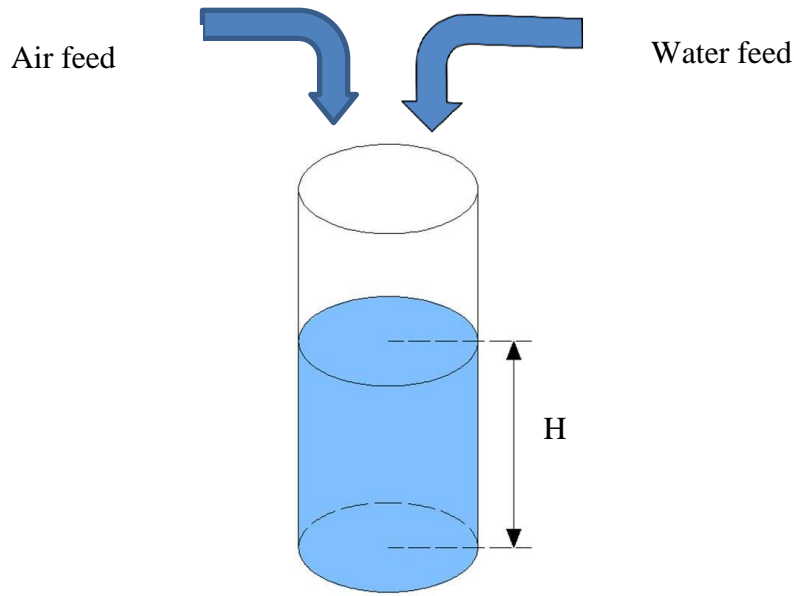


Figure 3.28 Aeration chamber

A total mass of the combined liquid and air entering the chamber can be written mathematically as [104] as derived in Eq. 3.9 to 3.13 :

$$m_{total} = m_a + m_w \quad (3.9)$$

With an equivalent combined volume

$$V_{total} = v_a + v_w \quad (3.10)$$

The ratio of the combined mass over and volume of the water and air can then be related as

$$\text{Density} \quad \rho_{total} = \frac{m_w + m_a}{V_w + V_a} \quad (3.11)$$

The equations has been derived thermodynamically by [104] that relates the inherent flow behaviour along the two-phase flow with emphasis given to the speed of sound in air a , as Eq. 3.12

$$a \approx \sqrt{\frac{p}{\rho_w C(1-C)}} \quad (\text{m/s}) \quad (3.12)$$

Where p , is the ambient pressure (Pa), ρ_w the density of water (kg/m^3), and C , the air concentrations which can be varied based on the experimental conditions as

$$C = \frac{Q_a}{Q_w + Q_a} \quad (3.13)$$

This is suitable for calculating speed of sound in aerated flow with varying air concentrations using the air concentration. Calculations conducted based on Eq 3.9 provided the pressure is kept the same, will mean that the speed of sound in aerated flow is only a function of air concentration. Hence, calculations can be generated for the Mach Numbers as the another important variable in aerated flow. The Mach number, M has been considered as the ratio of flow velocity to the speed of sound in the medium, expressed in Eq. 3.14 as

$$M = \frac{v}{a} \quad (3.14)$$

Where v , is the flow velocity (m/s). These calculation as shown Section 5.5 and simulated CFD calculation in Section 6.6 explained the flow behaviour in aerated flow further.

3.7.2 Pressure Wave front in aerated flows

The nature of the flow of water across varies in aerated and non-aerated flows especially in terms of the pressure waves generated during the flow. It has been experimentally confirmed as shown in Fig. 3.29, that the pressure wave front in aerated chamber using computerised signal detectors that the In an aeration 0 versus 10% comparison indicated increase in pressure wave

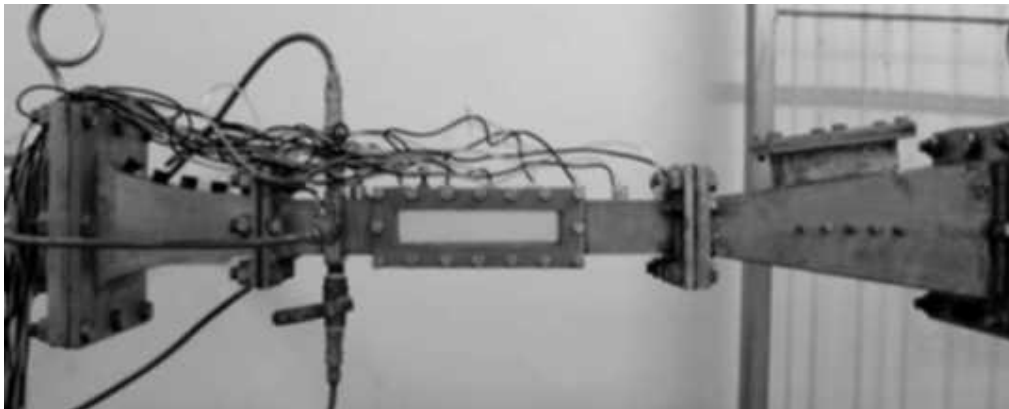


Figure 3.29 Experimental aerated chamber [56]

increase in almost 53kPa due to aeration as shown in Fig. 3.30 , indicating the suppression of cavitation due to aeration has further increases the pressure wave front.

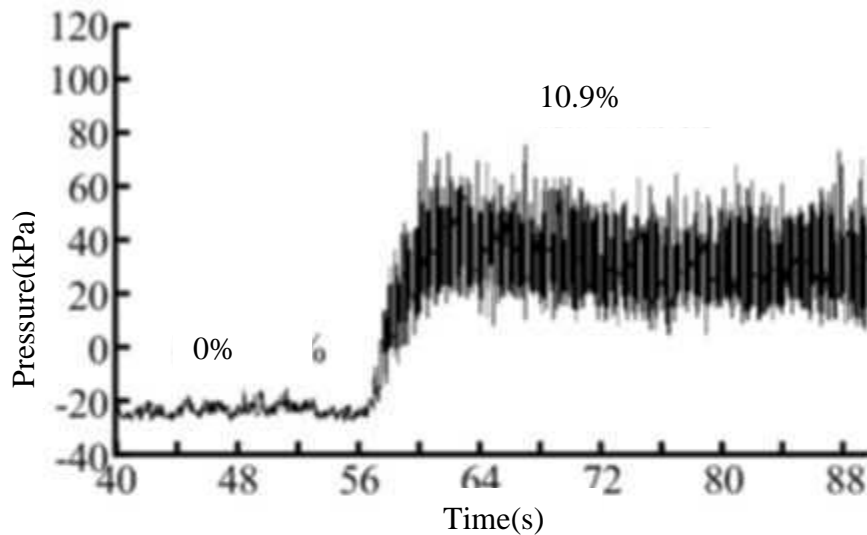


Figure 3.30 Pressure wave font with and without aeration [104]

However, increasing the aeration also increases the pressure wave font, which could subsequently enhance the impact when utilised for cleaning purposes. Other experiment conducted for low air concentration also confirm pressure enhancement in the left hand section shown in Fig. 3.31, and when the aeration was removed, the pressure became suppressed as shown in the right hand section.

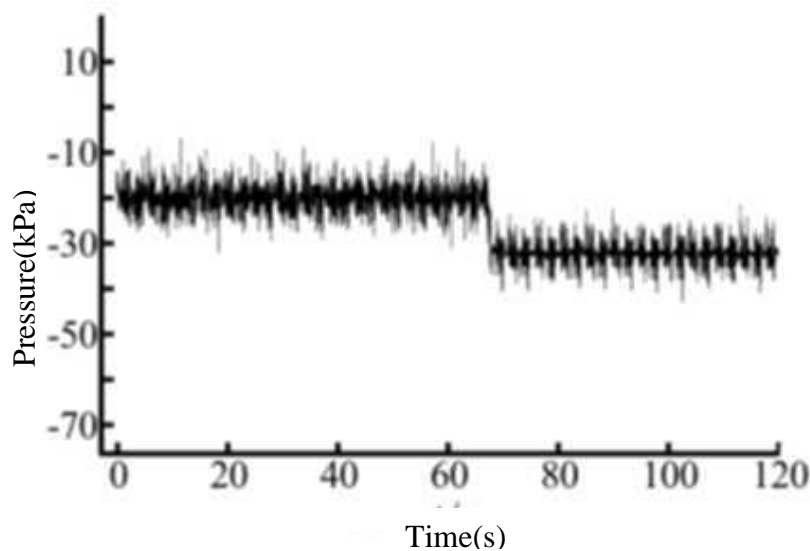


Figure 3.31 Aerate flow at low 1.6% air concentration [104]

As the of aerated flow scheme was successfully utilised in the construction industries, especially in dam spill ways for mitigating cavitation [104],[105],[110],[111],[112], further impact has been experimentally highlighted of capable to cause increase in pressure wave

font [104],[110], and the weakening effect of materials due to compressive stress they are subjected to by the aeration [113], as well as the application of Water Cavitation Peening(WCP) through aeration for improved fatigue life of metallic components [110],[103],[114],[115], such applications could be utilised to enhance erosional performance of surfaces during cleaning, which is suitable to compensate for the cavitation erosion effect exempted in high velocity jetting techniques upon aeration.

In this investigation, the air stream is solely utilised to pressurize the walls of the oil production tubing where mineral scales are, such that the compressive stresses exerted by the air on the scale surfaces play an additional role to eroding the scale when combined with the high pressure water from the flat fan atomizer. This has successfully led to enhanced scale erosion. This application could potential be improve to enhance erosion performance without using sterling beads.

3.8 Summary

The review of the various water flow behaviour has been conducted in this chapter and the following summary can be drawn:

- High velocity water flow in spray nozzles experience a substantial pressure drop at the nozzle *vena contracta*, leading to cavitation within and even downstream of the nozzle.
- The cavitation generates a micro bubbles which when collapse upon hitting a solid target generate a pressure shock leading to erosion called cavitation erosion.
- Cavitation erosion has attracted wide concern due to cost of repair /replacement of machinery parts, and also eroding concrete surfaces on water dams spill ways.
- Major oil companies took advantage of the cavitation erosion in successfully cleaning production tubing using spray jets on the surface, however, decreased erosion performance while in typical production tubing due to decrease in pressure has been a major limitation.
- The jetting techniques currently employ sterling beads(solid particles) in the water jets to compensate erosion decreased due to cavitation decrease with increasing depth, however, environmental concern, secondary clogging effects of the particles, damage to the production tubing itself and sophistication in pump design due to change in liquid density do not give a promising end to this technology.
- Forced air aerators have been successfully utilised in combating cavitation erosion in dam spill ways, by causing high pressure in the cavitation prone region, thereby eliminating cavitation erosion. However, the pressure wave front increase and weakening effect on the concrete surface due to aeration has also been a major concern.
- Application can then be sought of utilising the material weakening effect and enhance pressure wave font due to aeration to replace the use of sterling beads in scale cleaning as it compensate for high erosion effect.

Chapter 4

Experimental Set up and Procedure

4.1 Overview

This chapter introduces the experimental set up involved, procedures and description of detailed steps involved to ensure precise and accurate results are obtained. The Chapter covers the three phases including:

- (1) Phase 1: The measurement of the entrained-air velocities were performed with high precision Hot wire anemometer described in Section 4.2., it involves a non-intrusive measurement method with no calibration , however, the water sprays was also characterized in terms of drop size and velocities using Phase Doppler Anemometry(PDA) for the their momentum analysis across the scale surface described in Section 4.3, and hence the impact pressure was measured across the spray width using a pressure transducer in Section 4.4.

- (2) Phase 2: The qualitative monitoring of the cavitation bubble length under varying air concentration with partially submerged conditions downstream of the atomizer (Section 4.5). The cavitation was qualitatively investigated at various aerated pressures under submerged conditions , to ascertain the decay of cavitation along the stand-off distance in order to ensure no cavitation erosion is responsible for the erosion test trails conducted.

- (3) Phase 3: The scale removal trials were then conducted using an aerated chamber constructed specifically for this investigation at similar conditions during the characterisation and cavitation test for the hard, medium and soft scales which are typically found in the oil and gas wells. The scales are of different chemical composition based on the geology of the oil field and the chemistry of the injected water. Details of the experimental scheme and steps are provided in Fig. 4.1.

The experimental set ups, procedures as well as precautionary measures and sources of error are detailed in each respective section.

Section 4.2

Section 4.3

Section 4.4

PHASE 1

PHASE 2

PHASE 3

EXPERIMENTAL

CFD VALIDATION

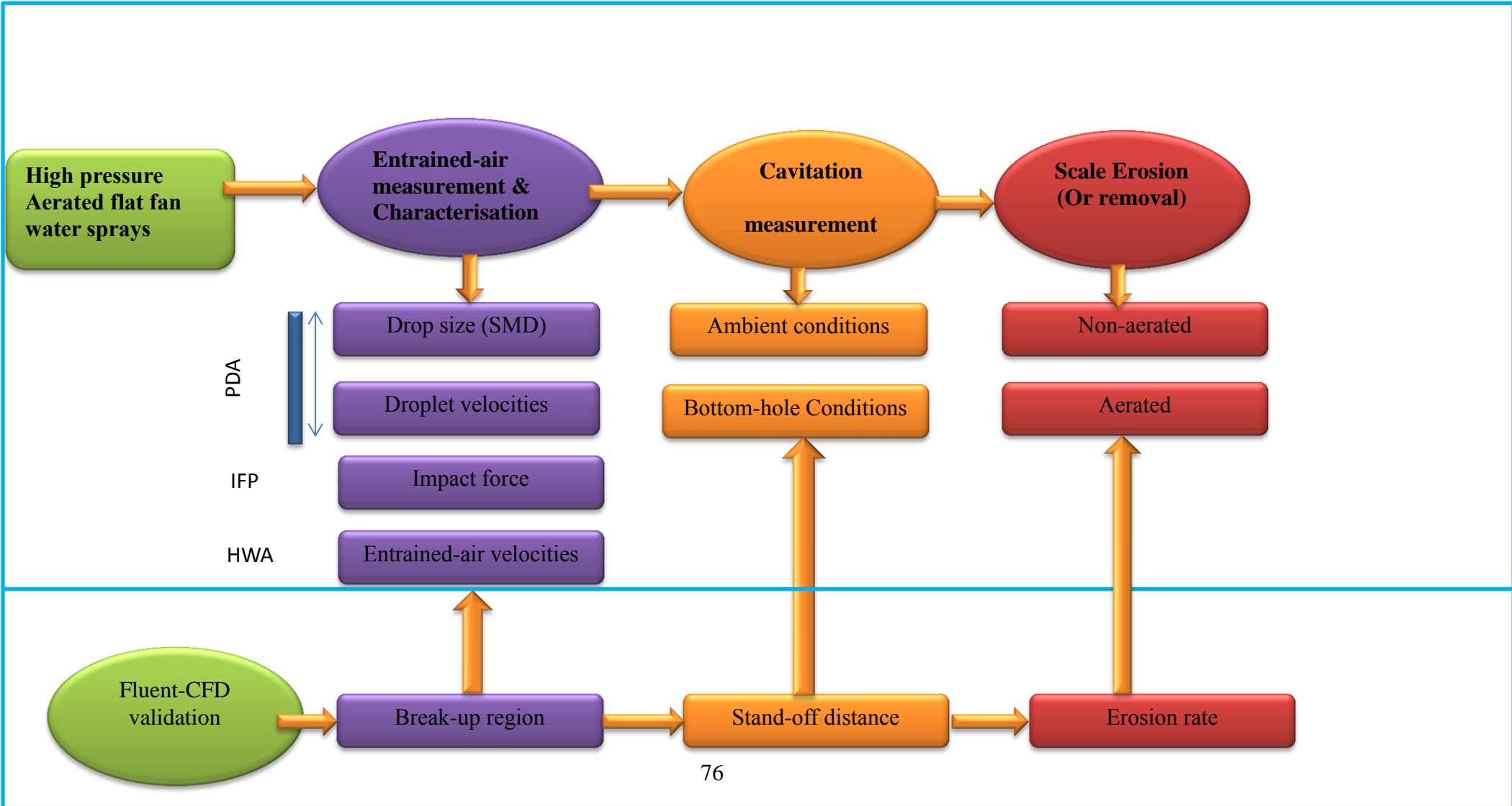


Figure 4.1 Experiment and simulation validation stages

4.2 Entrained-air Measurements and Spray Characterizations

4.2.1 Experimental set up

The measurement of the entrained air velocity was performed according to the set up shown in Fig. 4.2, using a High pressure pump to delivered water through the atomizer via a pressure gauge for ensuring the targeted pressure was achieved. The hot wire probe set around a grid lines corresponding to the measurement position, and the air velocities were then displayed. The water tank collects and recycles the water through the pump during the test. A Hot-wire sensor was kept 5mm away along the edge of the spray end to avoid destruction by the High pressure water jet and interference causes by condensing water heat transfer along the hot wire. Axial and radial measurements were performed as shown in the Fig. 4.2.

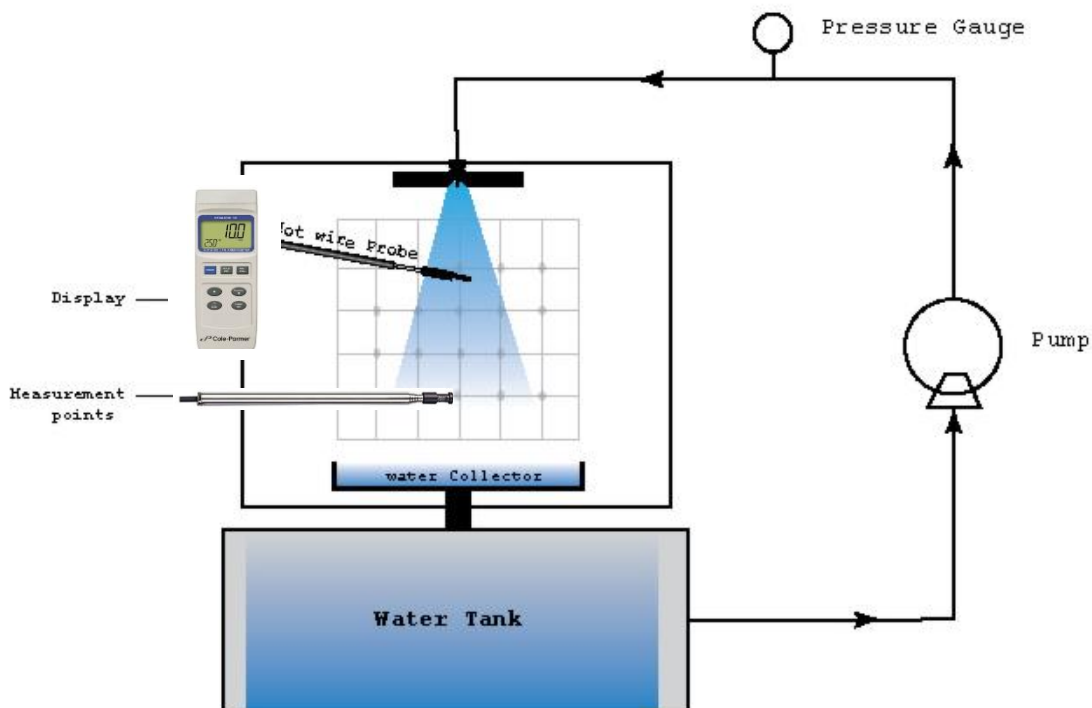


Figure 4.2 Entrained-air set up

4.2.2 Experimental apparatus

The measurement of the entrained-air around a high pressure water sprays includes apparatus connected together as shown in Fig. 4.2 to carry out the measurement, the following are the main apparatus use in this experiments

Hot Wire Anemometer

The application of a Hot-wire anemometer has been drawn based on the principle of convective heat transfer across a heated sensing element; which is generated upon perturbed by flow unto its surface, leading to changes in the heat transfer coefficient of resistance. It is currently applied in many industrial applications despite the availability of other non-intrusive measurement methods such as multi-component laser Doppler Velocimetry, still two other advantages such as (i) measuring accurately entropy changes and (ii) its capability to measure flow parameters. It operates on the basic principle that electrical output can be established by heat transfer from the cold surrounding air to the heated wire; as such the heat transfer which is a function of fluid velocity can then be accurately measured, which the electrical circuit is used to provide controlled amount of current to the wire to maintain a constant voltage. Although to maintain a constant temperature, the amount of supplied current may be varied to ensure isothermal conditions despite variation in the heat transfer rates. The simplified view of the Hot-wire section is shown in Fig. 4.3.

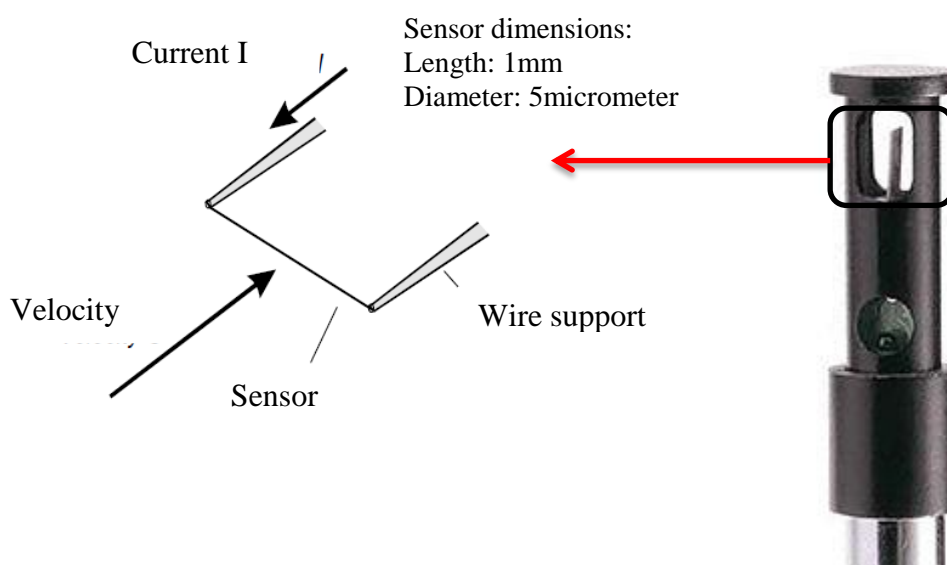


Figure 4.3 Hot Wire cross section[116]

A thin wire is placed across a path of moving cold air, with a velocity U , I , is the current, R , resistance. While a current is passed through the wire, an amount of heat equivalent to I^2R_w which, when at equilibrium, will compensate for the heat loss to the surroundings. Whenever the velocity changes, the heat transfer changes as well, and ultimately changes the temperature and a new equilibrium established.

Most practical applications require effective material to be used for the Hot-Wire, therefore the following properties were suggested:

- i. High coefficient of Temperature resistance
- ii. Suitable electrical resistance which can conveniently heat wire at practical currents and voltages
- iii. Availability of wires at very low diameters
- iv. Adequate strength to overcome aerodynamic stress even at high velocities

The governing equation for the energy transfer between the Hot wire and the surrounding air is:

$$\frac{dE}{dt} = W - H \quad (4.1)$$

Where E =Thermal energy stored within the wire C_wT , with C_w =heat capacity of the wire

W = Power generated by the Joule heating I^2R_w

H =Heat transferred to the surrounding by conduction, convection and radiation. Considering the overall Energy balance equation generated by the heat transfer,

$$H = \sum (\text{Convection to fluids} + \text{conduction to supports} + \text{radiation to surroundings}) \quad (4.2)$$

The convection equation heat transfer is governed by the equation

$$Q_{conv} = Nu \times A \times (T_{wall} - T_{air}) \quad (4.3)$$

Where Nu , is the Nusselt Number given by

$$Nu = \frac{hd}{k_f} \quad (4.4)$$

Hence, Eq. 4.1 can be written in terms of static heat transfer as follows:

$$W = H \Rightarrow I^2R_w = hA(T_{wall} - T_{air}) \quad (4.5)$$

Leading to transformation in form of dimensionless Nu , as

$$I^2 R_w = \frac{Nuk_f A}{d} (T_{wall} - T_{air}) \quad (4.6)$$

For Forced convection heat transfer, where $Re \approx Gr^{1/3}$ having a value between 0.02 in air and $Re \approx 140$

$$I^2 R_w = E^2 = (T_{wall} - T_{air})(A + B \times U^n) \quad (4.7)$$

According to King's law[116].

4.2.3 Experimental procedure

The connection between the digital display and the hot wire were mounted on the experimental rig as shown in Fig. 4.6 and placed, according to the grid established in Section 4.3. The pump was then primed and started, with subsequent pressure increases until the desired pressure was established using the pressure gauge on the nozzle top. The flow was then maintained for 2 minutes until stability of the water and air flow was achieved. The reading of the air velocities was then taken for 10 seconds to ensure accuracy and then subsequently repeated for axial positions at 25, 50 and 75mm and radial positions from 0, 5, 10, 15 and 20mm. Then it was traversed for -5, 10, -15 and -20mm. The results of the air velocity around the spray are shown in Section 5.2.2.2.

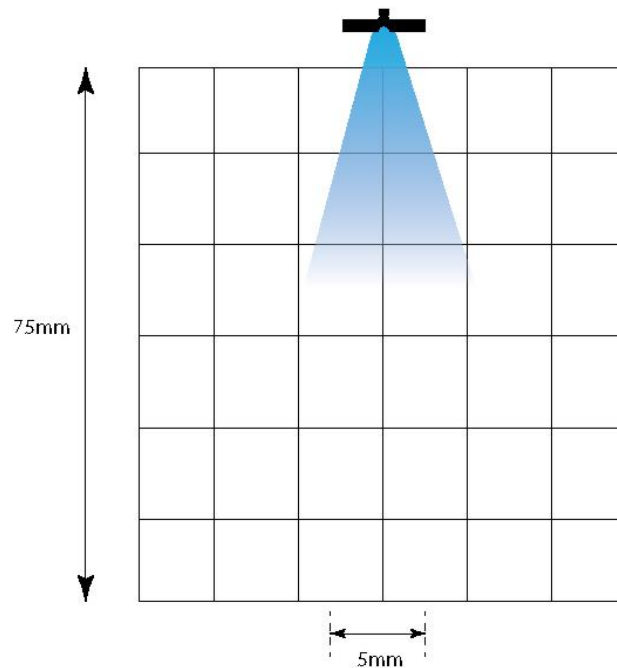


Figure 4.4 Entrained-air velocities measurement grid

The following steps were adopted for the measurement of the air velocities

1. The probe was connected to the probe input socket
2. The power on the meter was turn On
3. The unit for the velocity and temperature were chosen
4. The sensor slide cover was slid up to isolate the air velocity from the hot wire until the zero reading was observed at the display
5. The velocity meter was then zeroed at the isolation instance and then
6. The cover was slid down to allow air contact for the velocity measurement

4.2.4 Accuracy and Errors in Hot-Wire Anemometry

4.2.4.1 Precautions and accuracies adopted during the experiments

- Repetitive sensor drying to minimize water droplets fouling
- Liquid droplets not allowed to cascade in air
- Spray was allowed to stabilise before readings were taken
- Water vapour condensation was minimized on the hot wire during the experiments

4.2.4.2 Sources of errors

- Probe contaminations in air: The presence of dust, vapours, dirt's or chemicals affect the flow sensitivity of the hot sensor or experience a reduction in frequency of response. It is usually signalled as a drift due to particle contamination from the calibration curve shown in Fig. 4.3. This includes exposure to winter conditions or unfiltered air at 40m/s. Other effects includes low velocity due to the slight effect of dirt on the heat transfer
- Bubbles in liquids: In liquid components, dissolve gases generate bubbles on the sensors leading to reduced heat transfer rate and downward calibration drift.
- Readings taken within ± 1 mm along X and ± 1 mm along Y axis.

4.2.5 Hot Wire Calibration

The calibration principle of the Hot Wire Anemometer is derived from the King's law with its response derived as[116]:

$$E^2 = A + BU^n \quad (4.8)$$

Where E is considered as the voltage across the hot wire,

U , is the velocity normal to the wire, and A , B and n are constants. Using linear regression and plotting the velocity versus the voltage during the industrial calibration.

The measurement of the high pressure water spray characterization in terms of drop size and velocities were conducted using the PDA procedure detailed in Section 4.3.

4.3 Spray Characterization

4.3.1 Experimental set up using PDA

The PDA system was purchased from Dantec Particle Analyser. It comprises of the following components, as shown in Fig.4.5:

- a. Laser
- b. Transmitting Optics
- c. Receiving Optics (photo detectors)
- d. Signal Processor
- e. Computer processor package

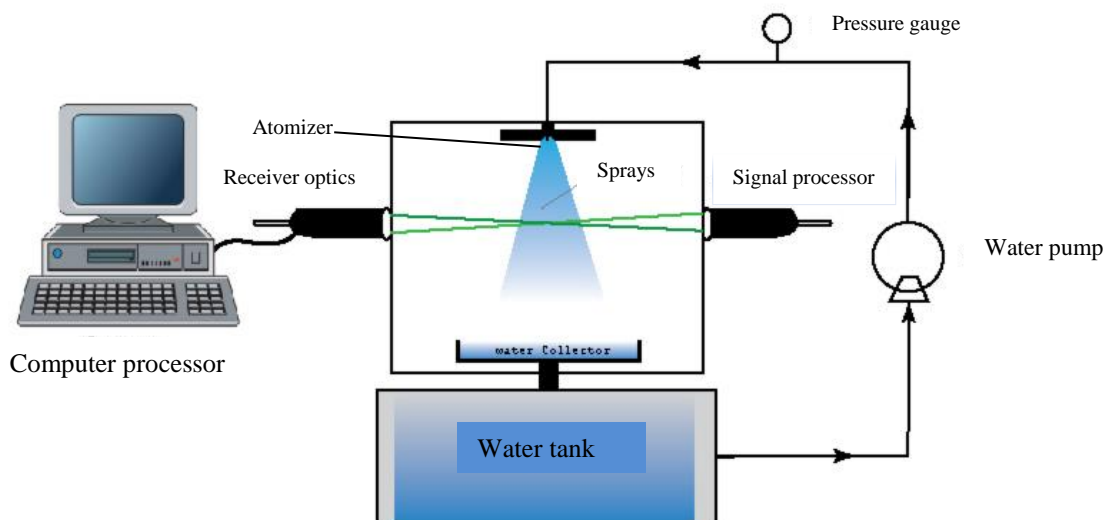


Figure 4.5 PDA set up

The technique adopted involves a hybrid of PDA and Laser Doppler Anemometry(LDA).This ascertains the velocities of the particles during the flow in combination with a particle sizing interferometer. The PDA system was set up as shown in Fig. 4.6, with the transmitting and receiving optics set to the values shown in Table 4.1. The only setting that can be adjusted on the transmitting optics is the power level of the laser. During the experiments the maximum power setting was used which has the effect of increasing the measuring volume.

Table 4.1 PDA set up

	Description	Symbol	Units	Value
Transmitting Optics	Laser power	P	mW	100
	Wavelength	λ	μm	514.5
	Beam Separation	df	mm.	38
	Focal length	f_{tr}	mm	400
	Beam diameter	d_b	mm	1.35
	Fringe Spacing	s	μm	5.42
	Number of fringes	N_f	-	37
Receiving Optics	Focal length	f_{rc}	mm	310
	Scattering Angle	θ	degrees	72
	Aperture setting	-	mm	0.5

The receiving optics were set to receive 1st order refraction from the particles, with the scattering angle being 72° which is the optimum forward refraction mode with reduced bias in the results due to the reflected light, thus ensuring good scattering light intensity levels (high signal to noise), thus making it suitable for measuring small particles.

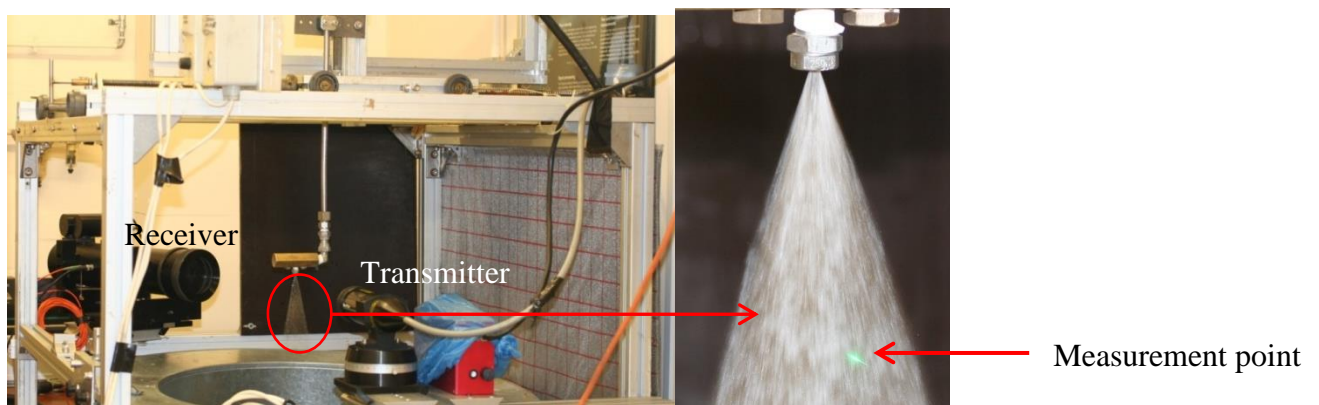


Figure 4.6 PDA Experimental set up cross section

The focal length of the receiver was 310mm. Table 4.1 provides the detail specification. Decreasing the focal length of the receiver increases the sensitivity of the optics allowing the receiver to measure smaller particles. However there are trade-offs with reducing the focal length such as reducing the size of the measurement volume and reducing the maximum droplet diameter that can be measured. The set focal length of 310 mm was suitable for measuring the range of particles in the experiments shown in Fig. 4.7.

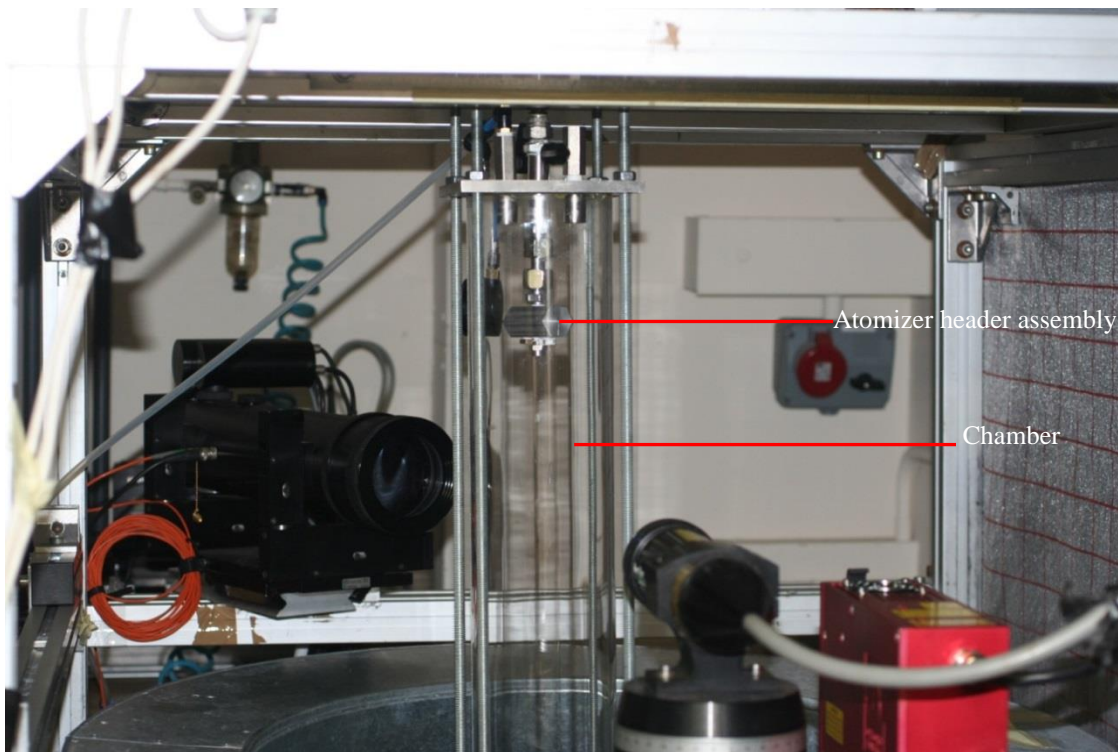


Figure 4.7 PDA aerated chamber

The concept of Doppler shift was first conceptualized in 1842 by an Austrian Physicist by observing a change in frequency due to movement of the wave source while propagating, it was however in 1964 that Yeh and Cummins introduced the idea of velocity measurement using Doppler shift. PDA, as a non-intrusive optical technique with an ability to determine droplet size and velocity simultaneously, with a more rigorous technique which analyse each droplet, and therefore wide spatial resolution is ensured.

4.3.2 Spray Characterization and Measurement grid

The position of the atomizer was centralized about the laser measuring volume and the atomizer was traversed in the radial plane with reference to the measuring volume (optics

fixed). As shown in Fig. 4.8, using a flat fan atomizer, droplet size and velocity measurements were taken at 25, 50 and 75mm at each of the edges as well as the centre of the atomizer exit for the 0.033kg/s, 0.045kg/s and 0.188kg/s (refer to Appendix E) corresponding to 4.8, 6.0 and 10MPa flow pressures. At each downstream location, three radial measurements were taken

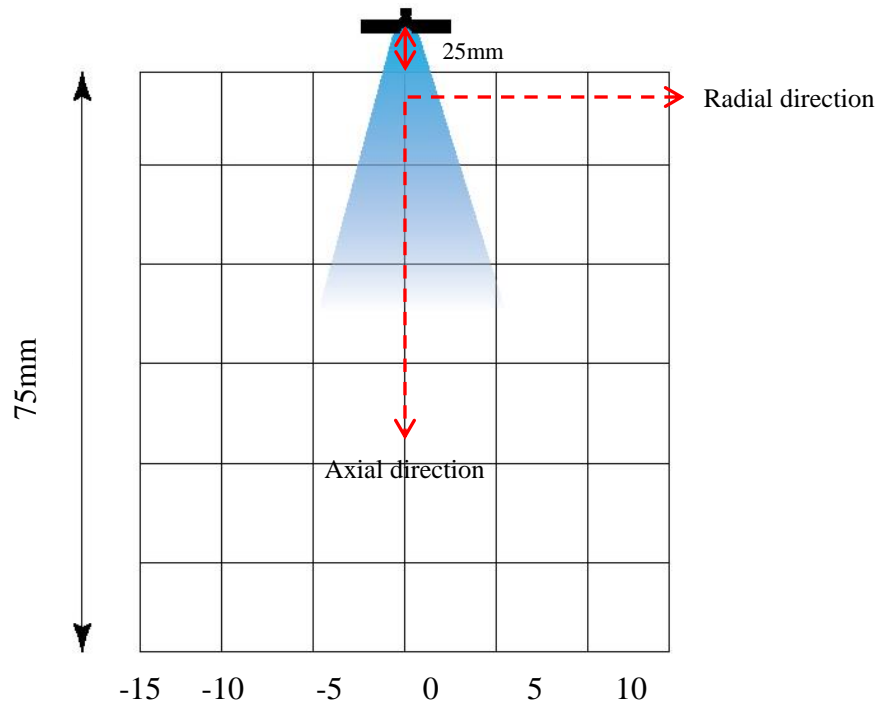


Figure 4.8 Measurement Grid

4.3.3 PDA Experimental procedure

The PDA measurements were carried out to study the structure of an overlapping flat fan spray used one, two and three atomisers at a range of supply pressure 4.8, 6 and 10MPa and downstream distances of 25, 50 and 75mm. The experimental procedures for characterising the spray using PDA was undertaken as follow:-

1. Secure the flat fan atomisers in the spray head and ensure the water supply is connected to the main spray head.
2. Attach the main hydraulic pipe to the pump and also to the head of the spray.

3. The pump was to initially deliver a high pressure of 4.8 MPa through the hydraulic pipe to one atomiser at a flow rate of 8 l/min under three different downstream distances of 25, 50 and 75mm.
4. The experiment was repeated twice for 4.8 MPa, 6.0 MPa and 10 MPa at a flow rate measured through a collection method for three different downstream distances of: 25, 50 and 75mm.
5. The laser is turned on and the crossing of the beams within the measuring volume is aligned using the eyepiece.
6. The laser was set to maximum power.
7. The water feeding the main hydraulic pipe to the spray atomiser was turned on to the desired flow rate.
8. The signal-to-noise ratio is checked for acceptable levels by using the oscilloscope.

The signals received from the three channels PD1, PD2 and PD3 and balanced by altering the supply voltage within the PDA software; to provide signals with equal orders of magnitude.
9. Data acquisitions starts or stops when either 20,000 validated samples were collected or a time out of 300 seconds is reached.
10. The data was saved to a file.
11. The flat fan spray atomiser was traversed to the next radial position and steps 9 to 13 were repeated.
12. Once the radial positions on the plane were taken, the optics is moved to the next downstream position and steps 9 to 13 are repeated until the remaining downstream positions were taken.
13. The data was saved to a file.

4.3.4 Accuracy and error analysis

4.3.4.1 Accuracy in PDA experiment

The transmitting optics delivered two stream of laser rays, although can be more in some cases, with equivalent intensities. These interfere along their path to form a region of measurement volume, this led to the formation of equally spaced fringes. Hence measurement of either the droplet velocities or mean size is done the moment the spray flow particles passes through this fringes. In the case of traversing particles across the measuring volume, shown in Fig. 4.9, there is usually a fluctuation of the amount of light received, causing the fringes scatter in all directions.

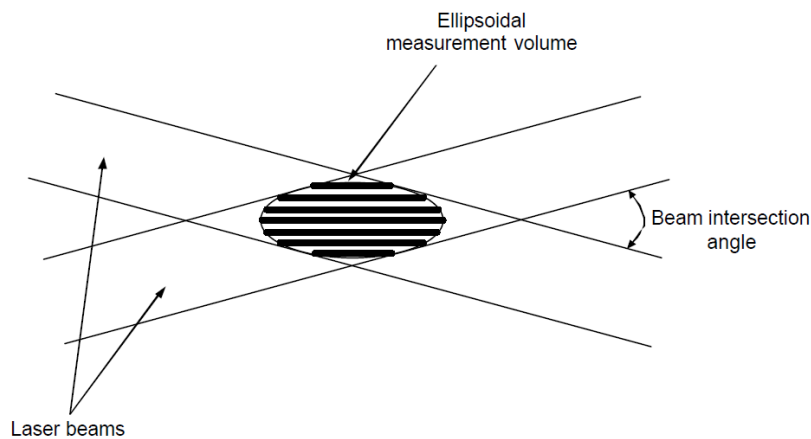


Figure 4.9 Measuring volume[117]

Part of this scattered light can be received by the the lens and then focused to the photodetector measuring the fluctuation burst shown in Fig. 4.10, for light to the voltage signal fluctuation, which is proportional to the particle velocity.

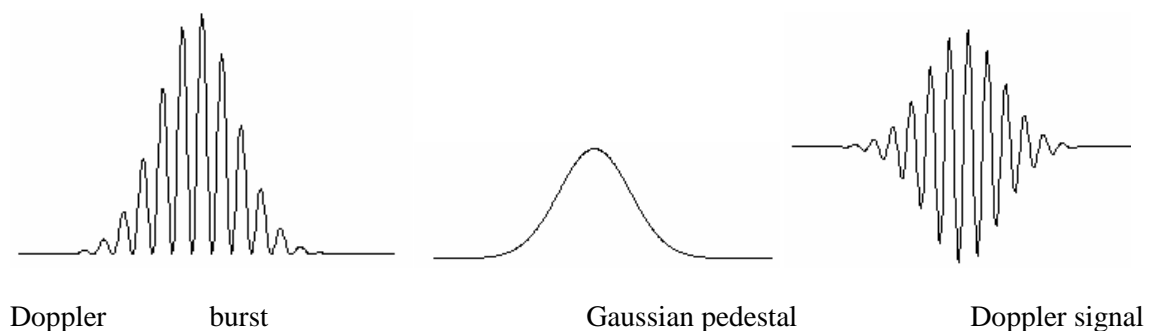


Figure 4.10 Doppler signal burst at measuring volume[117]

This frequency is termed as the Doppler shift, and its frequency can be determined through measurement of the Doppler frequency period, already known the wavelength λ of the laser as well as the angle intersection of two beams, θ , the Doppler frequency, f_D , the velocity U can be calculated using Eq. 4.9

$$U = \frac{\lambda}{2\sin(\theta/2)} f_D \quad (4.9)$$

However, the particle size D can be obtained based on the signals generated from the two detectors for both reflection and refraction shown in Eq. 4.10 and 4.11 respectively

$$\Phi = \frac{2\pi D}{\lambda} \frac{\sin \theta \sin \psi}{\sqrt{2(1 - \cos \theta \cos \psi \cos \varphi)}} \quad (4.10)$$

$$\Phi = \frac{-2\pi D}{\lambda} \frac{n_{rel} \sin \theta \sin \psi}{\sqrt{2(1 + \cos \theta \cos \psi \cos \varphi)(1 + n_{rel}^2 - n_{rel} \sqrt{2(1 + \cos \theta \cos \psi \cos \varphi)}}} \quad (4.11)$$

In order to successfully measure the particle size, the spatial frequency of the interference fringe produced by the scattered light must be known, which could be achieved through use of the photodetector to get simultaneous light from separate part of the interference pattern[117]

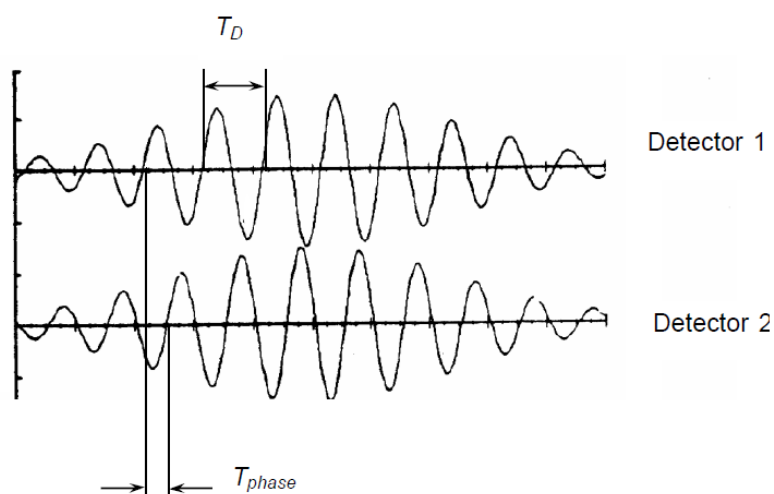


Figure 4.11 Doppler signal from different source[117]

The incidence ray of beam may undergo three different light phenomenon including the initial reflection unto the droplet, then refracted(1st order) through the droplet and finally refracted again(2nd order) shown in Fig. 4.12 according to the refraction pattern.

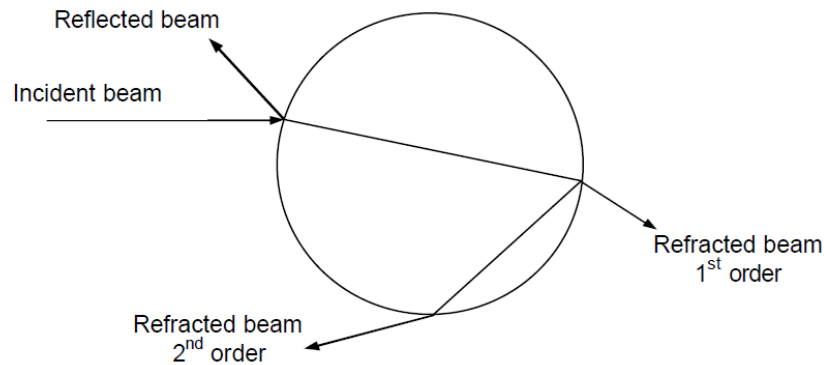


Figure 4.12 Light scattering models[117]

4.3.4.2 Sensitivity analysis

The PDA measurement is bound to a certain margin of error due to either the characteristics of the Doppler itself or the manner in which it is operated. In this investigation sensitivity and precautions were made to ensure accuracy of the results, however, the following factors were bound to cause errors in the measurements.

4.3.4.3 Shape of the particle

Accurate PDA measurements are suitable only for spherical particles, and high pressure water sprays undergo a violent break up scheme as in this case, producing either irregular or deformed particles. The effect of the aerodynamic forces changes the spherical particles to ellipsoidal shapes as shown in Fig. 4.13 as a result of the viscous and turbulent acceleration/deceleration.

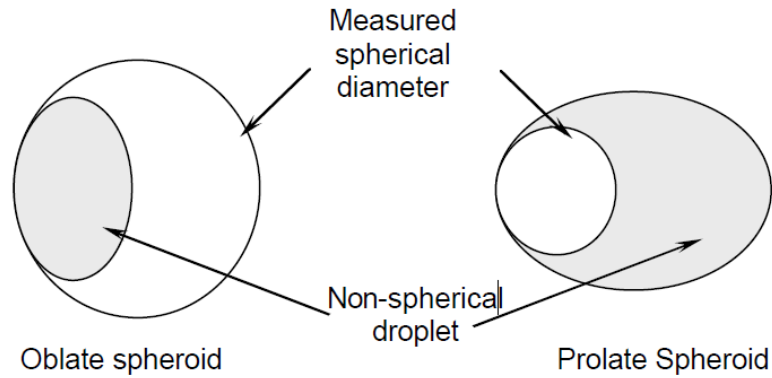


Figure 4.13 Ellipsoidal nature of droplets[117]

The literature suggests up to 45% over estimation in particle size due to non-sphericity[117]

4.3.2.2 Burst signal validation

In a PDA set up, signal passing through photomultipliers usually liberated at three different frequency, each corresponding to a threshold level. For the validation of a signal, it is expected to go beyond level 3 and below level 1 as shown in Figure 4.14

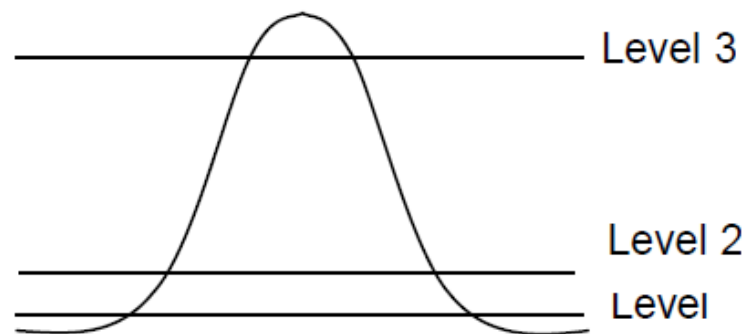


Figure 4.14 Burst validation[118]

4.3.4.4 Biased particle average

The measurement principle in PDA considers the average of the total sample particles passing through the measuring volume each time. This is distinctively different for low and high flow velocities due to variation of flow rate with time around the measuring volume. However, in turbulent flow measurement such as the experiment conducted in this work, averaging the population sample brings over-estimation leading to an error in the results.

4.3.4.5 Effect of slit

The effect limiting slit aperture in the receiver optical probe is often responsible for the suppression effect. The light scattering component considered for the particle size calculation using the measured phase difference is another possible cause of error in PDA measurement. A typical example is indicated in Fig. 4.15 where there is a suppression of the refracted light, exposing only the reflected scattered light become detected and hence used for measurement, which will automatically results in error.

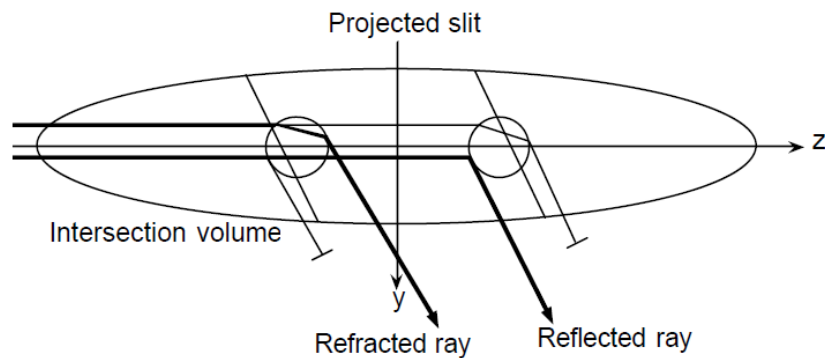


Figure 4.15 Slit effect in suppression scattered light

4.3.4.6 Trajectory ambiguity

A trajectory ambiguity, popularly known as Gaussian beam problem, occurs usually in measuring larger droplet sizes than the beam diameter. This causes non-uniform illumination which subsequently results in mixing of the refracted and reflected beams into the detectors. Usually one overshadow the other one, leading to erroneous results for larger droplets sizes. The effect is shown in Fig. 4.16 as the variation in Gaussian beam effects.

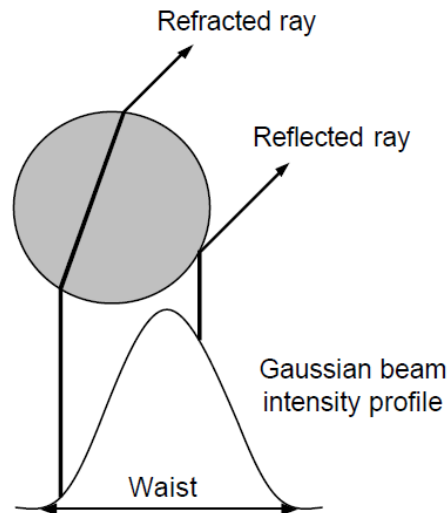


Figure 4.16 Gaussian beam imperfections[117]

4.3.4.7 Sources of Error in PDA measurements

The main systematic errors for the PDA system are due to measuring-volume positioning, velocity bias and doppler-frequency broadening. The random encounters are due to the statistical sampling uncertainty. Throughout the PDA experiments endeavours were made to keep these errors as small as possible. Statistical sampling uncertainty was kept to a minimum by using a sufficiently large sample size (20,000) per measurement data point.

Other systematic errors were calculated as:

- Traversing errors in the x and y direction for various planes downstream was ± 0.5 mm.
- The water supply for the fluid circuit was controlled to ± 2 ml/min.
- An estimated error in diameter measurement of ± 5 μm for the droplet sizes. Typical nominal errors for diameter suggested by the PDA system manufacturer are 4% on diameter.

4.4 Impact Pressure Measurement

4.4.1 Experimental set up

Measurement of impact force is considered as an integral part of this thesis, apart from being the force that dictates how much impact required for the scale cleaning process, also it enable analysis of the distance downstream at which the spray is the most effective cleaning process. The measurement was conducted with a High precision Load cell designed and manufactured by Omega limited, with a capability to sense up to 100N force with a resolution of $\pm 0.1\text{N}$, which can then be converted to pressure by dividing by the unit area covered by the spray. The setup consist of a high pressure water pump, pressure gauge, spray atomiser, and the load cell sensor and the display shown in Fig 4.17 and 4.18.

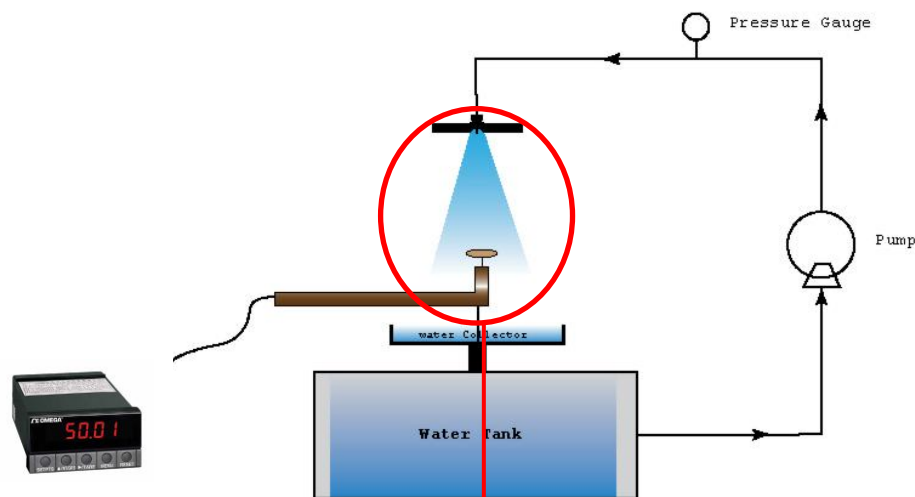


Figure 4.17 Impact pressure measurement set up

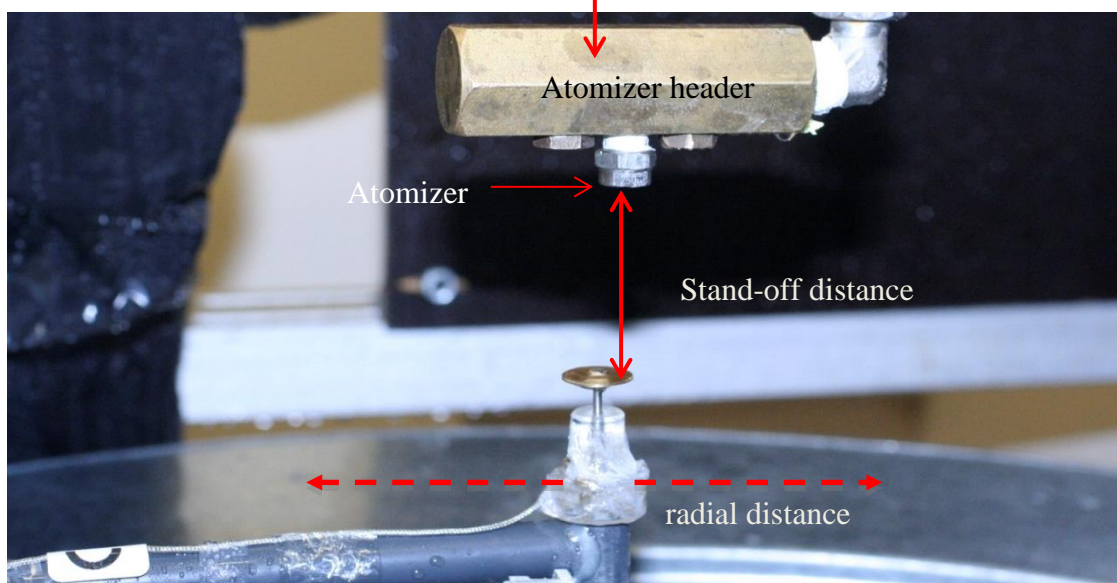


Figure 4.18 Load cell set up

4.4.2 Experimental procedure

The measurement of the impact force was conducted using the test procedure for the impact probe load cell in the following sequence:

1. The load was mounted to a rigid support, pivoted within a given downstream position which connect via a wire to the display screen.
2. The meter was calibrated using a known weight to ensure conformity and the graph was provided in Fig. 4.19
3. The display was then zeroed using the TARED function on the meter, which was checked after the experiment as well.
4. The High pressure pump was then ran until the targeted pressure of 4.8, 6.0 and 10MPa were achieved as indicated on the pressure gauge.
5. The flow was then allowed to stabilize for the first 15seconds.
6. Reading were then taken at each point over a period of 15 seconds and the average value considered.
7. The procededure was then repeated at varying downstream distances and radial positions.

4.4.2 Accuracy and error analysis

The main systematic errors for the impact force measurements were:

- Traversing errors for the downstream and radial distances were ± 0.5 mm.
- The water supply for the fluid circuit was controlled to ± 2 ml/min.
- Force measurements errors were calculated to be $\pm 0.2g$, comprising of the difference in readings between the displayed readings and know weights, resolution of the meter and drift between readings.

The calibration of the equipment was initially conducted to ensure an accurate response and repeatability over a range of forces measured in terms of mass. Although variation is shown in the Fig.4.19 during the calibration, it is acceptable as the difference is less than 5%.

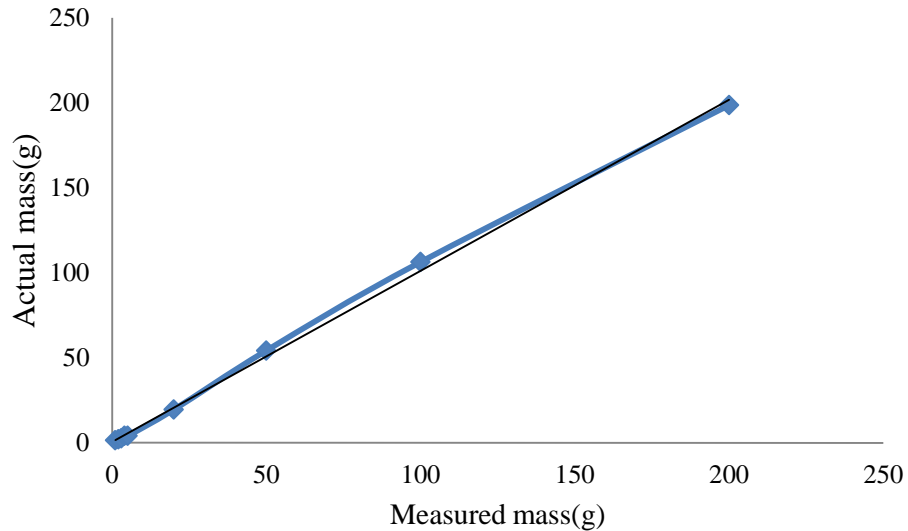


Figure 4.19 Impact force probe Calibration

A mathematical derivation can be used in line with Newton 2nd law of motion to express the impact force by a flat fan atomiser. Details of the Impact pressure theoretical calculations are provided in Section 3.2.4.5 Spray Impact Pressure.

4.5 Cavitation measurements

4.5.1 Experimental set up

The measurement of cavitation behaviour of flat fan atomizers were considered paramount in this investigation due to the erosion attributed to cavitation in scale cleaning. The set up considered an aerated chamber under submerged conditions for suitability to qualitatively measure cavitation bubble regions within 25mm downstream from the atomizer exit. The set up consisted of the aerated chamber filled with water over a shallow column of about 5mm just above the flat fan atomizer exit. A High pressure water pump supplied water to the atomizer via the pressure gauge. The water is collected and recycled through the water tank as shown in Fig. 4.20.

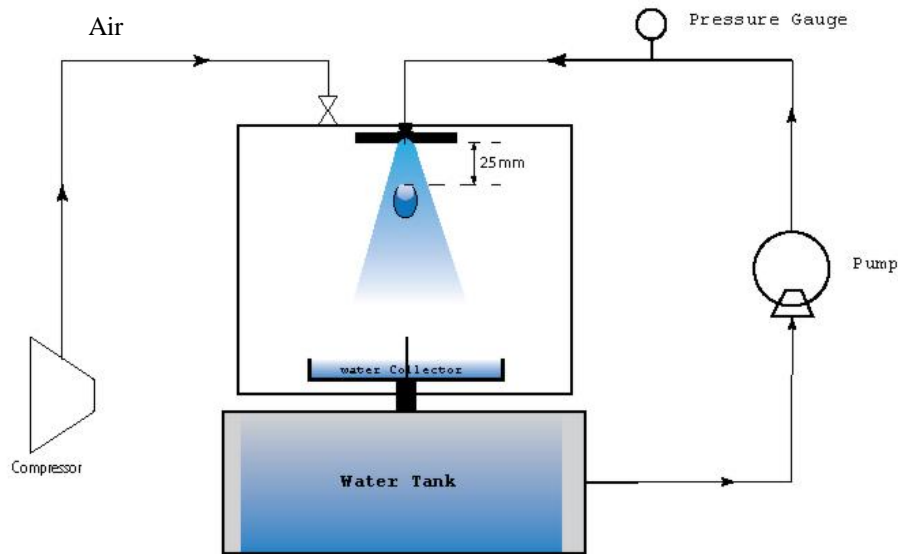


Fig 4.20 Cavitation experimental set up

4.5.1 Experimental procedure

The qualitative measurement of cavitation bubble length was conducted using the following steps:

1. The water level in the aerated chamber is raised to just above the atomizer(submerged), ensuring that the pressure head is not significantly high
2. The pump pressure was then increased to the desired value as indicated by the pressure gauge
3. The air supply was then connected using the isolation valve on the chamber top until the chamber pressure attained the desired aeration pressure(corresponding to the desired air concentration)
4. The cavitation bubble length is then photographed using a high resolution camera positioned from the same point throughout the experiment.

4.5.2 Source of error in cavitation measurement

1. A partial submerged condition is generated to ensure visibility of the bubble under this condition, which cannot be qualitatively measured otherwise due to the turbulent nature of the high pressure sprays.
2. The water level was kept just 5mm above the atomizer header to ensure no significant pressure head is acted upon the chamber due to the water column.

3. The water pressure fluctuation was maintained within $\pm 0.1\text{MPa}$
4. The air pressure fluctuation was maintained at $\pm 3\%$ of the actual air pressure

4.6 Scale Removal Set-up

4.6.1 Experimental set up

The measurement of scale erosion was conducted with the same aerated chamber set up in addition to including the scale sample clamped into the fixed position as shown in Fig.4.22. The experimental set up was designed to simulate realistic onshore oil and gas production tubing to suitably perform the test. The scale erosion experiment was set up as shown in Fig. 4.21 with (1) An air compressor to supply the aeration to the chamber, which will then be measured based on the air flow (2) A pressure gauge in order to calculate the aeration concentration into the chamber, (3) A simulated pressure chamber containing the scale sample, which is measured before and after each of the experimental trial. Water supply from the (6) High pressure pump, which passes through the (5) Pressure gauge for pressure and flow calculation. The Air and water are discharged out of the chamber using (7) Flow control valves, and then in the case of pressure build-up, (4) A relief valve is opened to restore normal operating conditions.

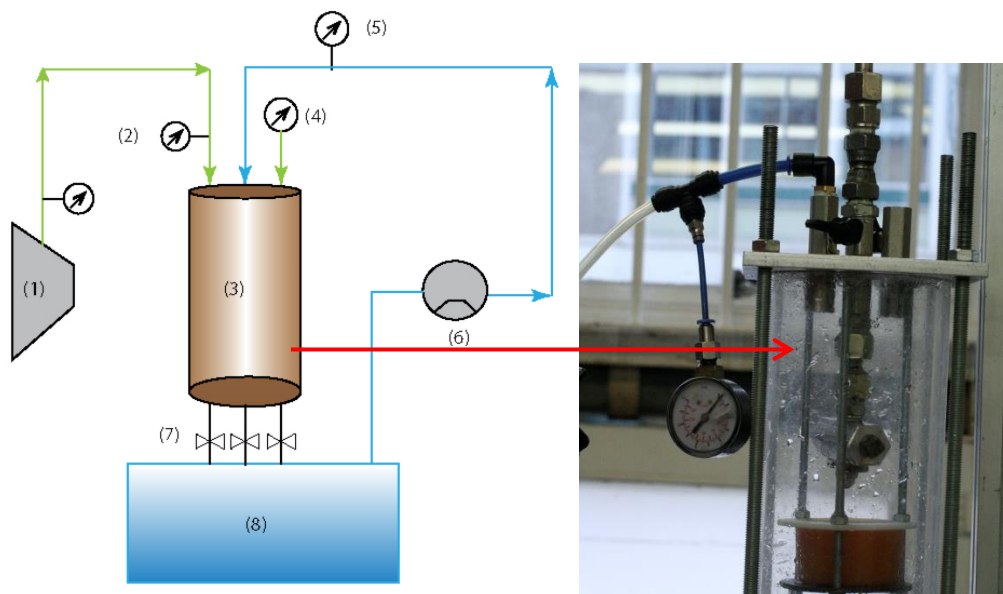


Figure 4.21 Descaling chamber set-up

4.6.2 Pressure Chamber Design, Construction and Set up

4.6.1.1 Design philosophy

Scale deposits are usually found at bottom hole along production tubing's several thousands of meters down the surface Christmas tree, since pressure increases with depth, a realistically high pressure chamber is necessary to understand the performance of the jetting technique with respect to scale removal and other properties of the jets especially impact forces, cavitation and erosion possibilities. The chamber model design is shown in Fig. 4.22.

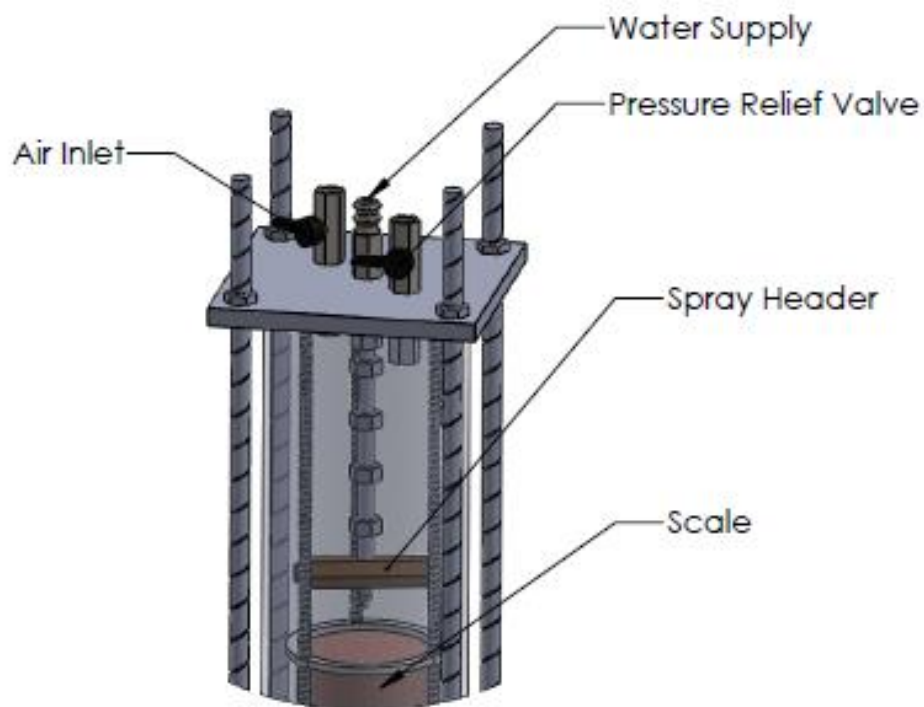


Figure 4.22 Design of the chamber

4.6.1.2 Design of aerated chamber

The material of construction selection was based on the ambient operating conditions of the chamber, since the pressure chamber requires holding higher pressure than the ambient, it was necessary to estimate the pressure rating of the chamber first, before deciding the type of material suitable. The various inner and outer components of the aerated chamber is shown in Fig. 4.23 and 4.24.

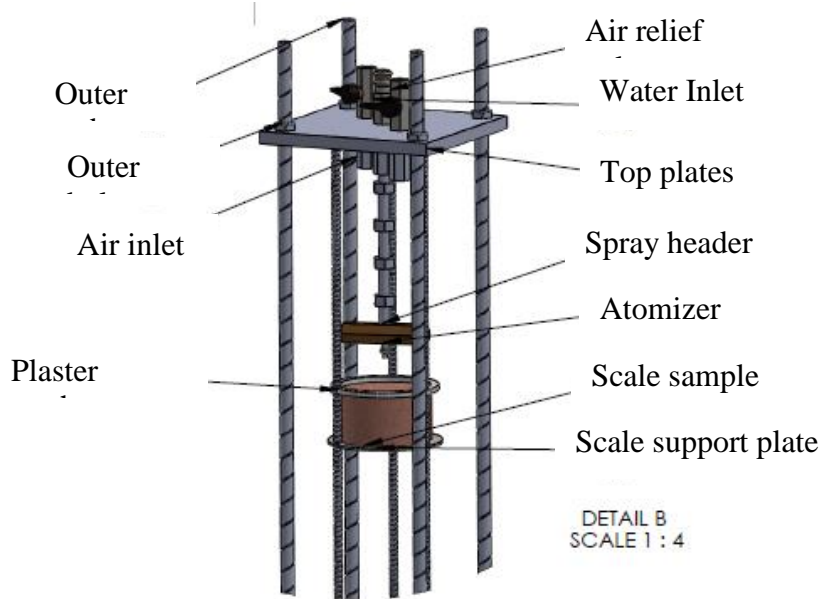


Figure 4.23 Interior section

The set-up consists of Outer rods, Top plates, Outer bolts, Inner rods, Scale sample, Scale support plate, Plaster washer, Air inlet valve, Air relief valve, Spray header, Water atomizer

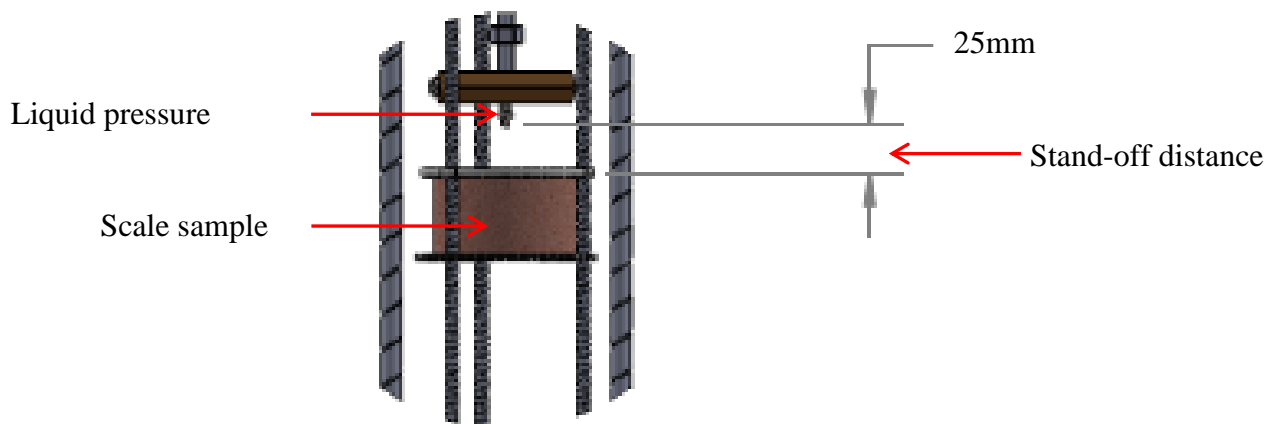


Figure 4.24 Scale holder details

The next section provides details of the plenum design used to hold and position the liquid pressure atomizer.

Plenum design

The atomizer header was re-designed to ensure minimum pressure loss with the inlet directly from the top instead of the previous set up shown in Fig.4.18, with the water inlet at the edge leading to higher pressure losses. A detail of the modified atomizer is provided in Fig. 4.25.

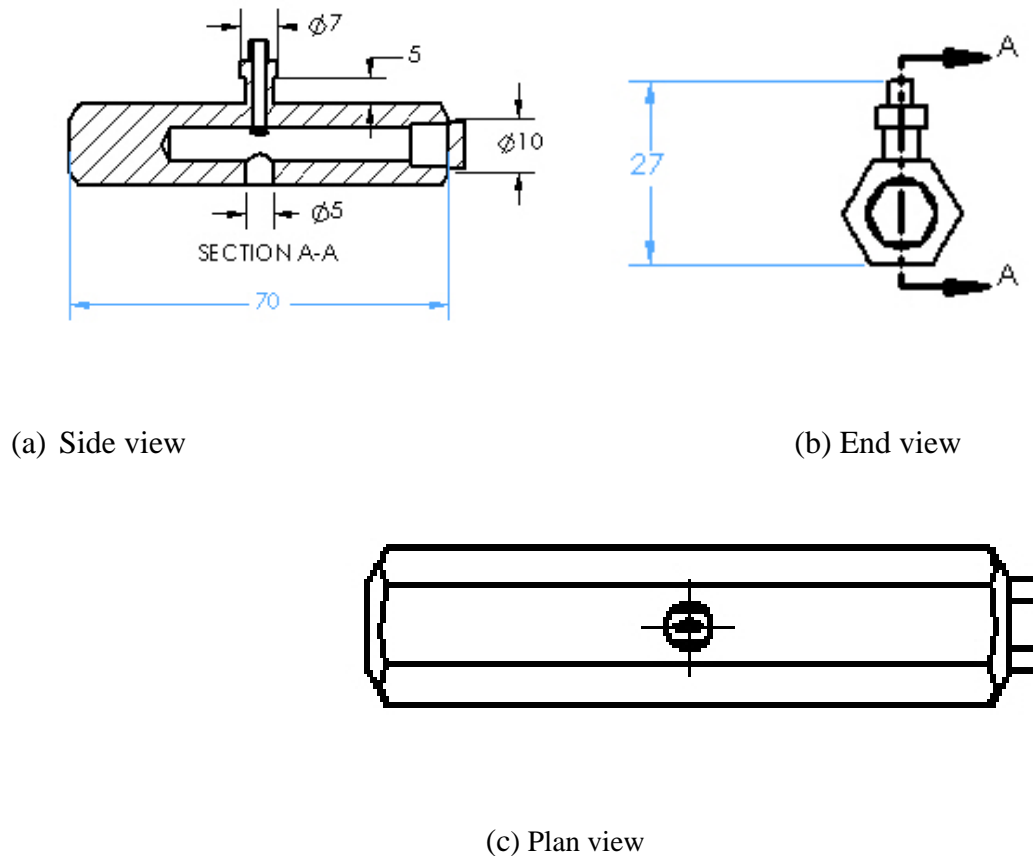


Figure 4.25 Atomizer plenum design

The pressure calculation was performed based on the ambient air pressure along the production tubing estimated to principally increase with depth as the major contributory factors, therefore using the pressure equation as:

$$P = \rho gh \tag{4.12}$$

Where P , is the bottom pressure, ρ the density of air along the empty column of production tubing during maintenance, g , as the gravity, and h , the depth to the scale formation. Taking the density of air as 1.224kg/m^3 , g 9.8m/s^2 and an approximate depth of 2000m , then

$$P = 1.224 \times 9.81 \times 2000 = 23,990.4 Pa = 0.24 bar \text{ _ gauge}$$

$$P = 0.24 + 1.013 = 1.25 bar \text{ _ absolute}$$

Having calculated the expected pressure along the tubing, despite the much availability of many materials capable of handling this pressure, a transparent acrylic tube was then chosen based on its pressure rating of 6 bar (maximum) and transparency to enable imaging the experiment and recording the observations.

4.6.1.3 Volume and Residence Time Calculations

The diameter of the chamber was based on the typical oil and gas production tubing by Saudi Aramco. As 4.5 inch (114.3 mm), then vendors specification of the diameters were available for selection. Table 4.2 provides the detail specifications.

Table 4.2 Clear acrylic tube vendor's specifications

Clear Acrylic Tube				Price
Reference	OD	ID	Wall thickness	£/Mtr
120/114XT	120mm	114mm	3mm	19.55
120/110XT	120mm	110mm	5mm	31.64
125/119XT	125mm	119mm	3mm	20.22
127/121XT	127mm	121mm	3mm	21.83
130/124XT	130mm	124mm	3mm	20.95

The appropriate diameter was chosen as the maximum thickness of 5mm (120/10XT) for this experiment, also it is similar to the intended 114.3mm as required.

The residence time calculation of the tube was then conducted which was used as a basis for a selection of a convenient length of 1m as available with the manufacturer,

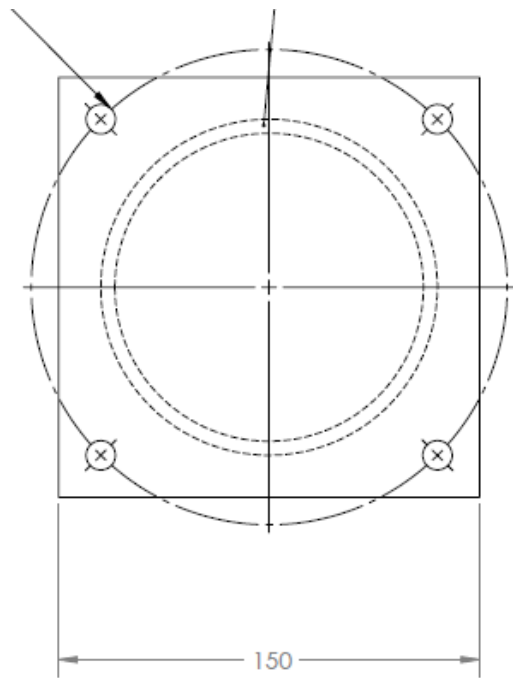
$$V = \frac{\pi d^2 l}{4} = \frac{\pi (0.11)^2 \times 1}{4} = 9.5 \times 10^{-3} m^3 = 9.5 \text{ litres} \quad (4.13)$$

Taking the flow rate of the flat-fan nozzle at 10MPa as 11.3 liter/min

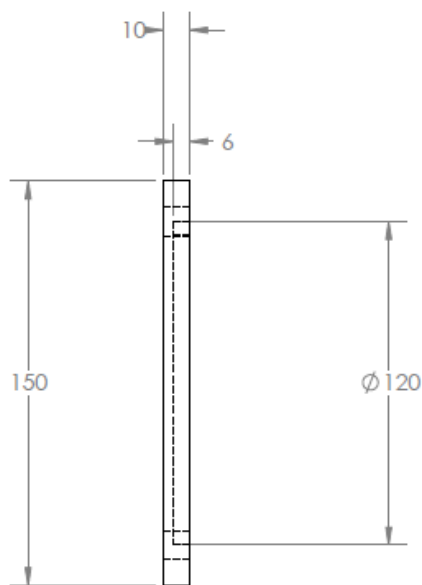
$$\text{Residence time of water} = \frac{\text{Volume}}{\text{Volumetric flowrate}} = \frac{9.5}{11.3} = 0.84 \text{ min} = 50 \text{ sec}$$

4.6.1.4 Chamber plate design

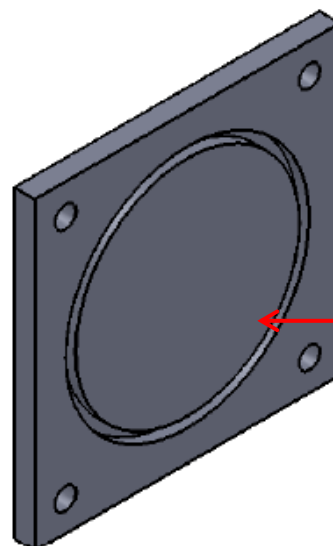
The design of the metallic cover plate was an integral part of the aerated chamber which connects holds and supports almost all the equipment attached to the chamber. A details of the design and construction of the chamber plate is shown in Fig. 4.26 and the top and the bottom plates assembly are shown in Fig. 4.27.



(a) Plan view

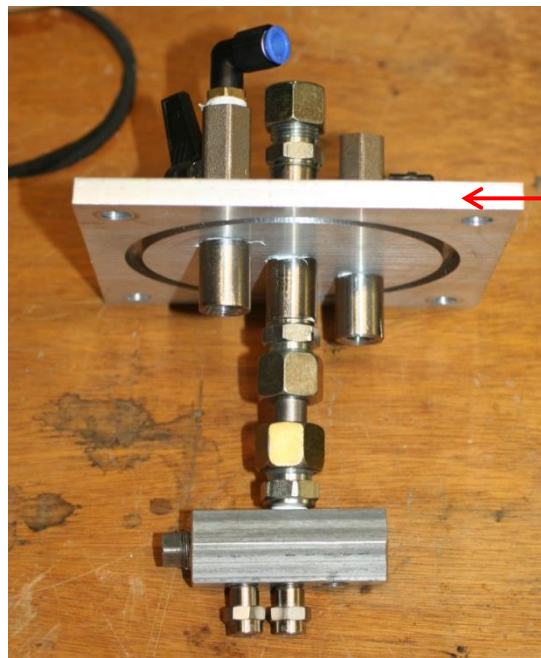


(b) Side view



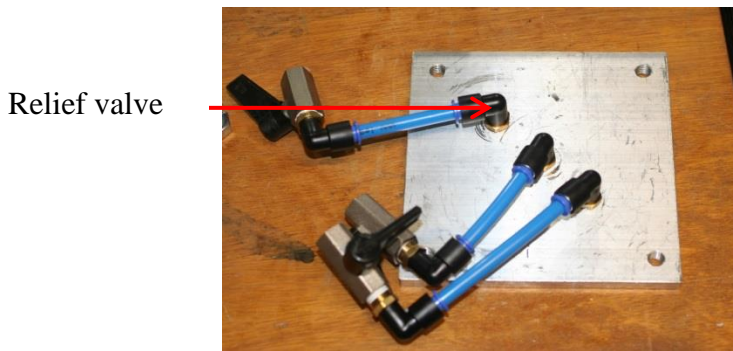
(c) 3D view

Figure 4.26 View of metallic cover



Assembled plate

(a) Top cover



Relief valve

(b) Bottom plate(outside view)



Outlets

(c) Bottom plate(inside view)

Figure 4.27 Assembled views of metallic cover

The metallic plate, water inlet, air inlet, relief valve, atomizer header as well as the scale made up the assembly. The assembly positioned suitable for positioning directly into the chamber as shown in Fig. 4.28. The pressure gauge and water connectors are made to be easily fitted into the assembly during the experimental trials.

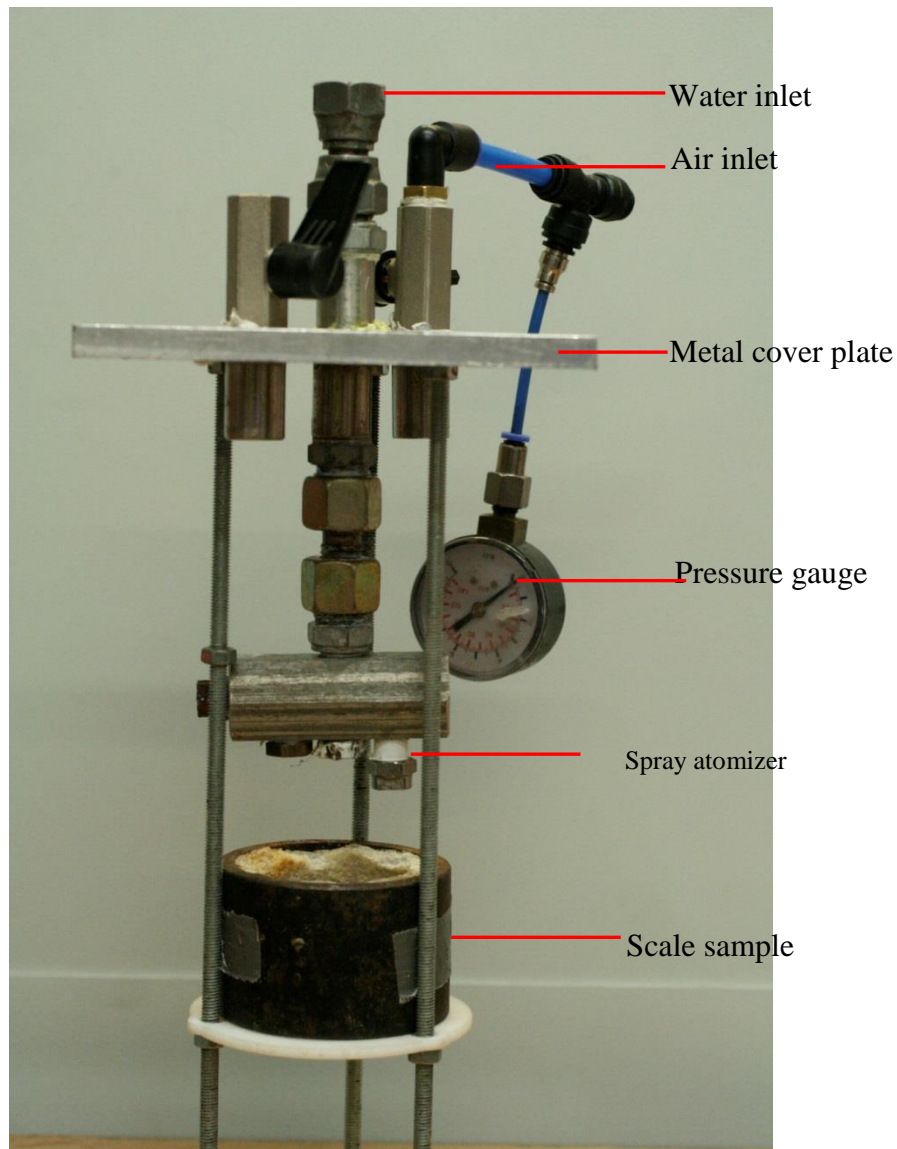


Figure 4.28 Scale sample assembly (without chamber)

4.6.3 Soft scale samples preparations

4.6.3.1 Introduction

The samples used in this investigation consist of three components that are typically similar to the scales encountered during oil and gas production. They includes the wax scale encountered when producing highly paraffinic hydrocarbons characterised with low API gravity. Although this scale sample is typically found on top-side facilities, it may be encountered along production tubing especially around the Christmas tree due to condensation of heavier hydrocarbons. Two other scale samples involve the real sample of oil field scale obtained from Libyan wells.

4.6.3.2 Wax scale preparations

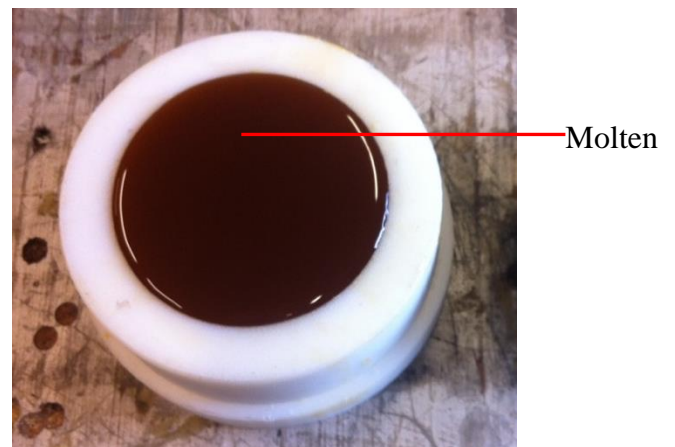
The sample of the wax scale was prepared using a wax material which was fragmented and melted and then inserted through a suitably designed holder to provide an appropriate shape, using a suitable material that can withstand the melting temperature as shown in Fig.4.29, 4.30 and 4.31



Figure 4.29 Scale holder



(a)



(b)

Figure 4.30 Wax scale preparation(a) empty holder (b) hot-filled wax



Scale in holder

(a)



Wax

(b)

Figure 4.31 Prepared wax scale samples (a) after cooling (b) prepared samples

4.6.3.3 Hard scale samples

The harder real scale samples used in the investigation were obtained from Libyan wells shown in Figure 4.32 in order to realistically investigate with the harder scale types typically encountered in petroleum production.



Hard scale

(a)



Medium scale

(b)

Figure 4.32 Scale samples (a) Hard (b) Medium

The combination of the scale and apparatus were assembly as shown in Fig. 4.33

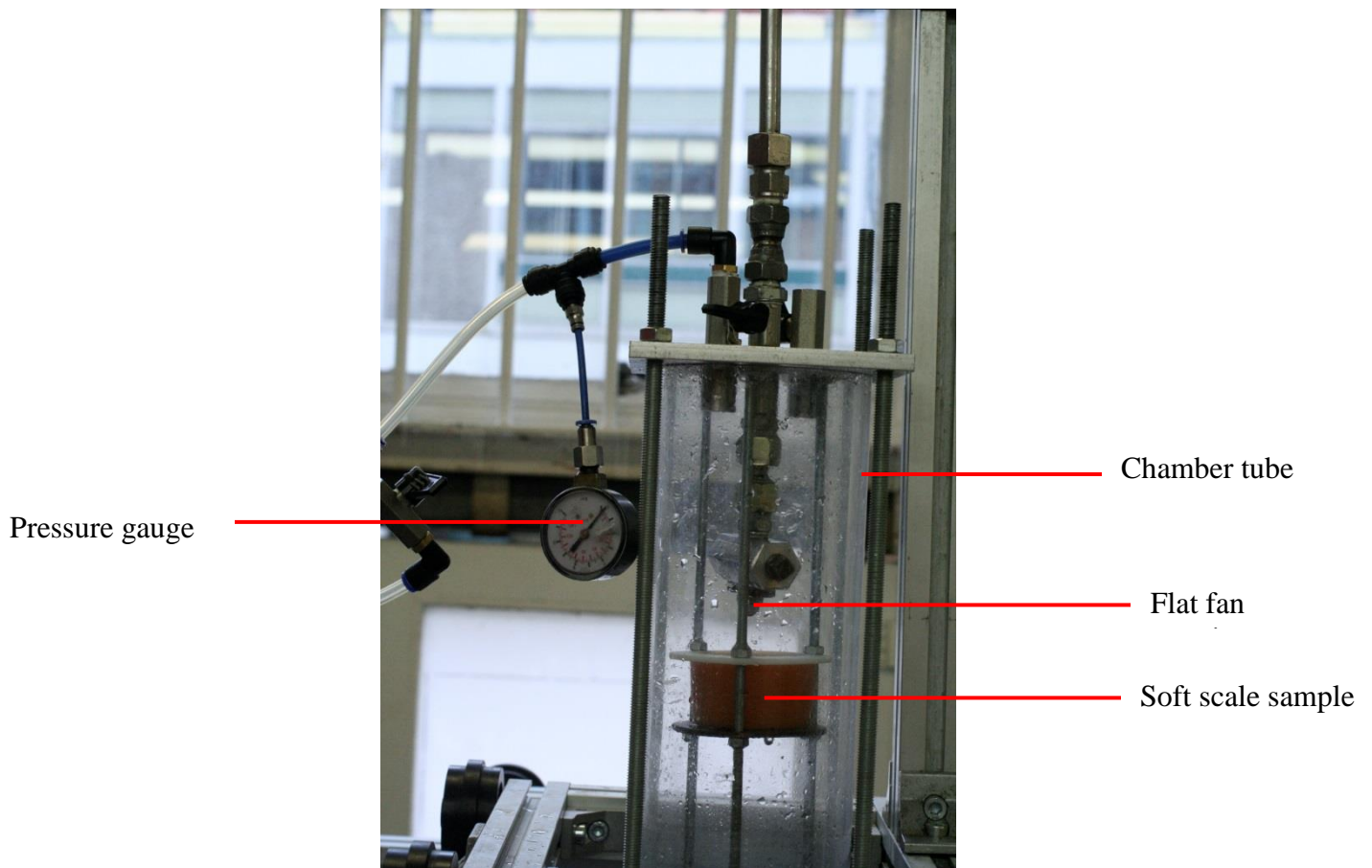


Figure 4.33 Chamber assembly

4.6.3.3 Experimental Procedures for Scale Removal

Prior to starting the experiment, there was the need for ensuring the safety, reliability of all equipment and devices used, during each test run. To prepare the candle wax for the experiment; the wax was first heated in a steel rectangle pan in order for it to take the shape of the pan. After cooling, the scale sample was placed and secured in the upper transparent Perspex tube of the experimental apparatus. This methodology was adopted only for the candle wax, as part of initial preparation for the scale removal trials.

The general experimental procedures are as follows:

1. Ensure all connections are appropriately situated, i.e. spray head, water tank and water pump.
2. Ensure that the scale sample placed on the aluminium base flange and secured in position.

3. Ensure that the spray head is adjusted to the required downstream distance from the scale sample.
4. Ensure that the scale sample with the aluminium base assembly was correctly placed to coincide with the vertical axis of the atomiser, fitted to the spray head.
5. Ensure that the water pump was primed to release air bubbles by turning on the pump.
6. Ensure that the inter connection of the hydraulic hose from the water pump to the spray head and to the water tank back to the pump is connected properly and firmly.
7. The image of each scale sample was taken, using a still Canon camera, before and after each test run.
8. The water pump was turned on first, at an initial low flow rate 8 l/min. and pressure 4.8 MPa, and then adjust to obtain the desired flow and pressure.
9. After 5 minutes with the aid of a stopwatch, the water pump was switched off. Then the particles of scale were collected from the scale sample through a sieve, positioned on top of the water tank.
10. The particles of the scale sample passed through the sieve were dried and weighed with a weighing scale (range \pm (0.1g)).
11. The image of the scale sample was taken again after each test run.
12. The procedure above was repeated for desired pressures of 4.8 and 6 and 10 MPa at the desired flow rate Flat fan spray atomisers respectively for 5 minutes each.
13. Record the different reading of each test run of the experiment for further analysis.
14. Repeat and apply all the above procedures on different scale samples
15. Repeat and apply all the above procedures on the Candle Wax Scale Sample

4.6.3.4 Safety Precaution

Safety and environment are the main concern at this point, they are the most significant risks that require severe attention and improvement in our world today. *Safety* measures are actions and *precautions* engaged to enhance *safety*, i.e. decrease risk associated with human health.

The safety precautions taken in during the trials are as follows.

1. All fittings and installations were properly verified and tightened to avoid a loss in pressure via leakage.
2. Circuits breakers were installed to avoid equipment damage, which could arise

from surplus voltage.

3. The different units of the apparatus were kept in their proper position in order to function correctly to their maximum efficiency.
4. The water tank was filled with water to the required maximum water level.
5. The power supply was switch off to the water pump after usage.
6. Personal protective equipment was worn as well as safety gloves and ear protection to avoid harm or injuries to the operator.
- 7 A Fire extinguisher was available in case of fire.

4.6.3.5 Qualitative technique

Various forms of imaging devices were used to capture and record all tests procedures. The Cannon Eos Kiss F was used to take stills of the testing process. An 18-55mm 1:3.5-5.6 IS zoom lens was used to take close-up images with a resolution of 3456 x 2304 pixels, as shown in Fig. 4.34. Images taken during drop size, velocity and mass flux tests were all recorded from a distance of 300 mm. It was set to 1280 x 1024 resolution during all of the tests. All high speed imagery was captured at downstream distances of 25, 50 and 75 mm.



Figure 4.34 Canon Eos Kiss F

4.6.3.6 Source of Errors in the Scale Removal Test

1. The high pressure pump (500bar maximum) was operated within a tolerance of ± 1 bar
2. The pressure differential was kept constant by adding the chamber pressure during the aerated test due to increase in back pressure in the pressurized chamber.
3. The possible Laser Traversing error during the PDA test positioning (Y-direction) of the spray head in the downstream distance at the measuring volume were kept within ± 1 mm.
4. The measurement for the mass of the scale recovered during each test was kept within ± 0.1 g to account for the mass of water soaked by the scale during the experiment which could not be dried off due to time constraint.

4.7 Summary

The methodology of this investigation followed a sequential approach to scale removal using the following scheme:

- Due to environmental and cost benefits, the application of high pressure water sprays in aerated medium was solely adopted to replace the use of solid particles in combination with the water currently utilized for industrial scale removal.
- The analysis of the aeration system was conducted using a Hot Wire Anemometer to measure axial and radial velocities of the entrained-air around the spray.
- The water spray was then characterised using PDA to establish the drop size and velocities at a selected stand-off distance of 25, 50 and 75mm downstream of the atomizer.
- The cavitation investigation was conducted qualitatively to confirm the position of scale removal in this investigation was not prone to cavitation, and therefore scale erosion was purely due to impact of the sprays and not cavitation bubble collapse.
- The scale removal trials were conducted at the characterised conditions of the spray in terms of drop sizes and velocities, in addition to the air envelope which was meant for increased stress on the scale in addition to the spray impact pressure during the removal of the scale.

The next chapter provides the results from the various experiments in this chapter, as well as the analysis. The results are presented in the same manner in which the experimental description followed as shown in Fig 4.1.

Chapter 5

Results and Discussions

5.1 Overview

This chapter introduces the results obtained from the experimental investigation conducted according to the scheme set out in Fig. 4.1. According to the original target of this investigation, in utilising aerated high pressure water sprays for cleaning mineral and organic scale deposits across an oil production tubing. Prior to the scale removal trials, both the velocities of the entrained-air around the high pressure water spray was measured using hot wire anemometer, and the high pressure water was characterised using PDA in terms drop size, velocities as well as Impact pressure distribution using a pressure transducer probe to enable establishing the scale cleaning conditions and target stand-off distance from the atomizer exit to the point of impact over the scale surface. The results are categorized into sections (phases) in which the experimental sequence followed:

- Phase 1: Characterizations of air and high pressure water sprays: Section 5.2 highlights the measurement of the air velocities axially and radially using a two component hot wire anemometer and the resultant velocities were then tabulated according to Eq. 4.1. The spray characterization was performed using PDA then followed at similar grid measurement point as the air velocities. The droplet sizes in terms of SMD, and the velocities were then tabulated. The impact pressure results from the spray at the designated PDA and air velocities were also recorded, and analysed as the principal erosion impact force for the scale removal trials. The results are given in Section 5.2.2.1.
- Phase 2: Cavitation along flat fan atomizer is measured qualitatively using imaging techniques, as detailed in Section 5.3. The measurement of the cavitation bubble region length is important to establish the region of spray cavitation as a function of increasing aeration concentration in order to ensure applicability of the aerated spray erosion results in wells of realistic depth of thousands of meters where cavitation does not exist.
- Phase 3: The scale removal trials of the non-aerated and aerated chamber were analysed and the results presented in Section 5.4 using the characterized spray conditions around the measured air velocities. The validations of the results were also conducted using Fluent-CFD in Chapter 6.

The next section provides details of the entrained air analysis obtained in Section 5.2.

5.2 Entrained-Air Velocities Measurement and the High Pressure Water Sprays (Phase-I)

5.2.1 Entrained-air velocities analysis

The measurement of the entrained air velocities (aeration) is an integral part of this noble investigation as the combined application of aeration and high pressure water sprays are utilised for scale removal in oil production tubing. The measurement of the air velocities around the spray was conducted according to the grid set-up around the spray as shown in Fig. 5.1, in order to establish the air behaviour around the high pressure water sprays.

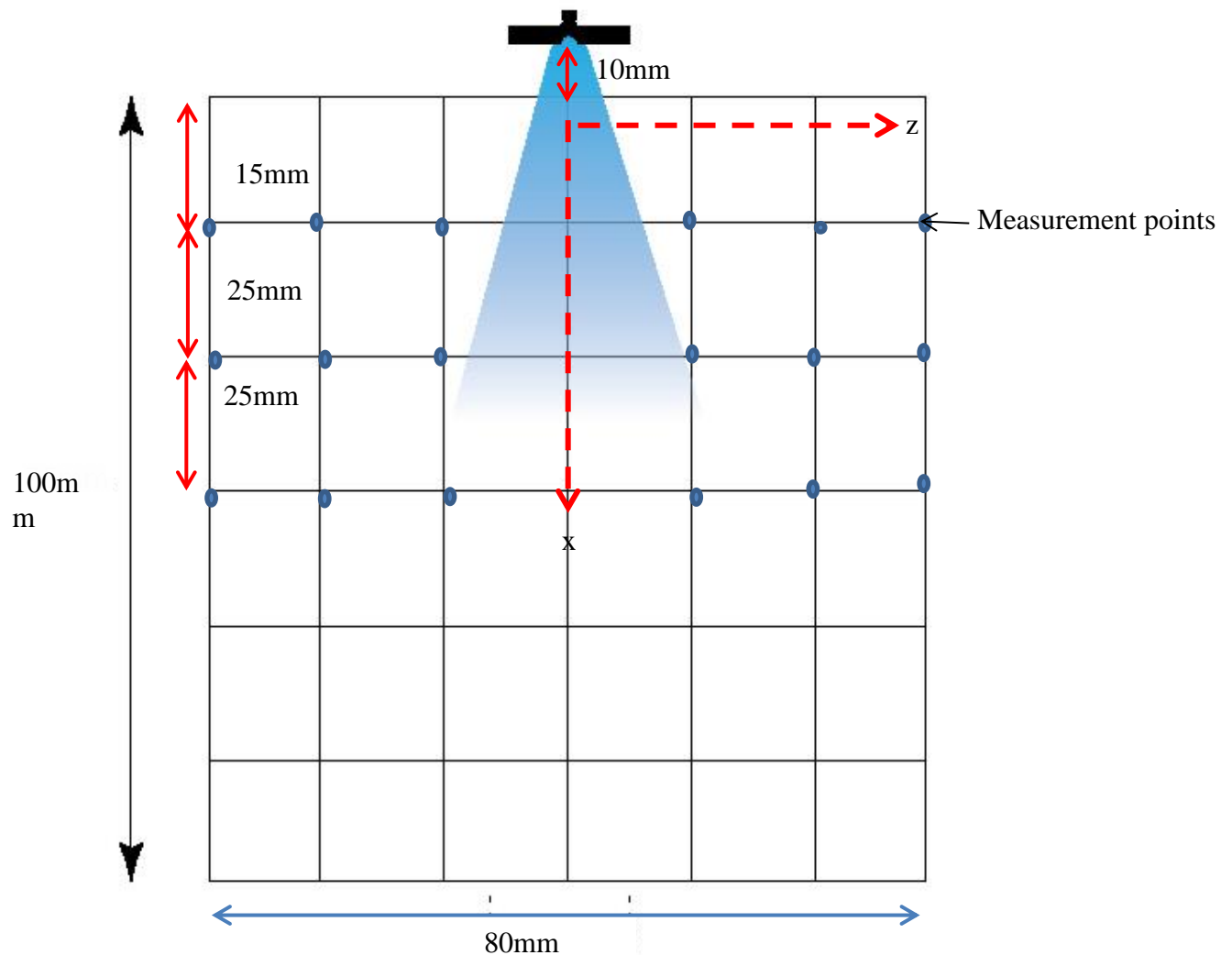
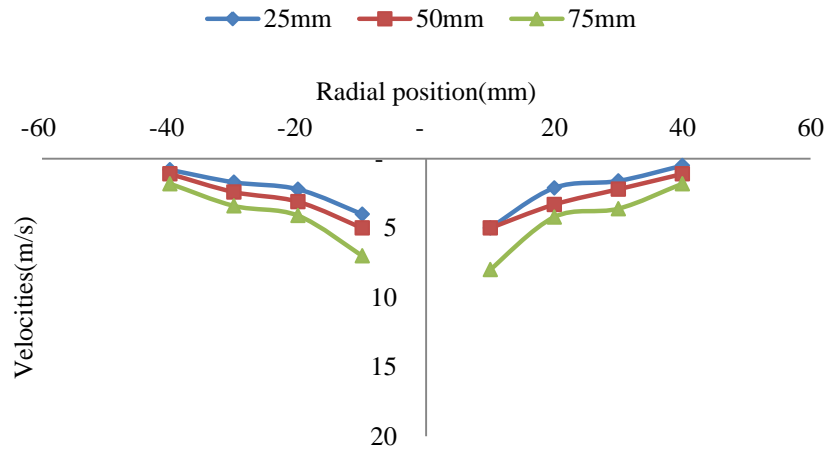


Figure 5.1 Entrained-air measurement grids

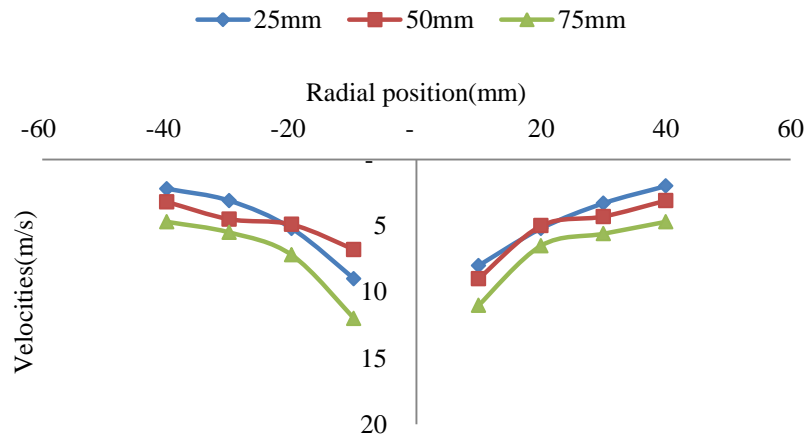
Adopting the grid system around the sprays, measurements of the air velocities were taken at the axial positions of at $x = 25, 50$ and 75mm downstream of the spray and the radially outwards positions $10, 20, 30$ and 40 and then $-10, -20, -30$ and -40mm .

Several researchers have considered the entrained-air around spray jets, particularly for water jets, with emphasis on the mass flow rate of the air around the spray [119]. This investigation consider employing the entrained-air behaviour around the sprays region to both understand the air behaviour around the break-up regions and then utilised the structural benefits of weakening solid structures upon contact with air [89 and 100] as applied to dam constructions, to provide a novel approach in the oil industry existing problems relating to scale cleaning, to which, little or no contributions has been made in the velocities profile measurement for the entrained-air behaviour around the sprays.

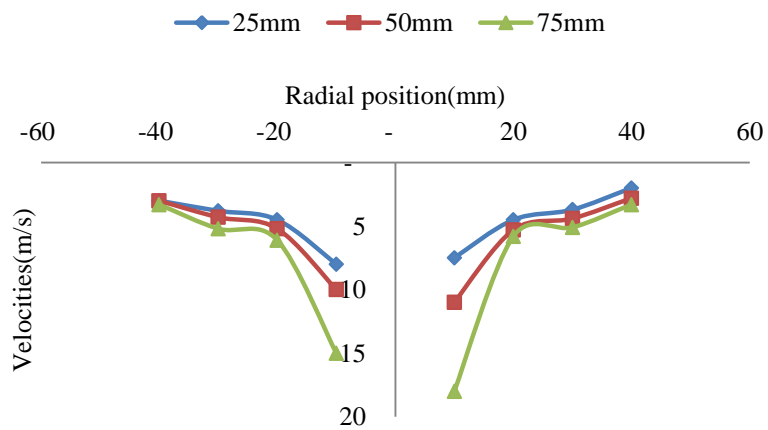
Additionally, the understanding of such interactions will add significantly to better understanding of the behaviour of spray break-up, especially in turbulent flow atomization applications. Previous work relates to air entrainment applications in dam spill ways, [120],[121], while others consider such applications as the combustion of fuel spray in air streams, [122],[123]. Currently, to the best of the current author's knowledge, no-one has attempted utilising the air velocities behaviour for scale cleaning applications. Therefore, most of the reported results in this investigation could not be compared with other research. Entrained air gained velocity as a result of its interactions with the high pressure water sprays as the water spray runs through a stagnant air stream and causes displacement of the air by the water which, when continuous flow continuous is maintained, a stream of air flow continuously around the water. The velocity measurements as indicated in Fig. 5.2 show the increasing manner of the air velocities with increasing axial distance solely due to the corresponding increasing in spray width, despite the turbulent fluctuation of the air velocities due to the high pressure nature of the sprays. The air velocities also substantially decays away from the spray centre from values of up to 14 and 7 m/s down to nearly 3 and 0 m/s at 4.8 and 10 MPa respectively as shown in Fig. 5.2(a, b and c) at the far edge of the sprays, located $z = 40\text{mm}$.



(a) 4.8MPa



(b) 6.0MPa



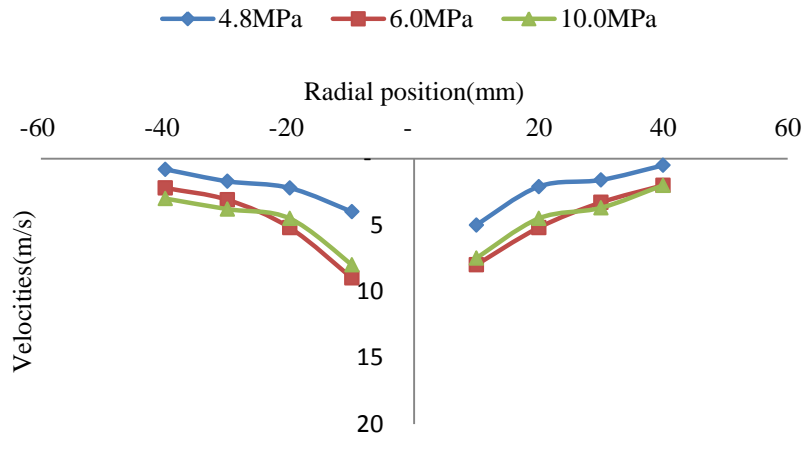
(c) 10.0MPa

Figure 5.2 Entrained-air velocities at various downstream positions

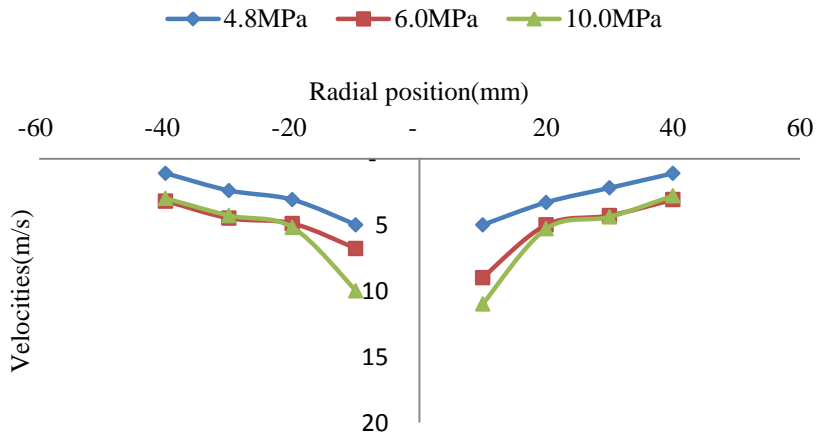
However, the results do not indicate a substantial interaction between the entrained-air and the high pressure spray break-up, although the behaviour shown indicates that the two streams depend on each other. This is confirmed by increasing the axial spray inlet pressure at each of the axial positions, which indicated a linear relationship between the water spray velocities and the entrained-air velocities. Furthermore, the design nature of the hot wire anemometer senses two directional velocities corresponding to x and y directions which record u and v velocities respectively upon positioning the anemometer sensor in either of the two directions. As a result, the tabulated results combined the magnitude of the resultant velocities in two-directional axis u and v performed and the resultant air velocities were computed using the Eq. 5.1.

$$U = \sqrt{u^2 + v^2} \quad (5.1)$$

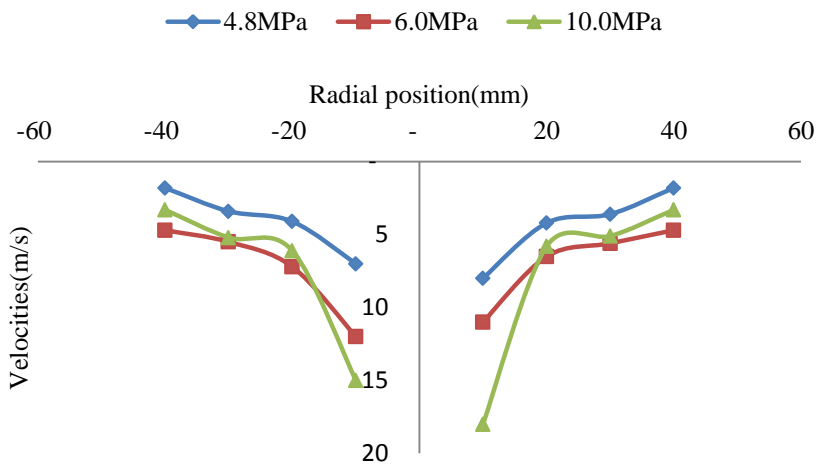
The investigation consider the varying the flow rate of the water through a range of pressure from 4.8MPa, through 6.0 and 10MPa corresponding to a liquid flow rate of 0.133, 0.145, and 0.188kg/s, respectively, which effectively causes an increase in aerodynamic forces due to flow pressure increase as shown in Fig 5.3(a, b and c), and subsequently led to the velocity increases. Although, at 4.8MPa spray pressure, there exist a wider margin compared to the velocities observed at 6.0 and 10MPa because the water sprays droplets undergo deceleration further downstream[124] especially when the buoyancy effect of the smaller droplets carried by the heavier spray droplets compensate the combined gravitational, drag and downward pulling forces by the heavier drops[64]. Similarly, increasing the spray injection pressure facilitates atomization to produce more smaller droplets, thereby decreasing the drag effect by the larger and heavier drops, and hence lesser influence on the air drag tendencies leading to insensitivity to air velocities increase despite the increasing pressure as typically observed in Fig 5.3(a, b and c) at 6.0 and 10MPa. Indeed, it is becoming evidently clearer that nature of sprays droplets sizes and velocities plays an important role in understanding the air behaviour around the sprays and vice-versa. Hence, characterization of the high pressure water sprays using PDA technique become the next analysis in order to give detailed sprays droplet distribution while employing same technique for descaling oil wells. The next section 5.2.2 provided a highlight of the analysis of the droplet size and velocities.



(a) 25mm downstream



(b) 50mm downstream



(c) 75mm downstream

Figure 5.3 Entrained air velocities at various injection pressures

5.2.2 Spray Characterizations Measurement using PDA

In trying to highlight the relevance of the air velocities distribution relating to the spray droplets distribution, it became relevant to establish the droplet size and velocities distributions across the water sprays in order to ensure that their combination provide a suitable approach to descaling oil wells as mention in Section 5.2.1. This section employed the use of non-intrusive PDA measurements for the droplet size and velocities distribution of the high pressure water sprays.

5.2.2.1 Spray droplet size distribution

A drop size analysis was conducted as part of this investigation to enable the impact distribution of the flat fan nozzle to be established. This time unlike the air velocities distribution, the measurement positions is attached to the water sprays for both the droplet size and for the velocities along the spray width. As the target of this investigation relies on achieving conditions and positions of higher impacts, it is obvious that the droplet size be measured along the positions of expected impact on the scale surface. Hence, the measurement target position where the cleaning trials are proposed to be conducted as shown schematically in Fig. 5.4, utilising the laser beam as part of the PDA in achieving the measuring volume.

The drop size measurement has been categorized into different types, the most frequent being the Sauter Mean Diameter(SMD) in spray characterization, especially such instance like spray impact where properties of water as the atomized liquid and the geometry of the nozzle play an important role[125]. The distribution of the SMD across the spray width has been plotted at different water flow rates as shown in Fig. 5.5 indicating a general decrease in the mean size of droplet with increasing axial distance irrespective of the flow rates, due to secondary break up (see Section 3.1). Although the measurements were made based on the 20,000 droplet population captured at each point using the PDA as described in Section 4.3. Although the droplet sizes exhibit a similar behaviour as predicted by both experimental and numerical values, which are mutually exclusive parameters [56], still their distribution have indicated their suitability in carrying out high pressure cleaning, to which descaling forms part of. The results at various downstream positions according the grid are shown in Fig. 5.5.

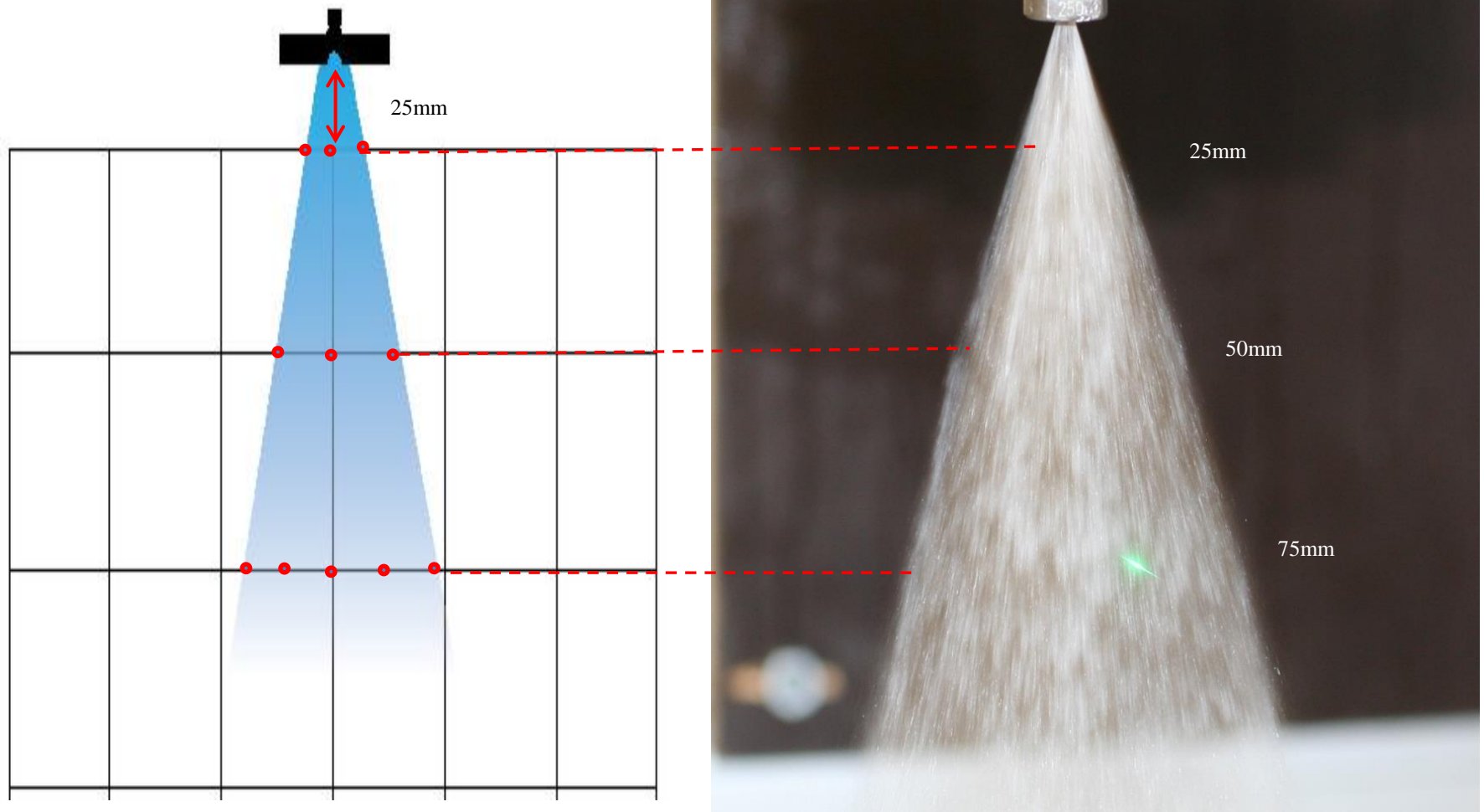
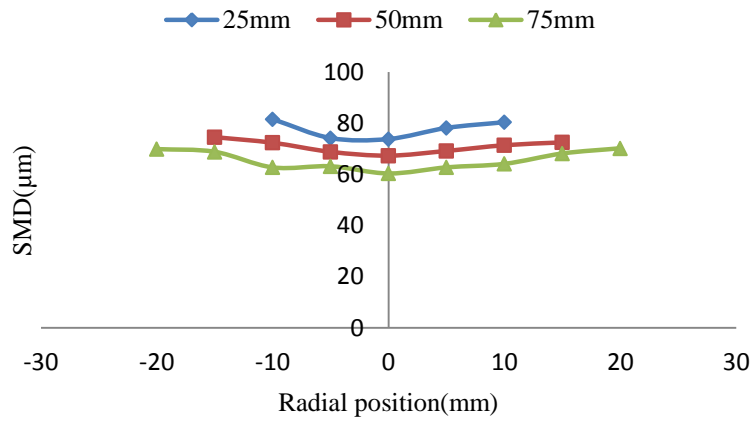
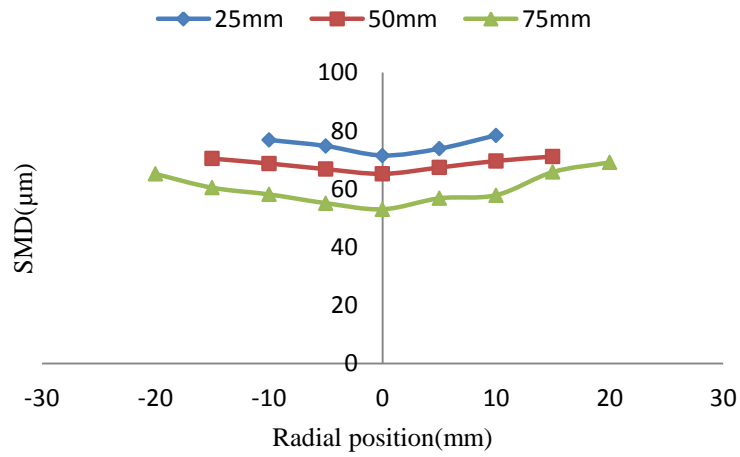


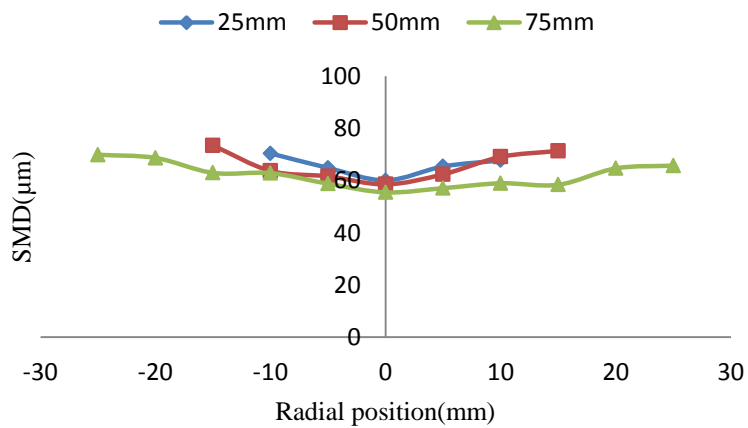
Figure 5.4 Spray droplets and velocities grid



(a) 4.8MPa



(b) 6.0MPa



(c) 10MPa

Figure 5.5 SMD across the spray width

As part of the effort to ensure momentum consideration and impact pressure analysis across the sprays width, selected points droplets sizes at the centre, negative and positive edge (shown in Fig. 5.6) of the spray were also compared, such that momentum analysis of the characteristic larger droplets with lower velocities will also be investigated to ascertain whether the increased in size has compensated the decreased velocities at the spray periphery. It has been well established that the droplet velocities of typical pressure atomizers like flat fan is highest at the centre due to lesser exposure to the aerodynamic forces [126], the results obtained and indicated in Fig. 5.7, the centre droplet sizes were observed to be lowest at the initial measurement positions of 25mm, although shows an abrupt increase towards the 50mm positions, still the size maintained smaller size compared to measurements at the other edges of the spray. Similarly the drop size at the edges of the spray were relatively larger although undergoes fluctuation in sizes due to turbulent nature of the high pressure sprays which are still very difficult to measure accurately[127]. Alternatively, increasing the liquid flow rate through pressure confirms decrease in SMD across as shown in Fig. 5.8, although the higher drop sizes recorded at further downstream position of 50mm were abnormally high. The next section will analyse the drop velocities obtained at same drop size positions for momentum computations.

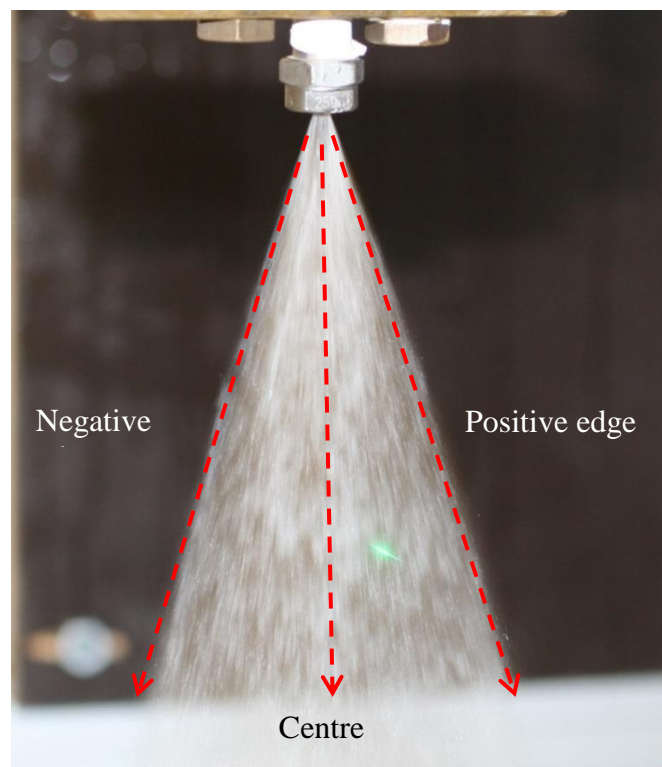
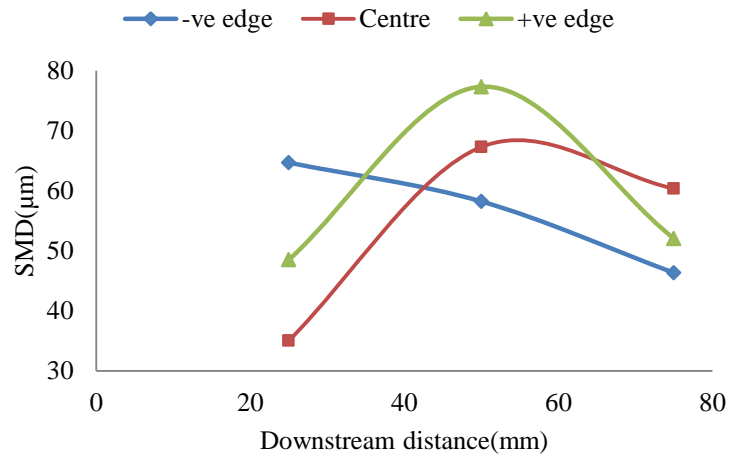
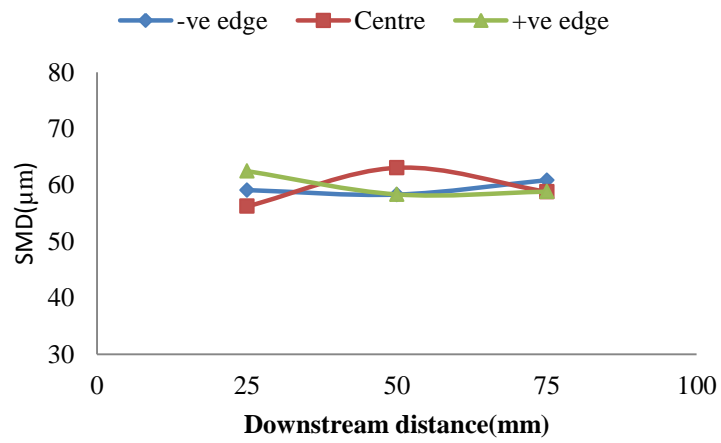


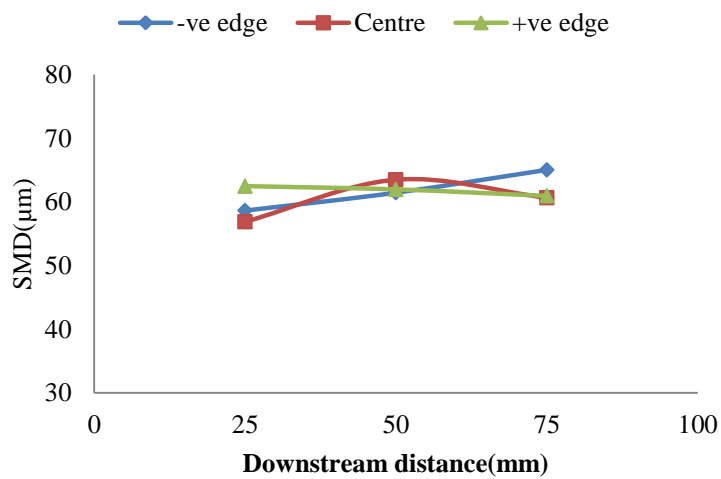
Figure 5.6 Typical measurement positions using PDA



(a) 4.8 MPa

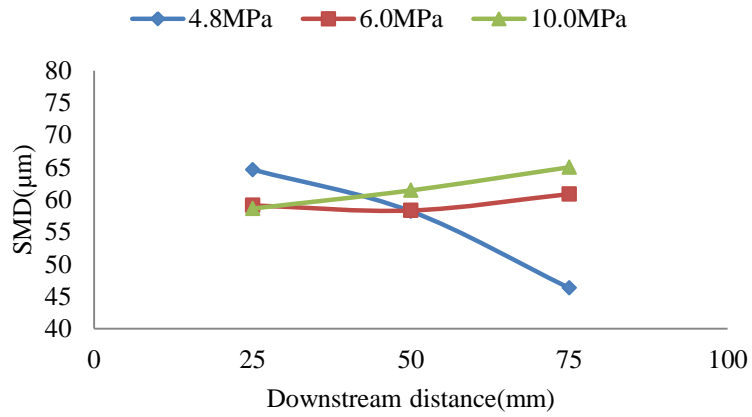


(b) 6.0 MPa

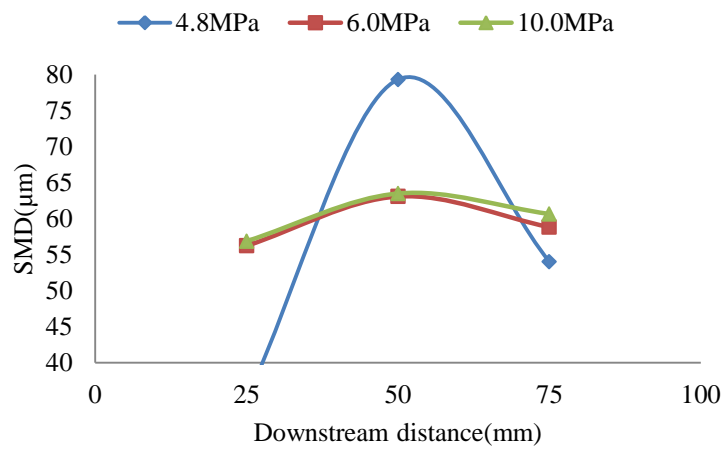


(c) 10 MPa

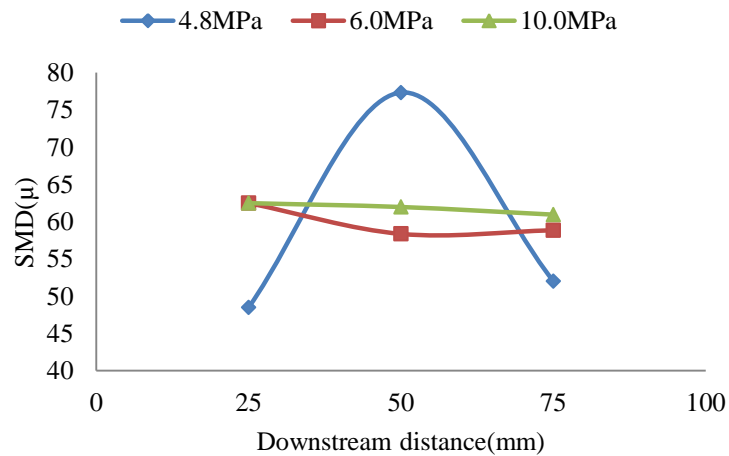
Figure 5.7 SMD at the centre and edge of spray



(a)



(b)



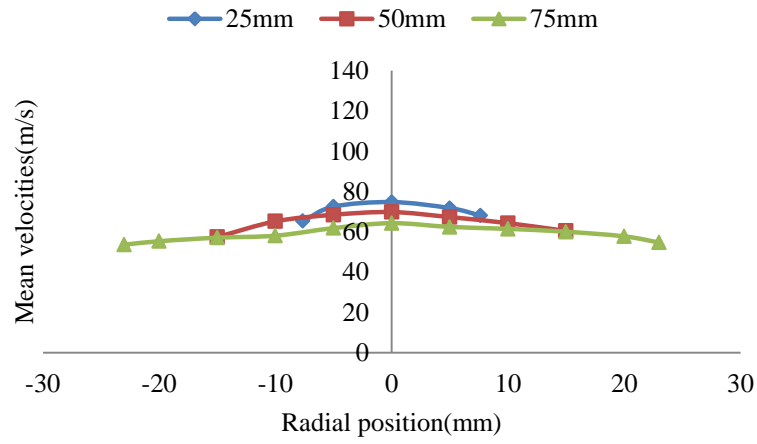
(c)

Figure 5.8 SMD at (a) negative edge, (b) centre, (c) positive edge

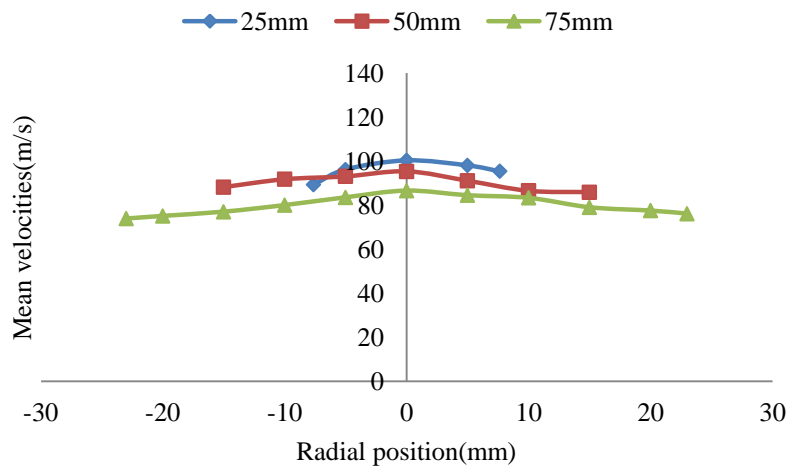
5.2.2.2 Spray droplet velocities

The measurement of droplet velocities is one of the most important characterization parameter as well apart from drop size, considering the aim of the investigation is to utilise high pressure water impact for descaling oil production tubing. The results obtained for the various runs of the characterization indicated that although mean velocities according to the grid used for SMD analysis shown in Fig. 5.8, generally increases with increasing the water flow rates as a results of increasing pressure drop from 4.0 6.0 and 10MPa, although the velocities at the centre of the spray appear higher and continue to decay towards the spray periphery due to competing aerodynamic forces at the edge[128], which despite the drop in velocities achieve momentum compensation by the growing larger droplets population. In this regard, the performance of the spray impact may likely be higher at the centre provided the impact pressure appears in similar pattern. Details of the impact pressure and momentum analysis is provided in Section 5.2.2.3, which will be used to establish the appropriate scale stand-off distance from the nozzle exit for the descaling trials in Section 5.4. The presence of aeration in the drop size and velocities measurement especially for flat fan atomizers could not be compared directly with other studies due to limited research of flat fan aeration especially using water instead of fuels, however, a reported droplet sizes $<100\mu$ in agricultural sprays systems using combined air and water streams[129].

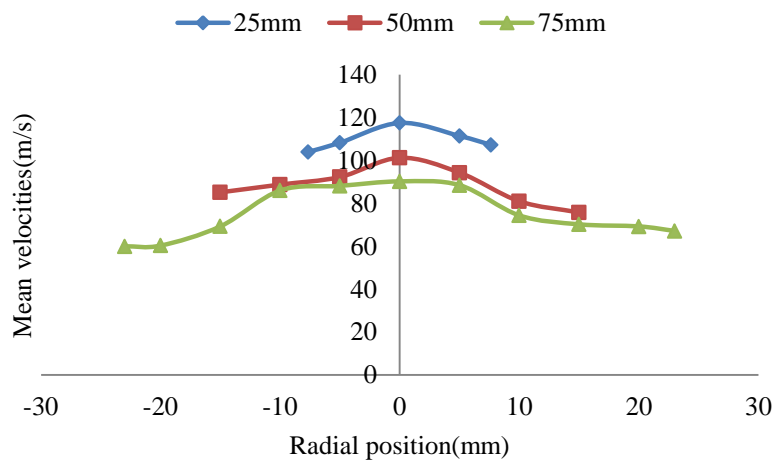
In addition, further measurements at selected positions similar to the SMD conducted according to Fig. 5.6 and shown in Fig. 5.10 indicated that at the edge spray droplets are affected by aerodynamic forces more than the central droplets, which as results experienced fluctuations with subsequent decrease and then increase at 10MPa as shown in Fig. 5.10 (a), and then vice-versa at 4.8MPa as shown in Fig. 5.11(c) instead of expecting a general decrease in velocities as shown in Fig. 5.11 (b). This also confirms that the increase in liquid loadings do not show an appreciable variation between 6.0 and 10MPa especially at the edge of the sprays as shown in Fig. 5.9 (a and c). Indeed, the mean velocities obtained at the centre of the spray seems to follow the expected order of highest velocities at 10, then followed by 6 and finally 4.8MPa as shown in Fig 5.9 and 5.12(b). Consequently, this could lead to higher performance in terms of momentum impact might be utilised in the selection of the descaling stand-of distance for the scale samples.



(a) 4.8MPa

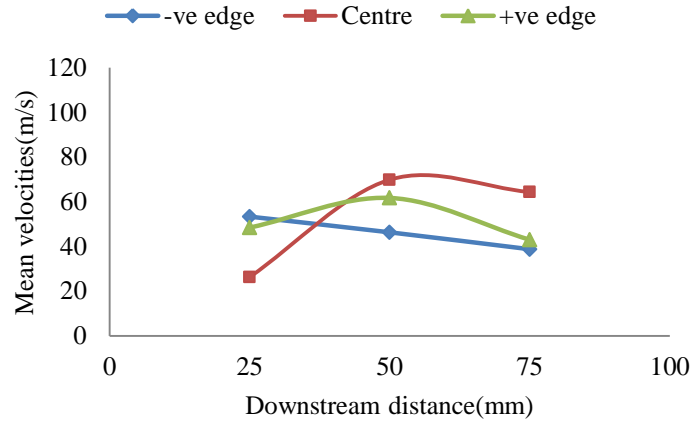


(b) 6.0MPa

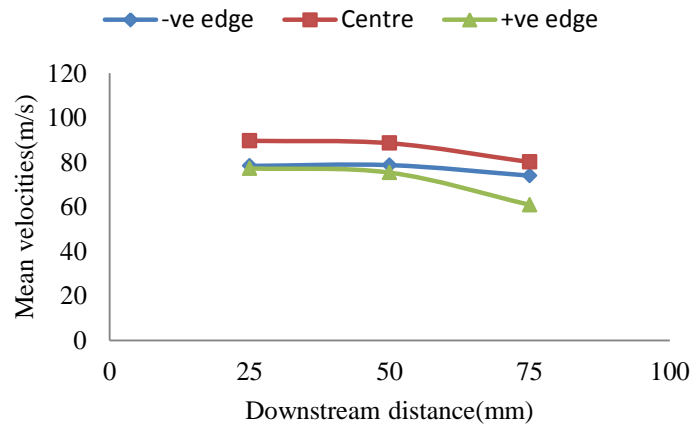


(c) 10MPa

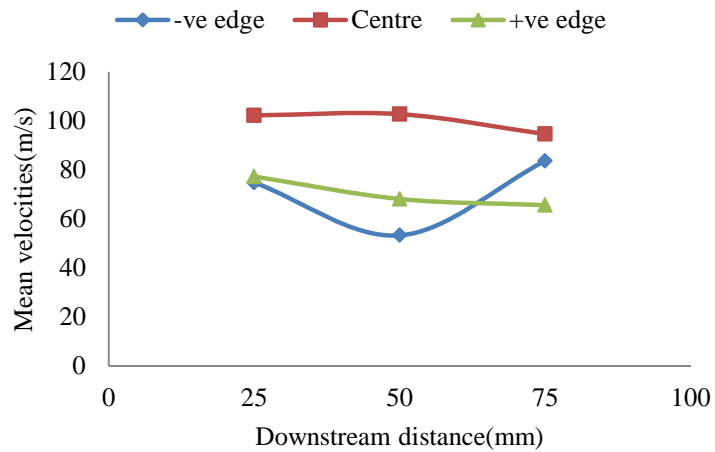
Figure 5.9 Droplet mean velocities at various stand-of distances



(a) 4.8MPa

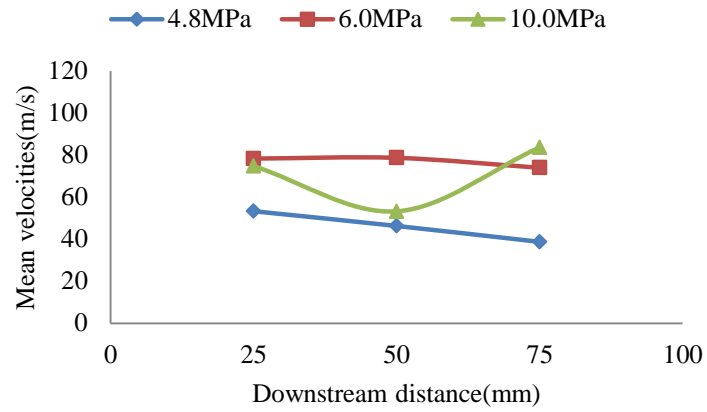


(b) 6.0MPa

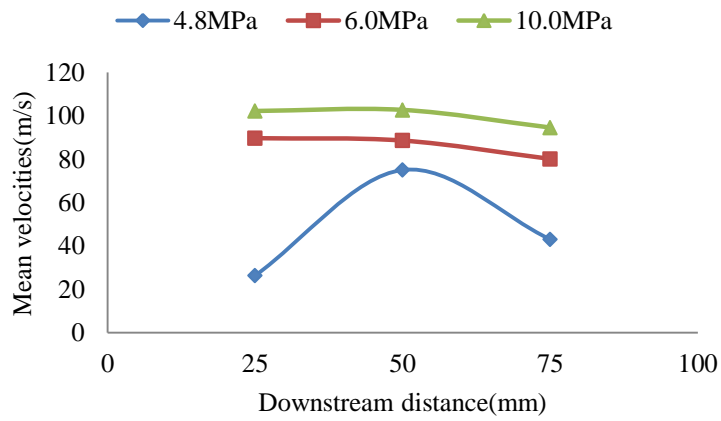


(c) 10MPa

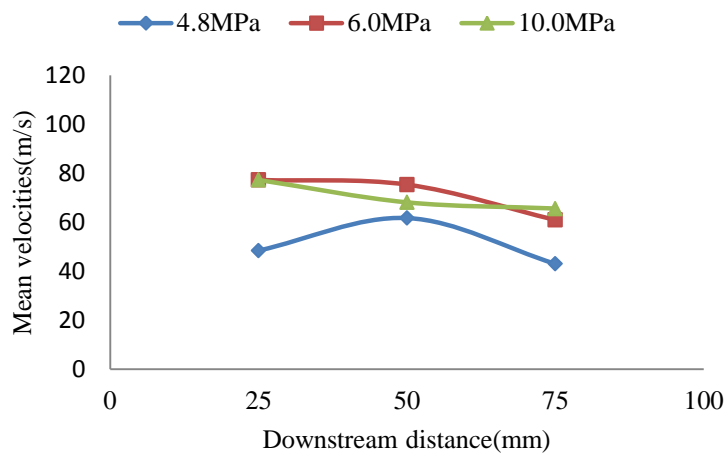
Figure 5.10 Droplet means velocities at various injection pressure



(a) Negative edge



(b) Centre



(c) Positive edge

Figure 5.11 Droplet mean velocities at centre and spray edges

The results obtained from the PDA measurement based on droplet sizes and velocities were used for the momentum calculations. A droplet of mass m , travelling with a velocity v will have a droplet momentum as:

$$\text{Droplet momentum} = m \times v \times n \quad (5.1)$$

Where m is mass of the droplet, v is velocity, and n is the number of droplet per second.

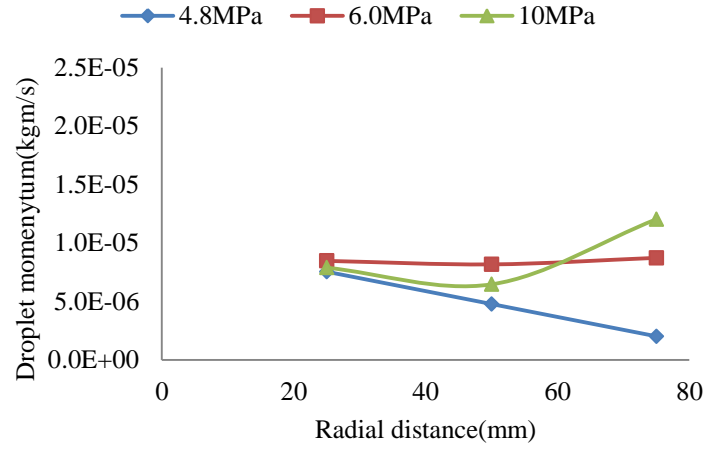
$$m = \rho \times V = \frac{4\pi\rho}{3} \left(\frac{\text{SMD}}{2}\right)^3 \quad (5.2)$$

$$n = \frac{\text{droplet capture}}{\text{time taken}} \quad (5.3)$$

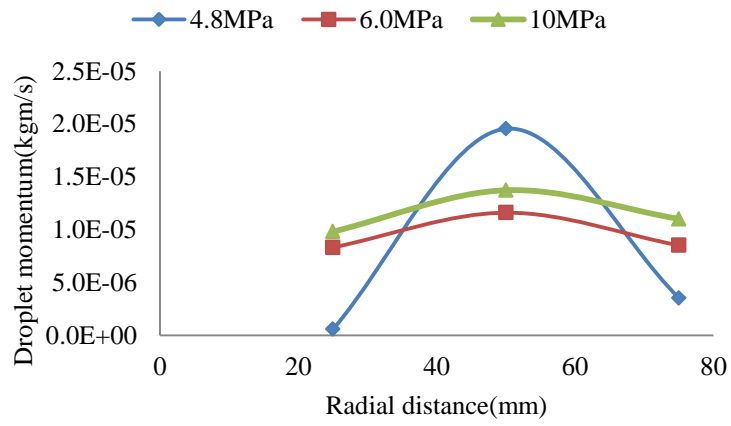
For 20000 droplets captured over a period of 20 seconds according the PDA set up, the number of droplet per time equals to 1000.

$$\text{Droplet momentum} = \frac{4\pi\rho}{3} \left(\frac{\text{SMD}}{2}\right)^3 \quad (5.4)$$

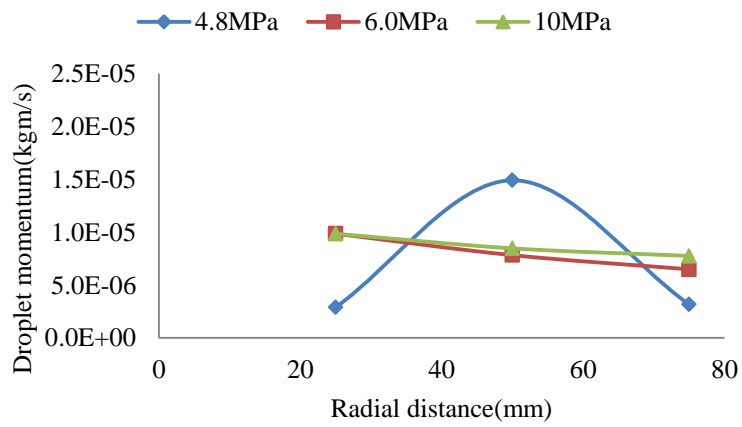
The momentum calculations was performed as per Eq.5.1 and shown in Fig. 5.12. The droplet momentum has indicated higher values at the centre of the spray compared to the edge where significant reduction can be observed as shown in Fig. 5.12(a, b and c). However, additional comparison of the momentum was conducted at the same pressure (water flow rates). The momentum of the droplets computed seems highest at the centre of the spray at all pressures regardless of the radial and axial positions as shown in Fig. 5.12. It is clearly evident that although spray characterization of flat fan nozzle was known to have lowest flow rate at the centre, and highest at the edge, momentum generates from the high droplet velocities at the centre could not be compensated by the increased liquid flow rate at the edge due to lower velocities.



(a) Negative edge

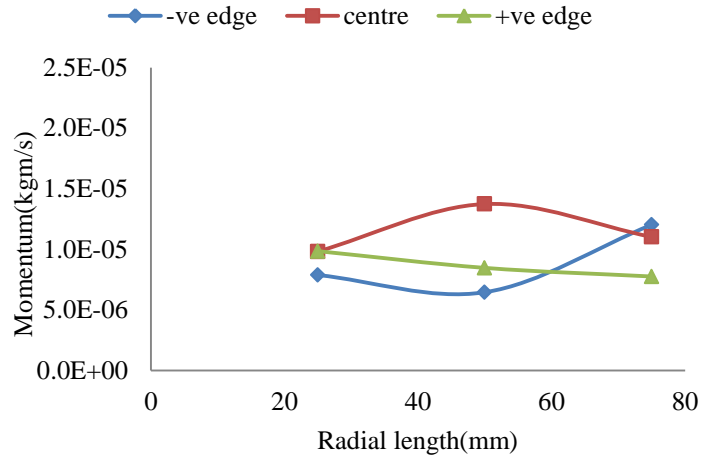


(b) Centre

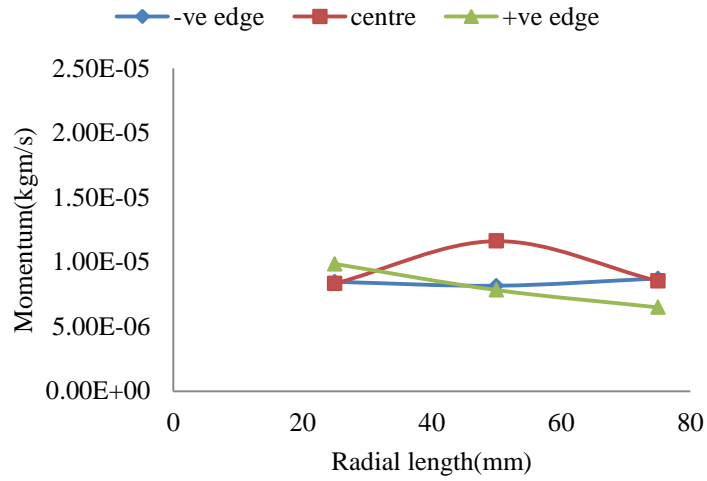


(c) Positive edge

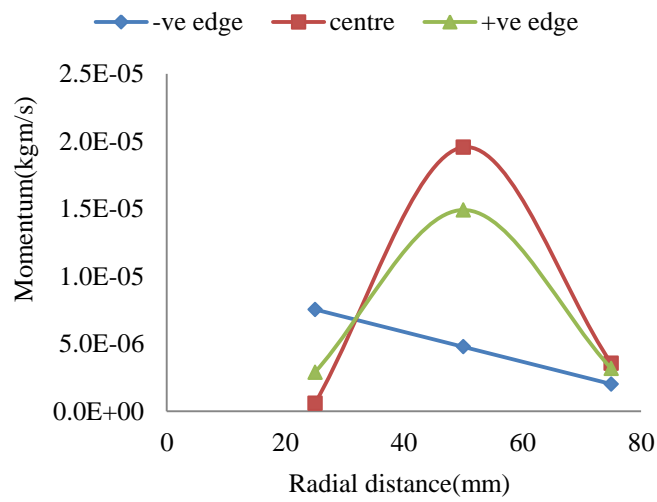
Figure 5.12 Droplet momentums at various injection pressure



(a)



(b)



(c)

Figure 5.13 Droplet momentums at various positions

5.2.2.3 Spray droplet impact pressure

In addition to the air-velocities; spray characterization in terms of drop size and velocities; momentum distribution across the spray, distribution of the impact pressure measurement using the impact pressure probe is necessary to realistically indicate the distribution across the spray width, especially that the flow may be subjected to cavitation, and the impact pressure wave has been reported to be affected by the aeration[105]. The measurement of the impact force used the grid pattern in addition the positioning of the impact force probe as shown in Fig. 5.14

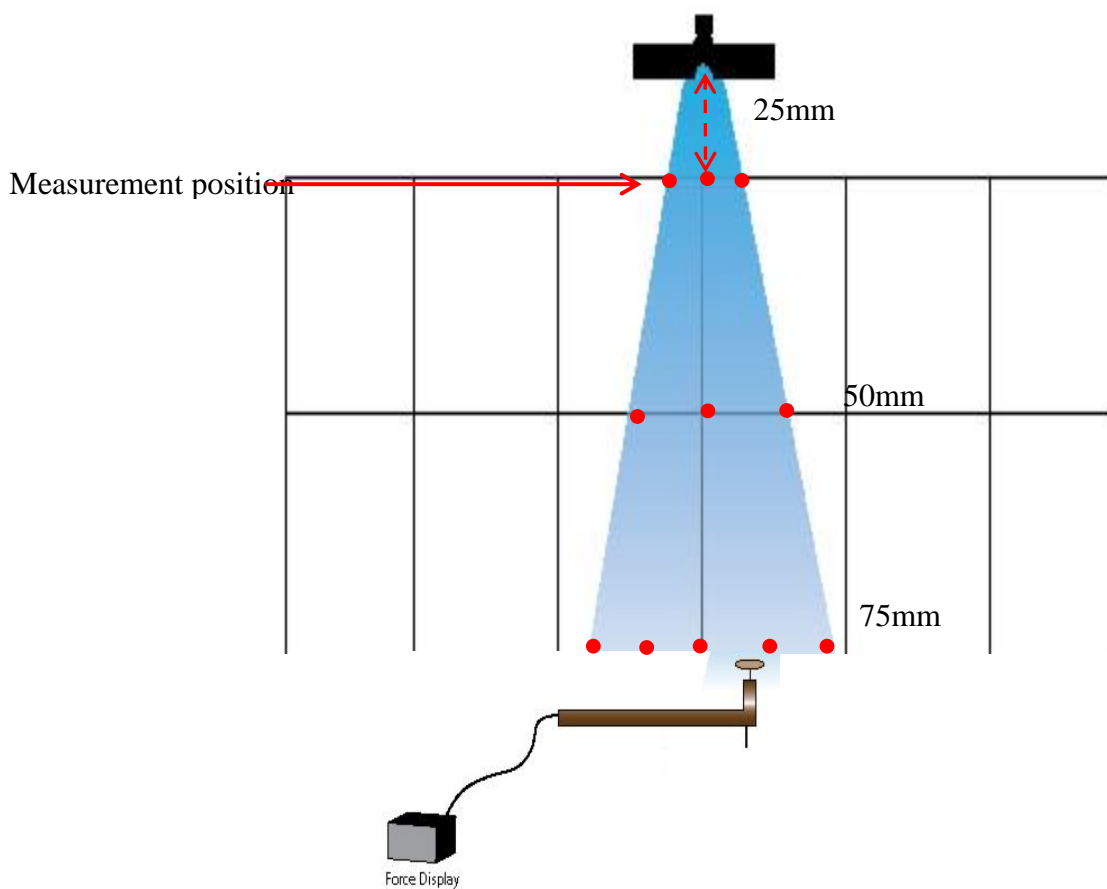


Figure 5.14 Impact pressure grid

The measurement of the impact weight were obtained on the display, which was converted to force and subsequently pressure using the cross sectional area on the sensor as 13mm^2 . The resultants obtained indicate a maximum impact pressure of 0.15MPa at the lowest stand-off distance of 25mm as shown in Fig. 5.15, with a corresponding decay in the impact pressure towards the spray periphery. Considering the atomizer used for this investigation was

designed with a spray angle of 25° , which was chosen for the suitability of providing higher impact pressure required for cleaning purposes. However, other applications such as agricultural sprays requiring a lower impact pressure onto the plants upon liquid sprays such as insecticide prefers higher spray cone angle[13][129]. Flat fan atomizers have been specifically designed to deliver high impact at low liquid flow rates as shown in Appendix E, however, even at the low flow rates impact pressure due reasonably vary across the spray width as shown in Fig 5.16(a, b, and c) in contract with the expectation that the higher droplet velocities at the centre with low flow rates compensates reasonably by the higher flow rates at lower velocities around the spray periphery[54].

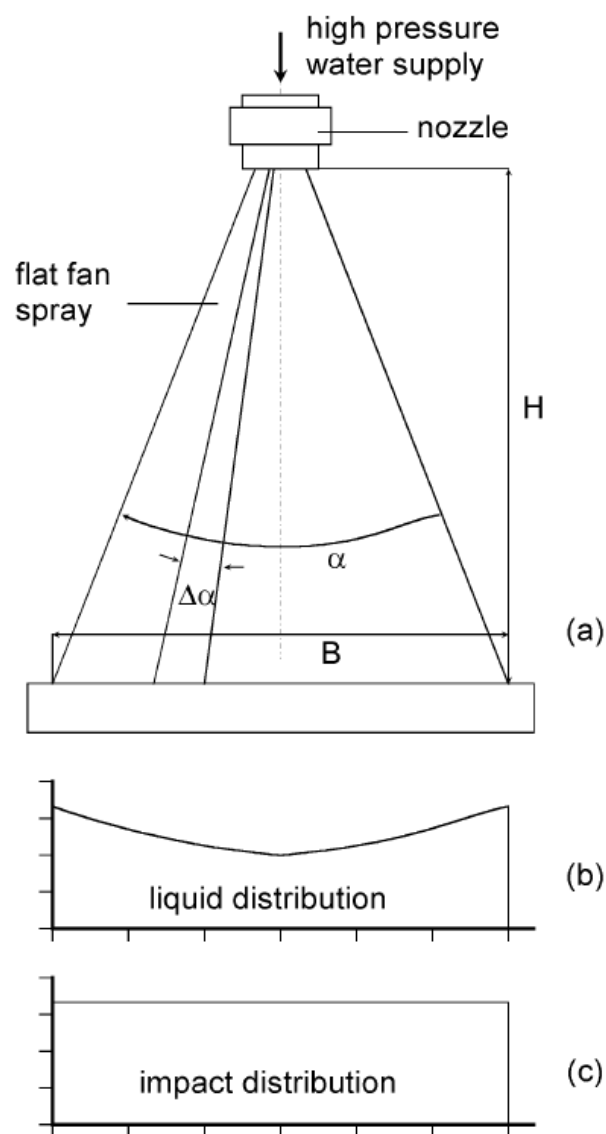
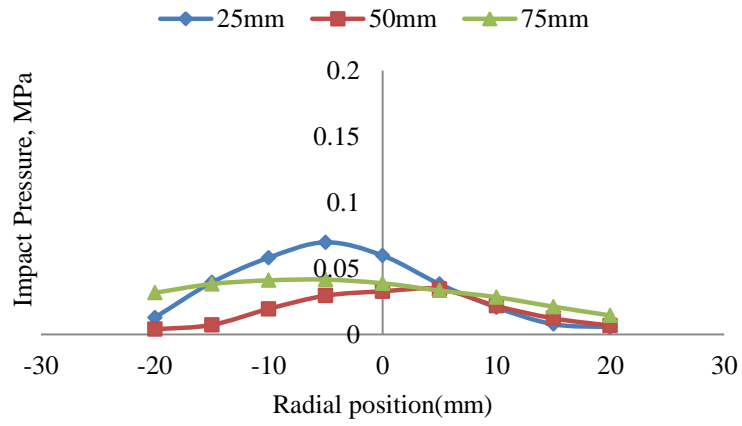
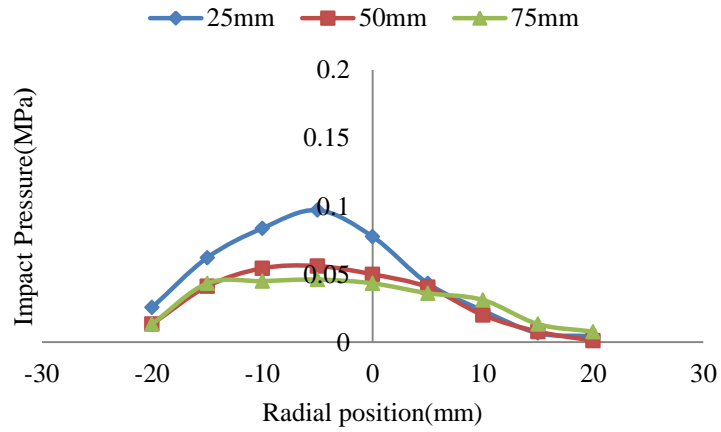


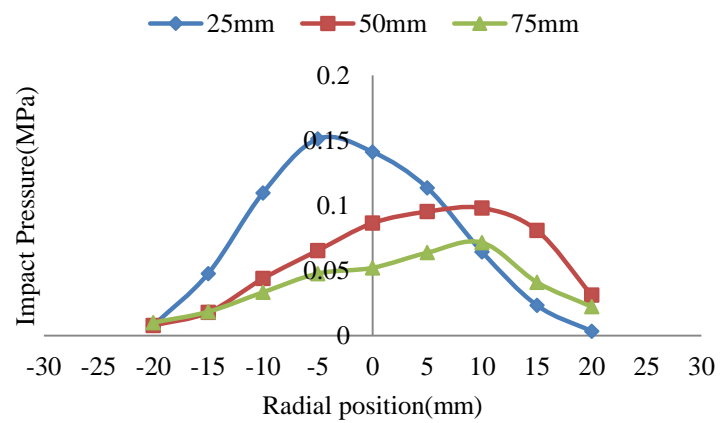
Figure 5.15 Impact pressure distribution proposed by Bendig [54]



(a)



(b)



(c)

Figure 5.16 Impact pressure distributions at (a) 4.8, (b) 6.0 and (c) 10MPa

Considering typical size of the oil production tubing's of around 30 to 60mm internal diameters[130] and the corresponding impact pressure performed in this section, it is evident that choosing the lowest stand-of distance of 25mm will not only give the highest impact pressure for the descaling operations, but will also be similar to realistic radial distance in oil and gas production tubing's.

The next section will investigate the cavitation possibilities in the flow along the nozzle, its behaviour in aerated flow systems and its contributions to the erosion of mineral scales.

5.3 Cavitation Measurements (Phase-II)

5.3.1 Overview of cavitation in multi-phase flows

Cavitation bubbles formation due to pressure drop to a value significantly lower or equal to the saturated vapour pressure of water has been responsible for the damage of several hydraulic machinery due to erosion caused by the pressure shock wave upon impingement with solid surfaces [131][132][133], however, it is equally beneficial to certain applications to which descaling process is one of them[1].However, increasing depth resulted in significant increase in pressure causing higher pressure surrounding affecting water cavitation tendencies, thereby causing partial or total absence of cavitation erosion.

While other test employ the solid particles to compensate for the cavitation erosion absence, this investigation however developed a novel approach of substituting the solid particles with aeration, which in addition to its suitability to providing a realistic pressure for laboratory test similar to the typical onshore production tubing's under maintenance(without oil flow) to be carried out, it also generate a compressive forces which enhances impact and subsequent erosion of the mineral scale.

This section analyse the formation cavitation bubble using a flat fan atomizer and also utilised aeration to prevent cavitation at the descaling stand-of distance of 25mm.The set up used to measure the cavitation bubble length is shown in Fig 4.21 and the grid obtaining the results is shown in Fig. 5.17.

Considering cavitation plays an important role in erosion, however, it decreases significantly with increasing depth due to back pressure; however, efforts of injecting solids were as

results of achieving increasing erosion despite cavitation suppression. In this investigation, however, aerated chamber is adopted to realistically measure cavitation bubble length along production tubing, to ensure cavitation bubble do not survive to the scale measurement position of 25mm, which evidently proves total absence of cavitation erosion in the mass of scale removed, but aerated chamber was then used to improve the erosion. Qualitative imaging utilised high resolution Cannon camera for its availability to be placed conveniently. The measurement consider a constant pressure water flow across a nozzle at 10 MPa, at varying ambient pressure as a results of changing air concentration (aeration) leading to cavitation suppression. The visibility of the bubble was affected by the turbulent nature of the flow in the aerated chamber.

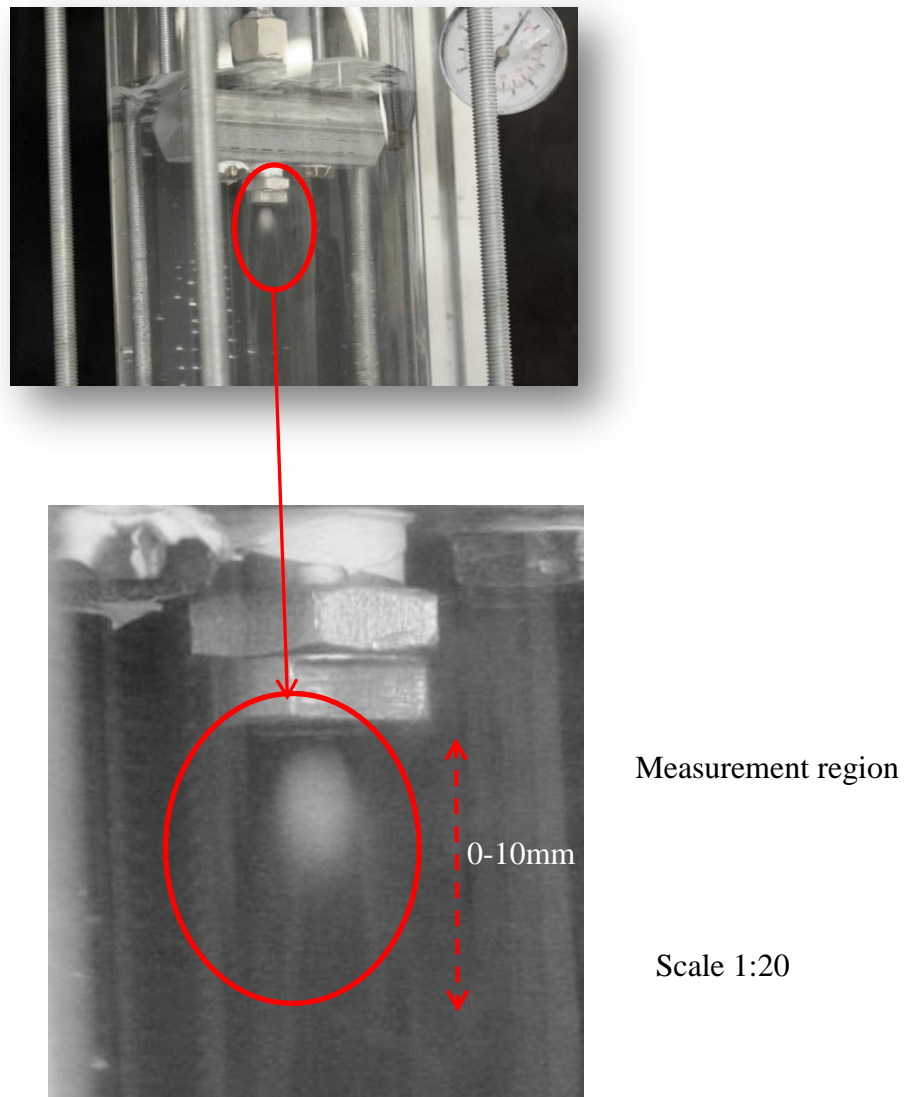


Figure 5.17 Cavitation region measurement positions

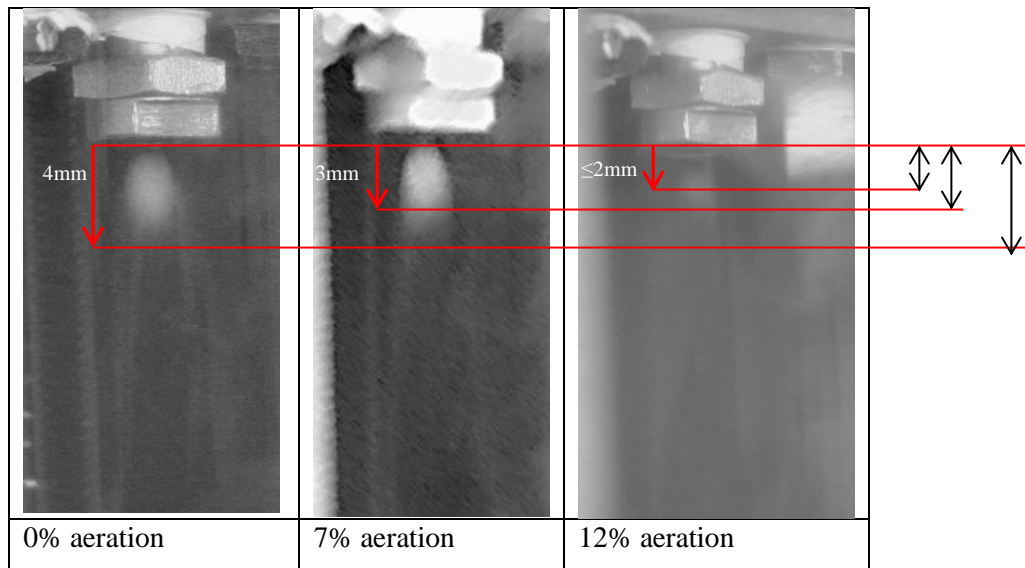


Figure 5.18 Cavitation bubble suppression with increasing aeration

The variation of air concentration in the submerged aerated chamber from 3 to 12% air concentration causes decay in the observed cavitation bubble length shown in Fig. 5.18. At the initial flow without aeration, sound attributed to cavitation was heard, which subsequently decayed to a minimum with increasing aeration. It is established that increasing in pressure with increasing depth causes a decrease in cavitation bubble length, however, when aerated spray is utilised, an improved erosion rate can be achieved as shown in Section 5.3. In addition to cavitation bubble length, cavitation number and speed of sound in aerated flow is also calculated. As such most investigation utilising the Cavitation Number of the flow of water across a flat fan nozzle otherwise referred to as Euler Number shown in Eq. 3.6, which was calculated at various pressure of 4.8, 6.0 and 10MPa similar to experimental flow conditions were noticed to show significant increase with downstream stand-off distance at all pressure due to continuous loss of flow pressure as the spray droplet moves far away from the atomizers similar to the results shown in Fig. 5.26 for the velocities variation measured using PDA.

Although several research has shown cavitation facilitates erosion[134][135][136][133][137][138][139], and aeration suppresses erosion[104][105][103][140][141], it becomes evident also aeration weakens the material strength due compressive stress[104][105] and therefore variation of cavitation number can be a substantial analysis to establish to establish the extent of cavitation as well as its suppression using aeration and the targeted descaling of production tubing as a novel application in oil and gas. Indications from the results obtained in Figure 5.28 suggest

decreased cavitation number with increased aeration except at far downstream position of 75mm, where due to low velocities of the water flow.

However, increased pressure especially around the cavitation-prone region by the aeration has been identified as the main cause for the cavitation number decrease[104], perhaps experimental evidence shown in Fig. 5.18 indicate pressure increase with aeration especially at far downstream position of 75mm, which can justify the increased in the impact pressure responsible for the increased erosion as suggested experimentally [103] using air concentration adequately could cause increased impact pressure[103]. Consequential effect of scale erosion in this experiment could be related to both impact pressure and the compressive stress resulted from the aeration as shown in Figure 5.30 and 5.31 for both the pressure and the pressure drop of the aerated flow.

5.4 Scale Removal (Phase –III)

5.4.1 Overview

While application of water cavitation peening(WCP) has been successfully employed in improving the fatigue life of metallic components, aeration has recently been proved as an important parameter for the intensity enhancement of WCP[110] components through inducing a compressive stress along the metallic surfaces[142] taking advantage of cavitation phenomena through Water Cavitation Peening, extension of the same stresses can then be utilized unto the target surfaces which are not necessarily metallic in nature, thereby rendering their surface to an additional stress due to aeration, leading to enhanced fatigue or subsequent erosion after impact by the water jet as an added stress. Perhaps, erosion mitigation in high dams spill ways has been successfully carried out with aeration, originally proposed by *Peterka* experimentally using 0.4-7.4% air concentrations to complete mitigation of cavitation after achieving attenuation of bursting and hammer-sound of water with increased aeration. It could then be a realistic application if aeration if applied into the downhole tubing scale erosion, where increasing pressure with depth in the same minimize the cavitation erosion, leaving the impact of the jet as the only contributory erosion factor, as such aerated flow along such tubing has been identified to weakness in concrete[104] with increased aeration, in addition to the improved pressure wave leading to an improved impact with aeration[104]. The results obtained in the subsequent section indicate the novel application of compressive stress due to aeration adopted in WCP, weakening tendencies of

target surfaces and improved pressure of impact all attributed to aeration as the solution to decreased erosion performance down the production tubing where cavitation is virtually non-existing.

Within the scope of this investigation, minerals scale cleaning was performed on three categories of oil and gas scale based on its composition and nature of formation which dictate its strength depending on the well chemistries, injection water types and its compositions as well as positions of the scale along the production tubing. The scale samples are categorized into three as shown in Fig.5.19 based on their hardness and chemical compositions and hardness index according to Mohs scale. They include:

- Hard scale (Hardness value of **3.0** in Mohs scale)
- Medium (Hardness value of **0.9** on Mohs Scale) and,
- Soft scales (Hardness value of **0.2** on Mohs scale)



Figure 5.19 Experimental scale samples

Each of the scale samples was tested under non-aerated as well as aerated conditions for the measurement of the mass of scale removed during the experimental trials. The following section provides details of the experimental results for the non-aerated trials.

- Section 5.4.2 Non-aerated scale removals
- Section 5.4.3 Aerated scale removals
- Section 5.4.4 Comparison of the Non-aerated and aerated trials

5.4.2 Non-aerated scale removal trials

The measurement of the scale removal without using aeration utilising high pressure water sprays is analysed in this section. The mass of scale removed as a result of water impact alone while keeping the air supply to the chamber shut as shown in Fig 5.20,

Shutter air supply valve

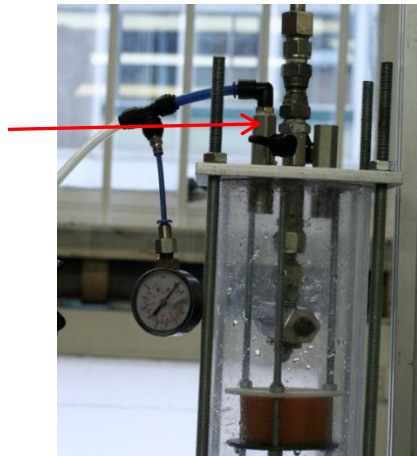


Figure 5.20 Non-aerated scale removal set-up

The results obtained for the soft scale sample shown quantitatively in Fig. 5.21 for the different scale samples. Soft scale sample erosion obtained is shown in Fig. 5.22 and qualitatively in Fig. 5.25 indicated the various masses of the soft scale removed during the trials. The increase in impact pressure measurement with increase in pressure provided a corresponding increase in the mass of scale removed as shown in Fig. 5.22. Although the mechanism of the scale erosion depends on its mechanical properties which guides the failure pattern of the scale sample [143], leading invariably to a non-linear relationship between the increase in injection pressure and the mass of scale removed. However, a general increasing trend in erosion is shown.

Similarly, the medium scale sample trials are shown in Fig. 5.23 and then qualitatively in Fig. 5.26 indicated similar manner of erosion with additional scale removed at each of the pressure increase. However, the chemical constituents of the medium scale composing of both hydrocarbons and minerals scale together, its scale was observed to have a characteristic low density, which as a results indicated lower mass removed compared to the hard scale and closer to that of soft scale. The Hard scale sample results indicated similar erosion pattern to the other scale types as shown in Fig. 5.24 and qualitatively using Fig. 5.27.

Commercial scale removal of oil scale types, typically found as mixture of mineral salts and other hydrocarbons possibly heavier in nature (such as grease) similar to that of soft scale sample or medium scale, applications of spray jetting's has proven to successfully causes erosion [11][132][144][145][146][147], which proved success at ambient conditions, however, success rate of most of the technologies was either achieved due to combined effects of either cavitation erosion, solid particles as well as droplet impact [132], perhaps the

position where oil scale exist such as the *Miano* gas field around 3400m subsea[22] , EW 873 Field in the Gulf of Mexico where the BaSO₄ scale of 11,000-12,000ft. Measured Depth(MD) (roughly 3500m) [49], potential increase in pressure with depth even to the ambient column of air during cleaning have resulted in decreased performance due to suppressed cavitation forces[11], rendering the jet performance to rely on the impact only. Indeed, in this novel approach, investigation into the depreciation effect of cavitation with increasing downhole length was conducted in Section 5.3.3, and also the length of cavitation bubble were found to exist only 3mm away from the nozzle exit as shown . Therefore, successful application of aeration as proven in this investigation enhances erosion without both cavitation and the solid particles as shown in Section 5.4.3.

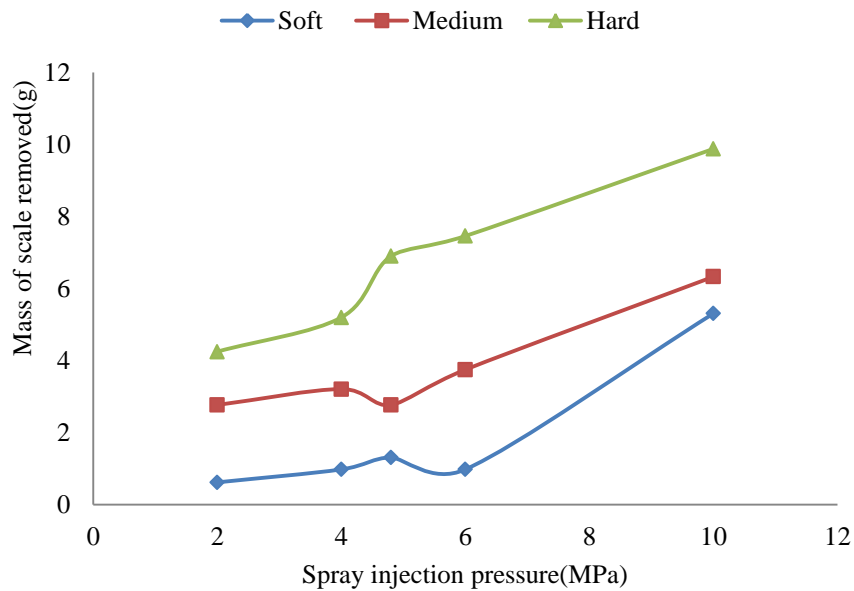


Figure 5.21 Comparison of scale removed

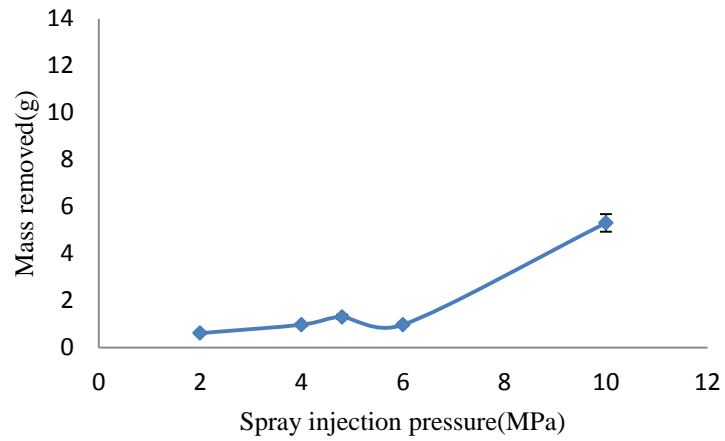


Figure 5.22 soft scales mass removed (non-aerated)

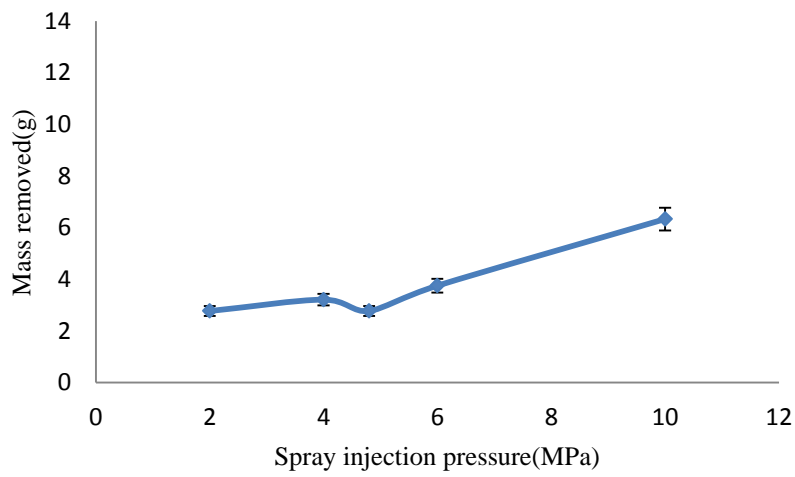


Figure 5.23 Medium scale removed (non-aerated)

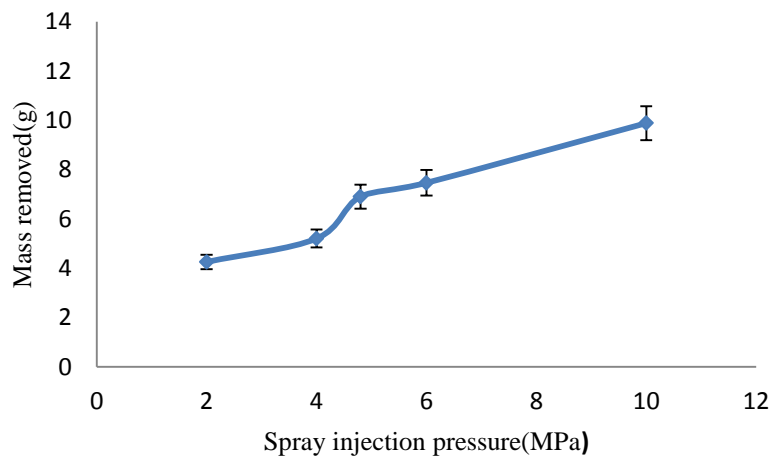


Figure 5.24 Hard scale removed (non-aerated)



(a) 4.8MPa

(b) 6.0MPa

(c) 10MPa

Figure 5.25 Soft scale samples after trials at various injection pressures



Figure 5.26 Medium scales after trials at various injection pressure

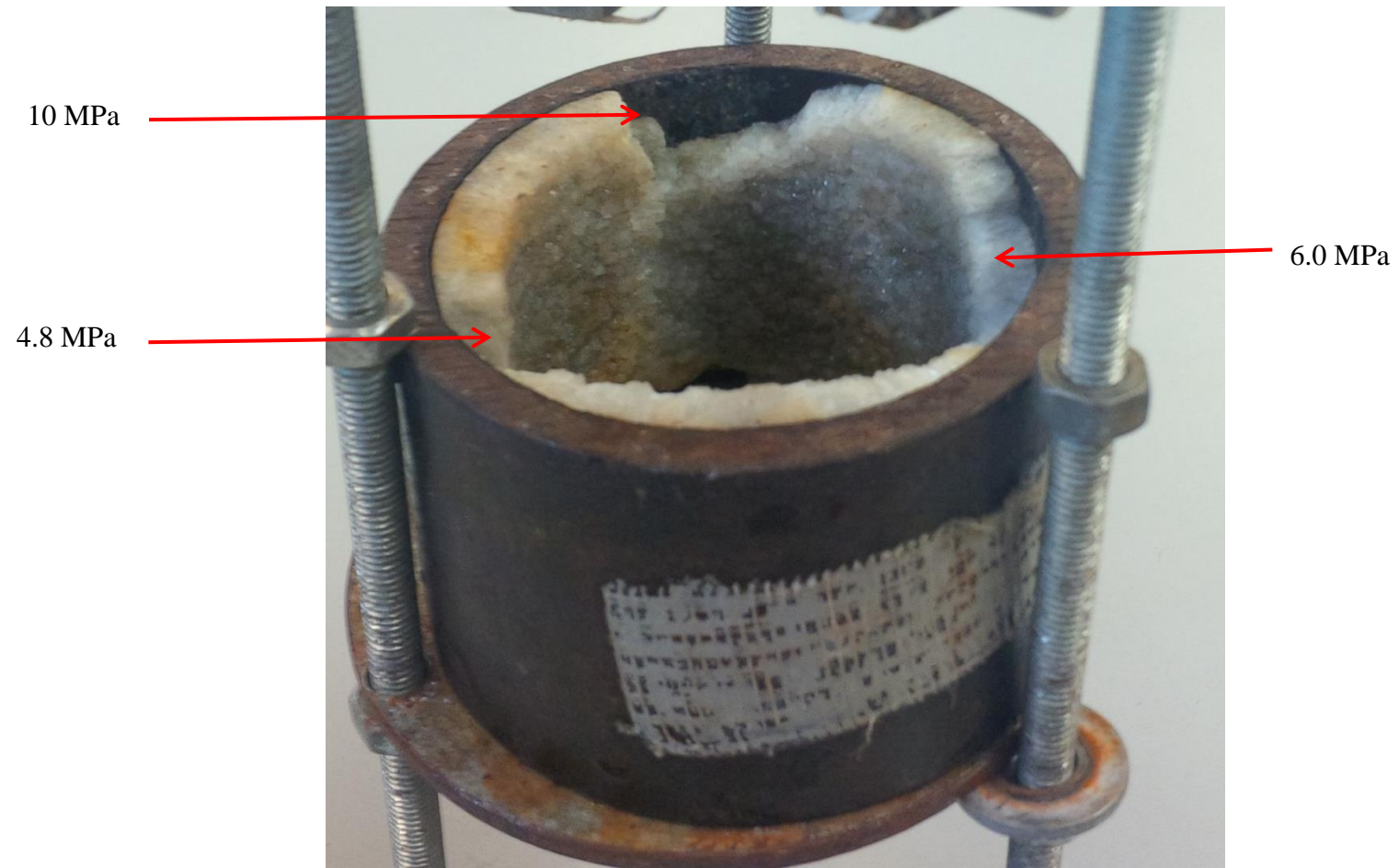


Figure 5.27 Hard scale removed (non-aerated)

5.4.3 Aerated scale removal

The novelty of this investigation is in utilising aeration in combination with high pressure water sprays up to 10 MPa at low water flow rate of 11.3 l/min in achieving an impact pressure up to 0.15 MPa for the mineral scale removal (descaling), The experiment was conducted under various air concentration through air supply to the aeration chamber ranging from 0, 0.5, 1.0, 1.5, and 2.0 bar (gauge), corresponding to air concentration of 0.0,7.0,10.0 and 12.0 % leading to increased erosional mass per time of 12.80, 7.31 and 65.80 g compared to non-aerated trial's having 9.88, 6.33 and 5.31g for the hard, medium and soft scales at 10 MPa within 5 minutes trial times. The soft scale erosion results indicated a sudden failure due to fatigue caused by the aeration as a compressive stress [110] described in Section 3.7.2 and shown quantitatively in Fig. 5.28 and qualitatively in Fig. 5.31. While the pressure increased from 6 to 10MPa at the varying air concentrations. Results obtained indicated the presence of additional stress resulted from pressure of up to 53 kPa[110] apart from impact pressure for both the medium and hard scale as well indicated by addition abrupt damage unto the scale samples shown qualitatively in Fig.5.31, 5.32, and 5.33.

The investigation having utilised the aeration to substantially suppressed cavitation limited to 2mm stand-off distance(see Fig. 5.18) at 12.0 %, implying the erosion was not attributed to cavitation in all cases, which make the investigation procedure similar to oil production tubing's at realistic depth of 25 mm stand-off distance, where cavitation is not found, This results erosion has been supported by the other researchers relating causes damage to the scale specimen on impact[103], indicating the capability of aeration exert additional force due pressure of around 53kPa, leading to erosion compensating the cavitation erosion impact. Similar test was conducted on the two oilfield scale samples obtained from Libyan, including CaSO₄ and Mixed type scale with high and medium *Mohs* scale index of 3.0 and 0.9 compared to the wax scale having 0.2. Results obtained across the aerated scale removal trials indicate the benefit of utilising low injection with a suitable aerated pressure (in terms of air concentration to improve erosion efficiency. This could be expressed in terms of efficiency of the process in terms of ratio of scale removed to the amount of water utilised, to ensure the flooding possibilities of the well is avoided. The efficiency could be expressed in Eq. 5.1:

$$Efficiency, \eta = \frac{Mass_of_scale_removed}{mass_of_water_utilised} \quad (5.1)$$

Using Eq. 5.1 typical comparison calculated have been done shown in Section 5.4.4.

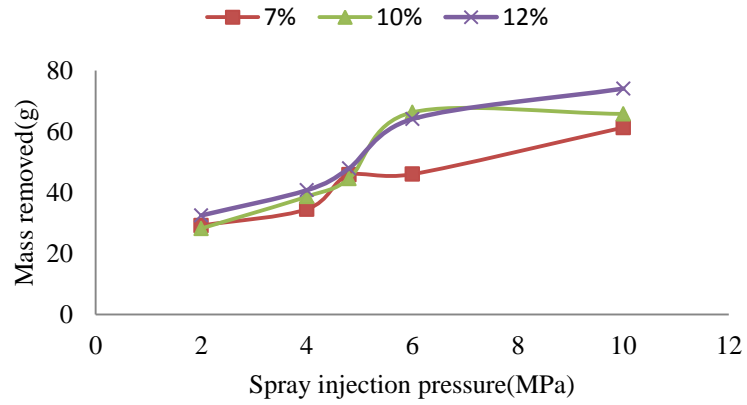


Figure 5.28 Soft scale removal (aerated)

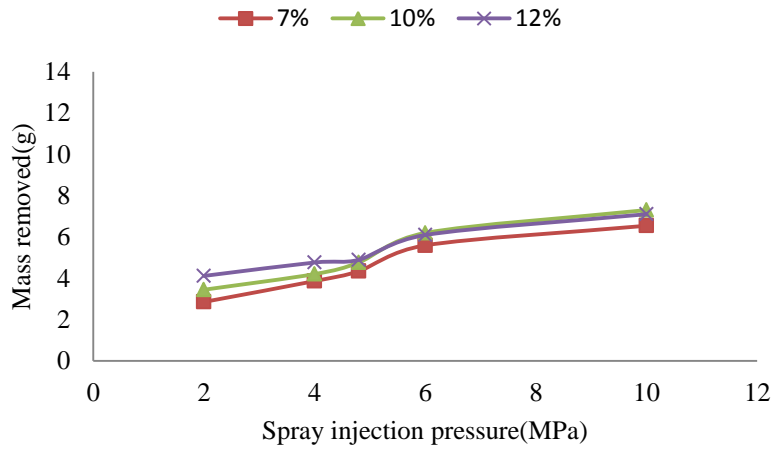


Figure 5.29 Medium scale removal (aerated)

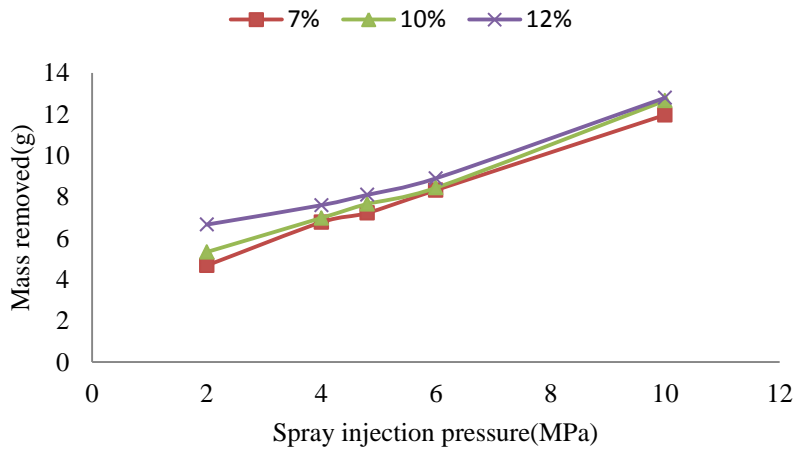
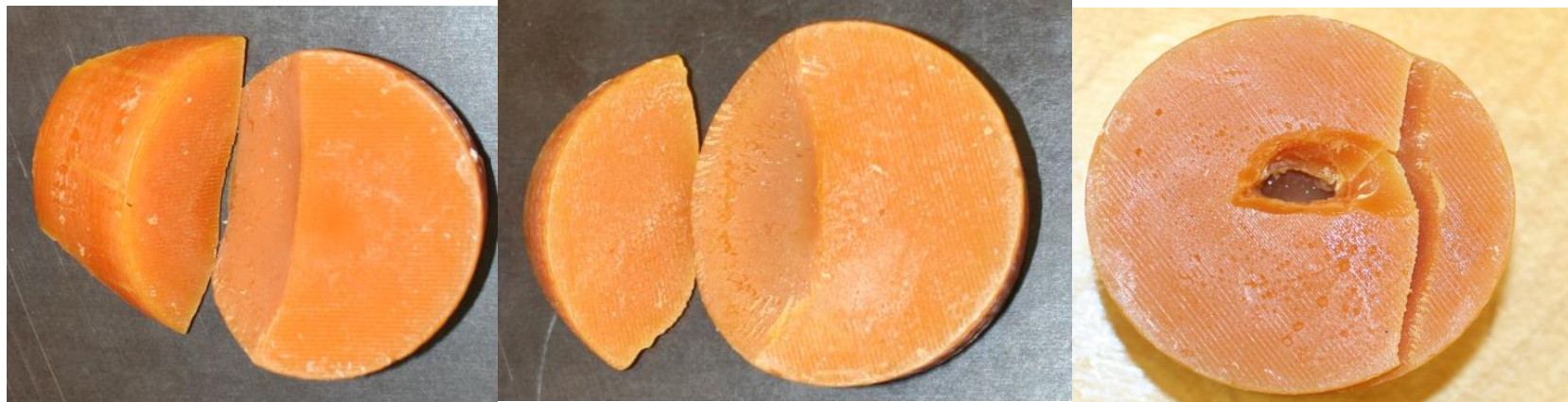


Figure 5.30 Hard scale removal (aerated)



(a) 4.8MPa

(b) 6.0MPa

(c) 10MPa

Figure 5.31 Soft scale samples after trials at various injection pressures (aerated)



Figure 5.32 Medium scales after trials at various injection pressures (aerated)

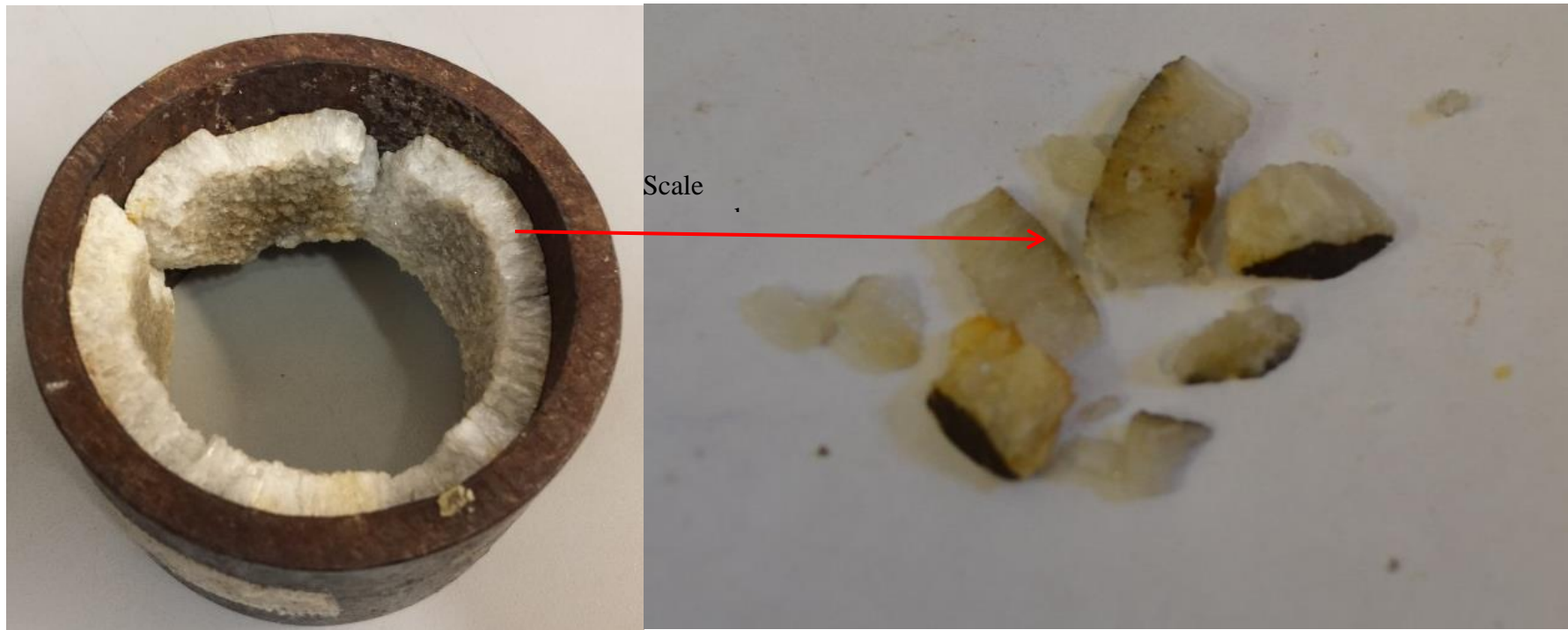


Figure 5.33 Hard scale removed (aerated)

5.4.4 Comparison of non-aerated and aerated chamber scale removal

Comparison of the non-aerated (0.0 % air concentration) and aerated (3.0-12.0 %) techniques was performed with the results shown in Fig 5.34, 5.35 and 5.36 results confirmed that the increasing concentration of the ambient air around the flat fan sprays in the chamber caused additional erosion mass of up to 12.80g compared to non-aerated trials of 9.88g due to fatigue caused by the compressive stress and pressure wave fluctuations.

Increasing hardness of scale present in oil wells poses additional risk to productivity, surveillance, wellbore access and intervention mechanisms[1] more than other types of scale which their removal were described in Section 5.4.1 and 5.4.2. As majority of scale samples are hard type, typically consisting of salts of Calcium and Silicates salts, part of this investigation consider such types of scales samples obtained from Libyan fields, which are tested for scale removal under ambient and pressurized (aerated) conditions as described in Section 4.5. The hardness of the scale itself in terms of the erosion achieved has significantly reduced compared to other types previously considered. Previous efforts to descale even the World's largest oil field Al Ghawar owned by the Saudi Aramco used the sterling beads for descaling Iron sulphide (Fe_7S_8) scale formed in one of the gas field[1], however, this investigation compensated the effect of the sterling beads with a pressurized environment capable of weakening the scale strength due to fatigue and hence removed upon subjected to the spray jet.

Payback period for descaling oil wells using chemical dissolvers was 3 days [2], although the these method possess higher profitability, however, lack of sustainability of this technique has enable consideration of the mechanical technique having up to 17 days' pay back period [2].

Alternative approach was later adopted by keeping the water spray pressure constantly at 4.8, 6.0 and 10MPa while increasing the aeration (through increasing the air concentration keeping the water flow rate unaltered as shown in Fig. 5.37, but maintaining a slightly added pressure at the pump to maintain the pressure despite the increase in the aeration chamber pressure).

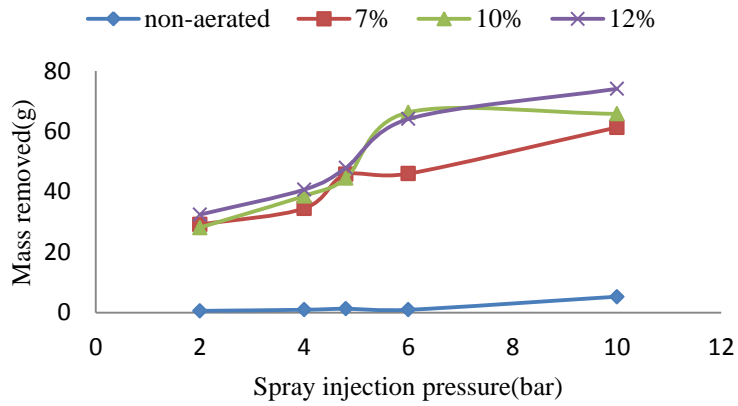


Figure 5.34 Soft scale removal comparisons

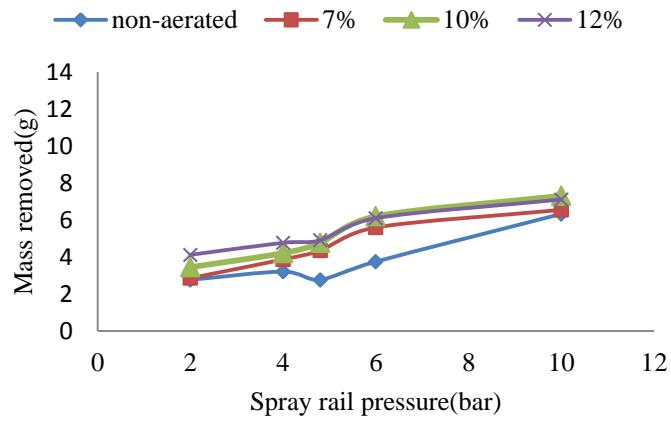


Figure 5.35 Medium scale removal comparisons

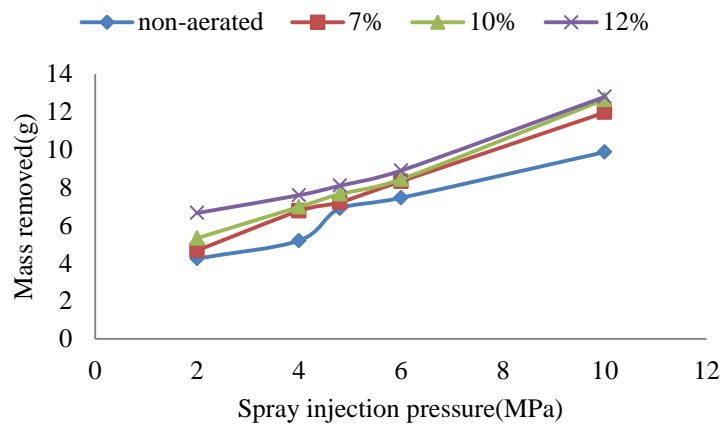
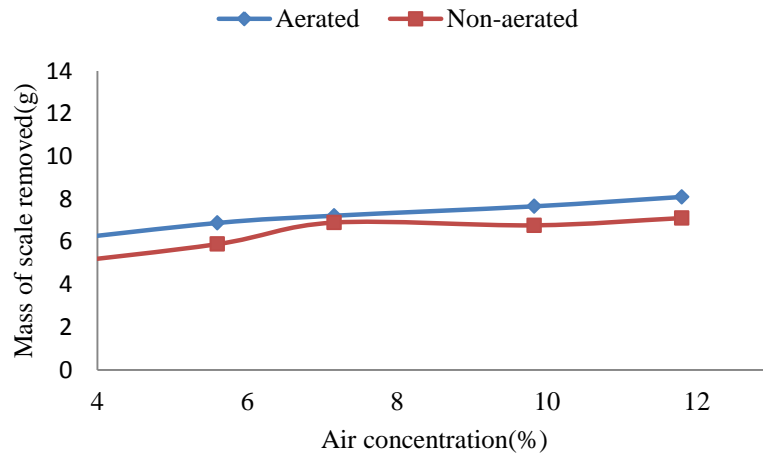
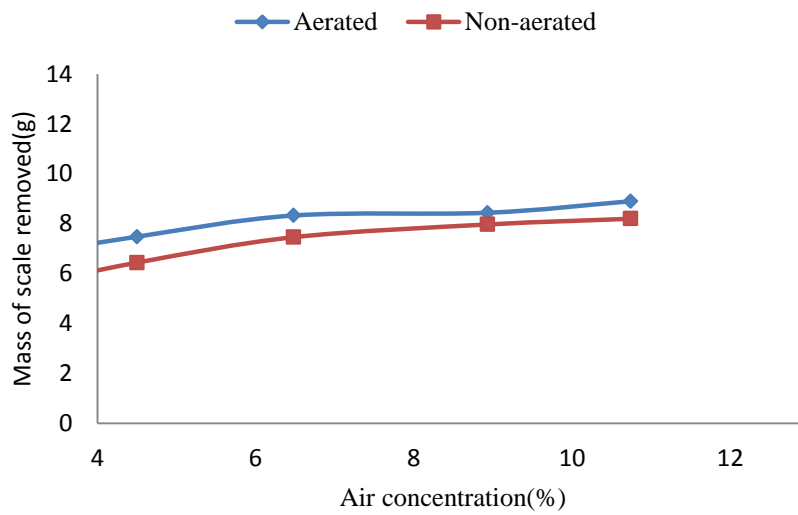


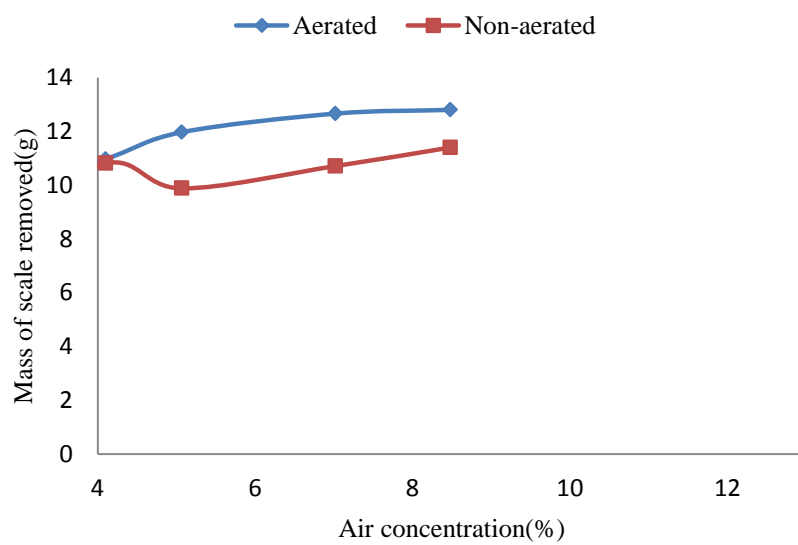
Figure 5.36 Hard scale removal comparison



(a) 4.8MPa



(b) 6.0MPa



(c) 10MPa

Figure 5.37 Aerated versus Non-aerated erosion at various pressures

Considering the aerated scale removal technique, the efficiency of the technique can be computed using Eq. 5.1 and the experimental data obtained and tabulated in Table 5.1.

Table 5.1 Scale removal efficiency comparison

Removal technique	10MPa		25MPa	
	Non-aerated	Aerated	Non-aerated	Aerated
Mass removed(g)	9.88	12.80	15.65	20.40
Water utilised(l/min)	56	56	89.5	89.5
Efficiency (%)	18	23	18	23

The aerated technique provides an avenue to remove scale at lower spray injection pressure compared to non-aerated technique as shown in Fig. 5.32, for instance, at a pressure of 10MPa utilising the aerated chamber, 56 litres of water will be used as shown in Table 5.1 to remove 12.88g of the hard scale. Whereas, conventional use of high pressure water sprays alone requires up to 17.5MPa removing same mass of scale, causing about 90litres of water being injected into the well which may cause flooding of the well and subsequent water evacuation more rapidly shown in Fig.5.38.

It therefore provide a significant improvement in increasing the efficiency of the descaling process from 18 to 23%, utilising less amount of water to achieve same level of scale removal action. Commercial technologies utilising solid particles(sterling beads) are also compared to this investigation in the next section.

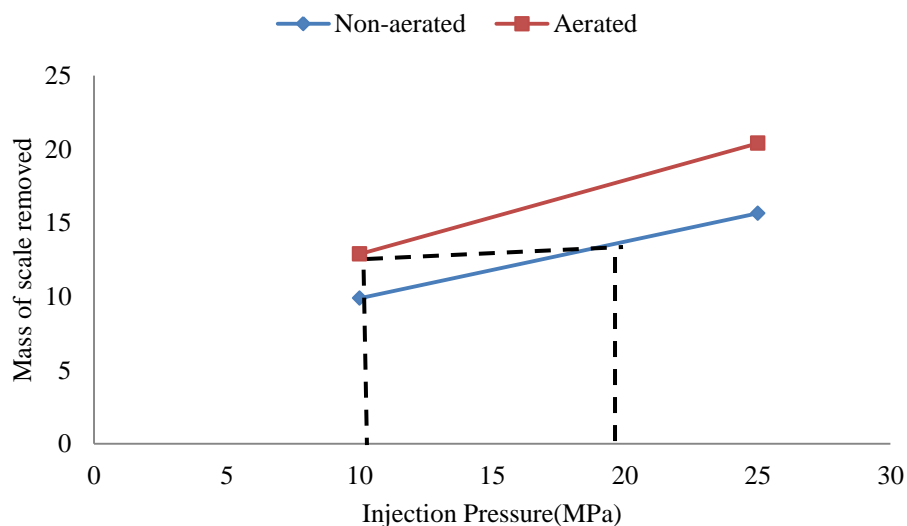


Figure 5.38 Comparison between laboratory and commercial pressure scale removal.

5.4.5 Comparison with current commercial scale removal techniques

5.4.5.1 Introduction

The experimental results obtained in this chapter are compared with the most recent scale cleaning operations performed with the view of establishing the benefits of exploring this new technique in oil and gas scale cleaning without using solid particles (sterling beads) in the spray jet. It is important to note that the current technique developed may not provide a substantial level of erosion to completely replace the use of water jets combined with solid particles, but has significantly shows an increase in erosion achieve with aerated chamber without using the solid particles, which can lead to another, greener, technology for environmental sustainability of descale operations. The comparison is performed indicated a 12.80 g removal using the aerated trials from this investigated compared to 6.1 and 25 g for the Khuff field and EW 873 field respectively compared in the following case studies:

- **Section 5.4.5.2** Khuff Reservoir Wells-Al Ghawar field Saudi Arabia
- **Section 5.4.5.3** Ewing Bank 873(EW 873) Field, Gulf of Mexico

Although the two case studies employed industrial scale descaling operations which are not suitable for laboratory investigations, the comparison used normalization technique in which the impact pressure attributed to each of scale erosion are compared to the mass of scale removed. The next section performed analysis for the Khuff reservoir located in the largest oil production site worldwide in Saudi Arabia.

5.4.5.2 Khuff Reservoir Wells in Al-Ghawar field Saudi Arabia

The Khuff gas wells are located in the current Al-Ghawar oil field in Saudi Arabia discovered in 1948 with a dimension of 225km long by 30km wide considered as the world largest oil production field. The field is subdivided into five regions from north to south. The company in charge of the field, *Saudi Aramco*, has successfully developed the field utilising an acid fracturing scheme for stimulation with optimum well productivity and completion and well productivity enhancement techniques. The Khuff field is a gas production field produced for over 20 years. The field has had a reported mineral scale deposits, which attracted attention. Recently Iron Sulfide has been the most challenging scale types which the removal used. Fig.5.39 provides the productivity performance of the well. The Mass of 2850kg of Iron Sulfide scale was removed over a period of 7 days. A detail data of the field is shown in Table 5.2 and the calculations is shown in Table 5.4.

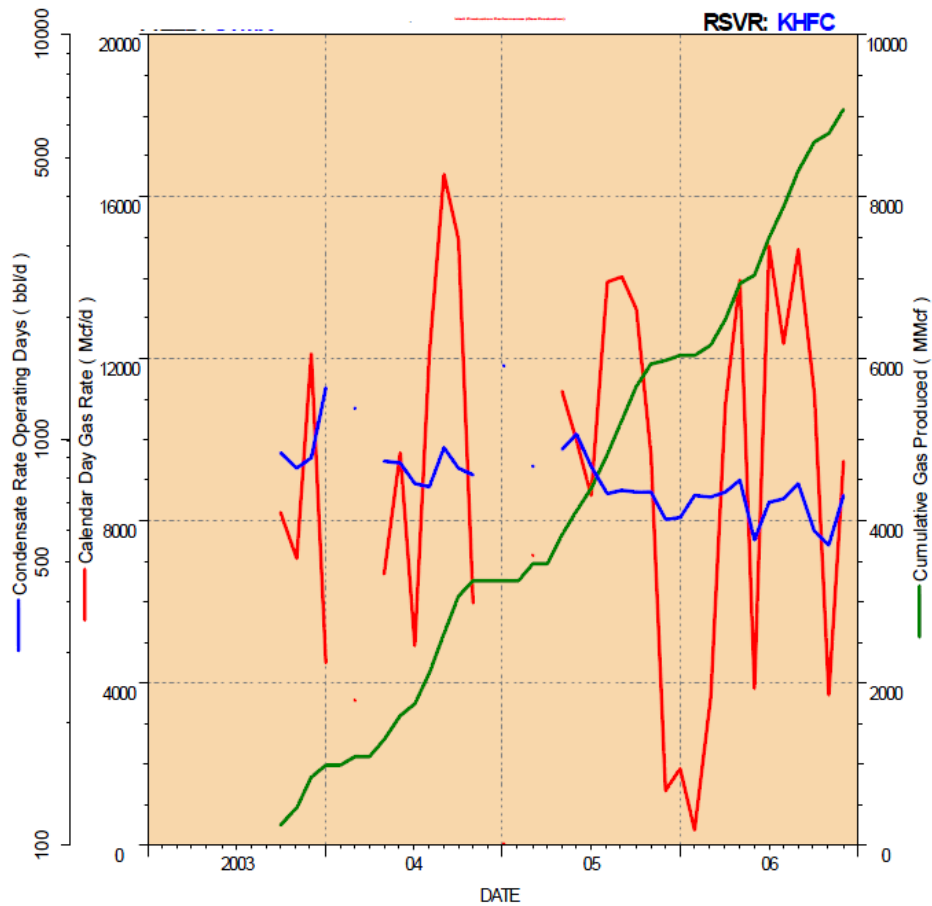


Figure 5.39 Khuff productivity performances[1]

Table 5.2 *Khuff* field descaling parameters

Parameter	Unit	Value
Tubing size	Inches	5.5
Scale thickness	mm	14
Number of nozzles	-	11
Jet Pressure Drop	MPa	23.8
Descaling duration	days	7
Scale type	-	Fe ₇ S ₈
Scaled depth	ft	11,000

Given the mass of scale removed within 7 days in the Khuff field, the amount of scale removed per atomizer per 5 minutes have been estimated in the Fig. 5.40 from both techniques, and also the profile of the Khuff scaled region is shown in Fig.5.41.

5.4.5.3 Ewing Bank 873(EW 873) Field, Gulf of Mexico

The Ewing bank field 873 discovered in 1991, is located 130 miles south of New Orleans in the Offshore Gulf of Mexico shown in Fig. 5.42, where Well A04 is among its wells which

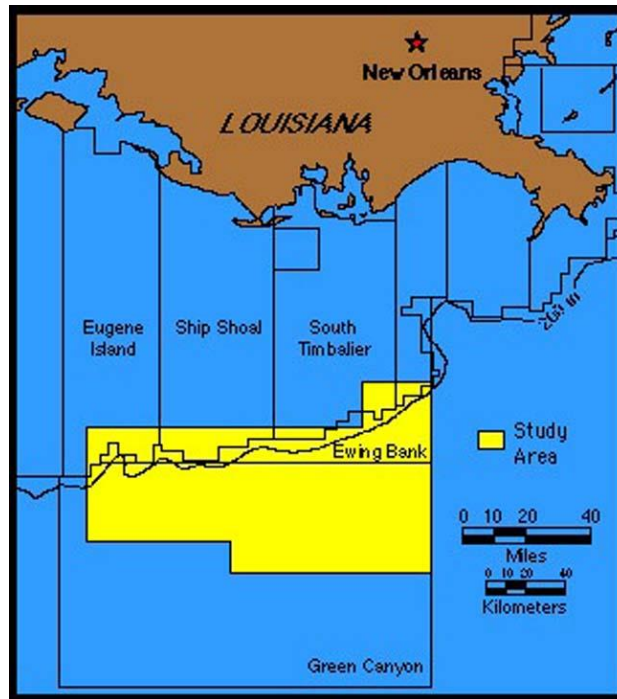


Figure 5.42 EW 873 Field location map[148]

Experienced severe production loss due to formation damage, as well as $BaSO_4$ deposit resulted from water incompatibility among injected formation water and the sea water inhibited by biocide, which was successfully removed using water jet blasting technique shown in Fig.5.43. Table 5.3 indicate the nozzle head specifications.

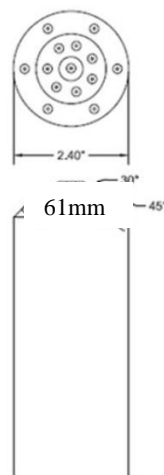


Figure 5.43 Atomizer assembly used for the EW 873 descaling

Table 5.3 Descaling conditions of EW 873

Parameter	Unit	Value
Atomizer Head OD	Inches	2.4
Number of jets	-	14
Jets ID	Inches	0.055
Jet Pressure Drop	MPa	23.8
Maximum tubing depth	m	3810
Scaled region	m	960.12
Descaling time	feet per min	5

The area covered by the scale sample in the tubing has been provided in Fig. 5.44, which can be used in generating the mass of scale removed during the operations

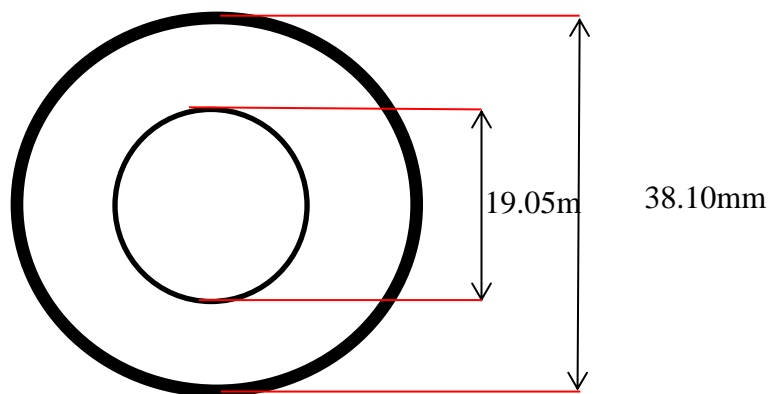


Figure 5.44 Scale deposition cross section in EW 873

$$\text{Area covered by the scale} = \pi(38.1^2 - 19.05^2) = 2563.53\text{mm}^2 = 0.002564\text{m}^2$$

$$\text{Volume of scale} = V = \text{Area of annulus} \times \text{Length of the scaled section}$$

$$\text{Volume of scale} = V = 0.002564 \times 960.12 = 2.46\text{m}^3$$

$$\text{Mass of scale,} = \text{volume} \times \text{density of BaSO}_4$$

$$V = A \times l = 0.00256 \times 960.12 = 3.28\text{m}^3$$

Mass of scale removed= $density \times volume$

Mass of scale removed, $M=4500 \times 2.56 = 11,077kg$

Descaling time can be calculated as 10.5hrs (See appendix G)

Table 5.4 Khuff field descaling data

Parameter	Unit	Value
Total mass of BaSO ₄ removed	kg	14760
Duration	Hrs.	3.5
Number of Nozzles	-	14

Mass of scale removed per Nozzle per 5 minutes performed experimentally in this investigation can then be calculated in Appendix G

5.4.5.4 Results comparison of this investigation and the commercial scale removal technologies

The impact pressure achieved through the two nozzles can be calculated using Eq. 3.5, using the data obtained experimentally for the Flat fan nozzles and the data provided by the two separate operations. Compared results is shown in Table 5.5

Table 5.5 Atomizer characteristics comparison

	Flat Fan Atomizer	Khuff Atomizer	EW 873 Atomizer
Spray angle(°)	25	90	90
Liquid velocity(m/s)	117.5	218	218
Injection	10	23.8	23.8
Pressure(MPa)			
Impact	4.99E+11	2.50097E+13	2.5E+13
Pressure(N/mm ²)			
Impact Pressure Ratio	1	50	50

The calculations performed shown in Table 5.5 indicated a scale removal of 12.80g using the aerated flat fan atomizer higher than the commercial Khuff field of 6.1 g. However, the results obtained using the aerated flat fan atomizer is lower than the 25.0g obtained at EW 873 commercial technology due to type of atomizer used in that case, which is a solid stream

atomizer. Although, the solid stream atomizer indicated higher impact pressure (see Section 6.5.1, Fig.6.34) enabling higher erosion rate limited to smaller surface area compared to flat fan atomizer. Additionally, using solid stream atomizer has a potential of eroding larger fragments of mineral scales due to narrower velocities distribution compared to flat fan atomizer characterised in Section 5.2.2.1, which could lead to tubing blockage and longer maintenance duration than normal. The wells descaled were then compared in Table 5.6.

Table 5.6 Scale removed comparison

Nozzle Pressure Drop(MPa)	Mass of scale removed(g)		
	Flat fan	Khuff field	EW 873
10	12.88	6.1	25
8	10.2	2.7	10.8
6	8.9	0.89	3.6
4	8.1	-	-
2	4.5	-	-

The comparison of the scale removed using two different descaling operations in the Al-Ghawar field (largest oil production site in the world) and the EW 873 in the Gulf of Mexico are made in this section as shown in Fig. 5.45. It is evident that utilising aeration during descaling oil wells has shown significant improvement with a value of 12.80g over that of Leal et al having 6.1g although lower than Spongwi et al with 25.0 g due to the use of solid stream atomizer characterised with low cleaning impact area in addition to scale fragments potential to cause blockage during maintenance.

The results obtained using involved normalizing the operating conditions of the both trials through comparing the mass of scale removed and the pressure applied. The impact force attained was then taken as ratio of the laboratory experimental scheme as An Impact Pressure Ratio (IPR).

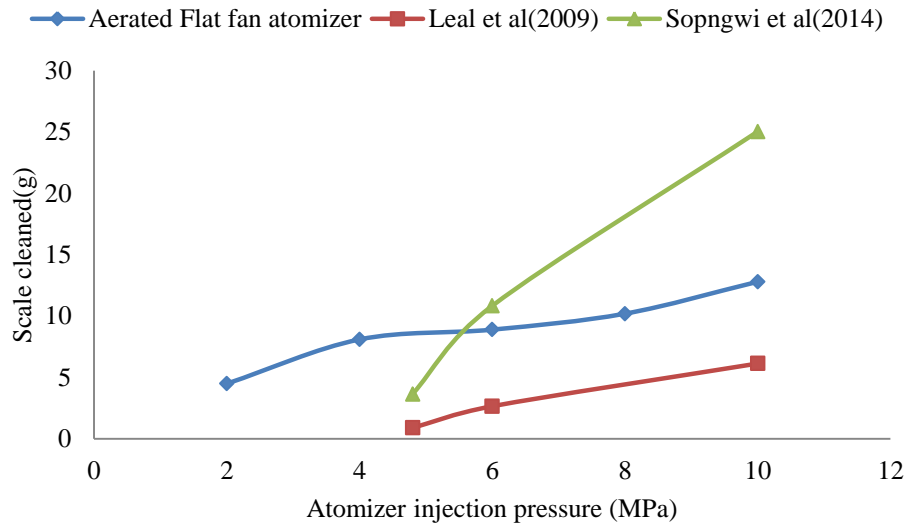


Figure 5.45 Comparison of results from this investigation and the commercial technologies

Improvement in the aeration research application especially for on-shore oil well descaling will reduce substantially the use of sterling beads as a means of achieving enhanced erosion.

5.5 Summary

The following summary has been drawn from this chapter

1. Interactions of air around a high pressure water sprays induced drag effect unto the surrounding air, leading to generation a air velocity distributions around the sprays with varying axial and lateral values ranging from 4 to 14m/s.
2. The droplet size ranges of 55 to 81 μ and droplet velocities of 75 to 117m/s, enabling the droplet momentum and impact pressure at the highest at the centre of the spray to be up to 1.45e-05kgm/s and 0.15MPa
3. Aeration has shown significant increase in the compressive stress around the scale samples leading to increased erosion by about 30% compared to non-aerated trials.
4. Aeration has been shown to significantly reduce or even eliminates cavitation within 2-4mm away from the atomizer eliminating the tendency of cavitation erosion at 25mm where the scale sample stand-of distance was chosen for this study.
5. Comparison of the current research with similar commercial descaling processes utilising solid particles confirms the suitability of employing aeration in descaling instead of the solid particles.

Chapter 6

Spray Jet Breakup and Cavitation's Modelling using CFD-Fluent

6.1 Overview

Despite the substantial experimental measurements conducted in the previous chapter, it is essential to validate some of the measured values through modelling the experimental behaviour in the Computational Fluid Dynamics (CFD) package, not only to validate the results obtained but also to carefully investigate other non-experimentally suitable measurements. Considering some of the design and experimental limitations which were beyond the capability of the test-rigs, in addition to highlights the relevance of parameters such as sprays' cavitation's along a flat-fan nozzle and other nozzles, ambient medium conditions, erosion tendencies of such parameters. In this chapter, the analysis is categorized into three (3) phases:

- **Section 6.4:** Entrained air around high pressure sprays as well as the characterization of the water sprays droplet sizes and velocities. However, instead of impact pressure measurement, turbulent kinetic energy was substituted in the *Fluent* models to enable impact pressure validation.
- **Section 6.5:** Cavitation behaviour of the sprays emerging from the flat fan atomizer was considered to establish the suitable stand-of distance where cavitation bubbles do not attain. This ensures the scale removal trials do not consider erosion attributed to cavitation.
- **Section 6.6:** Scale erosion validation was conducted to using various type of scale sample built-in the CFD-Fluent package at the wall.

The next section provides the basic concept of CFD applications in solving engineering related problems.

6.2 Principle of Spray and Cavitation Flow Models in CFD

The techniques of CFD Modelling has been recognised to have powerful and sufficient span of applications in both industrial and non-industrial relevance[149][150][151][152][82].Modelling spray injections have been developed due to its wider applications in combustion, spray drying agricultural sprinkling, fire-extinguishing

medical application and recently in cleaning oil and gas production tubing etc. using built-in Eulerian-Lagrangian spray models[153][154], discrete droplet parcels with their sub-models capable of predicting droplet motion, collisions, heating, evaporation, dispersion as well as breakup. Section 3.4 has described the interplay of forces during Primary and Secondary Atomisation. Although, conventional models such as Taylor-Analogy Breakup (TAB), Wave model (K-H instability of jets surface), stochastic breakup has been used for simulating the spray break-up. Computation fluid dynamics consist of basically three (3) segments, (i) the pre-processor, (ii) the solver and (iii) the post-processor.

The initial segment consists of the pre-processor with an interactive profile to enable model geometry and positioning, grid and mesh generation, physical phenomena, fluid characteristics as well as boundary conditions. The solver section enables the user to monitor the iterations as well convergence for the momentum, energy, continuity, turbulence as well as Pressure and Volume relations among others[134]. The post-processor interface is then used to view and analyse the results obtained into charts, vector and Cartesian plots.

Among the first steps in carrying out Fluent-CFD simulation is the geometry design of the typical flat fan atomizer as well as selecting appropriate models. Details are provided in the next Section.

6.3 Nozzle Selection for Erosion and Impact performance

6.3.1 Turbulent models

While Fluent code has utilized as commercial CFD simulation package principally for solving flow problems using the laws of conservation of mass, momentum, energy, chemical species interaction which are configured to handle finite volume of element and difference method. Equations built-in the code governing the model have been discretised using curvilinear grid in order to enable computation of complex and irregular geometries. The code computes through interpolation using first-order, second-order, or even higher order, power-law as well as up-wind scheme, solving the equations using line-by-line iterative matrix solver with multigrid acceleration. There are several turbulent models in Fluent code such as:

- Standard k- ϵ model
- Realizable k- ϵ model
- Standard k- ω model
- Renormalization Group(RNG) k- ϵ model

- Shear Stress Transport(SST) $k-\omega$ model
- Large Eddy Simulation(LES) model
- Reynolds Stress Model(RSM)

With k , turbulent kinetic energy, ϵ , as viscous dissipation rate, and specific dissipation ω . Considering the high cost of application of LES model and the time consuming nature of RSM models have been exempted in this analysis.

6.3.2 Geometry and Meshing

The geometry involves a pressure chamber connected to both water supply from a high pressure pump and air supply from a compressor as shown in Fig. 6.1(a), and the Fluent built geometry shown in Fig. 6.1(b) with a dimension of 100mm inside diameter and length of 1m. The water is supplied through a Flat-fan nozzle with a diameter of 1.5mm and a spray angle of 25° , held by an aluminium bar inside the chamber.

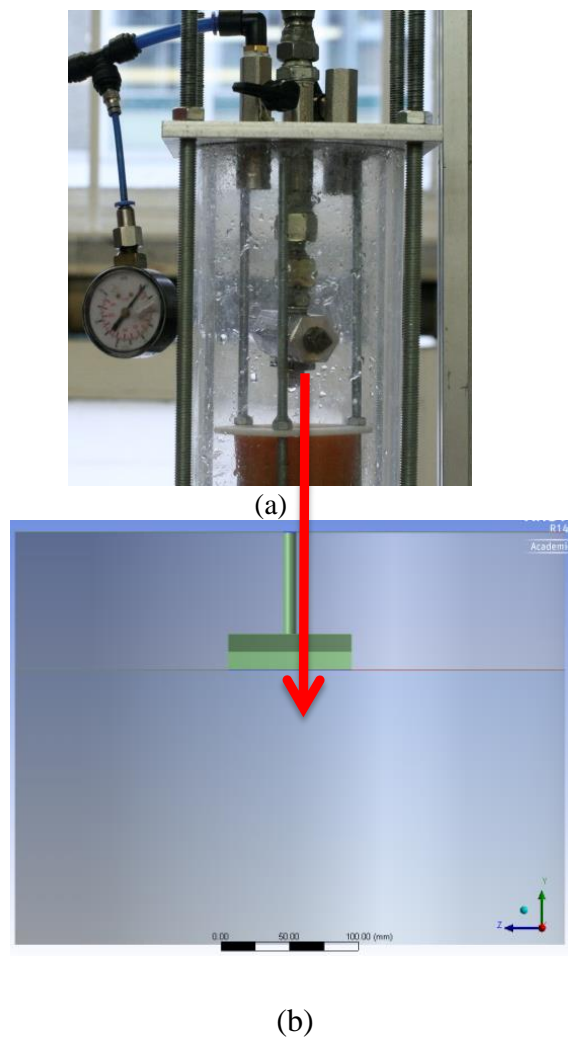
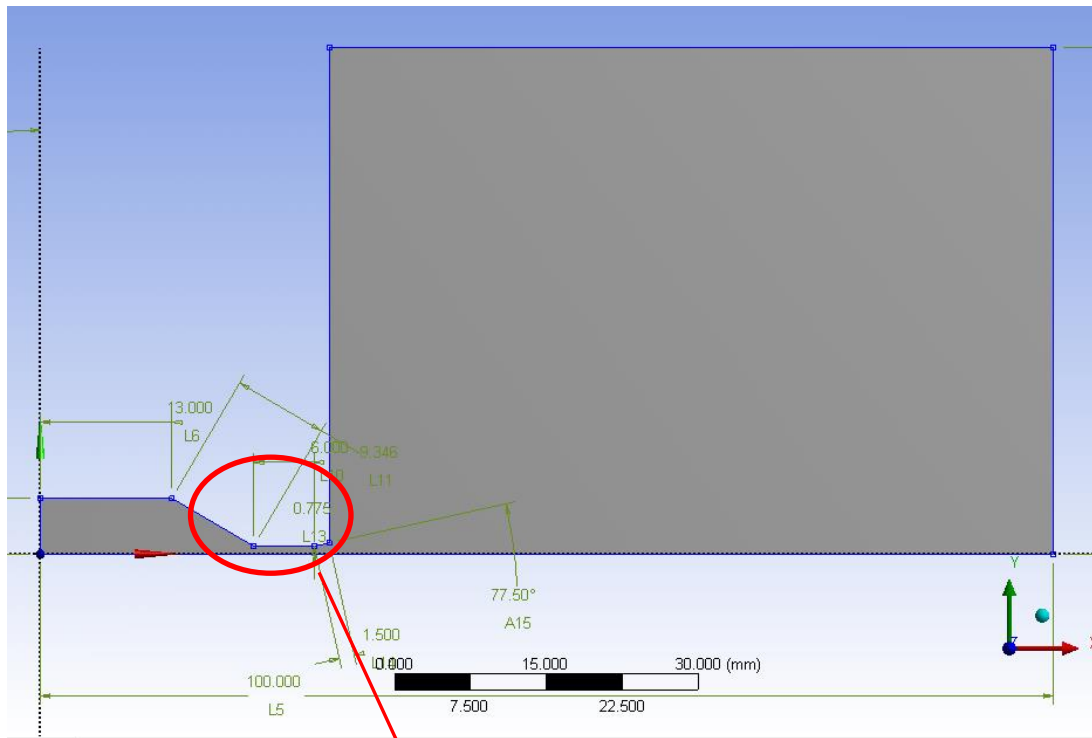
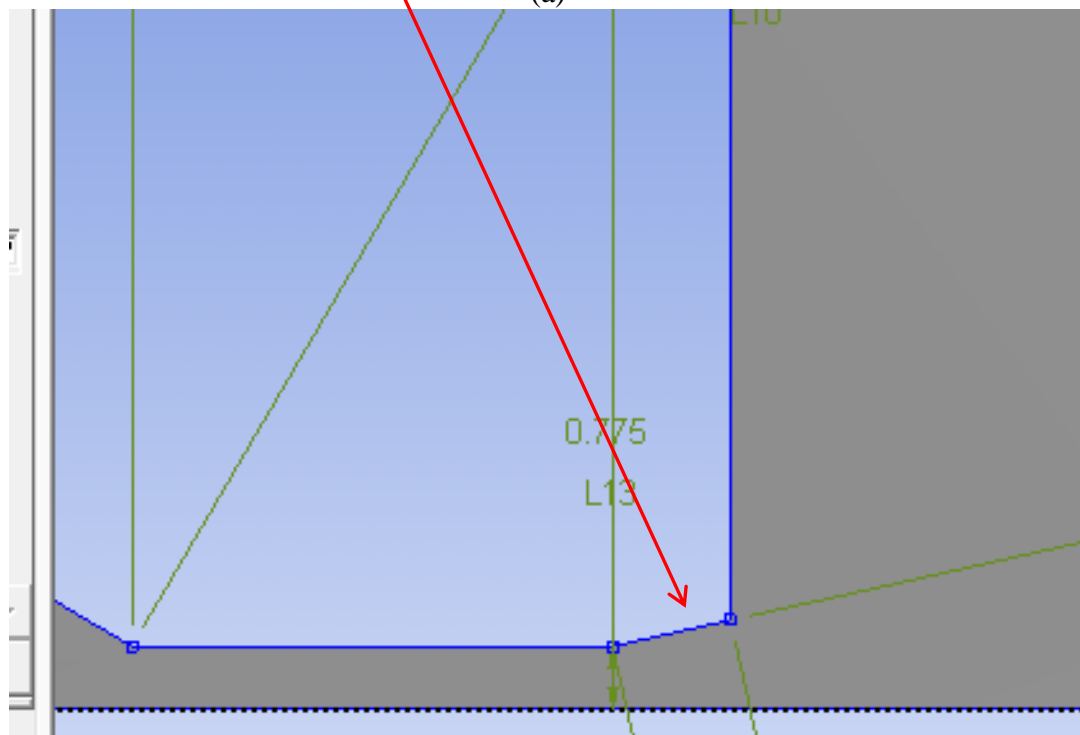


Figure 6.1 Geometry development (a) laboratory chamber(b) model development in 3D

The domain of the interaction between the water and the air and later with the scale were discretized, and an Axisymmetry geometry was chosen such that only half of the geometry is discretized. The model plane for the flow was then assembled to include the Flat-fan nozzle and the walls in a single diagram shown in Fig. 6.2 in 2D.



(a)



(b)

Figure 6.2 Flat-fan nozzle assemblies

The meshed was initially developed in 3D to conform to the design experimental rig and hence the plan selected for the 2D analysis was improved further for consistency.

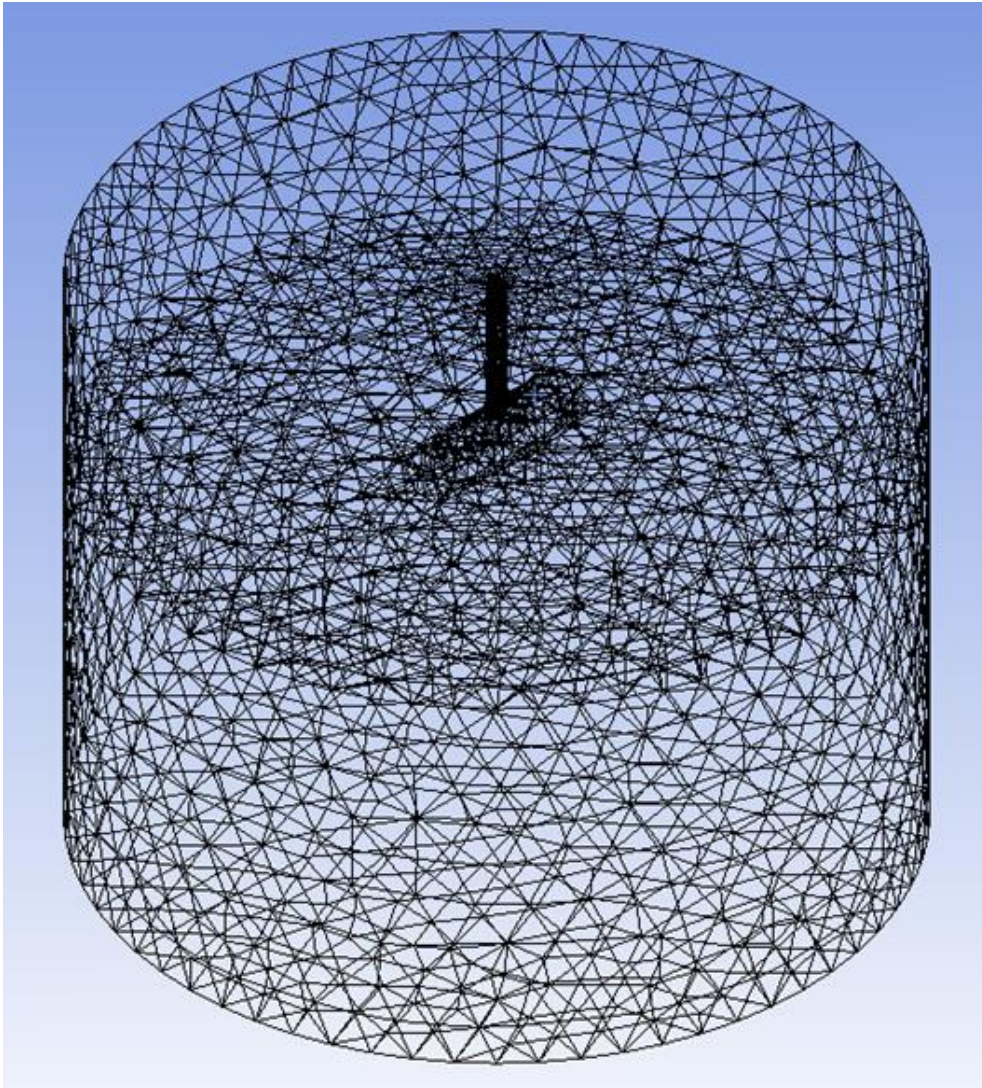


Figure 6.3 Chamber meshed model in 3D

The meshing stages involves the initial basic mesh, and then subsequent mesh improvement was applied with emphasis to areas of concern such as the nozzle throat where the pressure drop analysis is carried out further until the simulation results was independent of the mesh improvement. The final statistic includes 4635 nodes and 2343 elements.

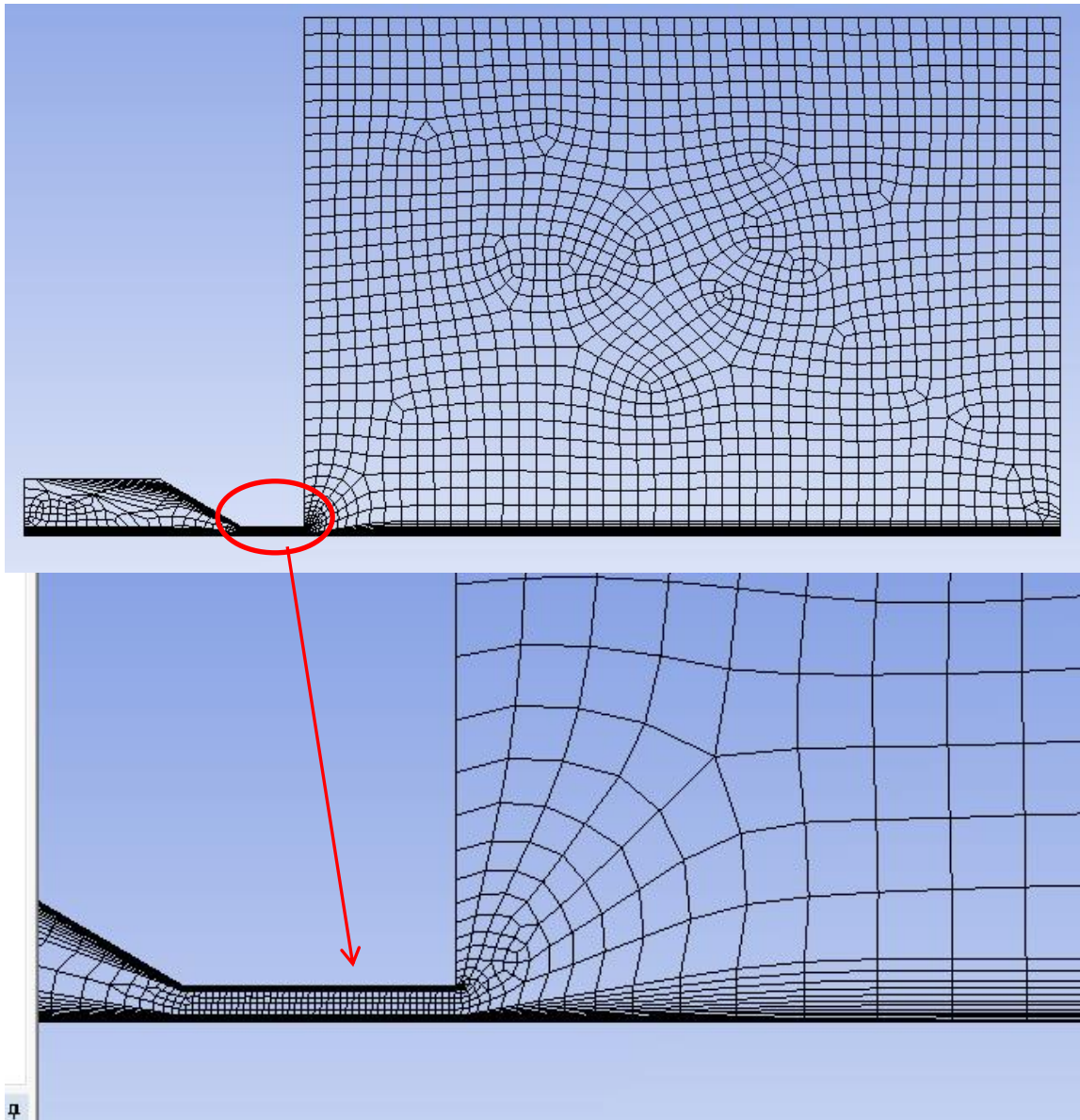


Figure 6.4 Exploded view of the Meshed domains for the flat fan nozzle in 2D

6.3.3 Boundary Conditions

The boundary conditions for the experimental rig were adopted for the Fluent simulation which includes the inlet pressure of 4.8, 6.0 and 10MPa pressure, the chamber pressure of 0-0.2MPa corresponding to various 0-12.0 % aeration was maintained for the variety of tests carried out.

Table 6.1 Boundary conditions

Section	Parameter	Value
Inlet	Pressure	4.8, 6.0 and 10MPa
	Temperature	300K
	Turbulent intensity	4.5%
	Hydraulic diameter	1.5mm
Outlet	Pressure	0.5, 1.0MPa
	Temperature	300 ⁰ K
	Turbulent intensity	4.5%
	Hydraulic diameter	100mm
Wall	Materials	CaSO ₄ , CaCO ₃ , BaSO ₄
	Roughness height	
	Interaction type	

6.3.4 Criteria for Convergence

The convergence of the simulation was achieved through specification of continuity parameters as stated in the Table 6.2. The iterations converged normally after 500 as shown in Fig. 6.5.

Table 6.2 Criteria for convergence

Residual	Criteria for convergence
x-velocity	0.00001
y-velocity	0.00001
z-velocity	0.00001
continuity	0.00001
Energy	0.000001
k	0.00001
Viscous dissipation rate	0.00001

6.3.5 Model Equations and Boundary Conditions

In a typical turbulent model where the Reynold's number has gone beyond critical value characterised with chaotic pattern in the flow properties especially for non-compressible fluid like water, such behaviour can be modelled using Navier-Stoke and continuity equations for the components along x, y and z axis as follows:

$$\frac{\partial u}{\partial t} + \text{div}(u \mathbf{u}) = -\frac{1}{\rho} \frac{\partial p}{\partial x} + \frac{\mu}{\rho} \text{div grad } u \quad (6.1)$$

$$\frac{\partial u}{\partial t} + \text{div}(v \mathbf{u}) = -\frac{1}{\rho} \frac{\partial p}{\partial x} + \frac{\mu}{\rho} \text{div grad } v \quad (6.2)$$

$$\frac{\partial u}{\partial t} + \text{div}(w \mathbf{u}) = -\frac{1}{\rho} \frac{\partial p}{\partial x} + \frac{\mu}{\rho} \text{div grad } w \quad (6.3)$$

$$\text{div } \mathbf{u} = 0 \quad (6.4)$$

Attempting to bring solution to the four unknown parameters (\mathbf{u} , \mathbf{v} , \mathbf{w} and \mathbf{p}) using the method in which the random turbulent model fluctuation of the instantaneous variable are decomposed as sum of the mean for the fluctuating parts. Application of truncation techniques can then be used to numerically solve the partial differential equations.

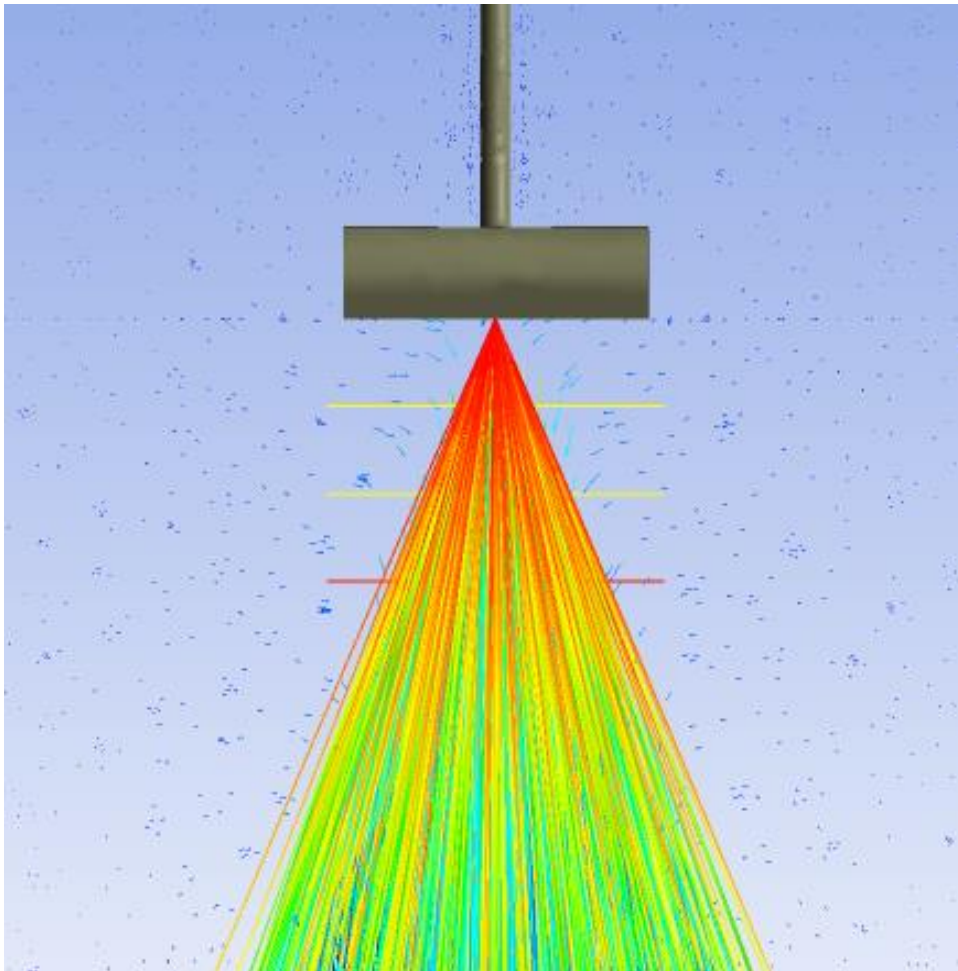
6.4 Entrained-air velocities measurements and Spray characterisation (Phase-I)

6.4.1 Entrained-air Velocities

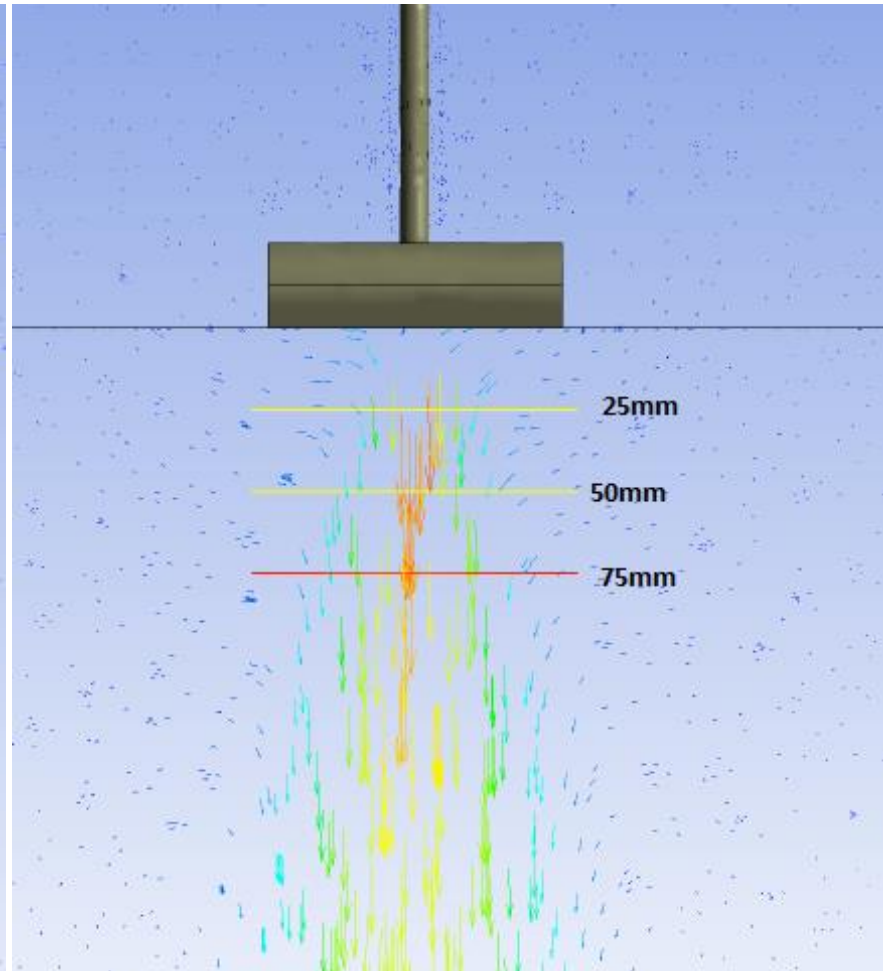
Along the spray jet path, drag forces usually initiate the flow of surrounding air to follow the path moves by the spray jet as well, although other researchers consider the measurement of total mass of air entrained and also the profile of the air flow pattern mostly for fuel based sprays, research gap still exist in the detail analysis of entrained-air around water jet break up and also the impact it may or may not have on the droplet mean velocities and SMD distributions. While Section 4.2.1(Entrainment measurement using Hot-wire anemometry) considered the profile of the entrained air, the CFD simulation become necessary to enable analysis of the entrained air inside the jet regions where physical measurements were impossible experimentally. The analysis of the air velocities was conducted while the water sprays (Fig.6.6(a)) and the with a hidden water sprays(Fig 6.6(b)) to enable more careful analysis be conducted, which the experimental procedure could not be possible.

The air vector diagram in Fig. 6.5 show the actual air profile along the region of spray with and without the jet droplet velocities, it is clearly to then view the air velocities even along regions covered by spray, with gridded lines of measurement at 25, 50 and 75mm downstream as shown in Fig. 6.6. This will provide answers to decay in the air velocities

axially and radially from the nozzle exit, so also the vectors provide detail flow pattern, and sources as well as obstruction to the air flow around the water jet. Varying of pressure shows little or no variation on the air velocities as shown in Fig. 6.7.

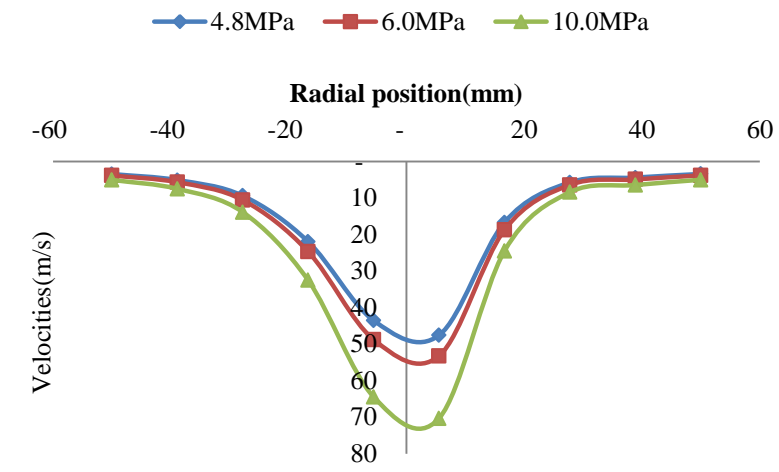


(a) Water and air

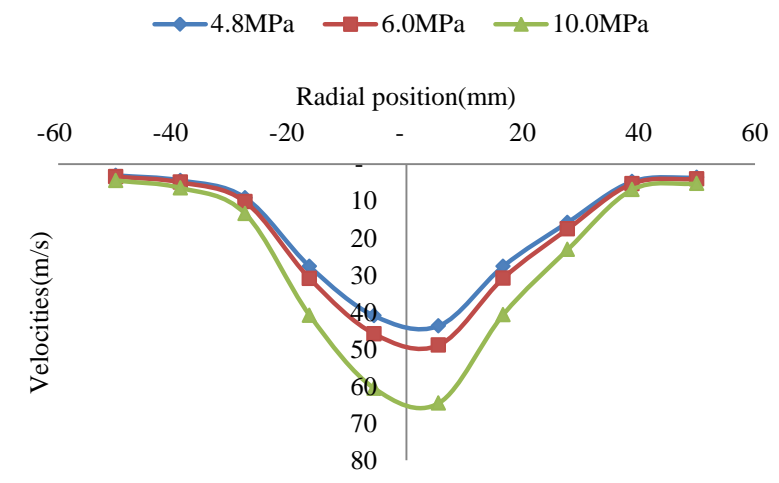


(b)air only

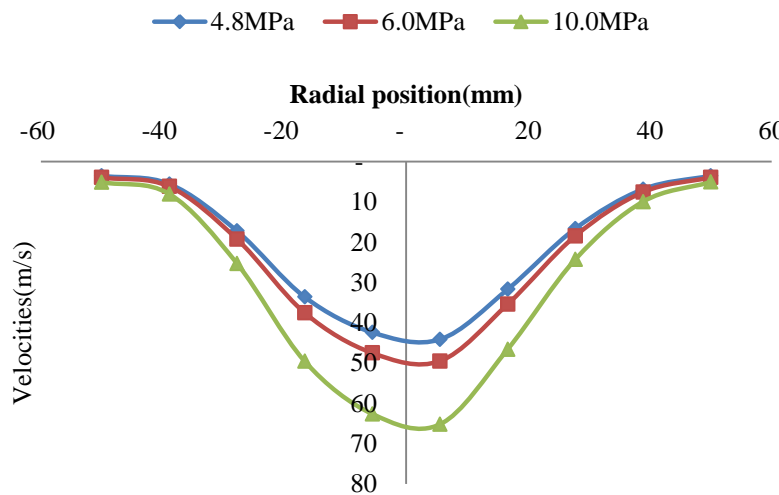
Figure 6.5 Entrained-air profiles (a) with, and (b) without the sprays



(a) 25mm downstream

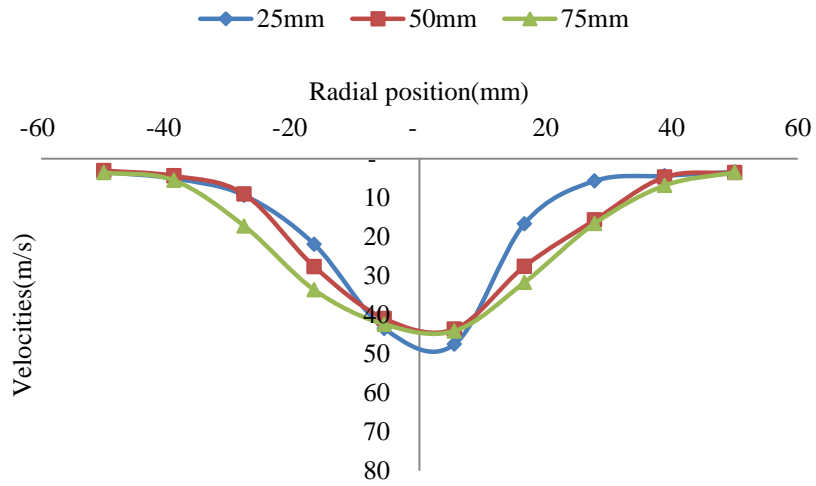


(b) 50mm downstream

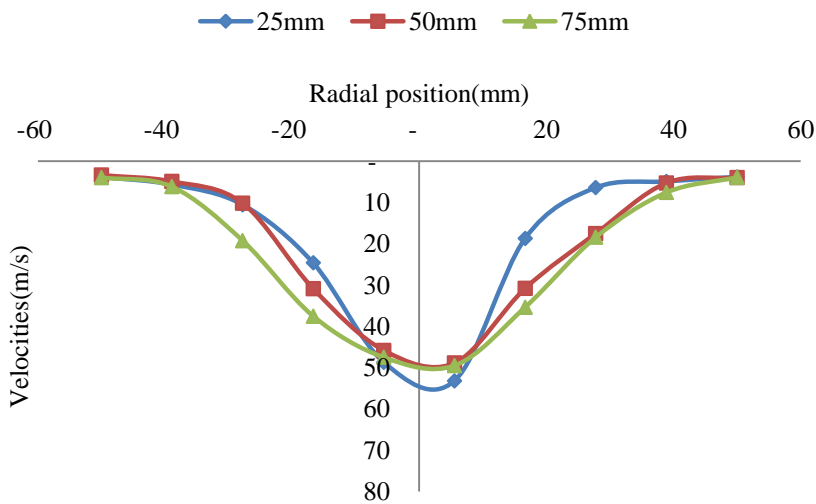


(c) 75mm downstream

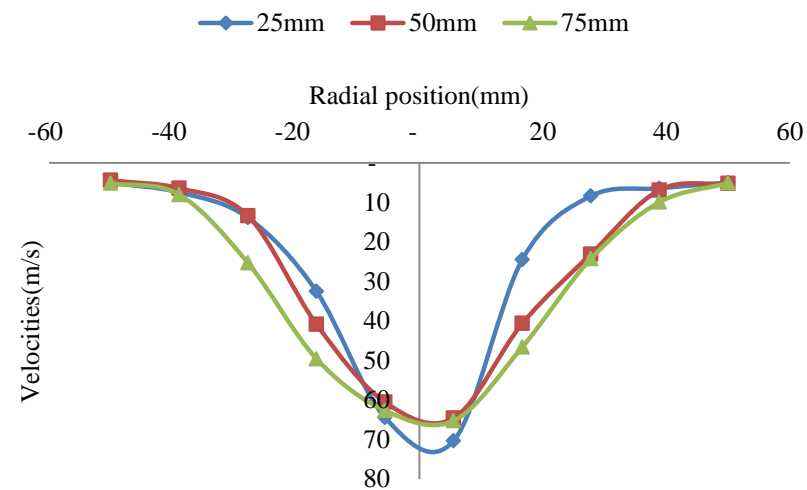
Figure 6.6 Entrained-air velocities at various stand-off distances



(a) 4.8MPa



(b) 6.0MPa



(c) 10MPa

Figure 6.7 Entrained-air velocities at various spray injection pressure

Comparison of the various experimental and simulated trials indicated a relative variation due to the nature in which the measurements were conducted. The air velocities could not measure inside the high pressure water sprays although, simulated results are obtainable as shown in Fig. 6.8, 6.9 and 6.10. The next section provides the high pressure water spray characterisations.

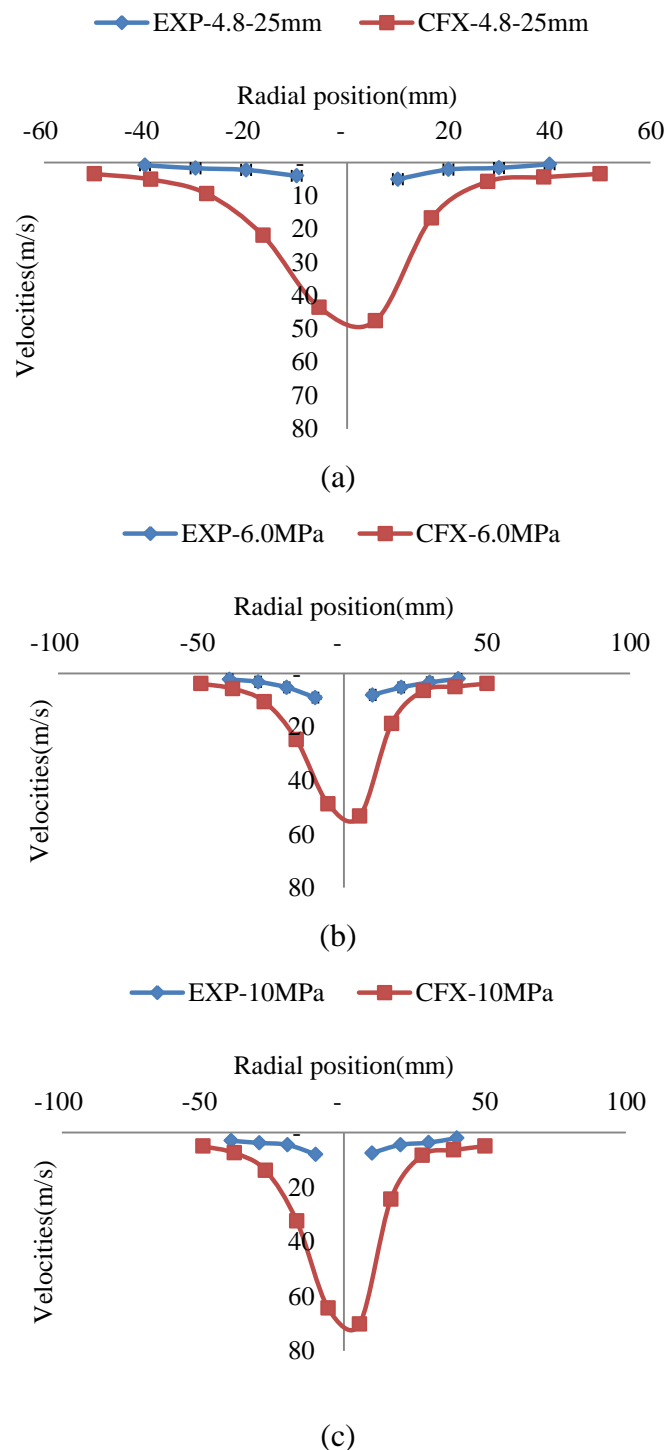
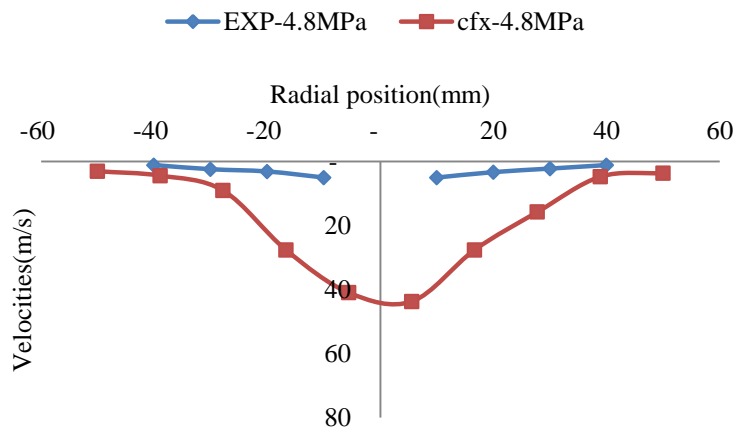
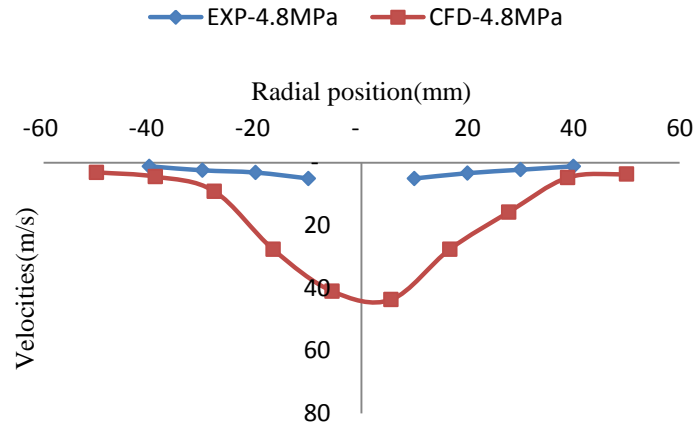
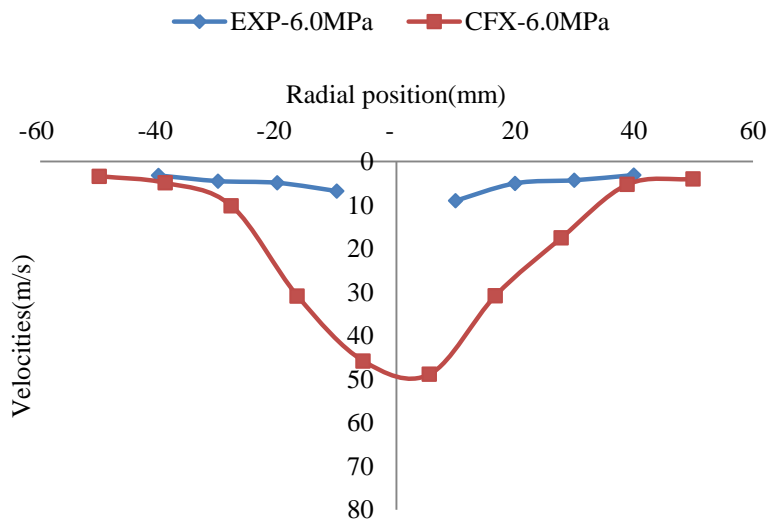


Figure 6.8 Comparisons of Entrained-air velocities between experimental and CFD, at different pressures



(a)



(b)

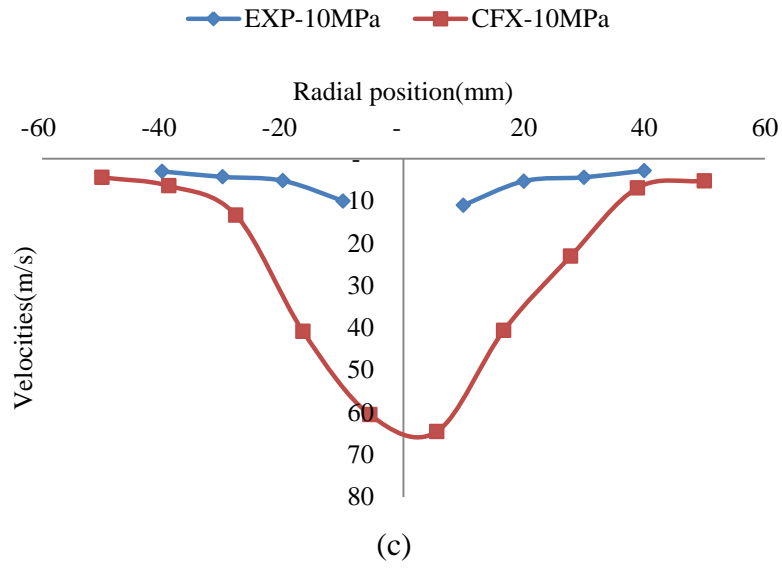
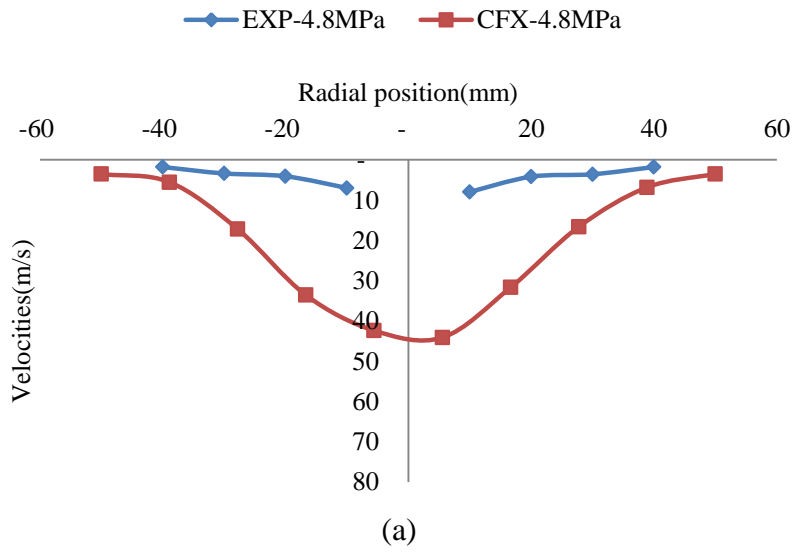
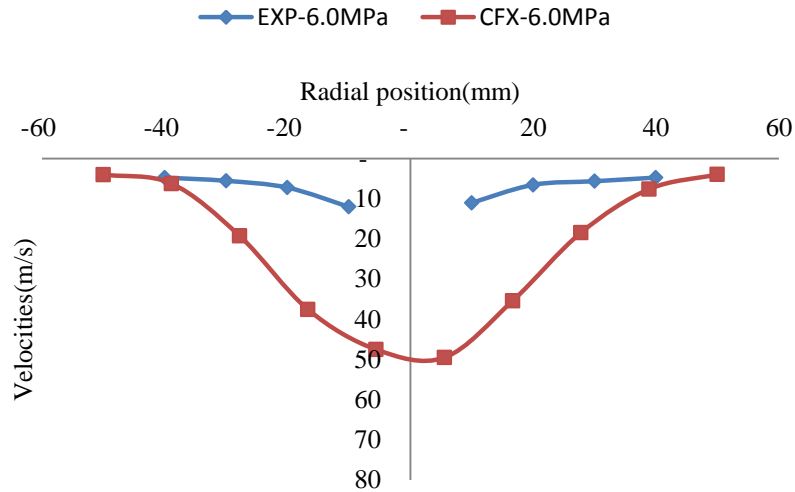
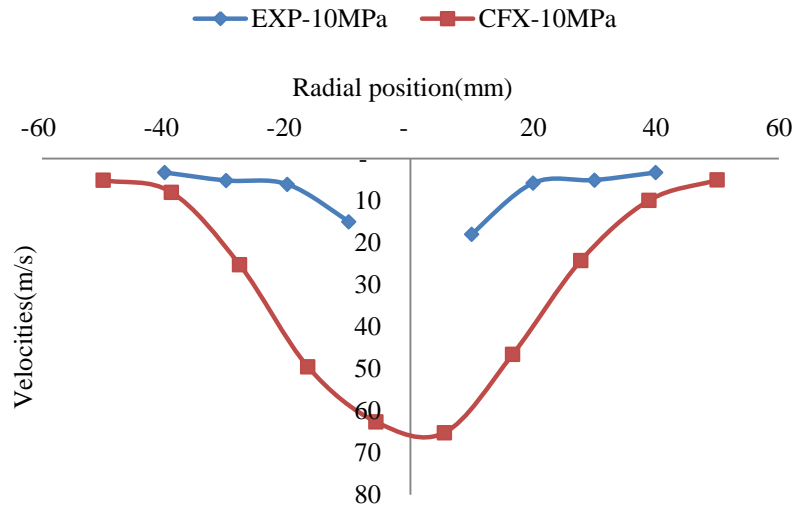


Figure 6.9 Comparisons of Entrained-air velocities between experimental and CFD at different pressures





(b)



(c)

Figure 6.10 Comparisons of Entrained-air velocities between Hot Wire Anemometry (HWA) and CFD at 50mm

6.4.2 Spray characterisations

6.4.2.1 Drop size validation

Measurements of droplet size provides adequate information with regards to momentum and breakup pattern of the flat-fan jet, especially at high pressure systems, the distribution will be useful for explaining whether or not it has impact on the erosion extent. The CFX profile is given in Fig.6.11 indicating the general distribution of the droplet mean size.

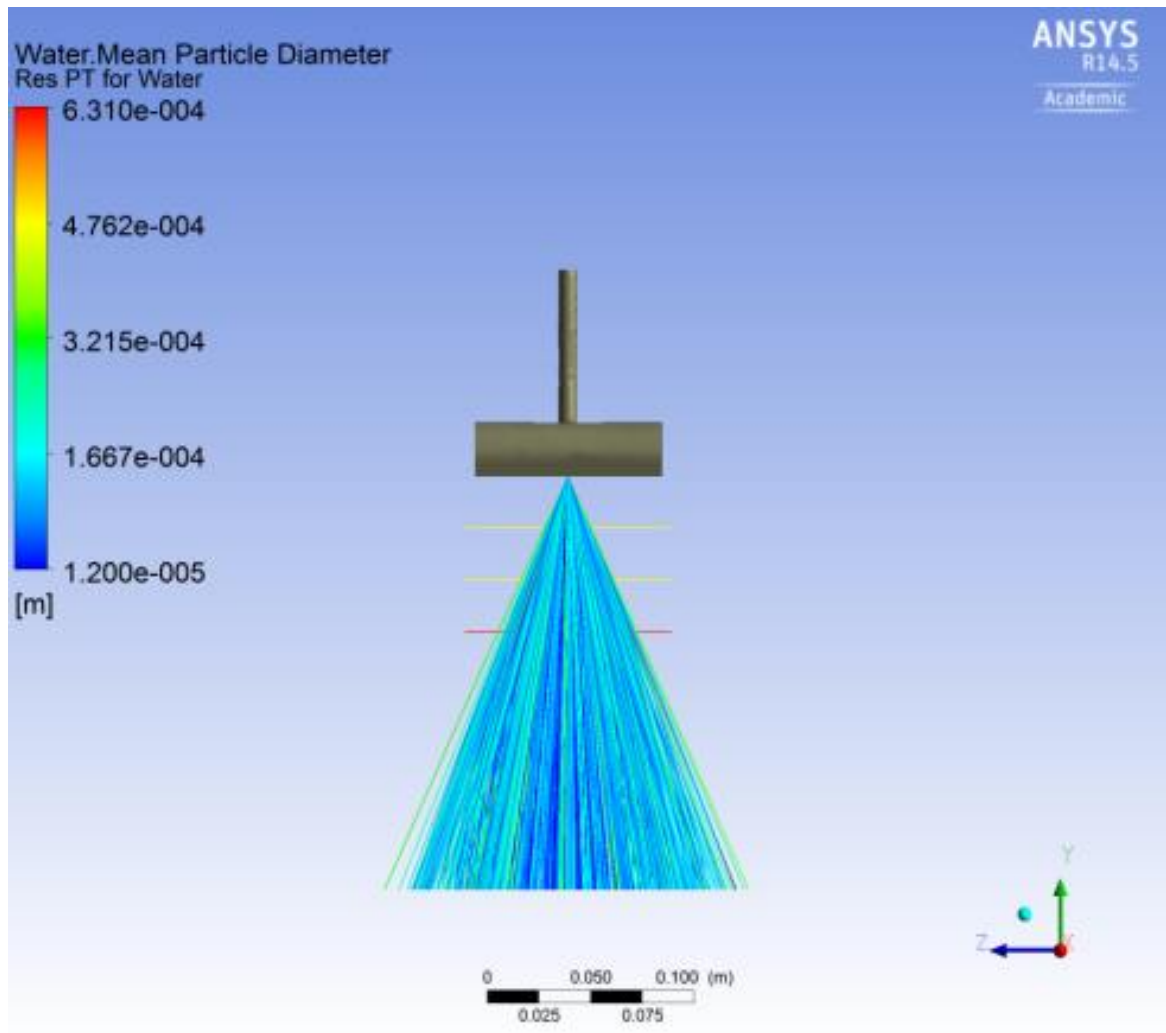


Figure 6.11 SMD profile using CFD

Droplet size distributions in Fig. 6.12 has shown increase in the spray injection pressure decreases the droplet sizes due to shrinkage in the breakup length of the jet, and subsequently changing the downstream positioning of measurements make the droplet sizes even further smaller, due to secondary atomisation.

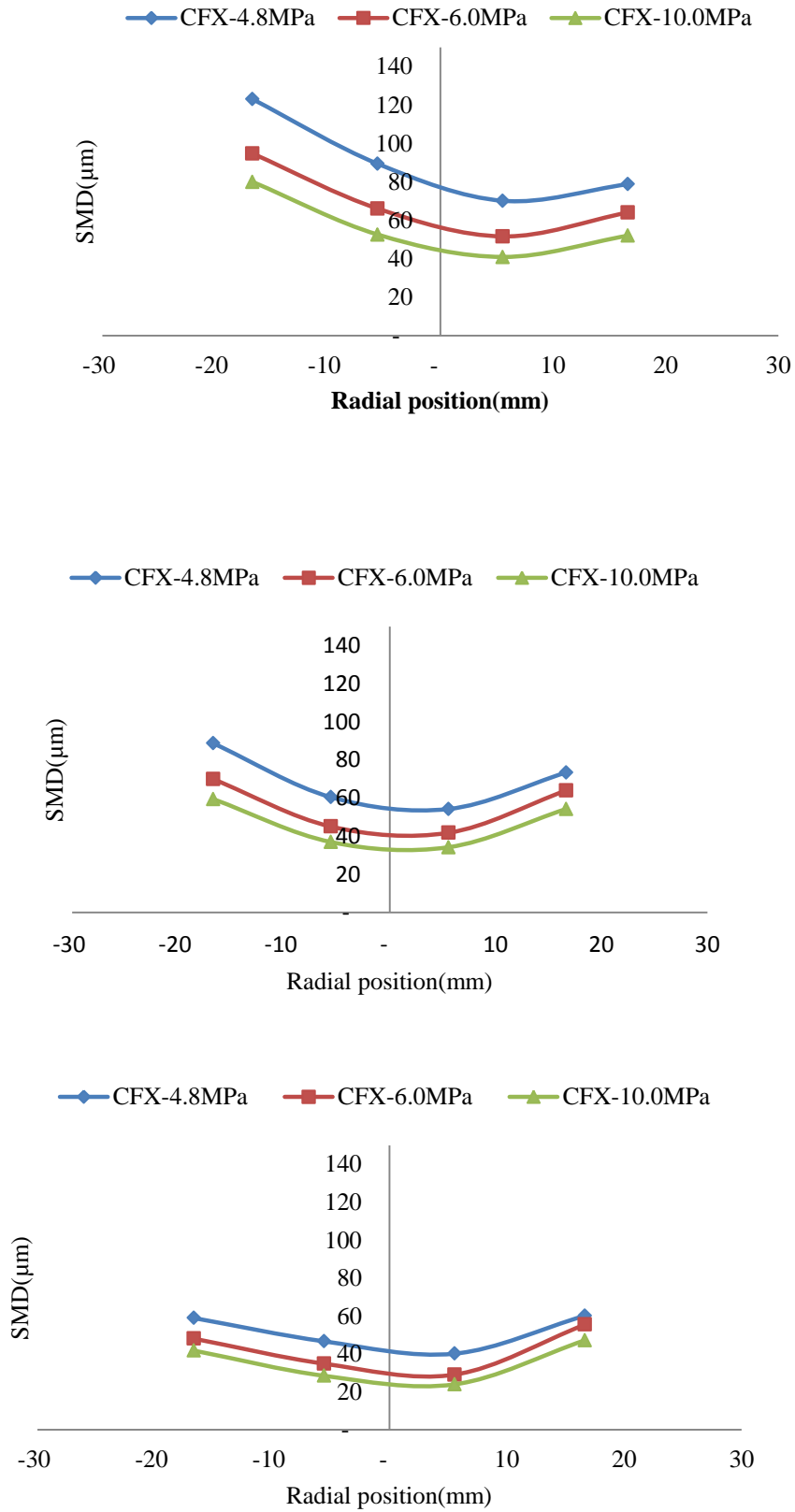
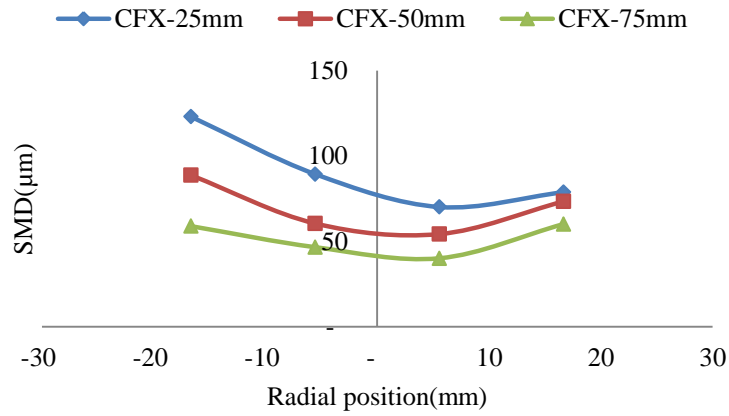
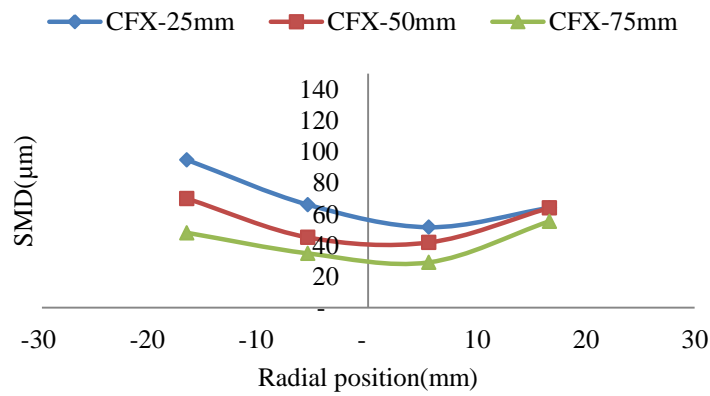


Figure 6.12 SMD at various downstream positions at 25, 50, and 75mm respectively

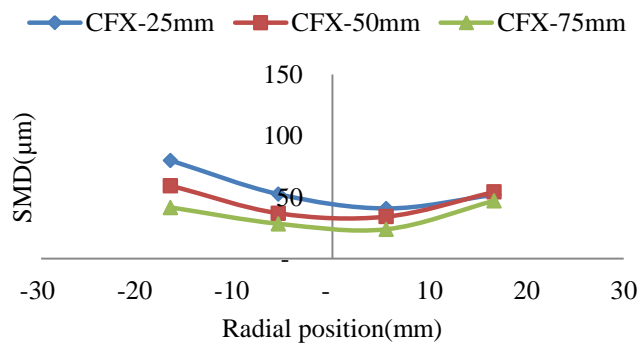
Further investigation shows in Fig. 6.13 that even at the same pressure, further downstream distances favours secondary atomisation's of water jets, still with more breakups at higher injection pressure.



(a)



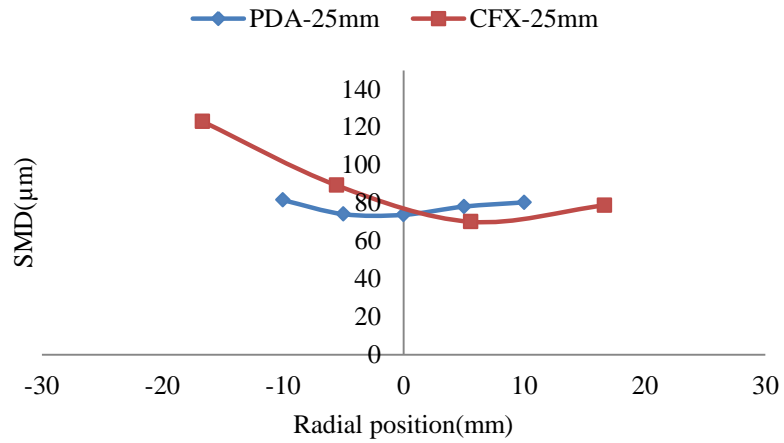
(b)



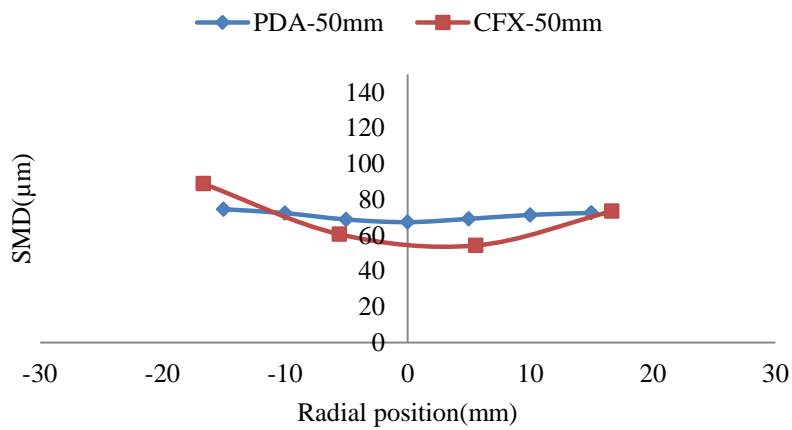
(c)

Figure 6.13 SMD at various pressures

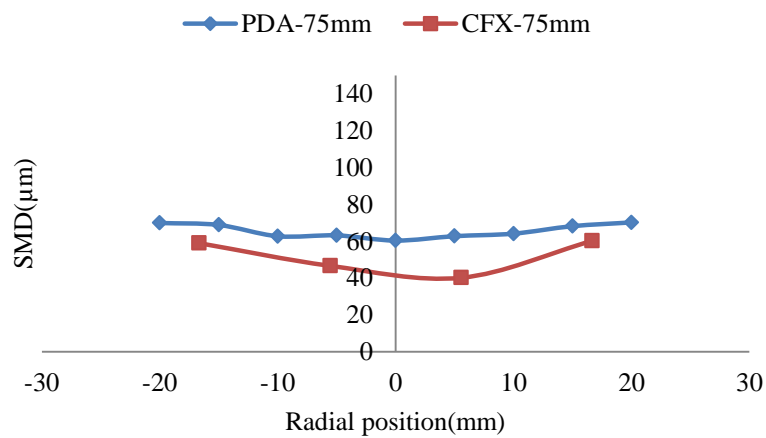
Comparison of the droplet sizes in terms SMD shows lower CFD drop sizes than their corresponding PDA measurements at all pressures shown in Fig. 6.14, 6.15 and 6.16, especially at the spray centre. Although deviations do occur at the spray edge but sensitivity analysis is required to answer such questions.



(a)

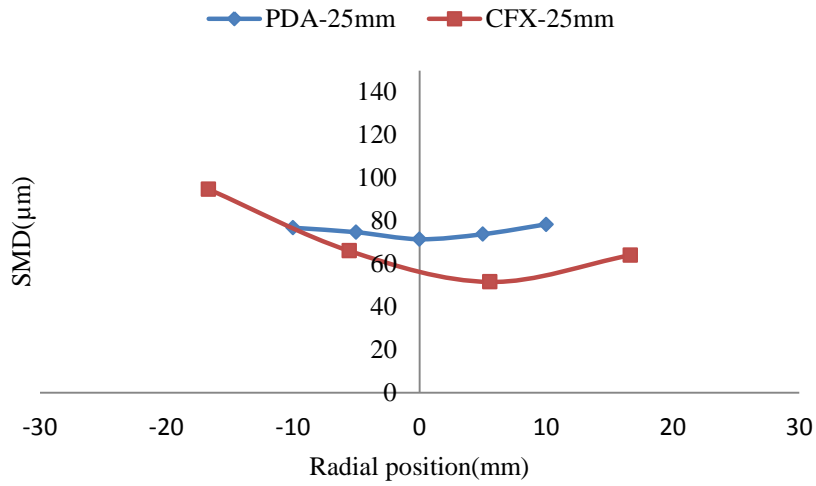


(b)

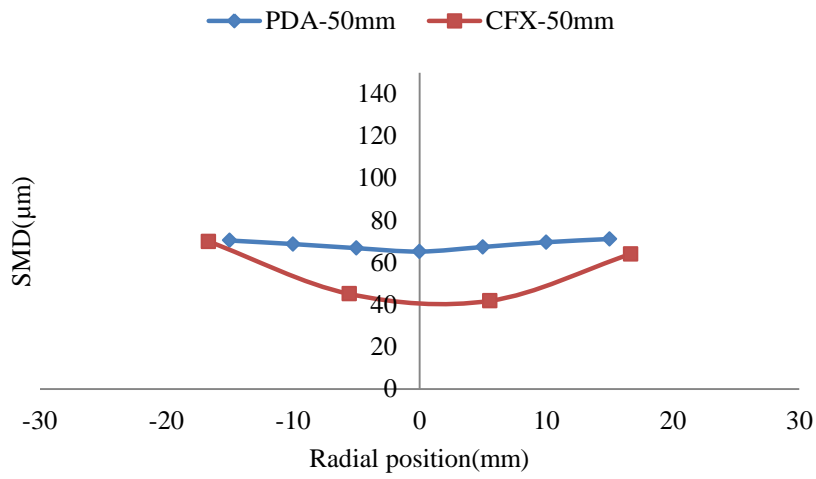


(c)

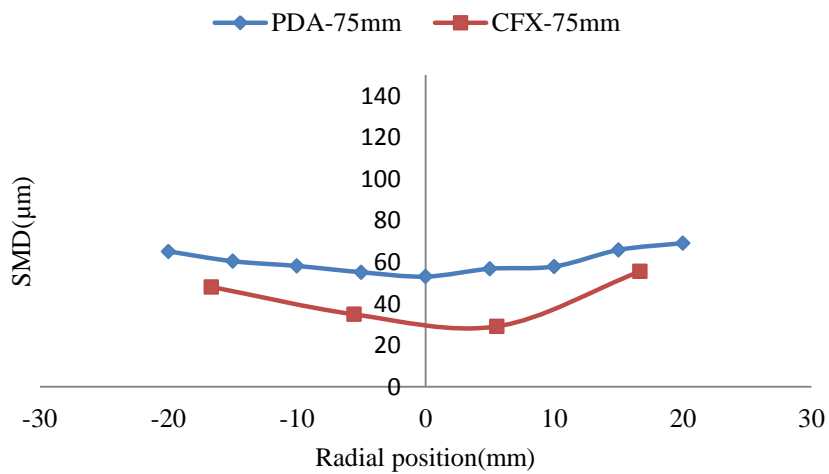
Figure 6.14 SMD comparisons between PDA and CFD at 4.8MPa



(a)

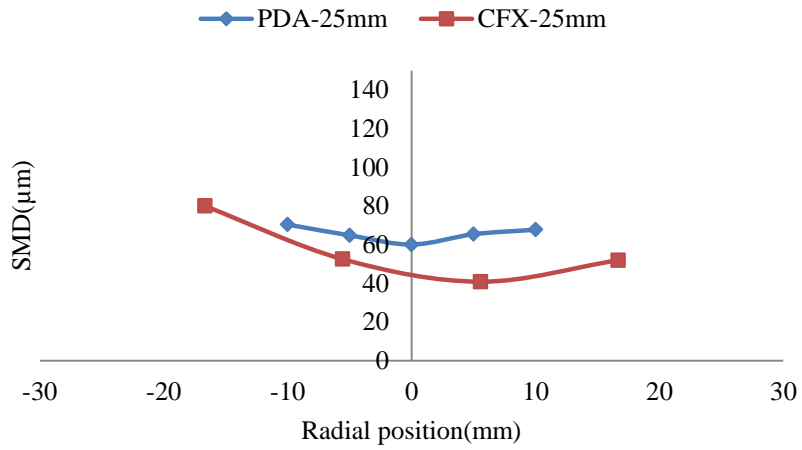


(b)

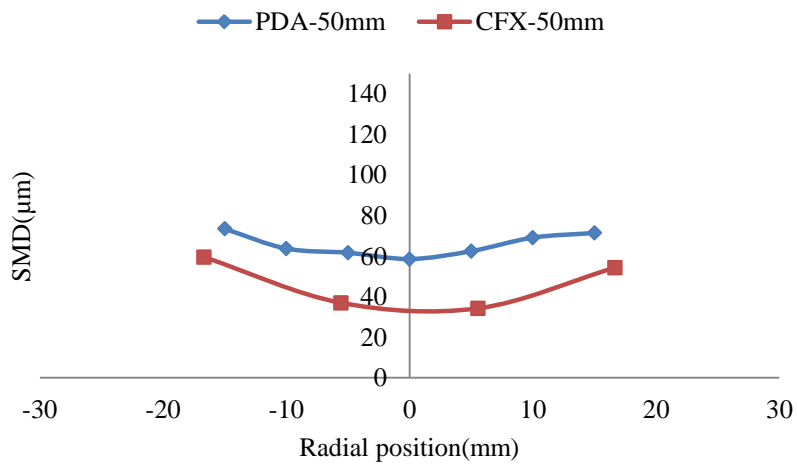


(c)

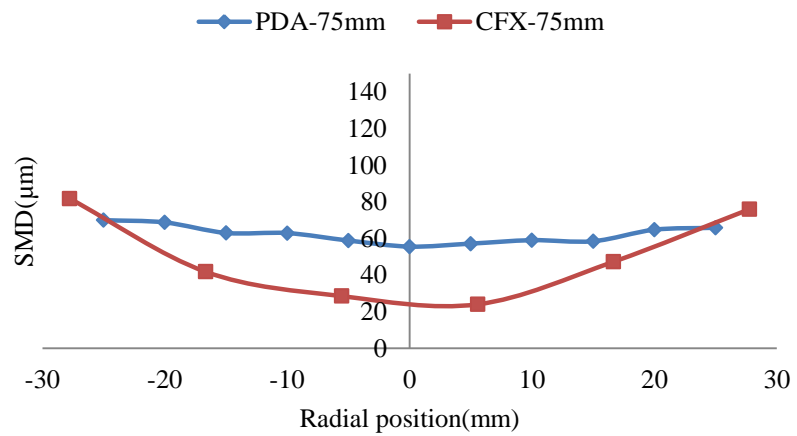
Figure 6.15 SMD comparisons between PDA and CFD at 6.0MPa



(a)



(b)



(c)

Figure 6.16 SMD comparisons between PDA and CFD at 10MPa

6.4.2.2 Drop velocities

Measurements of droplet velocities were simulated using Rosin-Rammler distribution in Ansys-CFX, with initial velocities at boundary set based on the continuity equation and the droplet size initialisation based on the PDA measurements. The velocities as one of the most important factor in determining the spray impacts is schematically shown in Fig. 6.17 indicating the exiting droplet near the nozzle to have the highest velocities'. However, when aerodynamic forces start acting across the spray, the droplets velocities tends to be decelerated with increasing downstream stand-off distance.

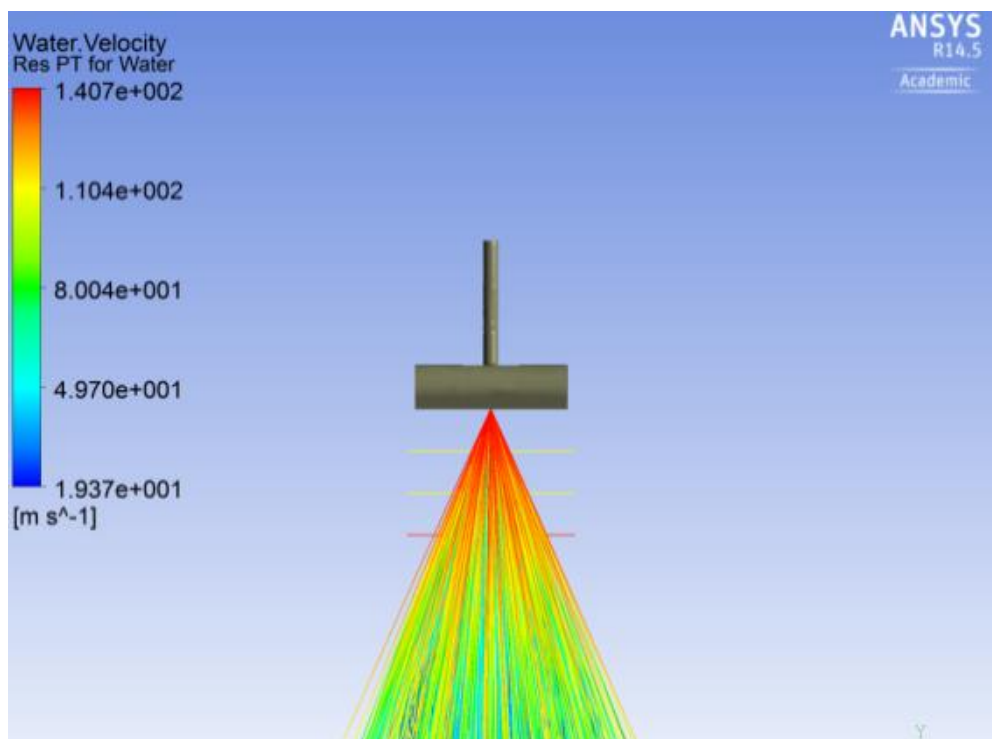
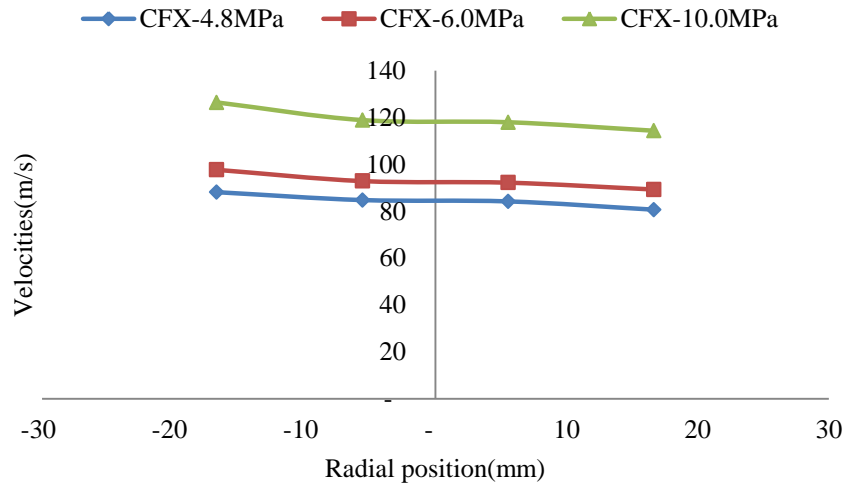
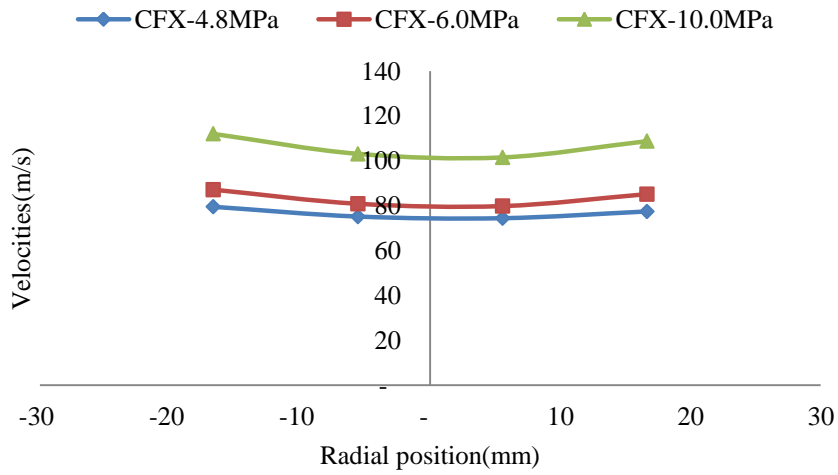


Figure 6.17 Droplet mean velocities

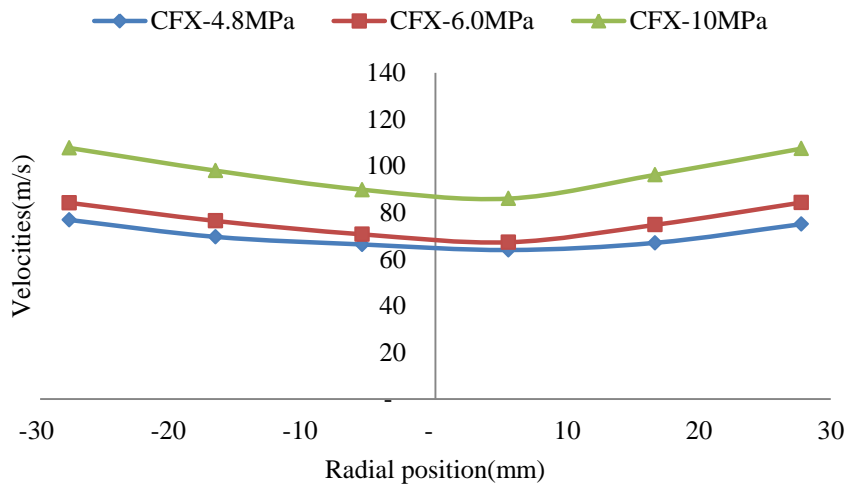
The velocities of the droplets increases with increasing injection pressure as shown in Fig. 6.18, also, vice-versa with downstream stand-off distance due to the effect of aerodynamic forces. The break up analysis using CFD generated mean droplet velocities as shown in Fig. 6.19, indication emerge that the droplet mean velocities increases with pressure in all scenarios, although experimental range of pressures as 10, 6.0 and 4.8MPa are not equally spaced, and therefore the velocity distributions are also higher margin between 10-6.0, contrast to 6.0-4.8MPa as shown in Fig.6.20 in the comparable results with experiments performed in Section 5.2.2.2. Appendix F4 shows the CFD velocities.



(a) 25mm

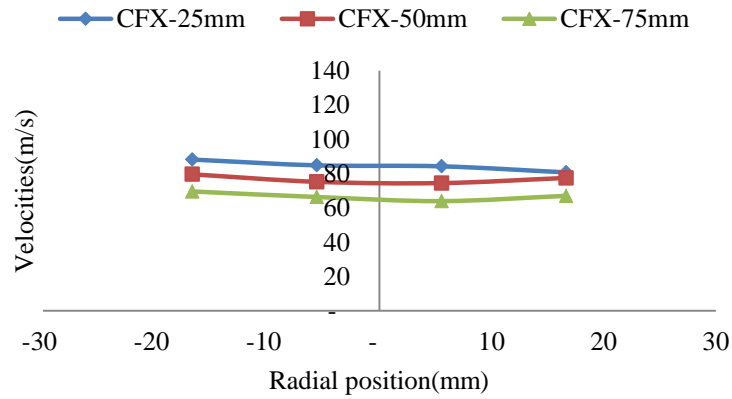


(b) 50mm

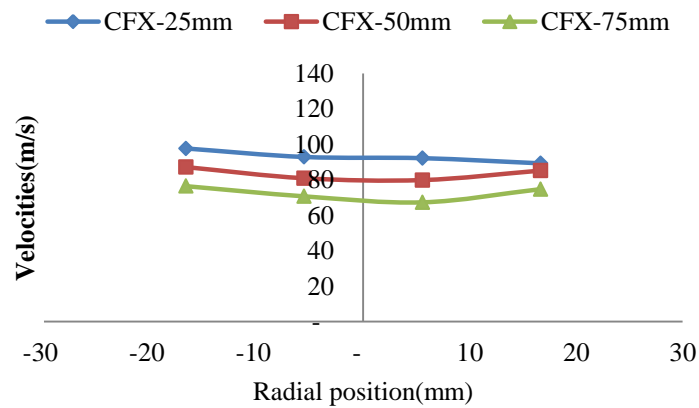


(d) 75mm

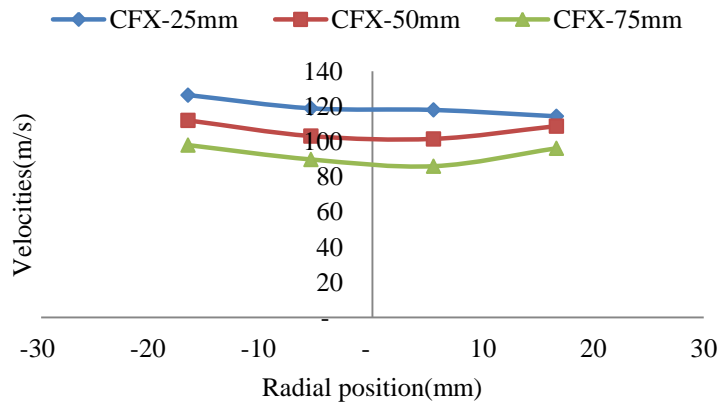
Figure 6.18 Droplet mean velocities at various downstream stand-off distances



(a)



(b)



(c)

Figure 6.19 Droplet mean velocities at (a) 4.8MPa (b) 6.0MPa (c) 10MPa

Increase in spray width has also shown a notable observation with regard to the edge velocities at 25mm, which seems lower even at all range pressures, but as the downstream distance increases to 50mm, the effect of the edge drag forces are partially shown by a mild curve, although further downstream distance of 75mm do not indicate same as shown in the comparable Fig. 6.20, 6.21 and 6.22.

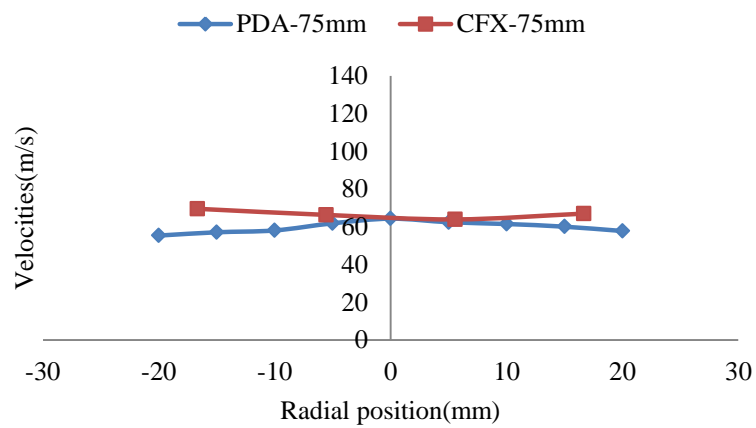
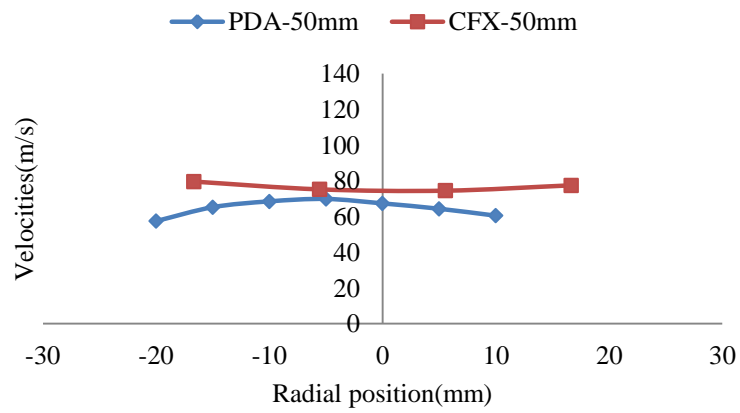
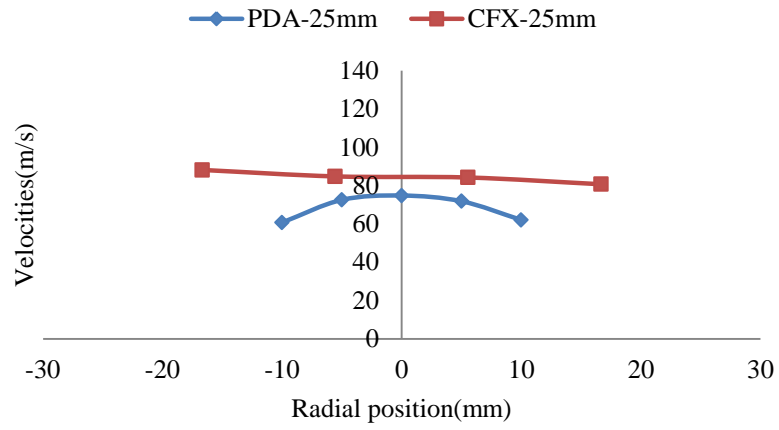
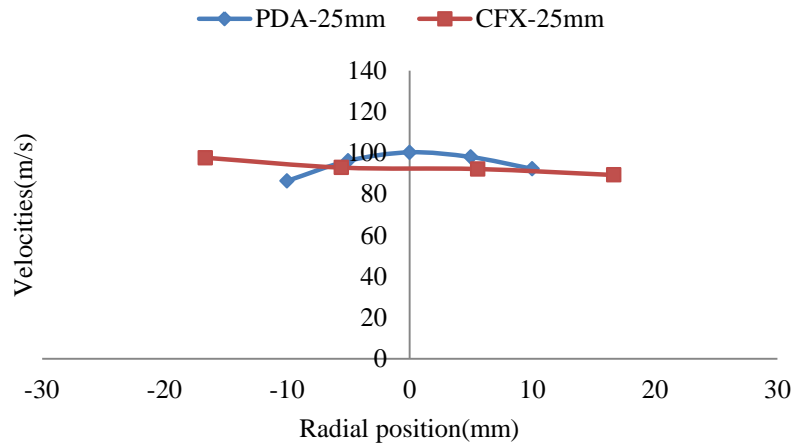
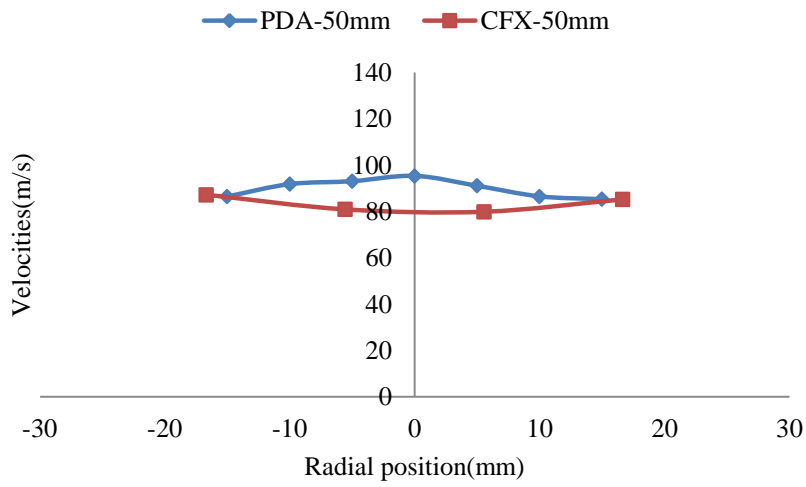


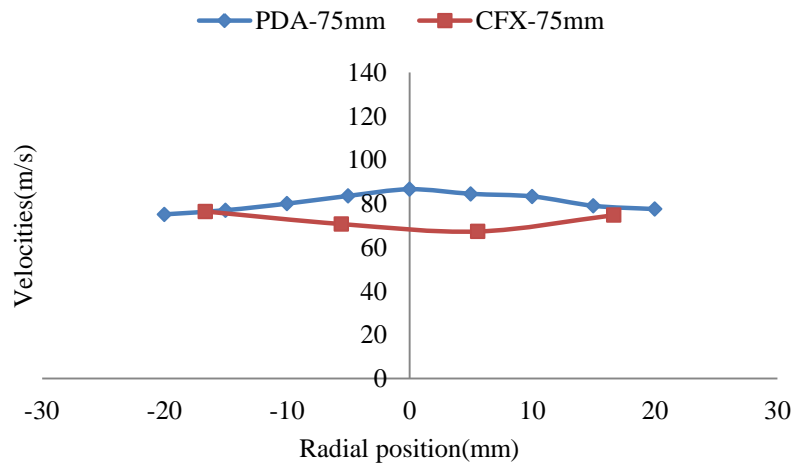
Figure 6.20 Droplet mean velocities comparison between PDA and CFX at 4.8MPa



(a)

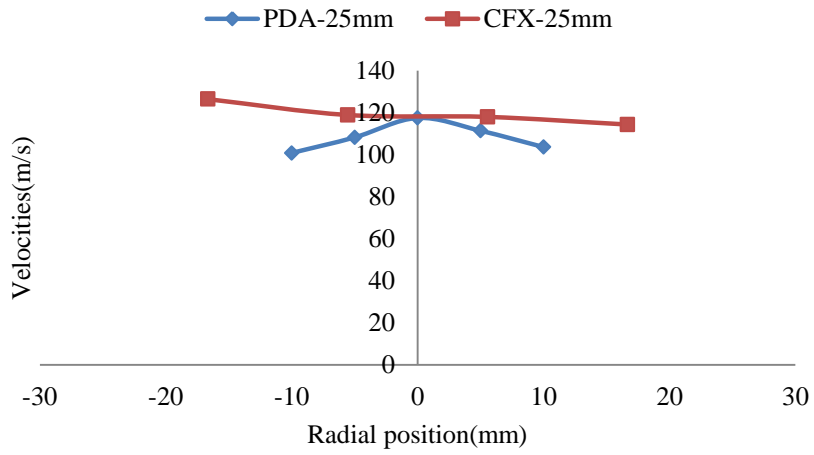


(b)

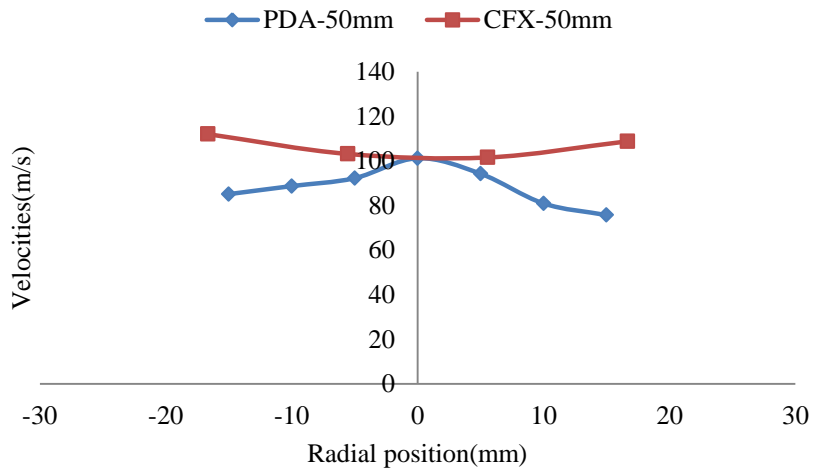


(c)

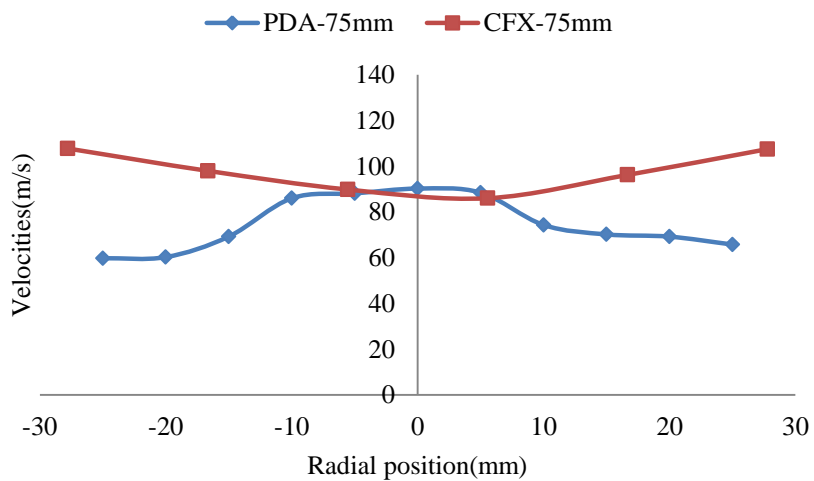
Figure 6.21 Droplet mean velocities comparison between PDA and CFX at 6.0MPa



(a)



(b)



(c)

Figure 6.22 Droplet mean velocities comparison between PDA and CFX at 10MPa

Comparison of the PDA and CFD simulations as shown in Fig. 6.20, 6.21 and 6.22 has shown higher velocities for CFD predicted velocities at 4.8 and 10MPa, still it is difficult to explain how the intermediate pressure of 6.0MPa provide higher PDA measured velocities than its CFD counterparts. As the break-up leads to characterised spray distribution, details of the spray break-up has been link to air-water interaction in Section 6.4.2.3

6.4.2.3 Break-up region using aeration

Understanding the propagation of a High pressure spray jet has been viewed been adequately analysed only to the distribution of the droplet velocities and sizes using sophisticated techniques such as PDA, PIV, Imaging etc., but fewer research contribution has ever related the multiphase behaviour of water jets and the surrounding air to predict regions of primary and secondary break up. Although, several model has been built in terms of the fundamental forces of surface tension, inertia force, gravity, viscous drag force etc. as to their dynamics in explaining the break up theories of spray jets, this research emphasize on using the surrounding air behaviour to qualitatively and quantitatively draw relevant assertions.

The analysis of the entrained-air and water spray droplets has been used in this investigation to estimate the pressure differential of the plane in which both water and air are interacting. Along the spray jets, continuous high velocity jet resulted in a partial vacuum around the nozzle exit to a distance of about 25mm downstream, although research conducted indicated the primary break up regions around 10mm downstream, which indeed, corresponds to the approximate regions of maximum air entrainment of many times than the spray regions. It is evident that after the primary disintegration region, secondary break up can then be noticed in Fig. 6.23, indicating both the spray image and models profiles for the air and low pressure regions. Although all the regions are dependent on the mass loading of different pressures, and it can be observed as in Fig. 6.24 that 10MPa primary and secondary atomization produces a wider low pressure regions than 6 and 4.8MPa shown in Fig. 6.25.

The next section provides the details of cavitation simulation using Fluent-CFD to establish the region of cavitation bubbles in order to select appropriate stand-of distance for the descaling trials in Section 6.6.

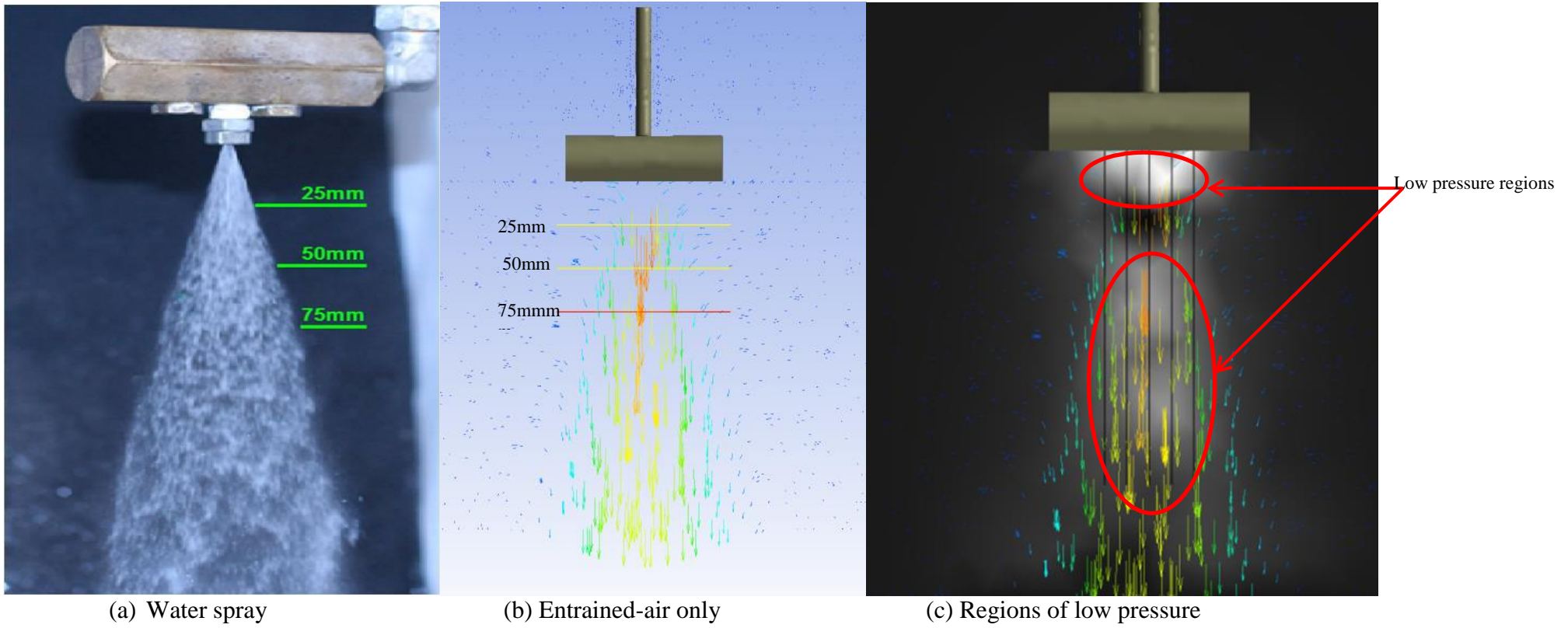
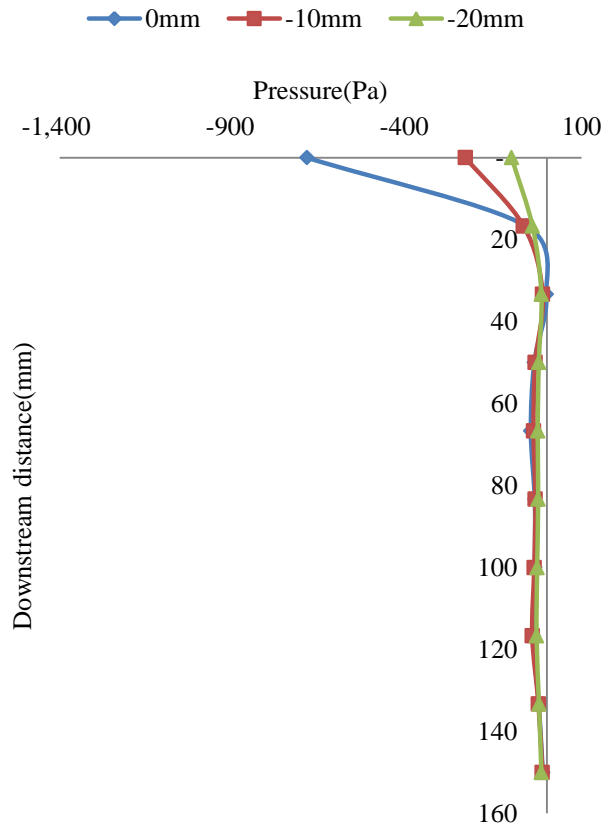
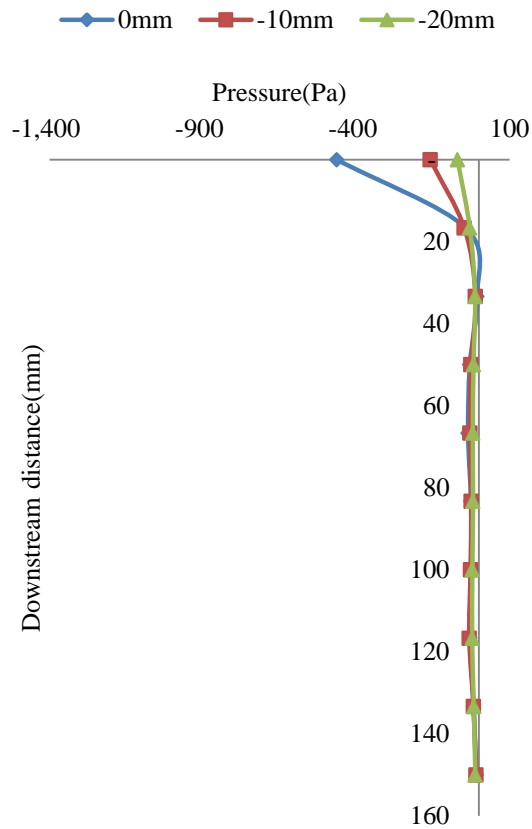


Figure 6.23 Spray jet image and models

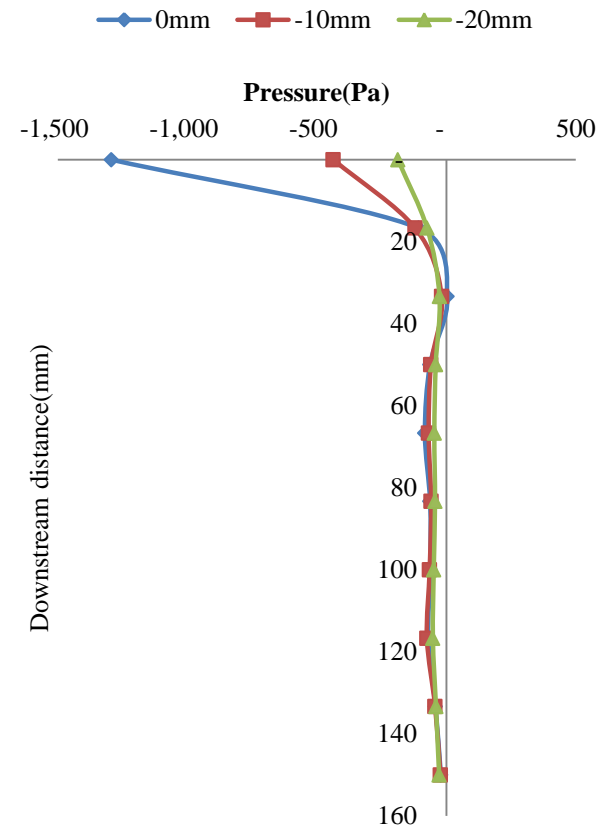
Distance from the spray centre



(a) 4.8MPa



(b) 6.0MPa



(c) 10MPa

Figure 6.24 Negative centre plane pressure profiles at different spray injection pressure

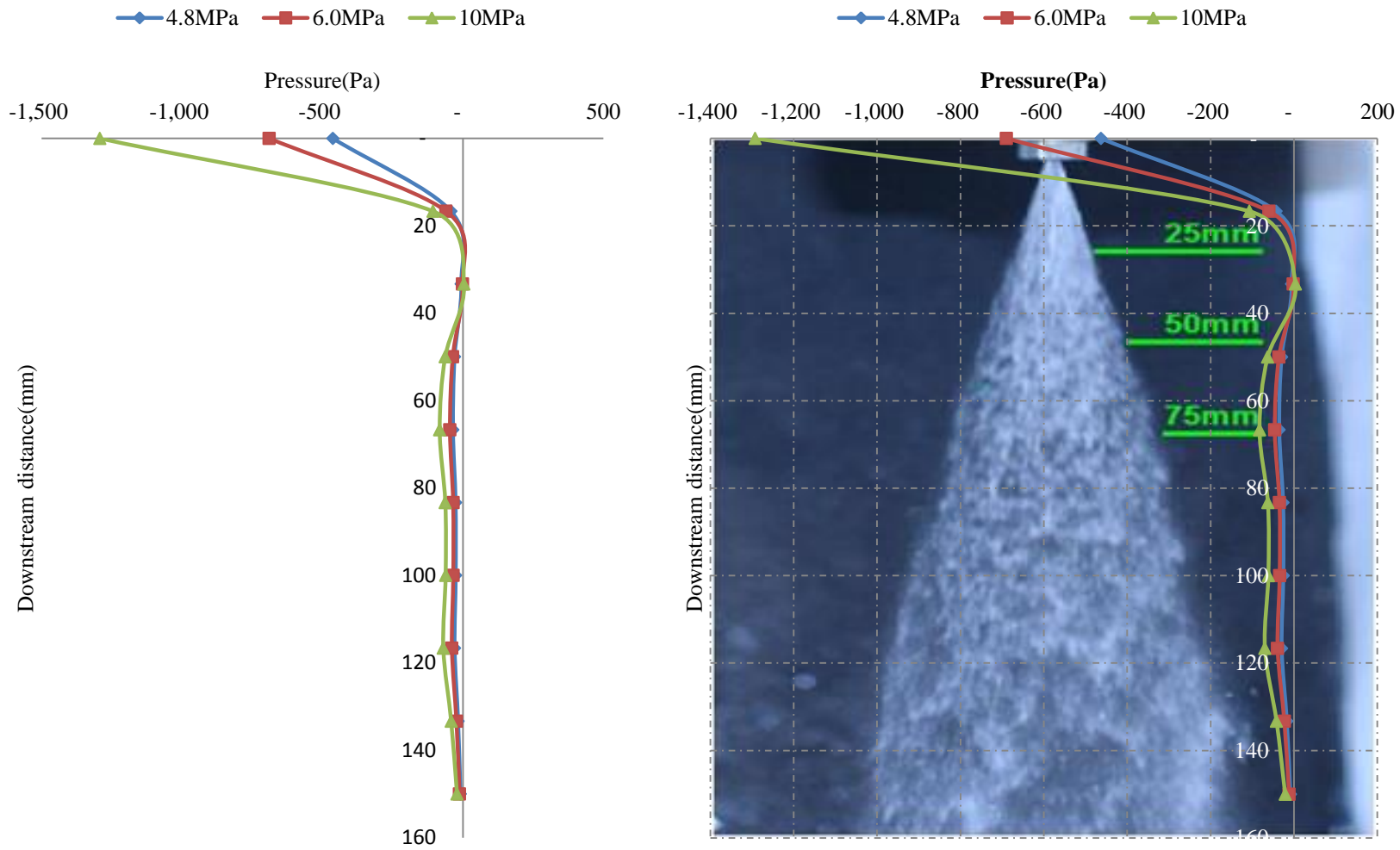


Figure 6.25 Negative plane pressures at centre-edge cross section.

6.5 Cavitation measurements (Phase-II)

6.5.1 Bubble generation

Spray jet cavitation's has been sought to have a contributory effect on the scale erosion, which occurs due to either the jet pressure falling below the saturated vapour pressure of water or due to pressure fluctuations along the nozzle. This section examines the possibility of generating a negative pressure at the *vena contracta* only along the flat-fan atomizer and solid stream jet as shown in Fig. 6.26.

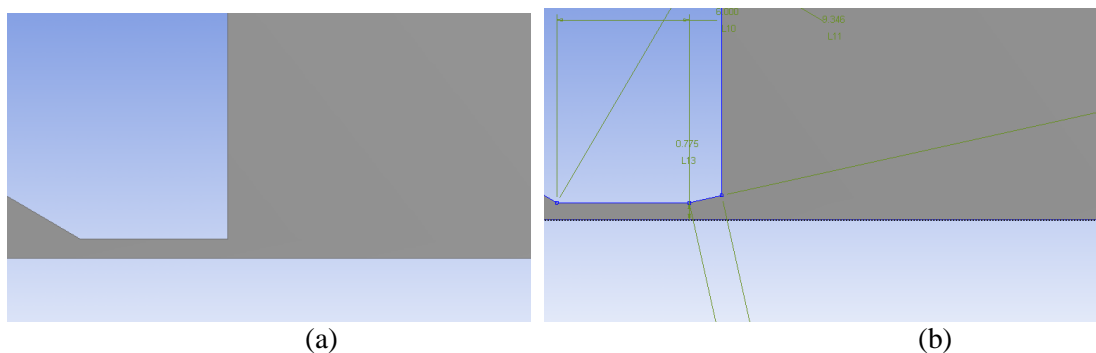


Figure 6.26 Fluent model nozzles(a) Flat-fan nozzle (b) solid stream nozzle

Results obtained as shown in Fig. 6.30 confirms the generation of substantial low pressure at the vena-contracta of a flat-divergent nozzle, although this has not been observed for the flat-fan nozzle. However, the effect of turbulent kinetic energy has favoured the flat-fan nozzle, which in-turn will provide much more impact and subsequent erosion at the targeted scale surface.



(a) Flat fan atomizer

(b) Solid stream jet

Figure 6.27 Experimentalt model nozzles(a) Flat-fan nozzle (b) solid stream nozzle

The flow properties of a water jet were also investigated with regards to the cavitation's possibility, in which a flat-fan nozzle confirms drop in water density to about 997.55kg/m^3 which is due to the bubble generation associated with cavitation, with no cavitation observed in solid stream nozzle as shown experimentally in Fig. 6.27 and validated through Fluent simulation shown in Fig. 6.28. so also liquid volume fraction fall below unity (1) for the flat-divergent nozzle as such as shown in Fig. 6.28. The length of the cavitation bubble generated has measured to be about 4.5mm from the flat fan atomizer exit.

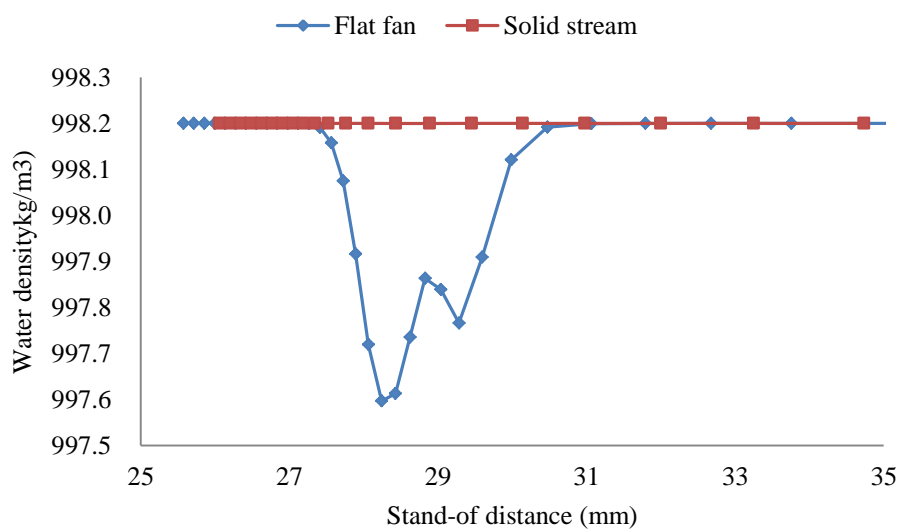
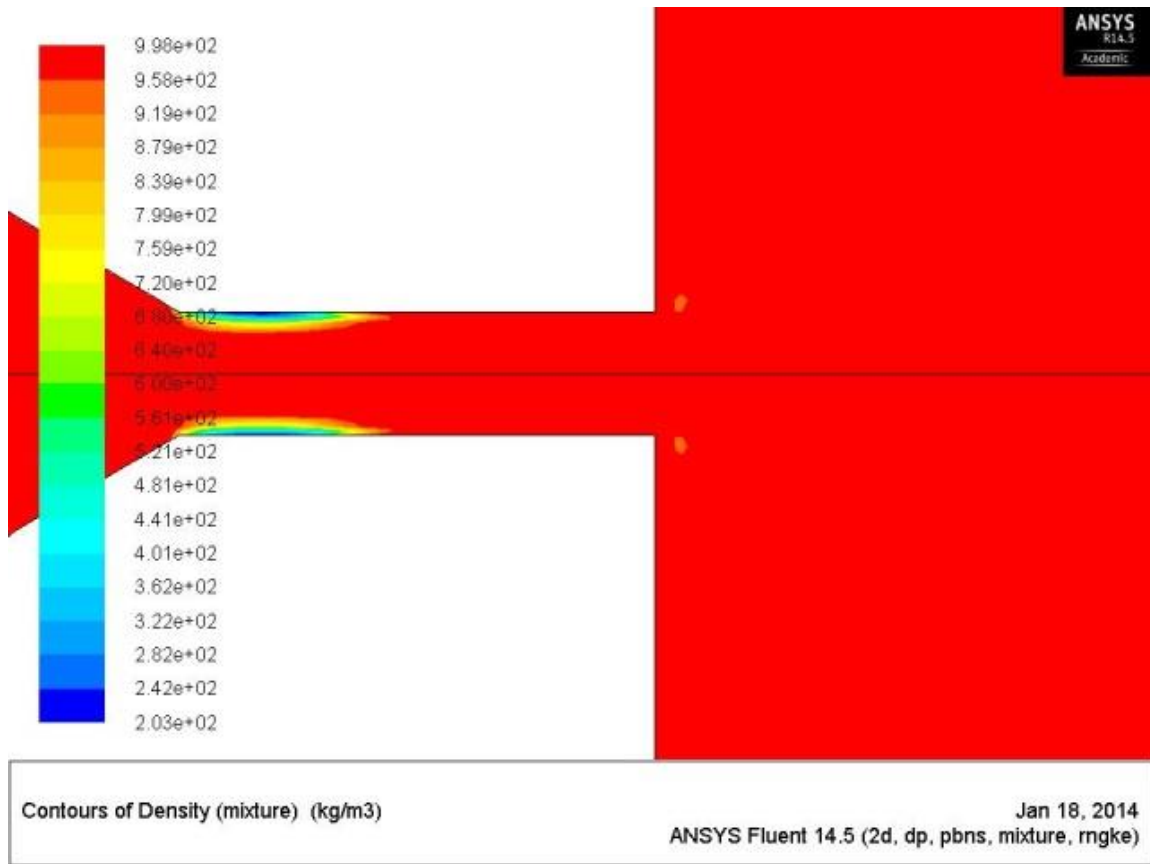


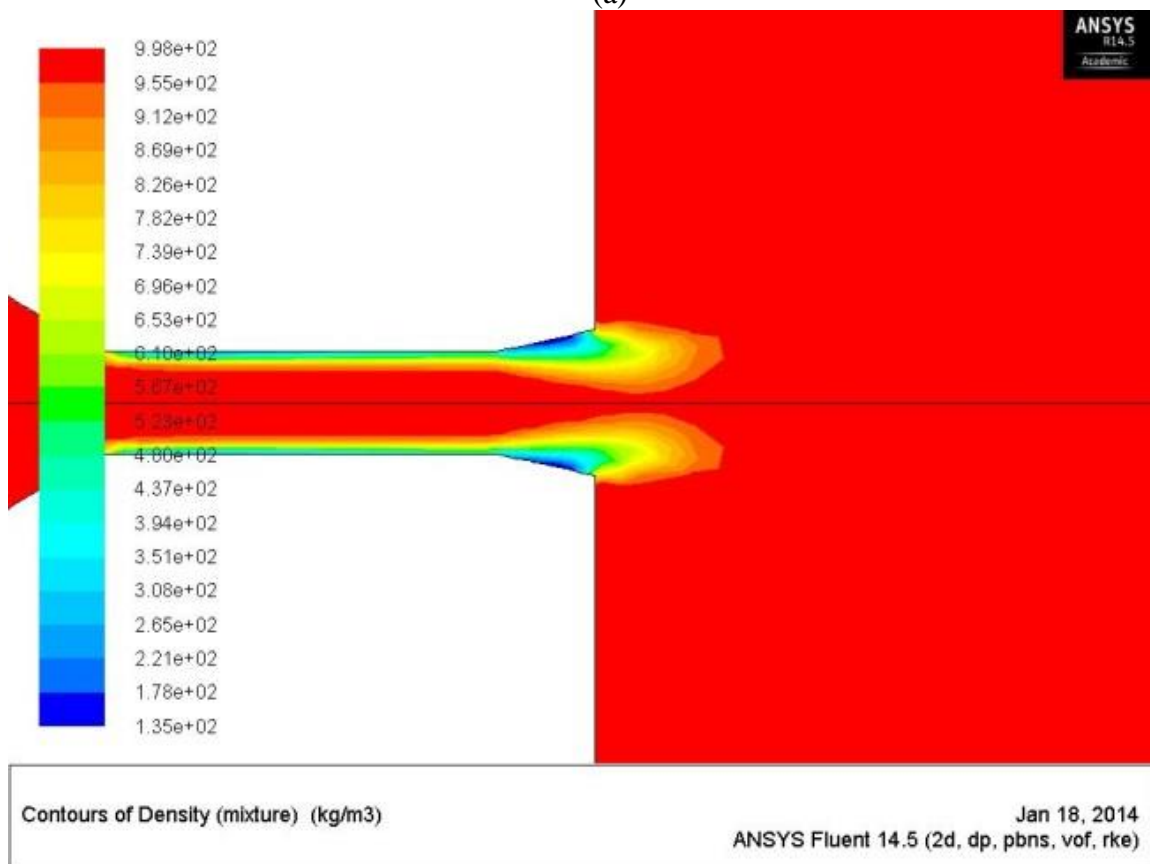
Figure 6.28 Cavitation bubble generation as a measure of density

Indications also emerged that the cavitation bubble do exist in both the flat-fan and the solid stream nozzles, only that the life time of the bubbles is shortened and limited to the nozzle vena contracta in solid stream nozzle, whereas flat-fan nozzle achieved a longer bubble life time extended and appeared outside the nozzle as shown in Fig. 6.29 (a) and (b).

Increasing the air concentration causes a decrease in the length of the cavitation bubble from 4.5 to nearly 2mm as shown in Fig. 6.30 using velocity vector shown in Fig. 6.31. It is now evident that within the range of injection spray pressure investigated in this work, the effect of cavitation erosion play no role in the mass of scale removed as reported in Section 6.6.



(a)



(b)

Figure 6.29 Cavitation bubbles regions (a) Solid stream (b) Flat-fan atomizer

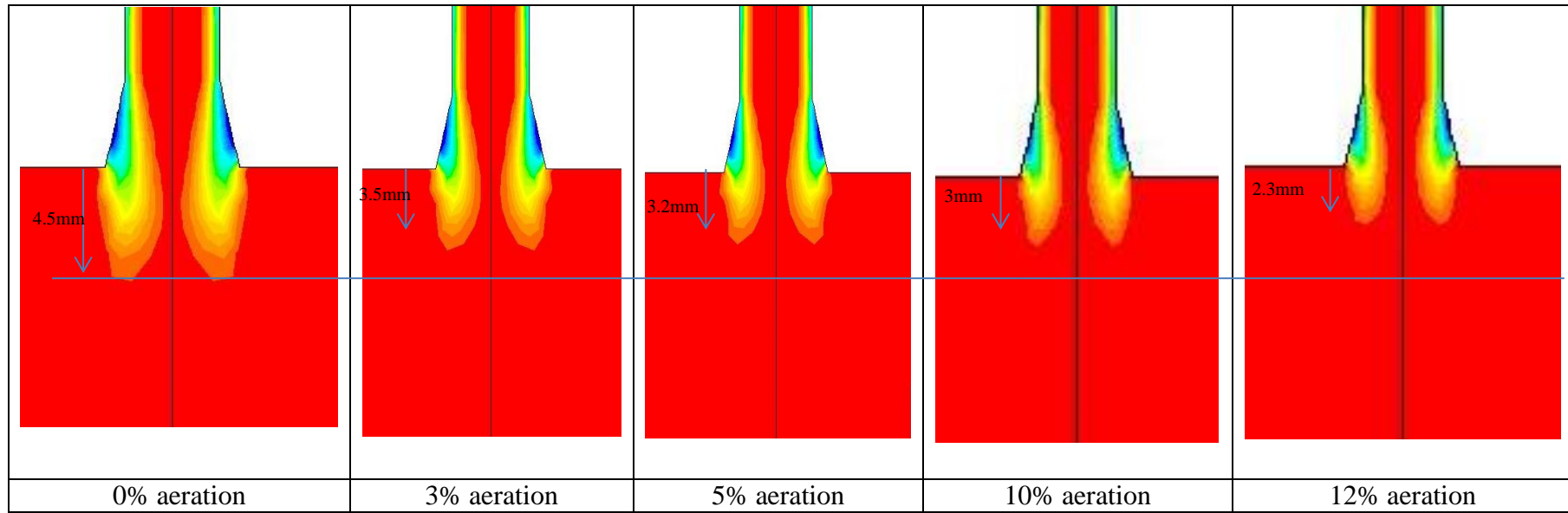


Figure 6.30 Cavitation bubble length validation

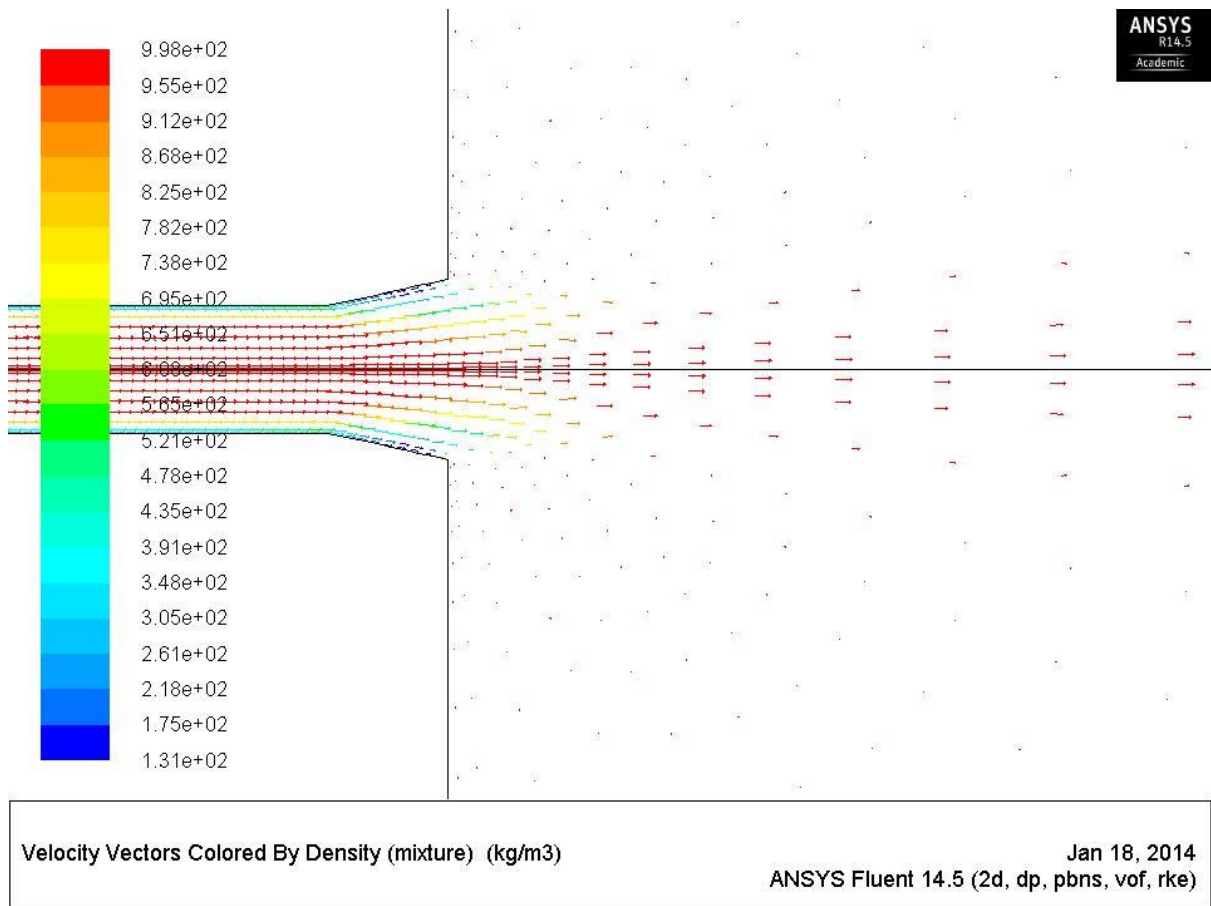


Figure 6.31 Density vector velocities

6.5.2 Turbulent Kinetic energy

Considering this research investigation the effect of cavitation bubbles downstream of the nozzle and its subsequent effects on aeration due to pressure effect with depth and the subsequent erosion possibilities, it is then favour proceeding with the Flat-fan nozzle for the further investigations, although other parameters such as the Turbulent kinetic energy plays an important role in the descaling impact, however analysis indicate such parameter do not survive up to $\leq 5\text{mm}$ downstream of the solid-stream nozzle as indicated in Fig. 6.32. This is in addition to its narrower spray width compared to Flat-fan atomizer, which ultimately determines the covered area of impact compared to solid stream atomizer shown in Fig. 6.33. Indeed, although increase in the spray angle of even the Flat-fan atomizer decreases impact pressure, 25° spray angle was chosen in these investigations to maximize impact.

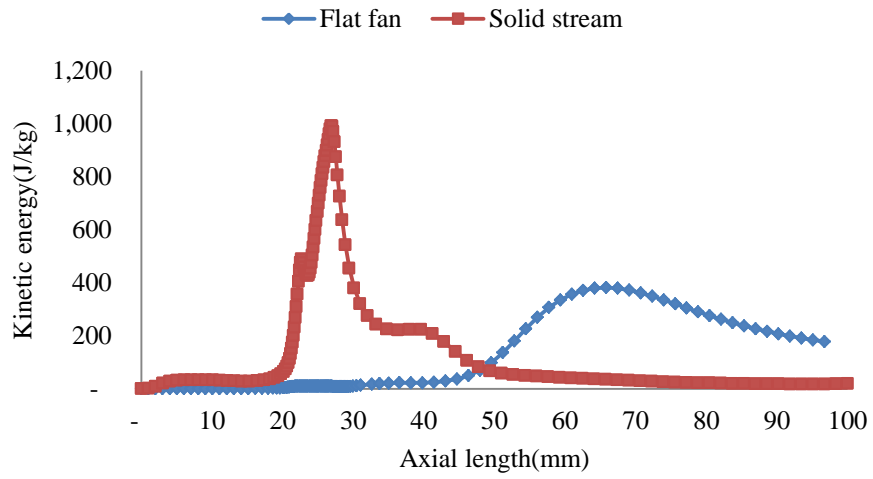
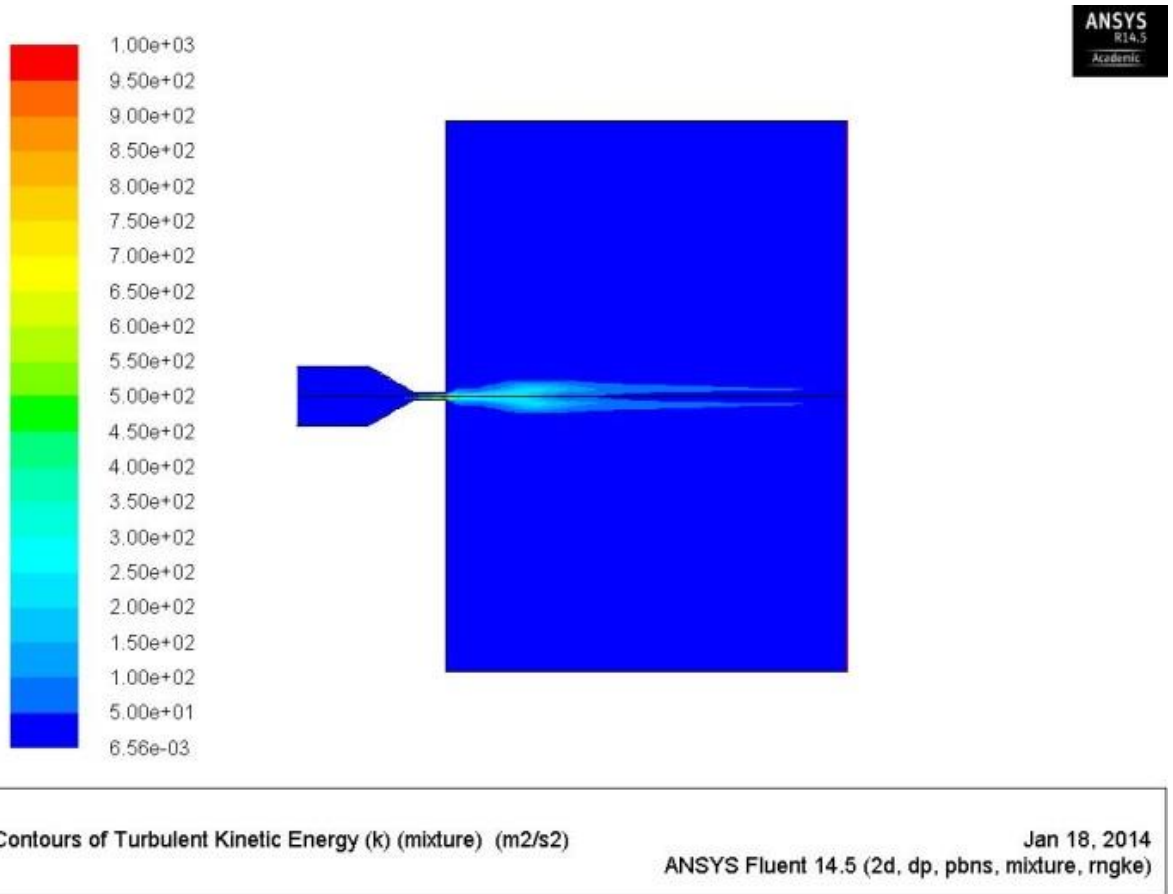
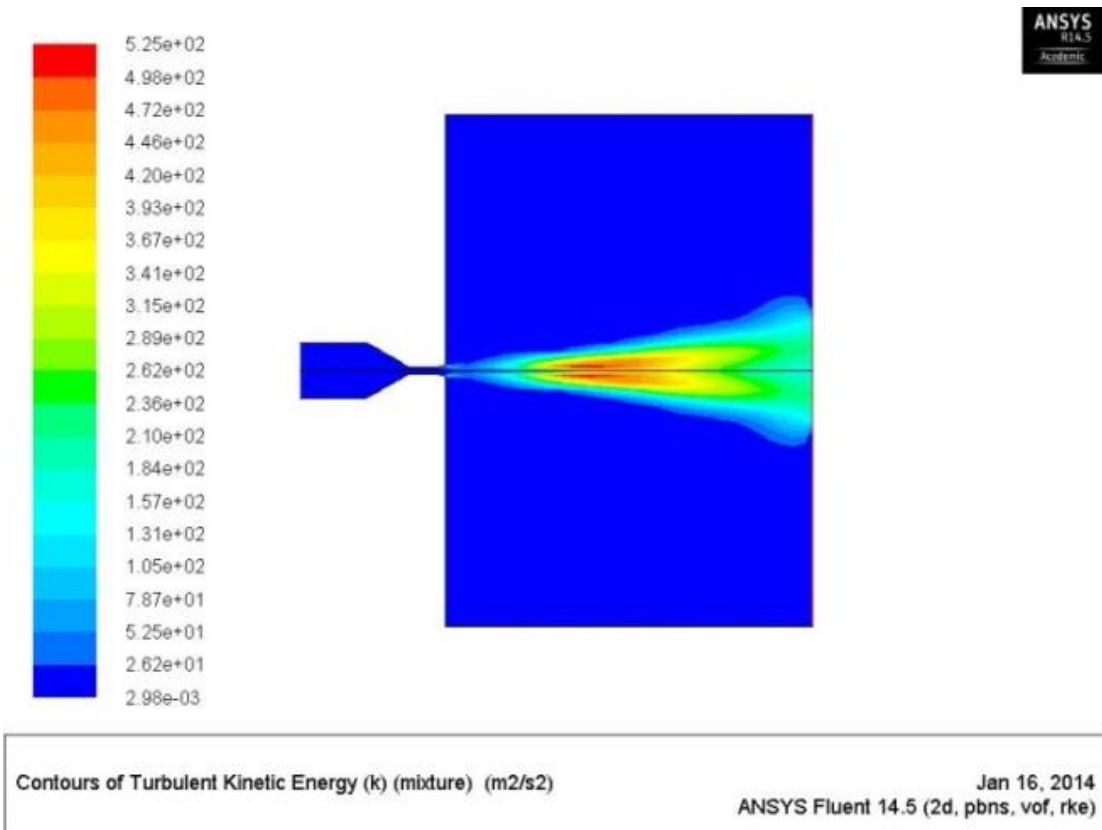


Figure 6.32 Turbulent kinetic energy comparisons



(a)



(b)

Figure 6.33 Fluent turbulent kinetic energy (a) solid stream (b) Flat-fan atomizer

Apart from the turbulent kinetic energy, droplet momentum analysis was conducted using the velocity profiles as the momentum factor in the next section.

6.5.3 Droplet momentum

The investigation further carried the analysis of the spray velocities as factor determining the momentum and subsequent impact upon hitting the target scale, the simulation indicated similarities in the velocities profile for both the Flat-fan and the solid-stream nozzle, indicating that both are capable to deliver similar effect upon impact. The results also indicated velocities of 110m/s at 25mm from the nozzle exit shown in Fig. 6.34, which is slightly lower than the 117m/s measured using PDA in Section 4.3. Profiles of the flow velocities images are also shown in Fig. 6.35.

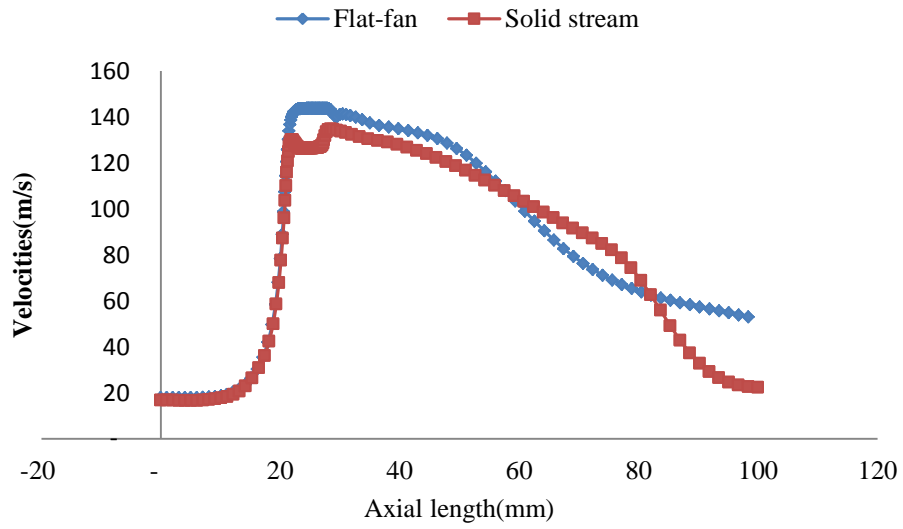
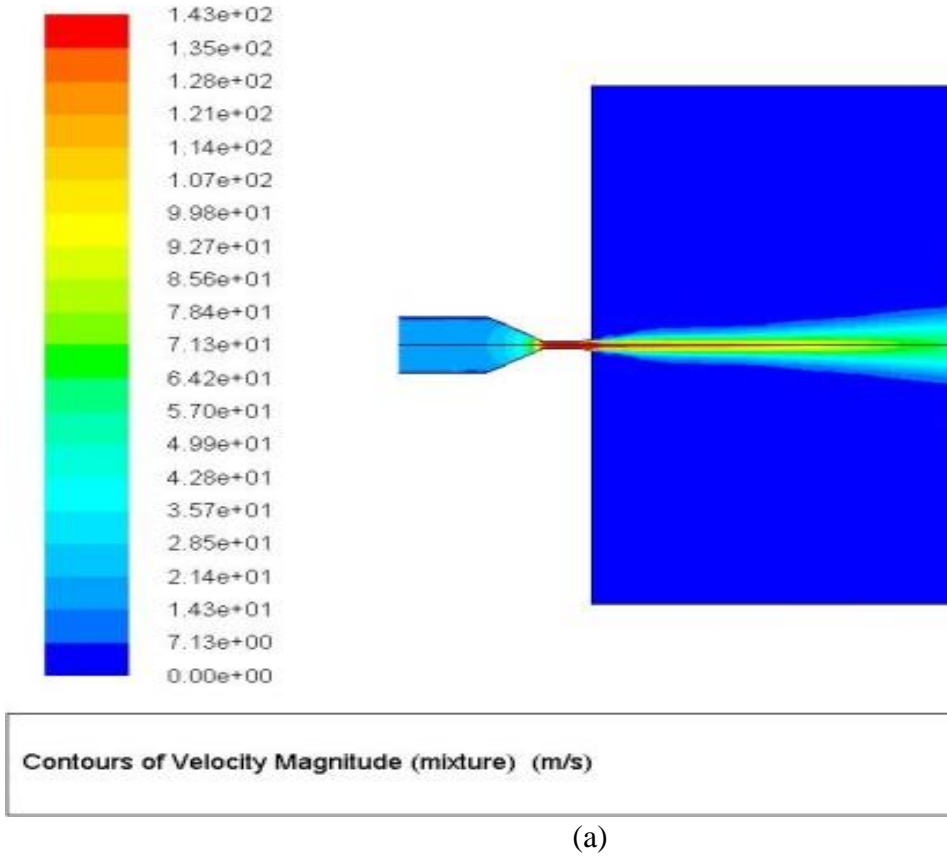
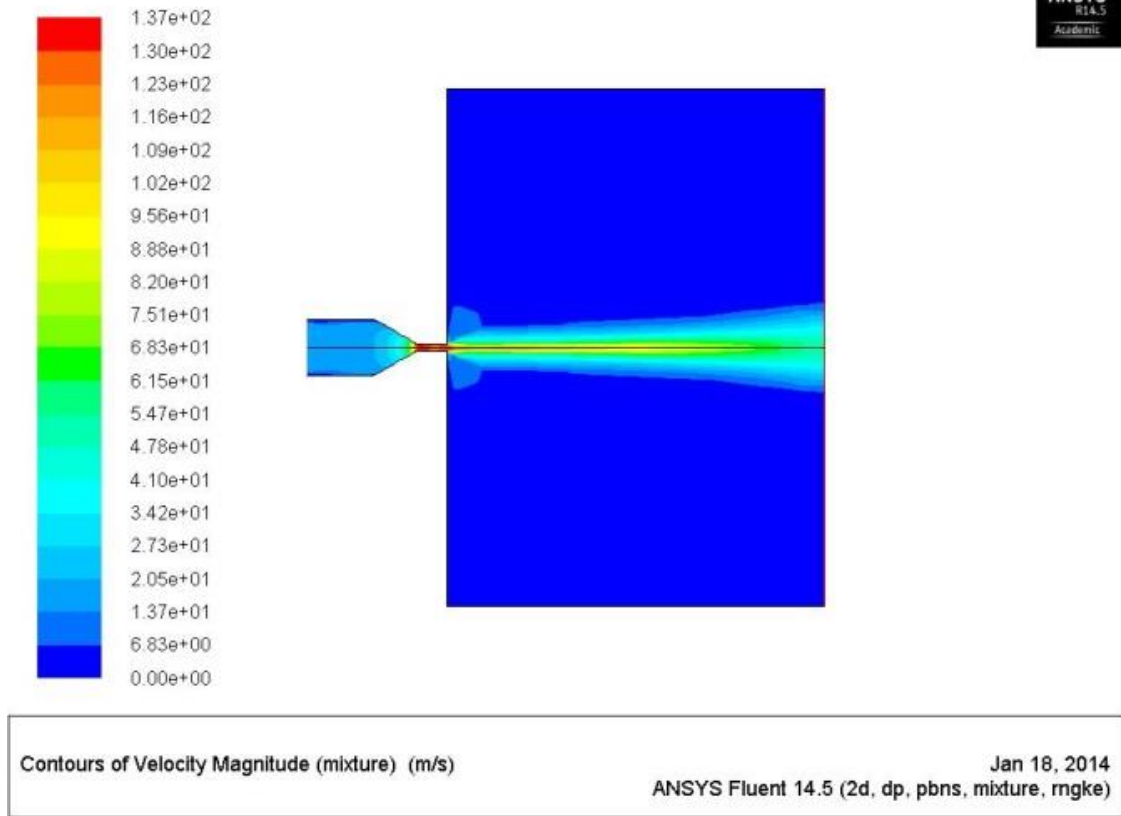


Figure 6.34 Velocities distribution in different nozzles





(b)

Figure 6.35 Velocities' colours for (a) solid stream and (b) Flat-fan nozzles

Moreover, while it is paramount to highlight the medium in which the scale cleaning is preferred, the next section highlight the suitability of both the air medium and the submerged considering the turbulent nature of the experimental trials, as being multi-phase behaviour in most cases, although it is air-water medium adopted for this investigation.

6.5.4 Flat fan operating conditions

Evidences shown in section 6.5 including the cavitation bubble longer life cycle and velocities profile leading to higher impact upon the target have favoured the selection of Flat-fan atomizer over solid stream, this section investigation the medium and operating conditions of the Flat-fan atomizer for the descaling experiment. The factors investigate includes the medium of the experiment(submerged or air), while considering the profile of pressure and the cavitation bubbles in both mediums, this enable an optimum conditions to be applied to the experiments.

6.5.4.1 Operating medium (Submerged and air medium)

While performing a descaling experiment, it is either performed with the water spray enveloped in air or water (submerged) as a medium. Analysis of pressure profile along the spray axis indicated that both the medium are capable of generating a pressure drop necessary required for cavitation bubbles formation as shown in Fig. 6.36, indeed, this has been shown experimentally in Fig. 6.27(a), also under submerged conditions shown in Fig. 6.37.

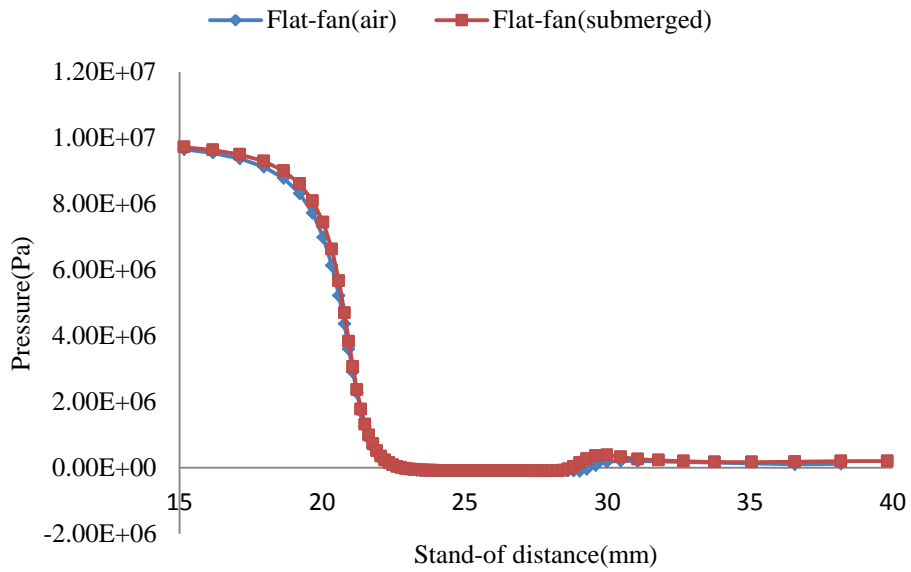
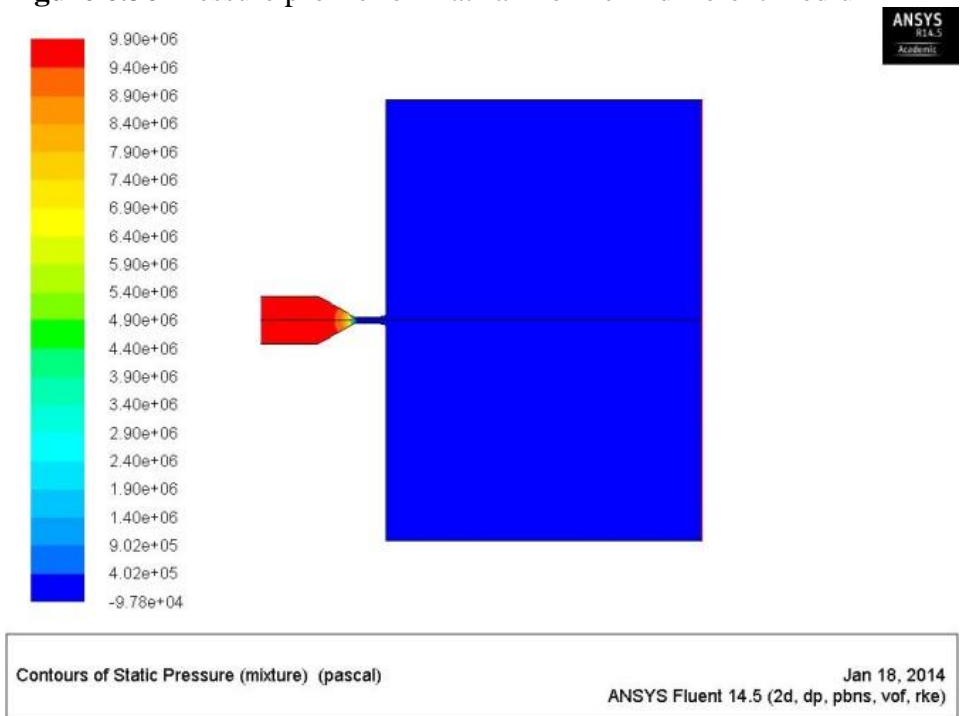
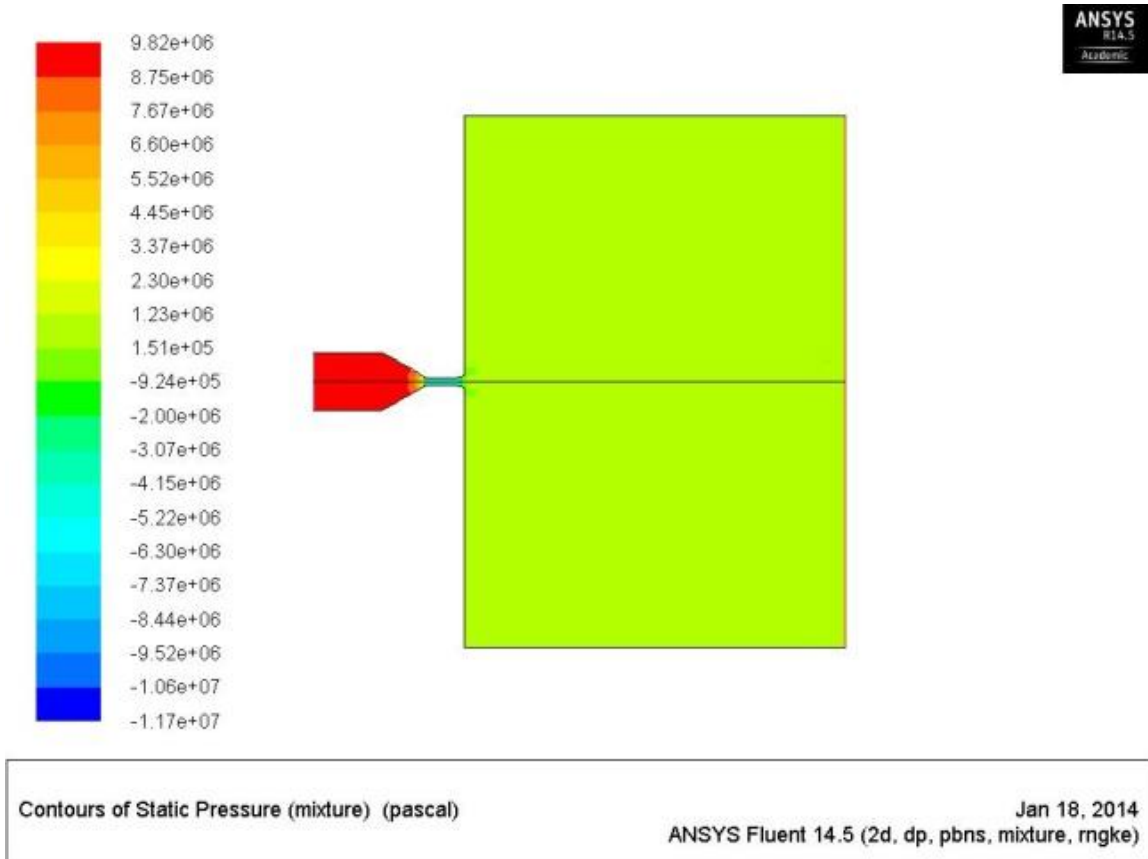


Figure 6.36 Pressure profile for Flat-fan nozzle in different medium



(a) Air medium



(b) Submerged medium

Figure 6.37 CFD pressure profiles for Flat-fan nozzle in different medium plane

6.5.5 Cavitation in Flat fan nozzles

Cavitation bubbles have emerged from the Flat-fan nozzle under both mediums due to the indications of the substantial pressure equal or even below the saturated vapour pressure of water. Although the extent of cavitation formation appeared higher for air medium with a density of water dropping to about 994kg/m³ at room conditions, submerged conditions only indicated density drop to about 997.6kg/m³ as shown in Fig. 6.38. Although experimental images captured are only possible for submerged conditions shown in Fig. 6.27.

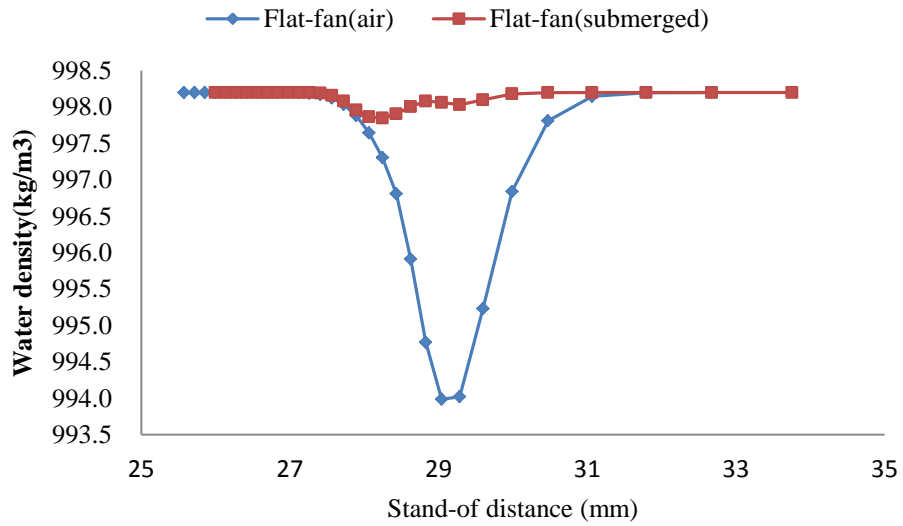


Figure 6.38 Density at ambient condition in different medium

So far, performing the scale removal experiment has been found to be more suitable using a Flat fan atomizer in air medium, in addition, increasing the air concentration will also enable presence of compressive forces to aid the scale removal, therefore, the next section provides the details of flow characteristics of the high pressure water sprays under aerated conditions as shown in Fig. 6.39.

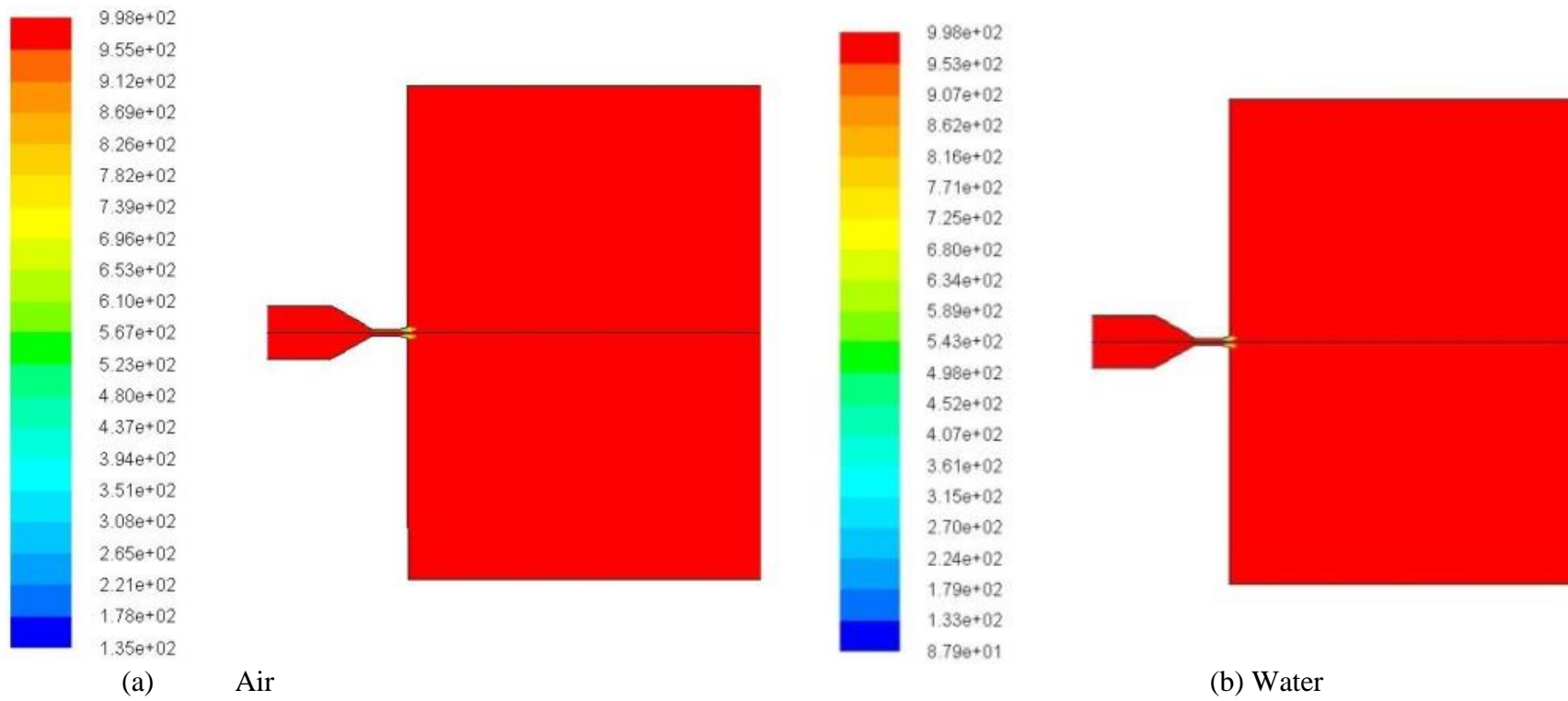


Figure 6.39 CFD Images of cavitation in Flat-fan atomizer in different medium

6.5.6 Aeration effect on cavitation length in Flat fan (Entrained-air medium)

A significant contribution has been made in this section by establishing the mitigation of cavitation damage through aeration especially in Flat fan nozzles. Research conducted by many scientist including Perteka, 1968, suggested 0.4-7.4% as the air concentration necessary to avoid cavitation in spill way dams, as he observed the increase in aeration causes reduction of bursting and hammer noise indication that cavitation has been eliminated. Others include Rasmussen with 1% air concentration for aluminium, Russell and Sheehan suggested 5.7% for concrete and subsequently Galipelins 3.0-9.7 % for a grade C10-C40 concrete [105]. In this investigation aeration of up to 12% were found to significantly eliminate the cavitation completely to nearly zero as shown in Fig. 6.40. Considering this research analyse high velocity flow of up to 140m/s at the immediate nozzle exit, most of the previous experiments were conducted for high dams spill ways, having a velocity of not more than 50m/s [104]. Beside the cavitation bubbles, other flow characterization parameters were further investigated in order to establish their effect on the scale cleaning as the major aim of this investigation. These include the kinetic energy, droplet velocities and pressure as shown in Fig. 6.41, 6.42, and 6.43, which do not show any variation with aeration. Perhaps these properties have not been affected by aeration, but rather stress was proved to have been induced[110] leading to enhanced erosion unto the scale surfaces considered.

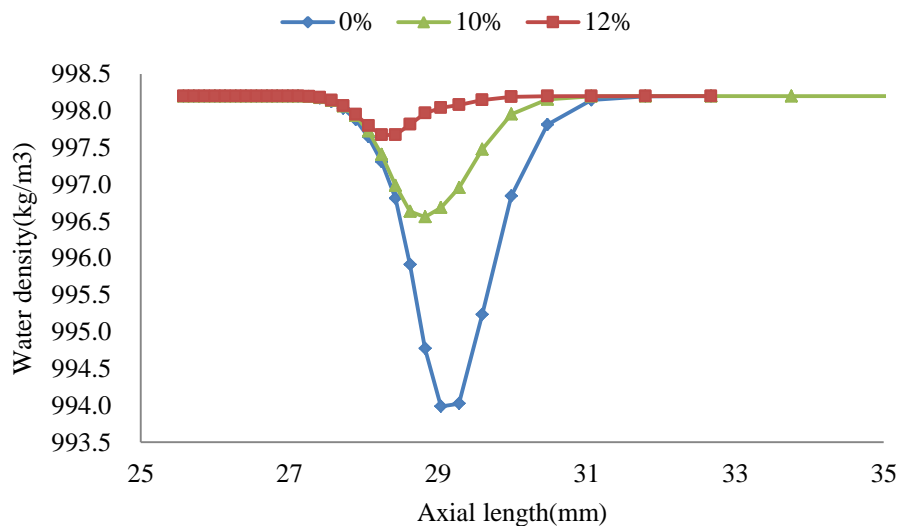


Figure 6.40 Aeration effect on cavitation

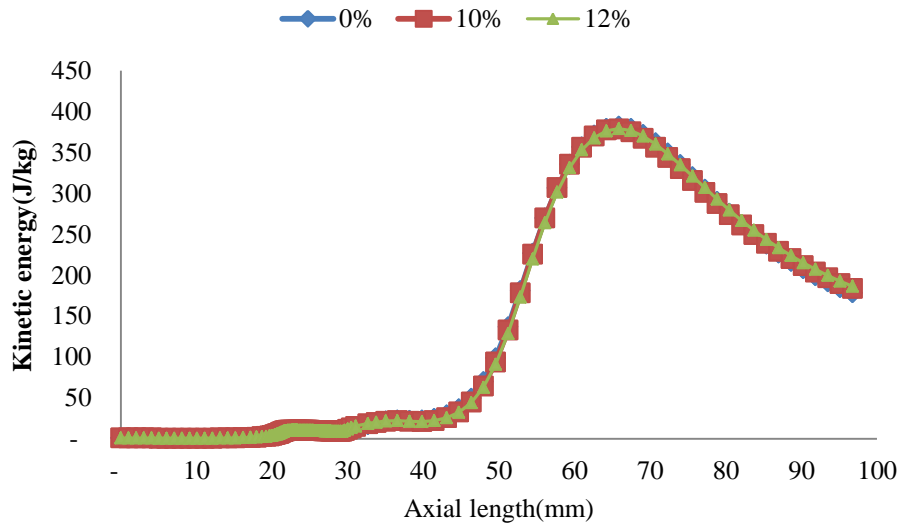


Figure 6.41 Aeration effect on turbulent kinetic energy

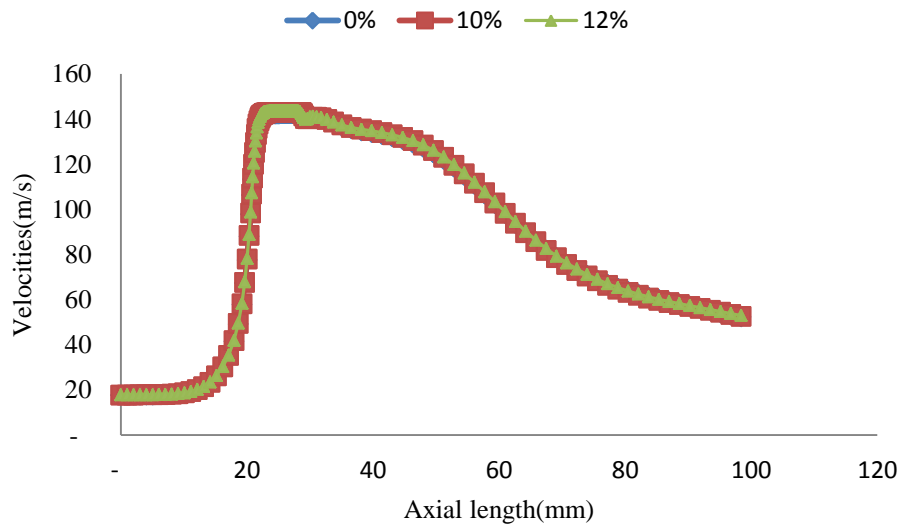


Figure 6.42 Aeration effect on droplet velocities

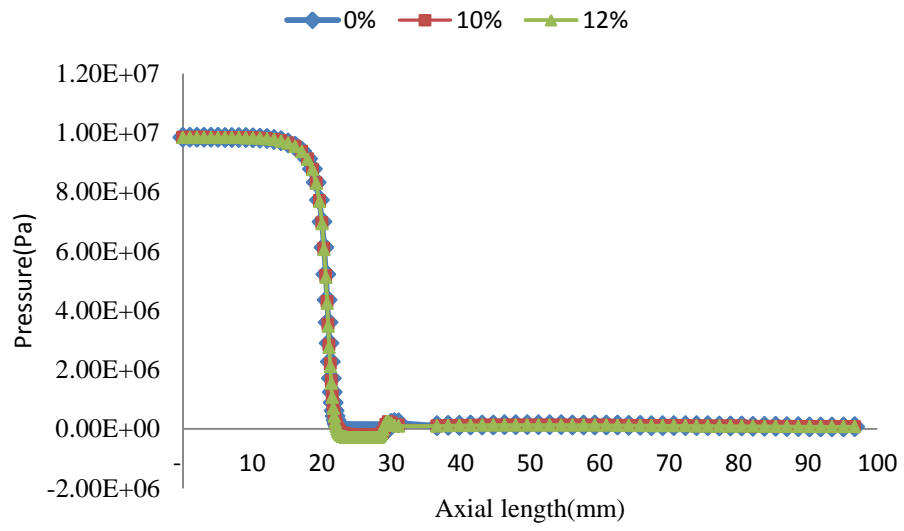


Figure 6.43 Aeration effect on pressure

6.6 Scale removal using measurement using CFD (Phase-III)

6.6.1 Scale removal set up

Scale removal prediction has been the primary target of this research work, and having carried out the detailed characterisation of the water jet using CFD as well as experimental measurements, validation will then be generated in this section to estimate the erosion rate of the flat jet at different operating pressure as well as varying ambient conditions. Initial results obtained using CFX-Fluent has shown the variation of the erosion along a wall hit by the spray jet as shown in Fig. 6.44.

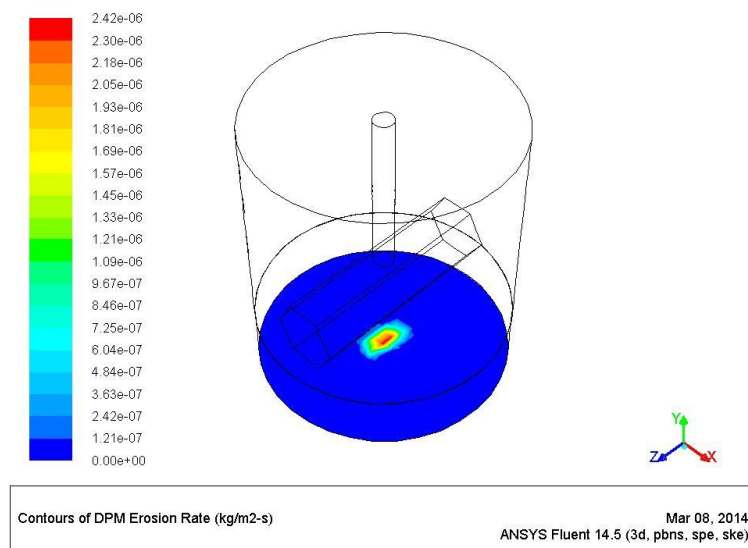


Figure 6.44 Erosion prediction using CFD

The plane selected for the scale removal simulations is indicated in Fig. 6.45, similar to the size of the samples used experimentally for the soft scale. The plane was varied using different scale samples available in the fluent models. The model shown in Fig. 6.45 is compared with experimentally eroded area of the soft scale sample shown in Fig. 6.46. The injection of the spray responsible for the erosion is shown in Fig. 5.47.

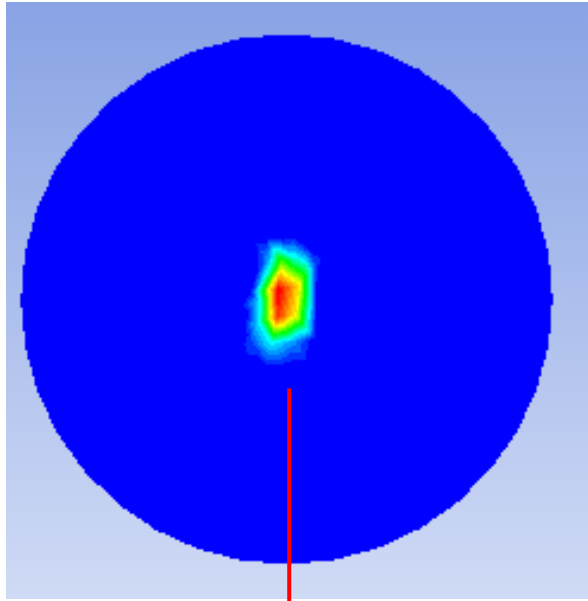


Figure 6.45 Erosion plane

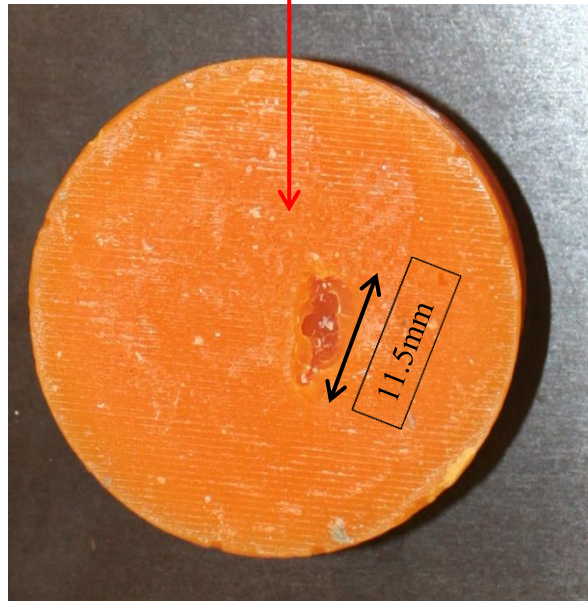


Figure 5.46 Experimental momentum impact variations

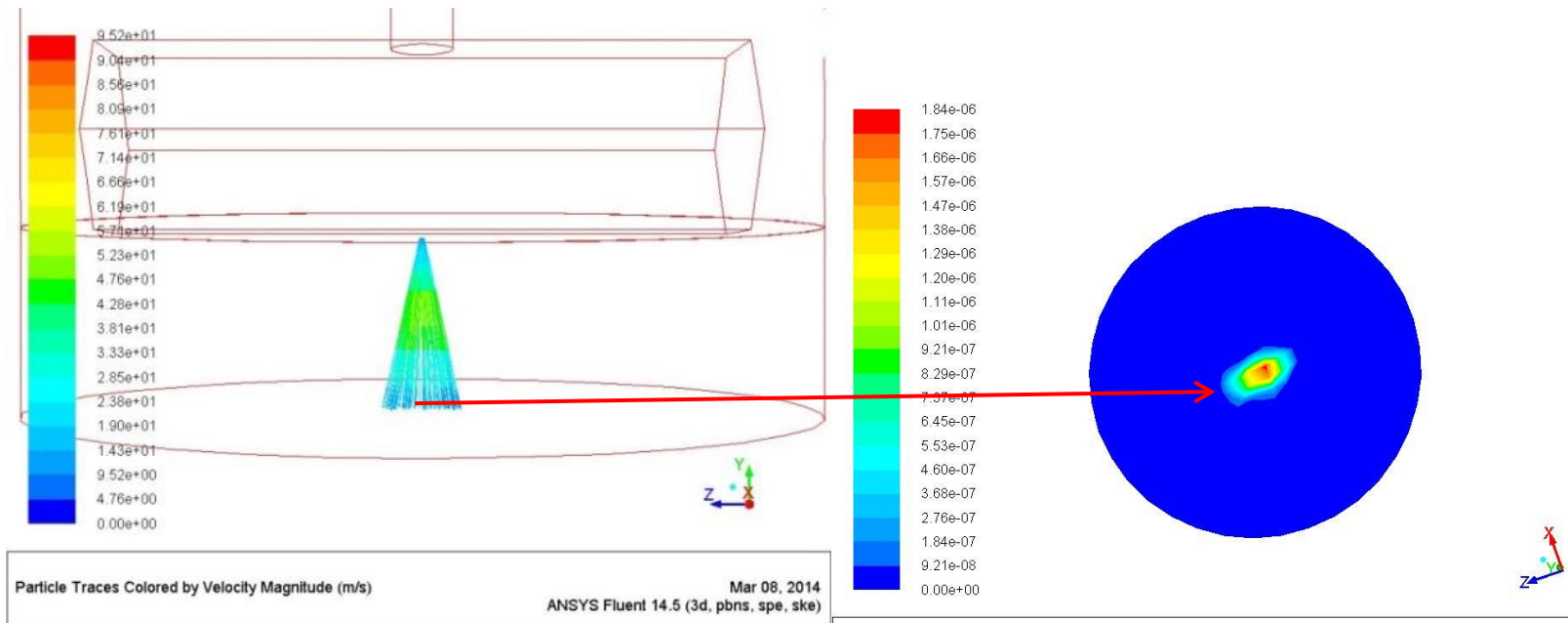


Figure 5.47 Simulated momentum impact variations

6.6.2 Comparison of aerated and non-aerated scale removal

This section provides the comparison of the CFD scale removal between the non-aerated and aerated results obtained. The sample for CaCO_3 and CaSO_4 were chosen from the *Fluent* built-in materials library and the results obtained is shown in Fig. 6.48 and 6.49 respectively. Also CaO and $\text{CaSO}_4 \cdot 2\text{H}_2\text{O}$ are shown in Fig. 6.50 and 6.51.

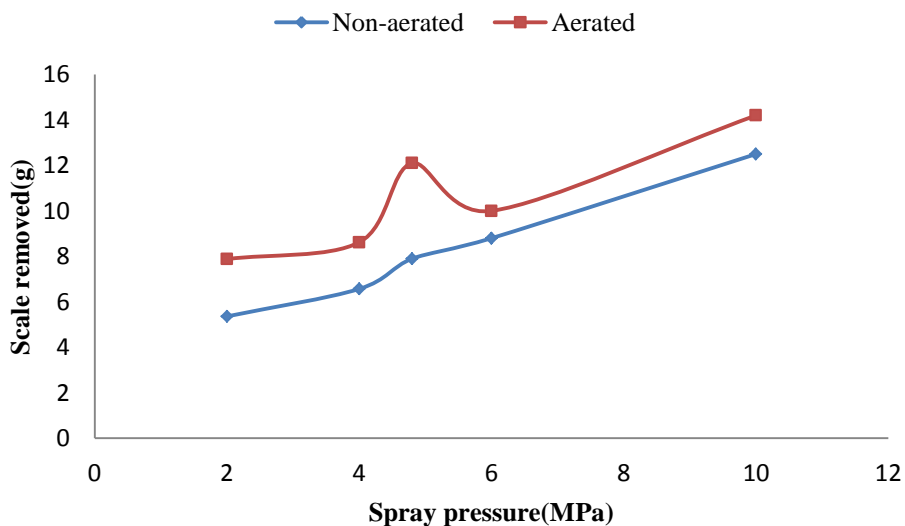


Figure 6.48 CaCO_3 comparison

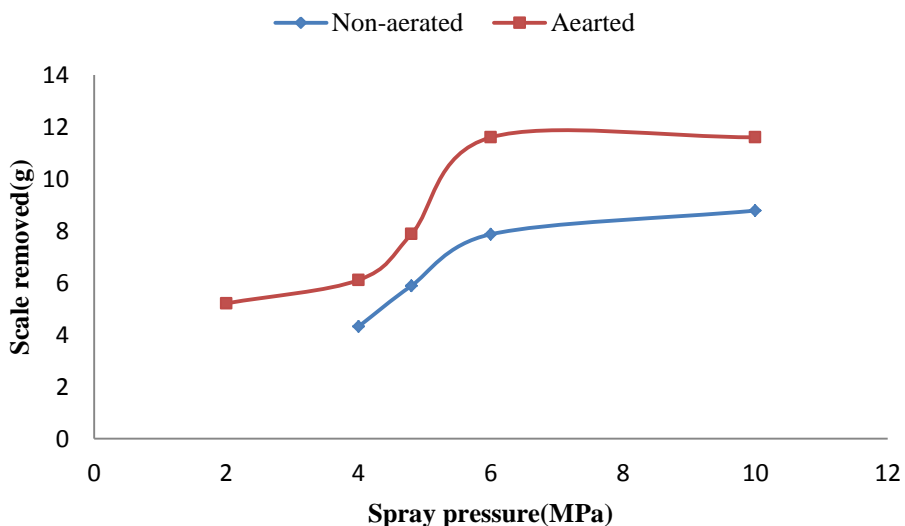


Figure 6.49 CaSO_4 comparison

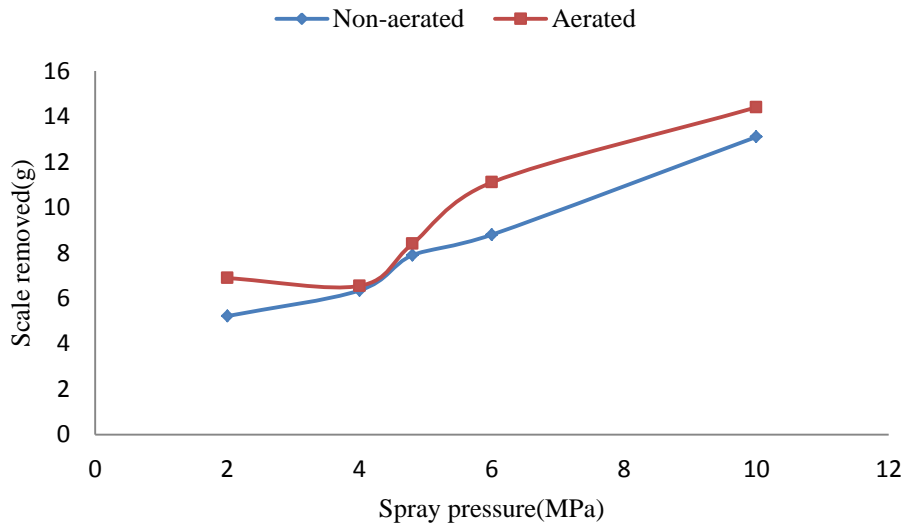


Figure 6.50 CaO comparison

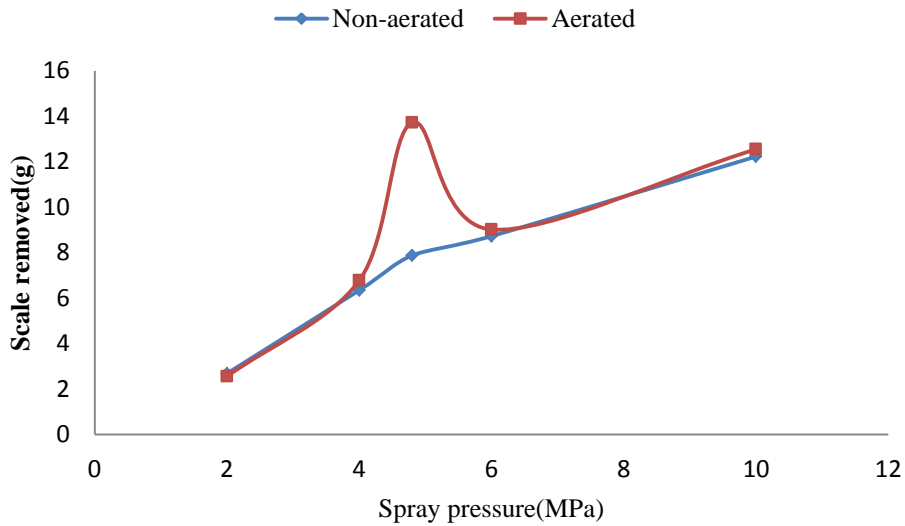


Figure 6.51 Gypsum (CaSO₄.2H₂O) comparisons

Further comparisons between the experimental and Fluent simulation results are shown in Fig. 6.52. Additionally, a general comparison between the mass eroded predicted using the Fluent models and the experimental investigation were further compared with in Fig. 6.53 indicating a good agreement between the results, with the aerated simulated trials showing higher erosion compared to the experimental results. This is possibly due to experimental errors which the Fluent simulation did not encounter.

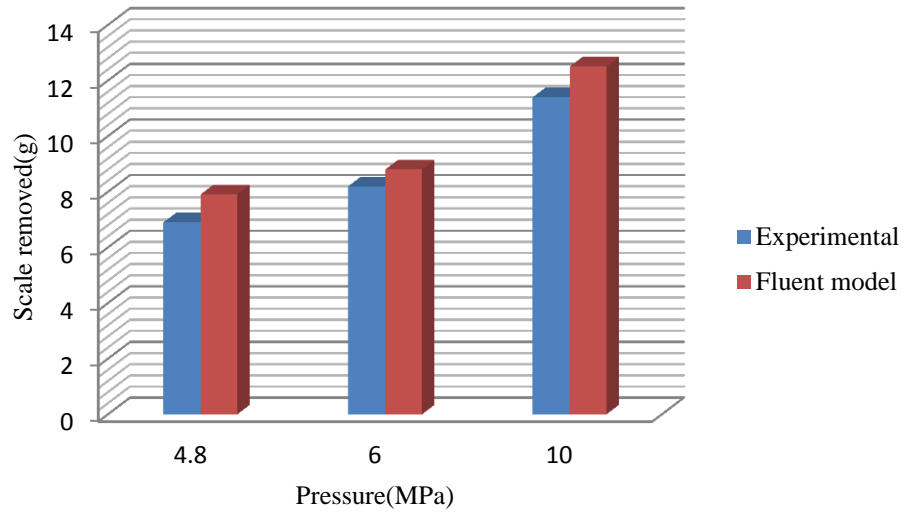


Figure 6.52 Experimental versus CFD simulation erosion

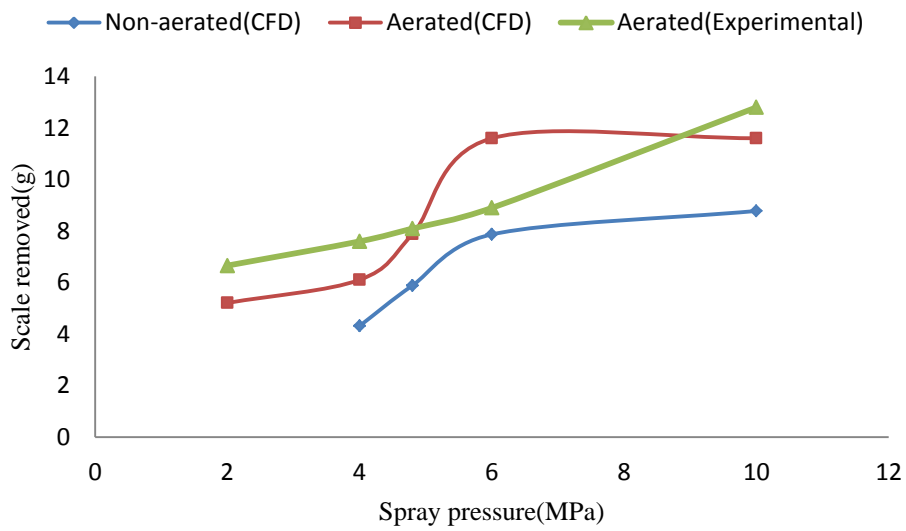


Figure 6.53 CaSO₄ comparison

6.7 Summary

Using Computational Fluid Dynamics (CFD) Fluent and CFX codes in validating the experimental trials investigated in this work, the following summary have been derived from the simulation results

- The five turbulent flow models namely Realizable k-e, RNG k-e, SST k-w, STD k-e, and standard k-w show similar capability in predicting the flow behaviour of air-water systems, especially the cavitation tendencies due to pressure drop across the atomizer throat which were confirmed experimentally through bubbles observed in the flow as well as noise presumed by the cavitation.
- The entrained-air velocities around the high pressure water sprays confirms a values between 5 to about 20m/s outside the spray width similar to the experimental results of 4 to 14m/s. However, within the sprays, CFD predicted velocities up to 70m/s in the region where experimental trials could not be performed.
- The spray characterization in terms of drop sizes determined numerically using CFD a value range of 40 to 80 μ m comparably similar to 55 and 81 μ m obtained experimentally using PDA. The droplet velocities of 80 to 120m/s compared to 75 to 117m/s at stand-of distance range of 25 to 75mm downstream of the atomizer.
- The air concentration variation from 0.0-12.0% has proven ability to mitigate cavitation bubble length from about 5mm to nearly zero in the aerated chamber; this led to the exemption of cavitation erosion at stand-off distance of 25mm where the scale removal trials were conducted.
- Scale removal erosion rate obtained using CFD is in agreement with the experimental trials within about 7%.

Chapter 7

Conclusion and Recommendations

7.1 Conclusions

The following conclusions can be drawn from this research which has successfully developed an option of adopting aeration into descaling oil wells operations in which three typical scale types involving hard, medium and soft samples having a Mohs hardness index of 3.0, 0.9 and 0.2 respectively, as follows:

- Air entrainment distribution was utilised to explain the variation of droplet impact pressure during the scale removal.
- Introducing aeration around sprays has been identified to cause compressive stresses onto the walls leading to improved erosion in downhole scale during descaling operations at even low spray pressure compared to the typical higher pressure used in the industry.
- Increase the aeration by changing the air flow rate between 3-12 % also increases the amount of scale eroded.
- Different scale samples respond to different erosion mechanism, which require a separate descaling conditions, although all the three samples considered in this research are eroded within 4.8-10MPa.
- The interaction between air-water developed a pulling effect forces enabling the air velocities increases towards the spray centre and decreases away from the spray centre.
- Interactions of air around a high pressure water sprays induced drag effect onto the surrounding air, leading to generation a air velocity distributions around the sprays with varying axial and lateral values ranging from 4 to 14 m/s.
- The droplet size ranges of 55 to 81 μm and droplet velocities of 75 to 117 m/s, enabling the droplet momentum and impact pressure at the highest at the centre of the spray to be up to $1.45\text{e-}05$ kgm/s and 0.15 MPa respectively.

- Aeration has shown significant increase in the compressive stress around the scale samples leading to increased erosion by about 30% compared to non-aerated trials.
- Aeration has been shown to significantly reduce or even eliminates cavitation within 2-4 mm away from the atomizer eliminating the tendency of cavitation erosion at 25 mm where the scale sample stand-off distance was chosen for this study.
- A scale removal of 12.80, 7.31, and 65.80 g was removed using the aerated chamber compared to be 9.88g, 6.33g and 5.31 g for the non-aerated chamber.
- Comparison of the current research with similar commercial descaling processes utilising solid particles confirms an erosion rate of 12.80g compared to 6.1 and 25g using a solid stream jets atomizer for 5 minutes, which poses a risk of fragmentation of scale with a potential of longer maintenance duration. This confirms the suitability of employing aeration in descaling instead using sterling beads (solid particles).
- The CFD simulation employ the five turbulent flow models namely Realizable k-e, RNG k-e, SST k-w, STD k-e, and standard k-w. These show similar capabilities in predicting the flow behaviour of air-water systems, especially the cavitation tendencies due to the pressure drop across the atomizer throat, which was confirmed experimentally through bubbles observed in the flow, as well as noise the presumed by the cavitation.
- The entrained-air velocities around the high pressure water sprays confirms a value of between 5 to about 20 m/s outside the spray width similar to the experimental results of 4 to 14 m/s. However, within the sprays, CFD predicted velocities up to 70 m/s in the region, where experimental trials could not be performed.
- The spray characterization in terms of drop sizes determined numerically using CFD give a value range of 40 to 80 μm compared to 55 and 81 μm obtained experimentally, using PDA. The droplet velocities of 80 to 120 m/s compared to 75 to 117 m/s at stand-of distance range of 25 to 75 mm downstream of the atomizer.
- The air concentration variation from 0-12 % has proven ability to mitigate cavitation bubble length from about 5mm to nearly zero in the aerated chamber; this led to the exemption of cavitation erosion at stand-of distance of 25 mm where the scale removal trials were conducted.

- Scale removal erosion rate obtained using CFD is in agreement with the experimental trials within about 7 %.

7.2 Recommendations

Although this investigation considered details procedures of design and construction and modification of the facilities used, therefore high level of breakthrough was achieved, still, it will be recommended to carry out other task which were considered out of scope of this research but may also contribute to knowledge gap:

- Multiple atomizers could be design to utilize an overlapping scheme which enables larger surface area of cleaning and combined impact pressure .
- The nozzle orientation in this investigation was maintained at 90° to the scale sample; however, alternative angular arrangement such as 30, 45 etc. might lift chunks again which could provide additional erosion during the scale cleaning.
- X-ray Diffraction to be carried out on the scale sample to confirm the actual chemical constituents of the scale samples.
- Fracture mechanics investigation be carried out to understand the erosion nature of the scale samples.
- The chamber for the experiment was designed with Perspex, with transparent material for imaging and observation purpose having maximum design pressure of 0.5 MPa, although improved material selection can be made to enable a pressure chamber that can withstand up to 1MPa could be used to investigate the effect of air concentration above the 12 % as considered in this investigation.
- The mechanism of erosion varies with the chemical and mechanical properties of the scale, therefore each oil well producing scale requires details mechanical data test for such scale sample prior to designing a suitable descaling scheme.
- While this investigation utilised only Flat fan nozzles which have a proven high pressure descaling capabilities, still, a combination of the Flat fan nozzles and solid stream nozzles could be investigated as most current technology adopts multiple number of nozzles.

REFERENCES

- [1] J. Leal, W. Nunez, S. Al-ismail, and J Ricardo Solares, "SPE 121404 Novel Mechanical Scale Clean-out Approach to Remove Iron Sulphide Scale from Tubulars in Vertical High Pressure and Temperature Deep Gas Producers : A Case History," 2009.
- [2] J. Al-ashhab, H. Al-matar, and S. Mokhtar, "SPE 101401 Techniques Used to Monitor and Remove Strontium Sulfate Scale in UZ Producing Wells," 2006.
- [3] Schlumberger, "Scale control," 2013. [Online]. Available: http://www.slb.com/services/completions/stimulation/sandstone/scale_control.aspx. [Accessed: 13-Dec-2013].
- [4] M. Brown, "Full Scale Attack," *The BP Technology magazine*, pp. 30–32, 1998.
- [5] E. Enerstvedt, H. Boge, and P. Petroleum, "SPE 68366 Scale Removal by Milling and Jetting With Coiled Tubing," no. July 2000, 2001.
- [6] F. A. Bajammal, H. M. Biyanni, A. P. Riksa, H. M. Poitrenaud, A. Mahardhini, E. Total, and P. Indonesia, "Scale Management in Mature Gas Field : Case Study of Peciko," no. May 2012, pp. 26–28, 2013.
- [7] A. R. Malik, T. M. Ogundare, Y. H. Ali, K. K. Waleed, D. A. Alaa, S. Aramco, R. T. Sebastian, and T. Bukovac, "IPTC 17665 Refracturing in Old , Mature and Depleted Carbonate Reservoirs in Saudi Arabia for Production Enhancement," 2014.
- [8] D. a. Axinte, B. Karpuschewski, M. C. Kong, a. T. Beaucamp, S. Anwar, D. Miller, and M. Petzel, "High Energy Fluid Jet Machining (HEFJet-Mach): From scientific and technological advances to niche industrial applications," *CIRP Ann. - Manuf. Technol.*, pp. 1–21, Jun. 2014.
- [9] R. Kayumov, A. Konchenko, A. Bairamov, A. Klyubin, O. Levanyuk, A. Chikin, V. Firsov, and E. Nikulshin, "SPE 168167 Experience of Carbonate Acidizing in the Challenging Environment of the Volga-Urals Region of Russia," no. Grace 2005, 2014.
- [10] A. Johnson, D. Eslinger, and H. Larsen, "SPE 46026 An Abrasive Jetting Scale Removal System," pp. 105–110, 1996.
- [11] M. Crabtree and A. Johnson, "Fighting Scale — Removal and Prevention," pp. 30–45, 1999.
- [12] M. L. Morkved, C. Knight, B. Bhagwan, A. Garcia, W. Zhuang, M. Oil, H. R. Christian, and A. C. Nelson, "IPTC 17456 Chemical Consolidation of Sand Propped Fractures in a Chalk Reservoir Offshore Denmark With Enzymatic Calcium Carbonate Scale," pp. 1–12, 2014.
- [13] H. Guler, H. Zhu, H. E. Ozkan, P. Ling, and T. Ohio, "CHARACTERIZATION OF HYDRAULIC NOZZLES FOR DROPLET SIZE AND SPRAY," vol. 22, no. 8, pp. 627–645, 2012.

- [14] B. K. Fritz, W. C. Hoffmann, G. R. Kruger, R. S. Henry, A. Hewitt, and Z. Czaczyk, "Comparison of Drop Size Data From Ground and Aerial Application Nozzles At Three Testing Laboratories," *At. Sprays*, vol. 24, no. 2, pp. 181–192, 2014.
- [15] M. Zahedzadeh and M. S. Karambeigi, "Comprehensive management of mineral scale deposition in carbonate oil fields—A case study," ... *Res. Des.*, pp. 1–9, Mar. 2014.
- [16] S. Hamid, O. De Jesus, C. M. Jacinto, R. Izetti, H. Pinto, E. Droguett, C. Edwards, J. Cassidy, H. Zhang, P. Dagenais, and M. Batocchio, "SPE 166673 A Practical Method of Predicting Chemical Scale Formation in Well Completions," no. 1992, 2013.
- [17] K. Mei, H. B. Qahtani, A. S. Al-kuait, L. A. Sukkar, and S. Aramco, "IPTC 16595 Formation Damage and Treatment of Offshore Water Disposal Wells in Saudi Arabia : Case Studies," 2013.
- [18] T. Chen, J. Lewis, P. Chen, R. Benvie, T. Hagen, H. Montgomerie, and N. Champion, "SPE 168154 Development of a New Squeeze Scale Inhibitor for Mitigating Formation Damage for High TDS High Temperature Tight Carbonate Reservoir," 2014.
- [19] E. Mackay, K. Sorbie, V. Kavle, E. Sørhaug, K. Melvin, K. Sjursæther, and M. Jordan, "SPE 100516 Impact of In - Situ Sul f ate Stripping on Scale Management in the Gyda Field," pp. 1–11, 2006.
- [20] R. Stalker, S. Solutions, I. R. Collins, S. P. E. Bp, E. Operating, and G. M. Graham, "SPE 80257 The Impact of Chemical Incompatibilities in Commingled Fluids on the Efficiency of a Produced Water Reinjection System : A North Sea Example," 2003.
- [21] A. Taheri, R. Masoudi, M. Zahedzadeh, A. R. Ataei, and R. Nioc, "SPE 113109 Simulation and Experimental Studies of Mineral Scale Formation Effects on Performance of an Iranian Carbonate Oil Reservoir U nder Water Injection," 2005.
- [22] M. Field, "SPE 135960 Scale Buildup , its D etection and Removal in High Temperature Gas Wells of," pp. 1–15, 2010.
- [23] R. Farrell, A. Leontieff, A. Strachan, B. Hughes, J. Muir, C. Etc, R. E. Stanley, and H. D. Smith, "Downhole Scale Management on the Alba Field : A Case History," no. May, pp. 6–9, 2013.
- [24] A. Kazemi, N. Korrani, K. Sepehrnoori, and M. Delshad, "SPE 168196-MS A Comprehensive Geochemical-Based Approach to Quantify the Scale Problems," 2014.
- [25] J. Pinango, "Design Simulation of A Pressurized Test Facility and Application Of CFD," University of Salford, 2003.
- [26] M. El-Kamki, "Investigation into Descaling of production tubing in Oil and Gas Wells," University of Salford, 2012.
- [27] Z. Wang, A. Neville, U. Leeds, and A. W. Meredith, "SPE 94993 How and Why Does Scale Stick — Can the Surface Be Engineered To Decrease Scale Formation and Adhesion ?," 2005.

- [28] A. B. Bin Merdhan and A. M. Yassin, "FORMATION DAMAGE DUE TO SCALE FORMATION IN POROUS MEDIA RESULTING WATER INJECTION," vol. 13, no. 3, pp. 69–79, 2008.
- [29] K. Skrettingland, E. I. Dale, V. R. Stenerud, A. M. Lambertsen, K. N. Kulkarni, Ø. Fevang, and A. Stavland, "SPE-169727-MS Snorre In-depth Water Diversion Using Sodium Silicate – Large Scale Interwell Field Pilot," 2014.
- [30] A. T. Kan, N. Zhang, W. Shi, K. Wang, L. Wang, C. Yan, F. Yan, M. B. Tomson, R. C. Tomson, H. Zhu, S. M. A. Razavi, and S. Water, "SPE 164127 Interrelationship of CO₂, Weak Acids, Bases, and pH in Scale Prediction and Control," 2013.
- [31] L. Sutherland, C. Johnston, and W. Taylor, "SPE 164070 The Influence of Turbulence (or Hydrodynamic Effects) on Barium Sulphate Scale Formation and Inhibitor Performance," pp. 1–9, 2013.
- [32] S. C. Ayirala, A. A. Yousef, and S. Aramco, "SPE-169048-MS Injection Water Chemistry Requirement Guidelines for IOR / EOR," no. April, pp. 12–16, 2014.
- [33] A. Shepherd, G. Thomson, R. Westacott, K. Sorbie, M. Turner, and P. Smith, "Analysis of Organic Field Deposits: New Types of Calcium Naphthenate Scale or the Effect of Chemical Treatment?," *Proc. SPE Int. Oilf. Scale Symp.*, May 2006.
- [34] A. Haghtalab, M. J. Kamali, and A. Shahrabadi, "Prediction mineral scale formation in oil reservoirs during water injection," *Fluid Phase Equilib.*, Apr. 2014.
- [35] C. Okocha and K. S. Sorbie, "SPE 168182 Sulphide Scale Co-Precipitation with Calcium Carbonate," no. February, pp. 26–28, 2014.
- [36] A. Kamari, F. Gharagheizi, A. Bahadori, and A. H. Mohammadi, "Rigorous modeling for prediction of barium sulfate (barite) deposition in oilfield brines," *Fluid Phase Equilib.*, vol. 366, pp. 117–126, Mar. 2014.
- [37] E. Oddo, M. B. Tomson, and U. Rice, "Why Scale Forms and How To Predict It," no. February, pp. 47–54, 1994.
- [38] J. S. Sopngwi, A. Gauthreaux, D. E. Kiburz, T. Kashib, E. A. Reyes, A. Beuterbaugh, A. L. Smith, and S. K. Smith, "SPE 168171 Successful Application of a Differentiated Chelant-Based Hydrofluoric Acid for the Removal of Aluminosilicates, Fines, and Scale in Offshore Reservoirs of the Gulf of Mexico," 2014.
- [39] D. N. Meehan, "Water Issues for Petroleum Engineers," 2010.
- [40] Z. Guimaraes, A. B. Franca, L. H. Duque, B. J. S. Co, R. B. De Souza, M. Porto, and D. Neves, "SPE 107063 Case Histories of Barium Sulfate Scale Removal in Offshore Wells, Brazil, Using a New Engineered Combination of Coiled - Tubing Tools," 2007.
- [41] F. Civan, "SPE 168164 Analyses of Processes, Mechanisms, and Preventive Measures of Shale-Gas Reservoir Fluid, Completion, and Formation Damage," 2014.
- [42] A. C. Todd and M. D. Yuan, "Barium and Strontium Sulfate Solid-Solution Scale Formation at Elevated Temperatures," no. February, pp. 85–92, 1992.

- [43] Window Cleaning Specialist, “We make 100% pure Water at our head office,” 2014. .
- [44] S. D. Bittner, K. R. Zemplak, B. D. Korotash, A. Canada, and P. Company, “SPE 60695 Coiled Tubing Scale Removal of Iron Sulfide – A Case Study of the Kaybob field in Central Alberta,” 2000.
- [45] A. A. Eltaib, O.E. & Rabah, “Crude Oil Pipeline Scale Deposition: Causes and Removal Methods,” 2012. .
- [46] C. J. Hinrichsen, “Preventing Scale Deposition In Oil Producing Facilities: An Industry Review,” *Corrosion*, vol. 98, no. 61, pp. 1–29, 1998.
- [47] et al Abbasi, “Scale Formation because of Water Incompatibility between Injection Water and Formation Water in Reservoir Pressure and Temperature Condition to Emphasis Thermodynamic Condition Changes- A Static Experimental Investigation,” *SPE*, 2013.
- [48] C. J. Hinrichsen, “Preventing Scale Deposition In Oil Production Facilities: An Industry Review,” no. 61, 1998.
- [49] J. S. Sopngwi, A. Gauthreaux, D. E. Kiburz, M. Oil, B. Sonnier, D. Moghalu, and S. K. Smith, “SPE 168255 Successful Mechanical Removal of Barium Sulfate Tubular Scale by Coiled Tubing : A Gulf of Mexico Case History of an Engineered Approach for Offshore Rigless Interventions,” 2014.
- [50] M. H. V Quiroga, J. C. N. Calmeto, S. L. Pinto, C. A. S. Assis, and I. Santos, “SPE 89627 Hard Scale Mechanical Removal : A Solution for Brazilian Offshore Operations,” no. May 2003, pp. 1–6, 2004.
- [51] Shlumberger, *Scale removal technology*. United Kingdom, 1999.
- [52] M. Nasr, G. G., Enyi, G.G., El-Kamki, M.E., & Burby, “Characterisation of Flat fan sprays for petroleum applications,” in *Institution of Liquid Atomization and Sprays Systems*, 2012, pp. 7–10.
- [53] J. Gholinezhad, “Evaluation of Latest Techniques for Remedial Treatment of Scale Depositions in Petroleum Wells,” *SPE Int. Oilf. Scale Symp.*, Apr. 2013.
- [54] L. Bendig, M. Raudenský, J. Horský, L. GmbH, C. Kg, U. Strasse, and M. Germany, “Descaling with high pressure nozzles,” no. September, 2001.
- [55] M. V. Panchagnula and P. E. Sojka, “Spatial droplet velocity and size profiles in effervescent atomizer-produced sprays,” *Fuel*, vol. 78, no. 6, pp. 729–741, May 1999.
- [56] M. Grac, D. Ayres, M. Caldas, V. Semia, and E. Carvalho, “Prediction of the droplet size and velocity joint distribution for sprays,” vol. 80, pp. 383–394, 2001.
- [57] M. Weclas and J. Cypris, “Diesel spray interaction with porous structure : space- and time-dependent analysis of fuel distribution in space and its vaporization,” vol. i, no. September, pp. 1–4, 2013.
- [58] T. Knorsch, M. Storch, L. Zigan, and M. Wensing, “Comparison of the Spray Evaporation and Inflammation of Alternative Fuels for Late Injection Timing Mode Experimental test-rig,” no. September, pp. 1–4, 2013.

- [59] M. Storch, T. Knorsch, L. Zigan, M. Wensing, and S. Will, "High-speed imaging of the sooting combustion of ethanol-gasoline blended fuel sprays under DISI cold start conditions," no. September, pp. 1–4, 2013.
- [60] A. Lampa and U. Fritsching, "Atomization and spray formation for PVP powder production," no. September, pp. 1–4, 2013.
- [61] S. Möller, G. Dutzler, E. Berg, P. Priesching, W. Payer, and J. V Pastor, "Detailed Investigation of Multi-Component Spray Model Capabilities for Diesel Engine Simulation," no. September, pp. 1–4, 2013.
- [62] K. Matsuura, K. Ide, Y. Yoshiura, S. Ohori, Y. Kurosawa, K. Shimodaira, T. Yamamoto, Y. Ohta, and S. Hayashi, "Phase Doppler characterization of burning sprays from an auxiliary emission control fuel nozzle of a lean two-stage low-NO_x combustor for an aero-engine at a simulated aircraft approach condition," no. September, pp. 1–4, 2013.
- [63] F. Pinkert, A. Gerds, I. Najar, C. Fink, and H. Harndorf, "On the use of 3D spray impulse topography for analyzing the effects of nozzle geometry on spray break-up," no. September, pp. 1–4, 2013.
- [64] Y. S. Tamhankar, J. R. Whiteley, M. R. Resetarits, and C. P. Aichele, "Spray Droplet Characterization Inside a Glass Column Through Dense Wall Flow," *At. Sprays*, vol. 24, no. 2, pp. 115–128, 2014.
- [65] N. Rimbart and G. Castanet, "Crossover between Rayleigh-Taylor instability and turbulent cascading atomization mechanism in the bag-breakup regime.," *Phys. Rev. E. Stat. Nonlin. Soft Matter Phys.*, vol. 84, no. 1 Pt 2, p. 016318, Jul. 2011.
- [66] P. C. Dombrowski, N., Hooper, "The effect of ambient density on drop formation in sprays," *Chem. Eng. Sci.*, vol. 17, pp. 291–305, 1962.
- [67] D. E. Dombrowski, N., Hasson, D. & Ward, "Some aspects of liquid flow through fan spray nozzles," *Chem. Eng. Sci.*, vol. 12, pp. 35–50, 1960.
- [68] R. P. Dombrowski, N., & Fraser, "A photographic investigation into the disintegration of liquid sheets," *Philos. Trans. R. Soc.*, vol. 247, pp. 101–130, 1954.
- [69] D. G. Yule, A J., Salters, "The structure and dimensions of time dependent break-up zone of diesel sprays," in *International Conference on Liquid Atomisation and Spray Systems*, 1994.
- [70] R. J. Rajendran S., Jog, M.A., Manglik, "Experimental Investigation of Liquid Jet Breakup at Low Weber Number," in *Institution of Liquid Atomization and Sprays Systems*, 2012, no. May.
- [71] H. Arai, M., Shimizu, M., & Hiroyasu, "Break-up length and spray angle of high speed jet," in *International Conference on Liquid Atomisation and Spray Systems*, 1985.
- [72] H. Liu, *Science and Engineering of Droplets: Fundamentals and applications*. William Andrew Publishing, 2000.

- [73] A. A. Ibrahim, "Comprehensive study of internal flow field and linear and non-linear instability of a annular liquid sheet emanating from an atomiser," University of Cincinnati, 2006.
- [74] A. H. Lefebvre, *Atomisations and Sprays*. Taylor and Francis, 1989.
- [75] G. Dombrowski, N. and Munday, *Spray Drying*. New York: Academic press, 1968, pp. 209–320.
- [76] R. Reitz, R.D & Diwakar, "Modelling atomisation processes in high pressure vapourising sprays," *At. Spray Technol.*, vol. 3, pp. 309–337, 1987.
- [77] J. Masden, "Computational and experimental study of spray from break-up of water sheets," Aalborg University Esbjerg, 2006.
- [78] G. Kamoun, H., Roberto, S., Lamanna, G., Weigand, "Velocity characterisation of a flashing ethanol jet with laser correlation velocimetry," in *Institution of Liquid Atomization and Sprays Systems*, 2012.
- [79] J. . Yule, A J; & Dunkley, *Atomisation of Melts for Powder Production and Spray Deposition*. Oxford: Clarendon press, 1994.
- [80] M. B. Abuhesa, "Investigation into Gas Flaring Reduction in the Oil and gas Industry," University of Salford, 2010.
- [81] G. I. Taylor, "Generation of ripples by wind blowing over a viscous Fluid," vol. 3, pp. 244–254, 1940.
- [82] J. R. R. Rivas, A. P. Pimenta, and G. a. R. Rivas, "Development of a Mathematical Model and 3D Numerical Simulation of the Internal Flow in a Conical Swirl Atomizer," *At. Sprays*, vol. 24, no. 2, pp. 97–114, 2014.
- [83] L. Nasr, G.G. Yule, A.J., & Bendig, *Industrial Sprays and Atomisations: Design, analysis and applications*. Springer and Verlag, 2002.
- [84] BETE, "Full Cone Nozzles - Air Atomising Design," 2014. [Online]. Available: <http://www.bete.co.uk/spray-nozzles/full-cone-nozzles/air-atomising-nozzles>. [Accessed: 29-Jul-2014].
- [85] Wikipedia, "Spray nozzles," 2014. [Online]. Available: http://en.wikipedia.org/wiki/Spray_nozzle. [Accessed: 29-Jul-2014].
- [86] BETE, "The basic spray patterns," 2014. [Online]. Available: <http://www.bete.co.uk/resources/engineering-resources/guide-to-spray-properties/2--basic-spray-patterns>. [Accessed: 29-Jul-2014].
- [87] BET, "Air actuated flat fan nozzles," 2014. [Online]. Available: <http://www.bete.co.uk/spray-nozzles/flat-fan-nozzles/air-actuated>. [Accessed: 29-Jul-2014].
- [88] S. E. Gant, *CFD modelling of water spray barriers*. HSL, 2006, p. 79.
- [89] D. L. Naber, J.D., Siebers, "Effects of Gas Density and Vapourisation on Dispersion and Penetration in Diesel Sprays," *SAE Pap.*, no. 960034, 1996.

- [90] Schlumberger, “Scale control,” 2013. .
- [91] M. S. Mirza, V. Prasad, and O. Company, “SPE 53345 Scale Removal in Khuff Gas Wells,” 1999.
- [92] J. M. Franc, J.P., & Michael, *Fundamentals of cavitation*. France: Grenoble sciences, 2003.
- [93] F. R. Young, *Cavitations*. McGraw Hill, 1989.
- [94] “Engineering Tool Box,” 2013. [Online]. Available: http://www.engineeringtoolbox.com/oxygen-solubility-water-d_841.html. [Accessed: 12-Nov-2013].
- [95] T. Koivula, “On cavitation in fluid power,” 2000, pp. 371–382.
- [96] W. E. . Lauterborn, *Cavitation and inhomogeneities in under water acoustics*. Springer and Verlag, 1980.
- [97] C. E. Brennen, *Cavitation and bubble dynamics*. Oxford: University press, 1995.
- [98] Y. Zhang, “Amazing bubble world blog spots,” 2012. [Online]. Available: <http://amazingbubbleworld.blogspot.co.uk/2012/05/classifications-of-cavitation.html>. [Accessed: 09-Nov-2013].
- [99] J. Desantes, J. M., Payri, R., Salvador, F. J. & Gimeno, “Measurements of spray momentum for the study of cavitation in diesel injection nozzles,” *Soc. Automot. Eng.*, 2003.
- [100] S. Martynov, D. Mason, M. R. Heikal, S. S. Sazhin, and M. Gorokhovski, “Modelling of Cavitation Flow in a Nozzle and Its Effect on Spray Development,” *Jets*, 2006.
- [101] F. G. Knapp, R. T., Daily, J. W. & Hammitt, *Cavitation*. McGraw Hill, 1970.
- [102] Y. K. De Chizelle, S. L. Ceccio, and C. E. Brennen, “Observations and scaling of travelling bubble cavitation,” *J. Fluid Mech.*, vol. 293, no. -1, p. 99, Apr. 2006.
- [103] B. Han, D. Y. Ju, and W. P. Jia, “Influence of water cavitation peening with aeration on fatigue behaviour of SAE1045 steel,” *Appl. Surf. Sci.*, vol. 253, no. 24, pp. 9342–9346, Oct. 2007.
- [104] Z. Dong and P. Su, “Cavitation Control By Aeration and Its Compressible Characteristics,” *J. Hydrodyn. Ser. B*, vol. 18, no. 4, pp. 499–504, Aug. 2006.
- [105] D. Zhi-yong, C. Lei, and J. U. Wen-jie, “CAVITATION CHARACTERISTICS OF HIGH VELOCITY FLOW WITH AND WITHOUT AERATION ON THE ORDER OF 50 m / s *,” vol. 19, no. 50579067, pp. 429–433, 2007.
- [106] H. Hajikandi, “c r v i h o e f c f,” vol. 3, no. 1, pp. 19–25, 2011.
- [107] J. Wu, B. Zhang, and F. Ma, “Inception point of air entrainment over stepped spillways,” *J. Hydrodyn. Ser. B*, vol. 25, no. 1, pp. 91–96, Feb. 2013.

- [108] M. Pfister and W. H. Hager, "Self-entrainment of air on stepped spillways," *Int. J. Multiph. Flow*, vol. 37, no. 2, pp. 99–107, Mar. 2011.
- [109] Y. Wang, L. Qiu, R. D. Reitz, and R. Diwakar, "Simulating cavitating liquid jets using a compressible and equilibrium two-phase flow solver," *Int. J. Multiph. Flow*, vol. 63, pp. 52–67, Jul. 2014.
- [110] M. Qin, D. Y. Ju, and R. Oba, "Improvement on the process capability of water cavitation peening by aeration," *Surf. Coatings Technol.*, vol. 200, no. 18–19, pp. 5364–5369, May 2006.
- [111] S. M. Chun, "Aeration effects on the performance of a turbocharger journal bearing," *Tribol. Int.*, vol. 41, no. 4, pp. 296–306, Apr. 2008.
- [112] K. Harby, S. Chiva, and J. L. Muñoz-Cobo, "An experimental study on bubble entrainment and flow characteristics of vertical plunging water jets," *Exp. Therm. Fluid Sci.*, vol. 57, pp. 207–220, Sep. 2014.
- [113] Z. Dong, Z. Liu, Y. Wu, and D. Zhang, "An Experimental Investigation of Pressure and Cavitation Characteristics of High Velocity Flow Over a Cylindrical Protrusion in the Presence and Absence of Aeration," *J. Hydrodyn. Ser. B*, vol. 20, no. 1, pp. 60–66, Feb. 2008.
- [114] D. Y. Ju and B. Han, "Investigation of water cavitation peening-induced microstructures in the near-surface layer of pure titanium," *J. Mater. Process. Technol.*, vol. 209, no. 10, pp. 4789–4794, Jun. 2009.
- [115] H. Soyama, "The Use of Cavitation Peening to Increase the Fatigue Strength of Duralumin Plates Containing Fastener Holes," *Mater. Sci. Appl.*, vol. 05, no. 06, pp. 430–440, 2014.
- [116] Test4less, "ATP AVM 888-Hot Wire Anemometer," 2014. [Online]. Available: <http://www.test4less.co.uk/details.asp?ProductID=2296#>. [Accessed: 02-Aug-2014].
- [117] J. Lacoste, "Characteristics of Diesel Sprays at High Temperatures and Pressures," University of Brighton, 2006.
- [118] Dantec Dynamics, "Phase Doppler Anemometry," 2014. .
- [119] S. A. MacGregor, "Air entrainment in spray jets," *Int. J. heat fluid flow*, vol. 12, no. 3, pp. 279–283, 1991.
- [120] C. Reilly, N. R. Green, and M. R. Jolly, "The present state of modeling entrainment defects in the shape casting process," *Appl. Math. Model.*, vol. 37, no. 3, pp. 611–628, Feb. 2013.
- [121] J. Wu, B. Fan, and W. Xu, "Inverse problem of bottom slope design for aerator devices," *J. Hydrodyn. Ser. B*, vol. 25, no. 5, pp. 805–808, Oct. 2013.
- [122] K. M. Breton, D. S. Nobes, and B. A. Fleck, "The Effect of Superheat on the Performance Characteristics of a Flash Atomized Spray," no. September, pp. 1–4, 2013.
- [123] C. Crua, G. De Sercey, M. Gold, and M. R. Heikal, "Image-Based Analysis of Evaporating Diesel Sprays in the Near-Nozzle Region Experimental test-rig," no. September, pp. 1–4, 2013.

- [124] M. A. Reddemann, F. Mathieu, and R. Kneer, “Zooming into the primary breakup region of engine-related sprays Experimental test-rig,” no. September, pp. 1–4, 2013.
- [125] V. Semião, P. Andrade, and M. D. G. Carvalho, “Spray characterization: Numerical prediction of Sauter mean diameter and droplet size distribution,” *Fuel*, vol. 75, no. 15, pp. 1707–1714, Nov. 1996.
- [126] M. Gorokhovski and M. Herrmann, “Modeling Primary Atomization,” 2008.
- [127] N. Hecht, Z. Bouali, T. Menard, J. Reveillon, and F. X. Demoulin, “Coupled modelling impact of liquid interface and dispersed sprays,” no. September, pp. 1–4, 2013.
- [128] S. Makhlouf, J. Hélie, and J. Cousin, “Investigation of some primary atomization aspects using double exposure and double view processes 1- Introduction 4- Image Analysis,” vol. 1, no. September, pp. 1–4, 2013.
- [129] L. Opfer, I. V Roisman, J. Venzmer, M. Klostermann, and C. Tropea, “Effect of air-induction on agricultural flat fan sprays,” no. September, pp. 1–4, 2013.
- [130] Q. Wang, H. Ajwad, T. Shafai, J. D. Lynn, and S. Aramco, “SPE 168063 Iron Sulfide Scale Dissolvers : How Effective Are They ?,” no. May, pp. 19–22, 2013.
- [131] M. Dular, B. Stoffel, and B. Širok, “Development of a cavitation erosion model,” *Wear*, vol. 261, no. 5–6, pp. 642–655, Sep. 2006.
- [132] J. E. Field, J.-J. Camus, M. Tinguely, D. Obreschkow, and M. Farhat, “Cavitation in impacted drops and jets and the effect on erosion damage thresholds,” *Wear*, vol. 290–291, pp. 154–160, Jun. 2012.
- [133] R. Fortes Patella, T. Choffat, J.-L. Reboud, and A. Archer, “Mass loss simulation in cavitation erosion: Fatigue criterion approach,” *Wear*, vol. 300, no. 1–2, pp. 205–215, Mar. 2013.
- [134] Z. Sun, X. Q. Kang, and X. H. Wang, “Experimental system of cavitation erosion with water-jet,” *Mater. Des.*, vol. 26, no. 1, pp. 59–63, Feb. 2005.
- [135] M. Hajian, A. Abdollah-zadeh, S. S. Rezaei-nejad, H. Assadi, and S. M. M. Hadavi, “Applied Surface Science Improvement in cavitation erosion resistance of AISI 316L stainless steel by friction stir processing,” *Appl. Surf. Sci.*, vol. 308, pp. 184–192, 2014.
- [136] S. Hattori, T. Hirose, and K. Sugiyama, “Prediction method for cavitation erosion based on measurement of bubble collapse impact loads,” *Wear*, vol. 269, no. 7–8, pp. 507–514, Aug. 2010.
- [137] J. E. Field, J.-J. Camus, M. Tinguely, D. Obreschkow, and M. Farhat, “Cavitation in impacted drops and jets and the effect on erosion damage thresholds,” *Wear*, vol. 290–291, pp. 154–160, Jun. 2012.
- [138] B. S. Mann and V. Arya, “An experimental study to correlate water jet impingement erosion resistance and properties of metallic materials and coatings,” *Wear*, vol. 253, no. 5–6, pp. 650–661, Sep. 2002.

- [139] R. Cottam, V. Luzin, H. Moody, D. Edwards, a. Majumdar, Y. C. Wong, J. Wang, and M. Brandt, "The role of microstructural characteristics in the cavitation erosion behaviour of laser melted and laser processed Nickel–Aluminium Bronze," *Wear*, vol. 317, no. 1–2, pp. 56–63, Sep. 2014.
- [140] J. Wu and C. Luo, "Effects of entrained air manner on cavitation damage," *J. Hydrodyn. Ser. B*, vol. 23, no. 3, pp. 333–338, Jun. 2011.
- [141] S.-J. Kim, K.-Y. Hyun, and S.-K. Jang, "Effects of water cavitation peening on electrochemical characteristic by using micro-droplet cell of Al–Mg alloy," *Curr. Appl. Phys.*, vol. 12, pp. S24–S30, Sep. 2012.
- [142] A. Sahaya Grinspan and R. Gnanamoorthy, "Surface modification by oil jet peening in Al alloys, AA6063-T6 and AA6061-T4: Residual stress and hardness," *Appl. Surf. Sci.*, vol. 253, no. 2, pp. 989–996, Nov. 2006.
- [143] Q. Zongyi, "Investigation of the cavitation mechanism and erosion of submerged high pressure water jets," University of Queensland, 2004.
- [144] M. Atkinson, E. V. Stepanov, D. P. Goulet, S. V. Sherikar, and J. Hunter, "High pressure testing sand erosion in 3D flow channels and correlation with CFD," *Wear*, vol. 263, no. 1–6, pp. 270–277, Sep. 2007.
- [145] J.-P. Franc, M. Riondet, A. Karimi, and G. L. Chahine, "Material and velocity effects on cavitation erosion pitting," *Wear*, vol. 274–275, pp. 248–259, Jan. 2012.
- [146] N. Kamkar, F. Bridier, P. Bocher, and P. Jedrzejowski, "Water droplet erosion mechanisms in rolled Ti–6Al–4V," *Wear*, vol. 301, no. 1–2, pp. 442–448, Apr. 2013.
- [147] J. O. B. Design, "Jet Blaster."
- [148] EMARC, "Petroleum systems of the northern Gulf of Mexico: Phase I: Green Canyon and Ewing Bank," 2014. [Online]. Available: http://emarc.colorado.edu/respubs/programs/GOM_phase1.html. [Accessed: 20-Jun-2014].
- [149] C. A. Chasos, G. N. Karagiorgis, and C. N. Christodoulou, "Gasoline direct injection internal injector flow CFD simulations for various bioethanol blends," no. September, pp. 1–4, 2013.
- [150] M. Shehadeh and A. I. Shahata, "Modelling the Effect of Incompressible Leakage Patterns on Rupture Area in Pipeline," vol. 5, no. December, pp. 132–142, 2013.
- [151] F. J. Salvador, J.-V. Romero, M.-D. Roselló, and J. Martínez-López, "Validation of a code for modeling cavitation phenomena in Diesel injector nozzles," *Math. Comput. Model.*, vol. 52, no. 7–8, pp. 1123–1132, Oct. 2010.
- [152] a. Alhussein, J. Capelle, J. Gilgert, S. Dominiak, and Z. Azari, "Influence of sandblasting and hydrogen on tensile and fatigue properties of pipeline API 5L X52 steel," *Int. J. Hydrogen Energy*, vol. 36, no. 3, pp. 2291–2301, Feb. 2011.
- [153] S. R. Gopireddy and E. Gutheil, "Numerical Investigation of PVP / Water Spray Flows in an Eulerian Framework 1 : Interdisciplinary Center for Scientific Computing (IWR),

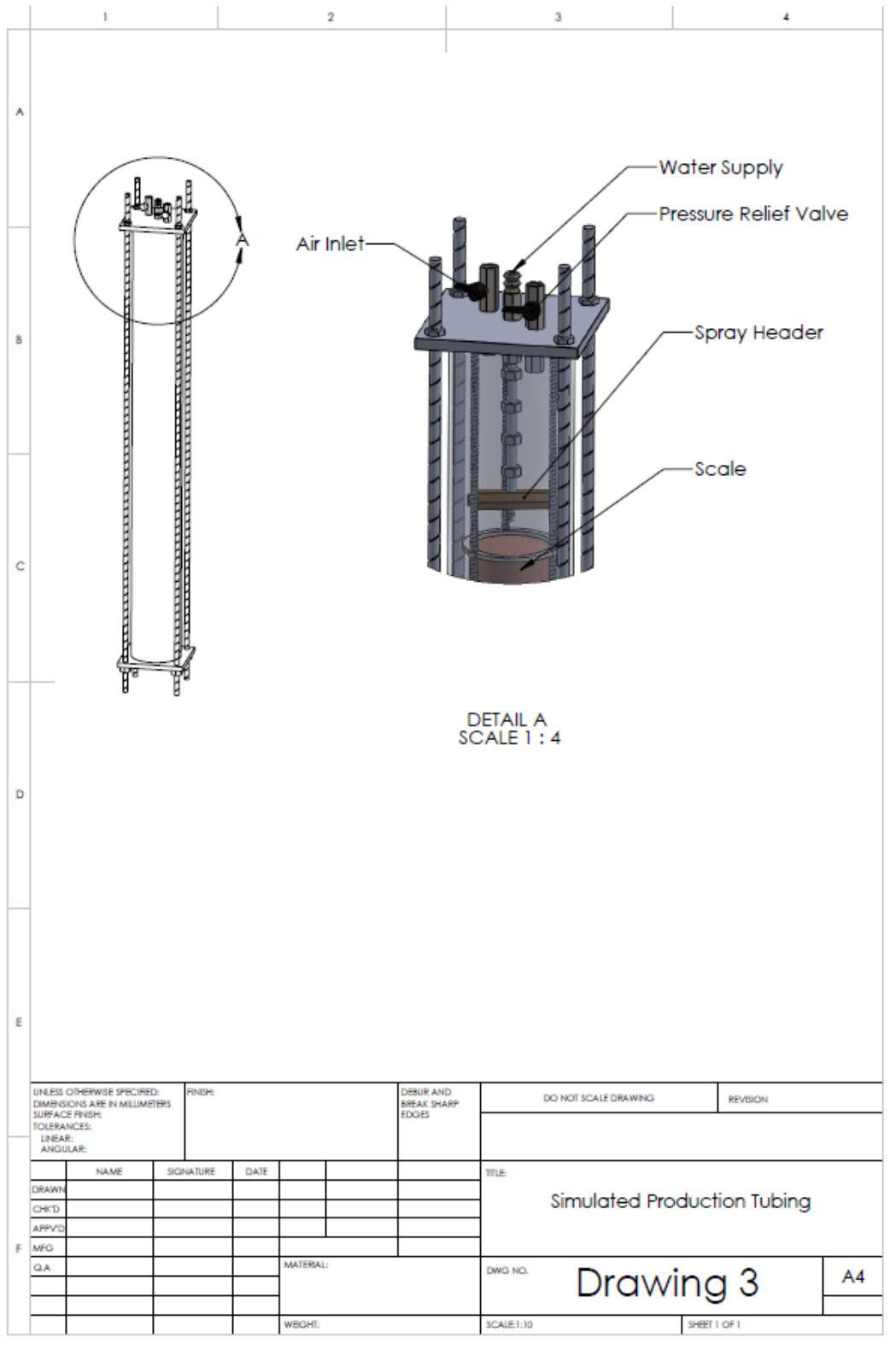
Heidelberg University , Germany Abstract Mathematical modeling,” no. September, pp. 1–4, 2013.

- [154] S. Systems, “A Gibbs free Energy Relaxation Model for Cavitation Simulation in Diesel injectors Chawki Habchi 1 1;,” no. September, pp. 1–4, 2013.

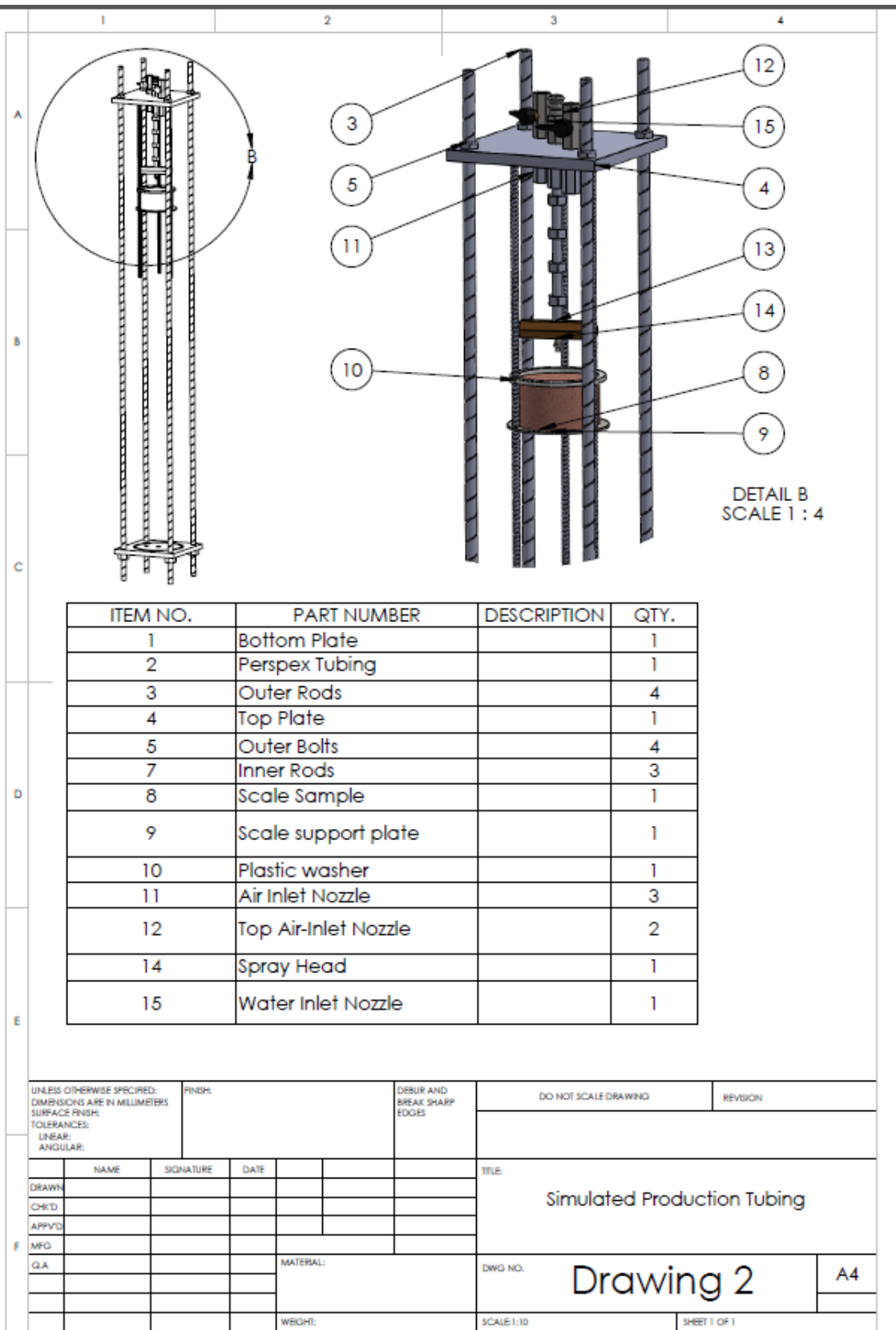
APPENDICES

Appendix A: Chamber Design

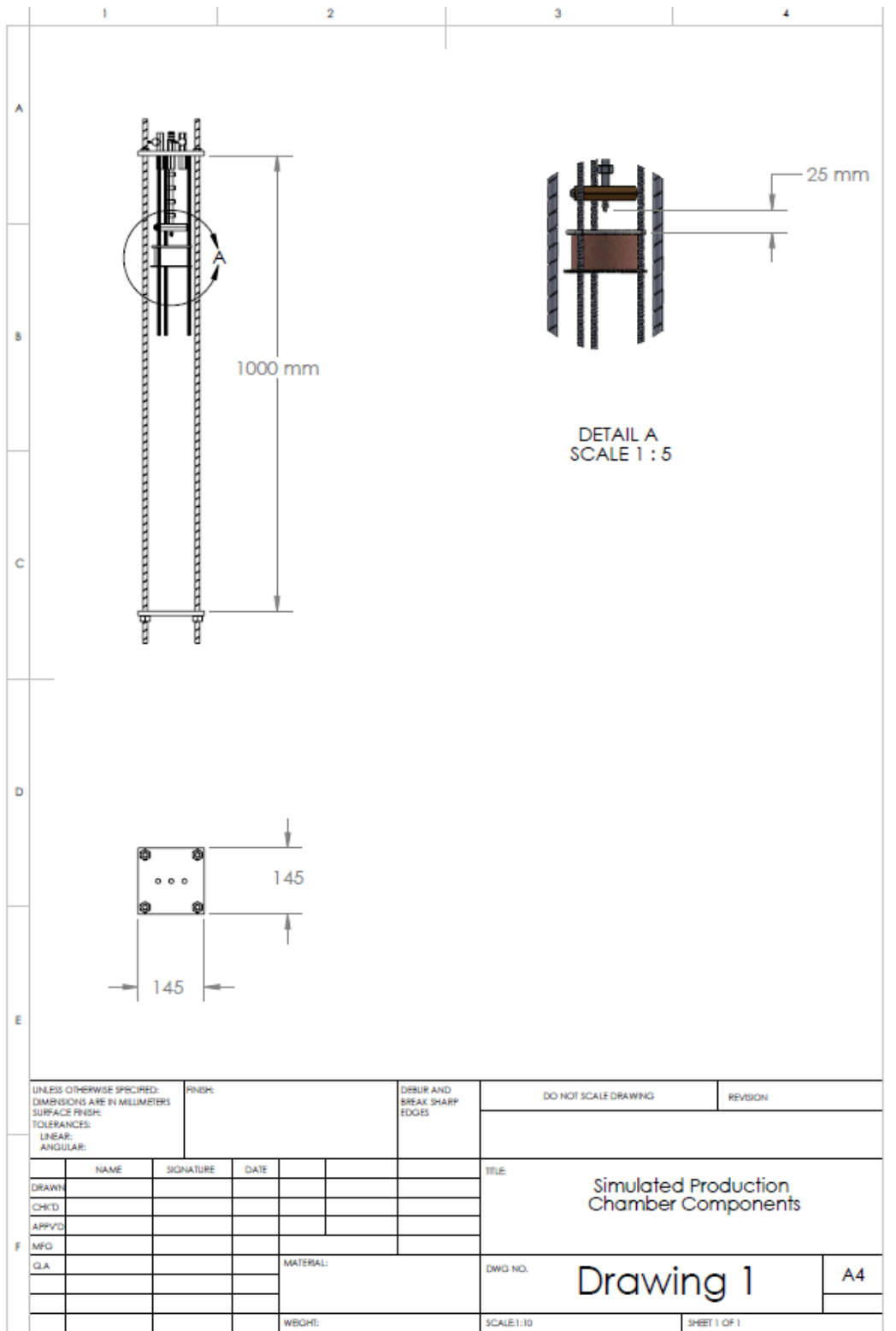
A1: Aerated chamber top section



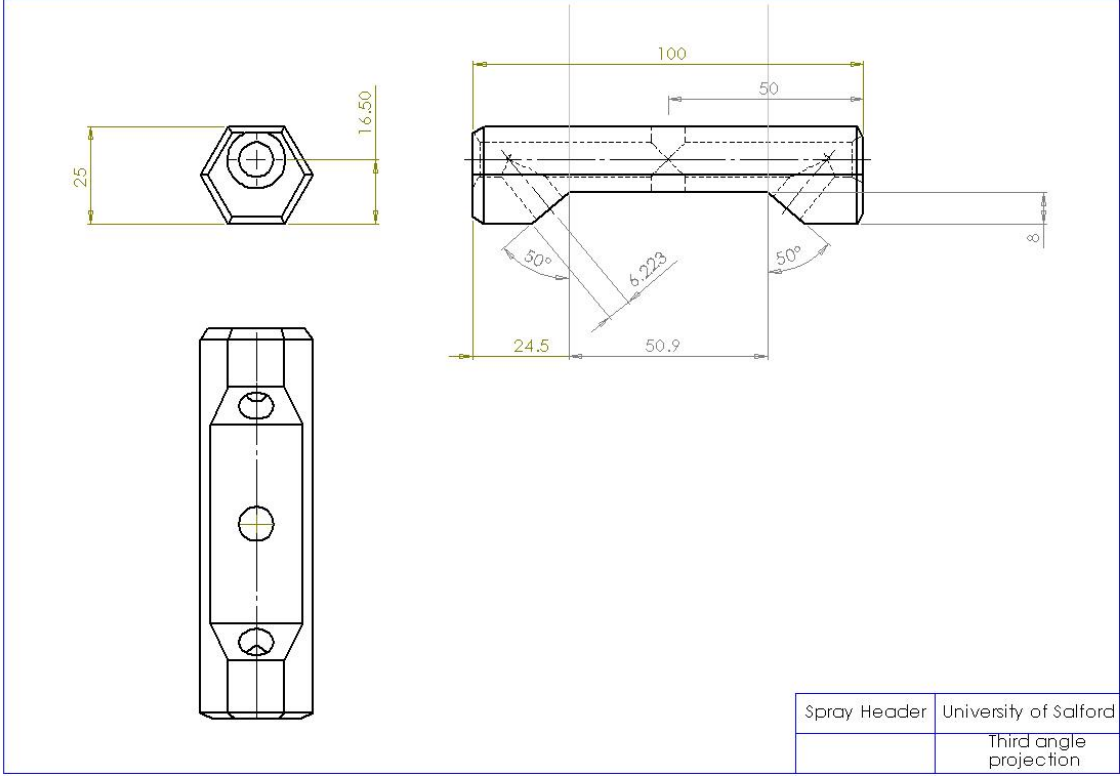
A2: Aerated chamber internals



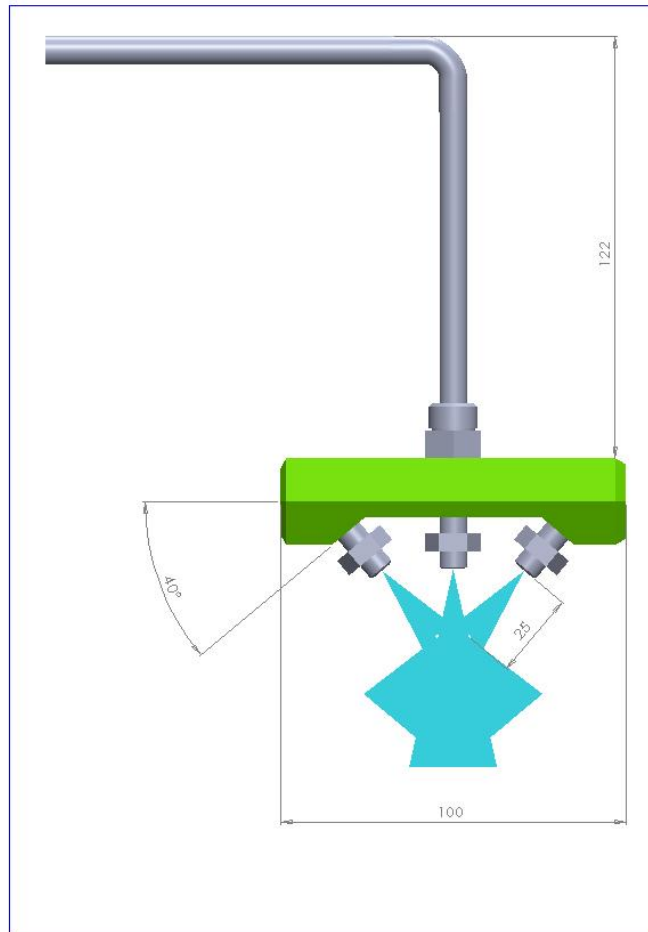
A3: Aerated chamber (scale section)



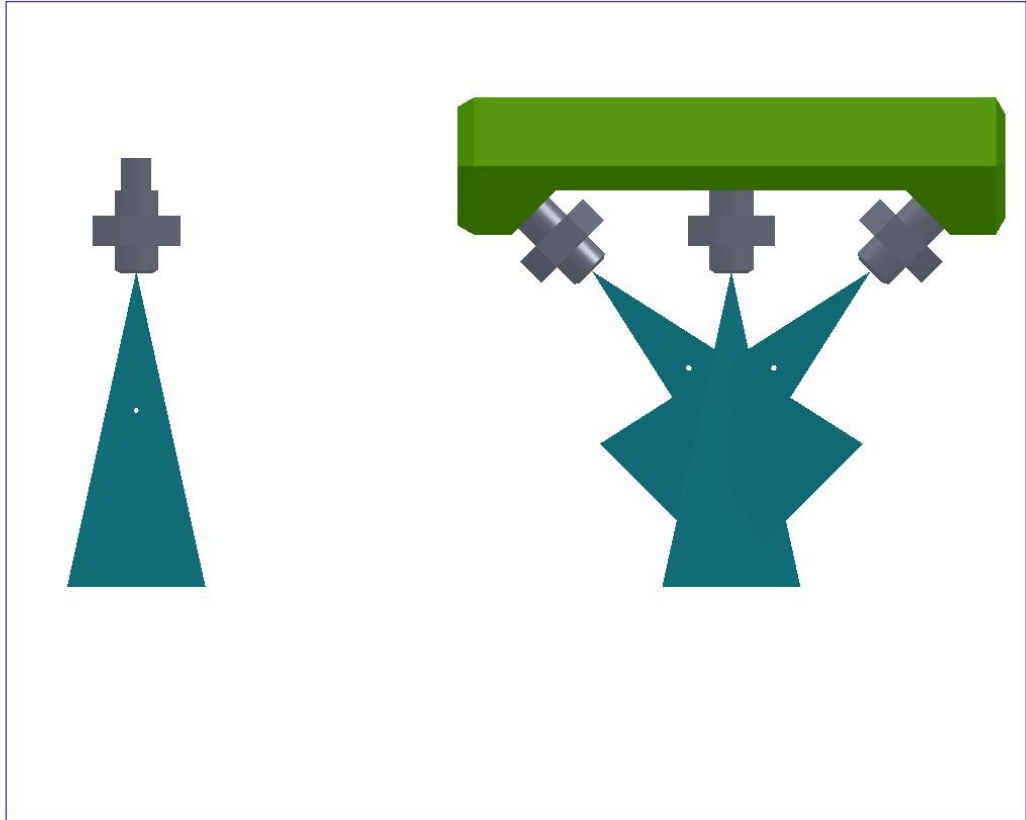
Appendix B: Atomizer Header Design



Appendix C: Overlap spray header design



Appendix D: Overlapping Spray Pattern



Appendix E: Flat fan Atomizer Chart

09

Nozzles & washing accessories

Further information about high pressure nozzles

Output in l/min depends on pressure in bar

Pressure in bar		30	40	50	60	70	80	90	100	110	120	130	140	150	160	175	200	225	250	300	400	500
02	1,00	2,5	2,8	3,2	3,5	3,7	4,0	4,2	4,5	4,7	4,8	5,0	5,3	5,4	5,6	5,9	6,3	6,7	7,0	7,7	8,9	9,9
025	1,10	3,1	3,5	4,0	4,3	4,7	5,0	5,3	5,6	5,9	6,1	6,4	6,6	6,9	7,1	7,5	8,0	8,5	9,0	9,9	11,4	12,7
03	1,18	3,7	4,3	4,8	5,3	5,7	6,1	6,3	6,8	7,1	7,4	7,7	8,0	8,3	8,6	9,0	9,6	10,2	10,7	11,8	13,5	15,1
035	1,30	4,2	4,9	5,5	6,0	6,5	7,0	7,4	7,8	8,2	8,6	8,9	9,2	9,5	9,8	10,3	11,0	11,7	12,3	13,8	15,5	17,8
04	1,35	5,2	5,9	6,6	7,3	7,8	8,4	8,9	9,4	9,8	10,3	10,7	11,1	11,5	11,9	12,4	13,3	14,1	14,8	16,3	18,7	20,9
045	1,40	5,5	6,4	7,1	7,8	8,4	9,0	9,6	10,2	10,5	10,9	11,4	11,8	12,2	12,6	13,2	14,1	15,0	15,8	17,4	19,9	22,3
05	1,55	6,2	7,1	8,0	8,7	9,4	10,0	10,7	11,3	11,8	12,4	12,9	13,4	13,8	14,3	14,9	16,0	16,9	17,9	19,7	22,6	25,3
055	1,60	6,8	7,8	8,7	9,6	10,3	11,1	11,8	12,4	13,0	13,6	14,1	14,7	15,2	15,7	16,4	17,5	18,6	19,6	21,7	25,0	28,0
06	1,72	7,4	8,6	9,6	10,4	11,3	12,1	12,8	13,6	14,3	14,9	15,5	16,0	16,7	17,2	18,0	19,2	20,4	21,5	23,7	27,1	30,3
065	1,75	8,0	9,3	10,4	11,3	12,3	13,2	14,0	14,7	15,4	16,1	16,8	17,4	18,0	18,6	19,4	20,8	22,0	23,2	25,6	29,3	32,7
07	1,80	8,6	10,0	11,2	12,2	13,2	14,1	15,0	15,8	16,6	17,3	18,0	18,7	19,3	20,0	20,9	22,3	23,7	25,0	27,1	31,3	35,0
075	1,90	9,3	10,7	12,0	13,1	14,2	15,2	16,1	16,9	17,7	18,5	19,3	20,0	20,7	21,4	22,4	23,9	25,3	26,7	29,4	33,7	37,7
08	2,05	9,8	11,3	12,7	14,0	15,1	16,1	17,1	18,0	18,9	19,7	20,5	21,3	22,0	22,8	24,5	25,9	27,3	29,4	34,4	39,0	43,0
085	2,08	10,4	12,1	13,5	14,8	16,0	17,1	18,1	19,1	20,0	20,9	21,8	22,6	23,4	24,1	25,3	27,0	28,6	30,2	34,5	39,8	44,5
09	2,10	11,1	12,8	14,3	15,7	17,0	18,0	19,2	20,2	21,2	22,1	23,0	23,9	24,7	25,5	26,7	28,6	30,3	31,9	35,1	40,2	45,0
10	2,30	12,3	14,2	16,0	17,4	18,9	20,1	21,4	22,5	23,6	24,6	25,6	26,6	27,6	28,5	29,8	31,8	33,7	35,6	39,2	44,9	50,2
11	2,42	13,4	15,5	17,3	19,0	20,5	22,0	23,3	24,5	25,7	26,9	28,0	29,1	30,1	31,1	32,5	34,7	36,8	38,8	43,4	50,1	56,0
12	2,50	14,6	16,9	18,9	20,8	22,4	24,0	25,4	26,8	28,1	29,4	30,6	31,7	32,8	33,9	35,4	37,9	40,2	42,4	46,7	53,4	59,8
13	2,55	15,9	18,3	20,5	22,5	24,3	26,0	27,5	29,0	30,4	31,8	33,1	34,4	35,6	36,7	38,4	41,1	43,6	45,9	50,5	57,8	64,7
14	2,60	17,1	19,7	22,1	24,2	26,1	28,0	29,6	31,3	32,8	34,2	35,6	37,0	38,3	39,5	41,4	44,3	46,9	49,4	55,0	63,5	71,0
15	2,70	18,5	21,3	23,9	26,1	28,3	30,2	32,1	33,8	35,3	36,9	38,4	39,9	41,3	42,6	44,6	47,7	50,6	53,3	58,7	67,2	75,2
20	3,05	24,7	28,5	31,9	34,9	37,8	40,3	42,7	45,1	47,2	49,3	51,3	53,2	55,1	56,9	59,5	63,6	67,5	71,1	78,2	89,6	100,0
30	3,90	37,0	42,7	47,8	52,4	56,6	60,5	64,2	67,6	70,9	74,0	77,1	80,0	82,8	85,5	89,4	95,6	101,0	107,0	118,0	149,0	151,0
40	4,20	49,4	57,0	63,7	69,8	75,4	80,7	85,5	90,2	94,6	98,8	103,0	107,0	110,0	114,0	119,0	127,0	135,0	143,0	157,0	198,0	202,0

Please find table which shows flow rates and pressures associated with nozzle size.

Your Lechler nozzle is a 2505 = 25° angle
05 orifice

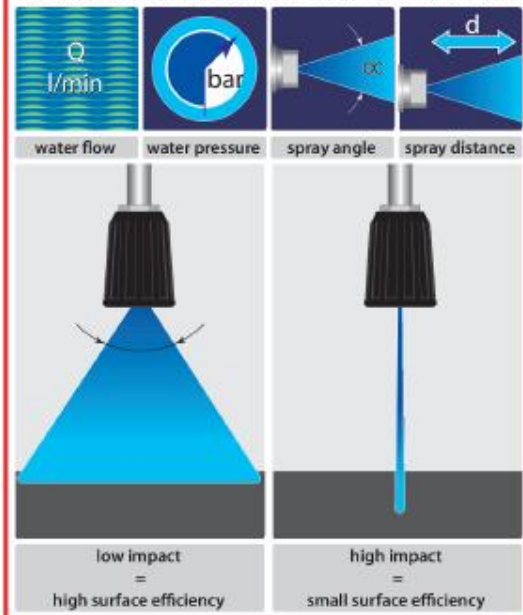
For flow rates - read the pressure (bar) along the top and follow it down to the marked box and this will show you your flow (lpm)

Please use the below formula to calculate the nozzle size required if you know your flow rate and pump pressure

$$\text{Nozzle Size} = \sqrt{\frac{20}{\text{Bar}}} \times \text{flow (lpm)}$$

I hope this helps

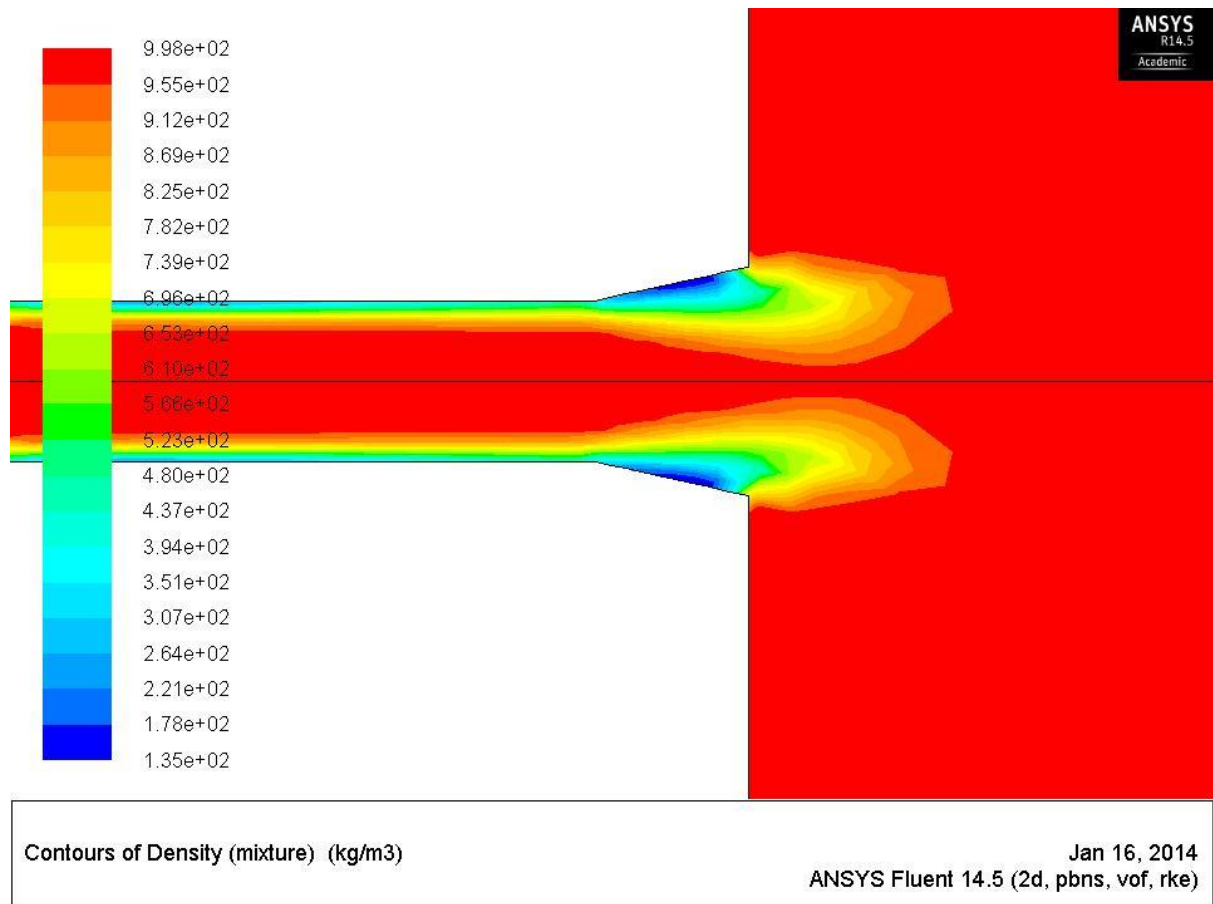
Important for excellent high pressure cleaning is the impact of the spray jet which is made up of 4 features.



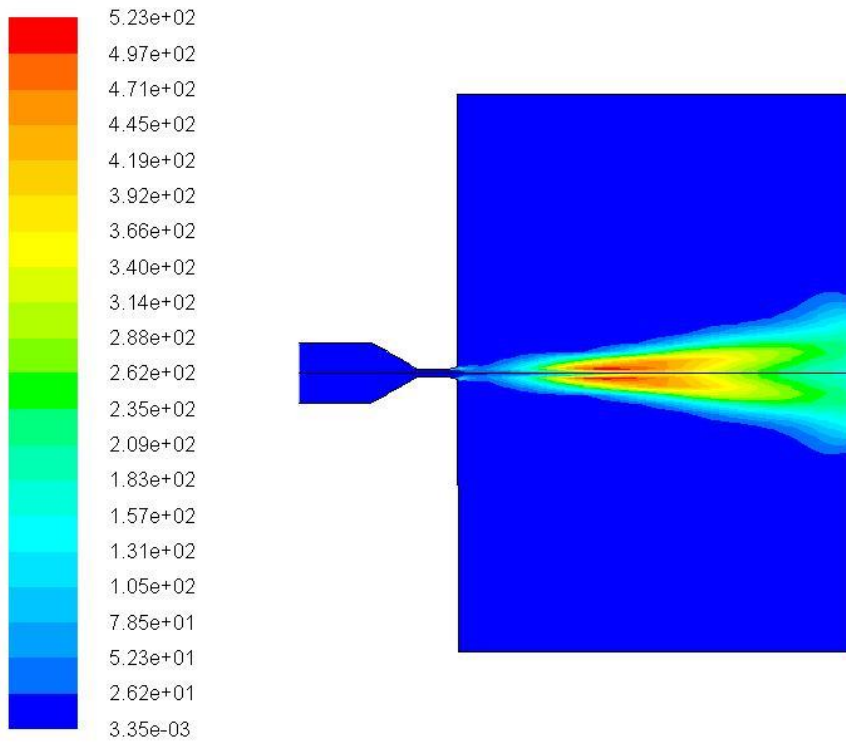
Symbols □ nozzle □ flow ⊙ diameter

Appendix F: CFD Graphics

F1: Density profile in flat fan atomizer(1bar)



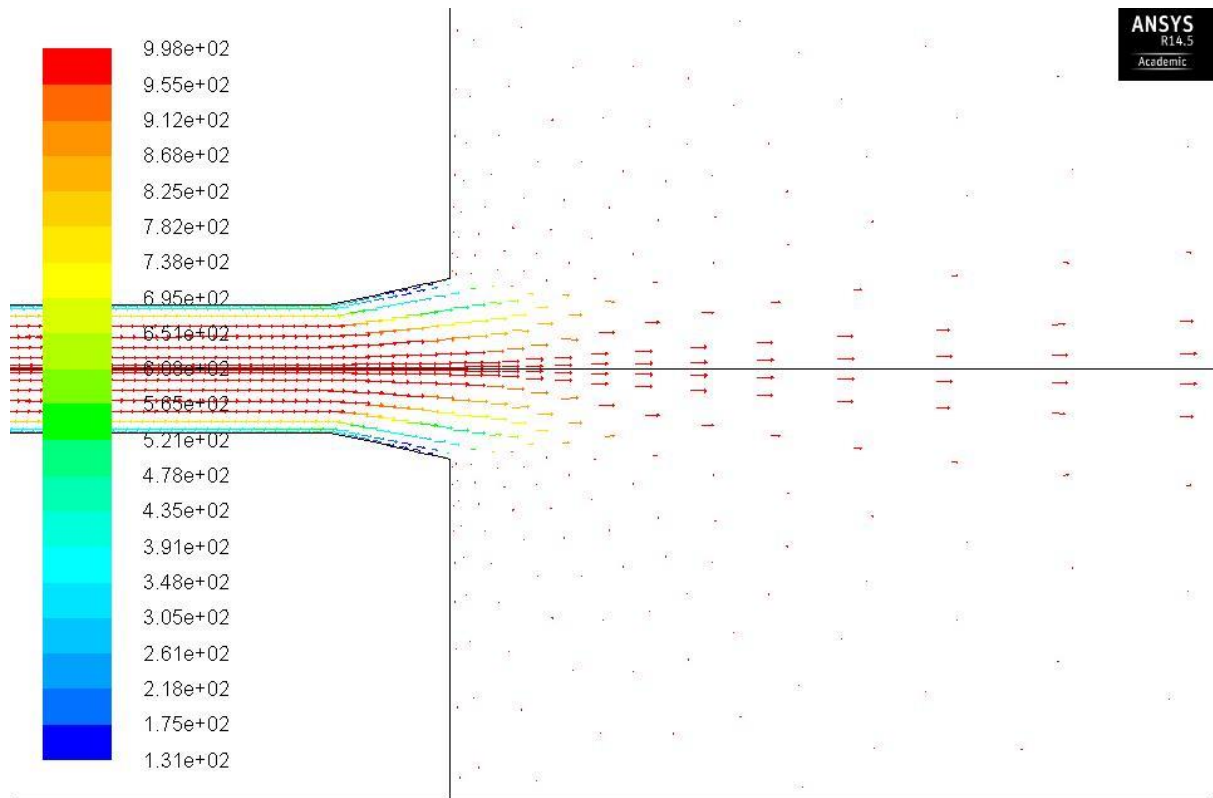
F2:Turbulent kinetic energy profile in solid stream atomizer



Contours of Turbulent Kinetic Energy (k) (mixture) (m2/s2)

Jan 18, 2014
ANSYS Fluent 14.5 (2d, dp, pbns, vof, rke)

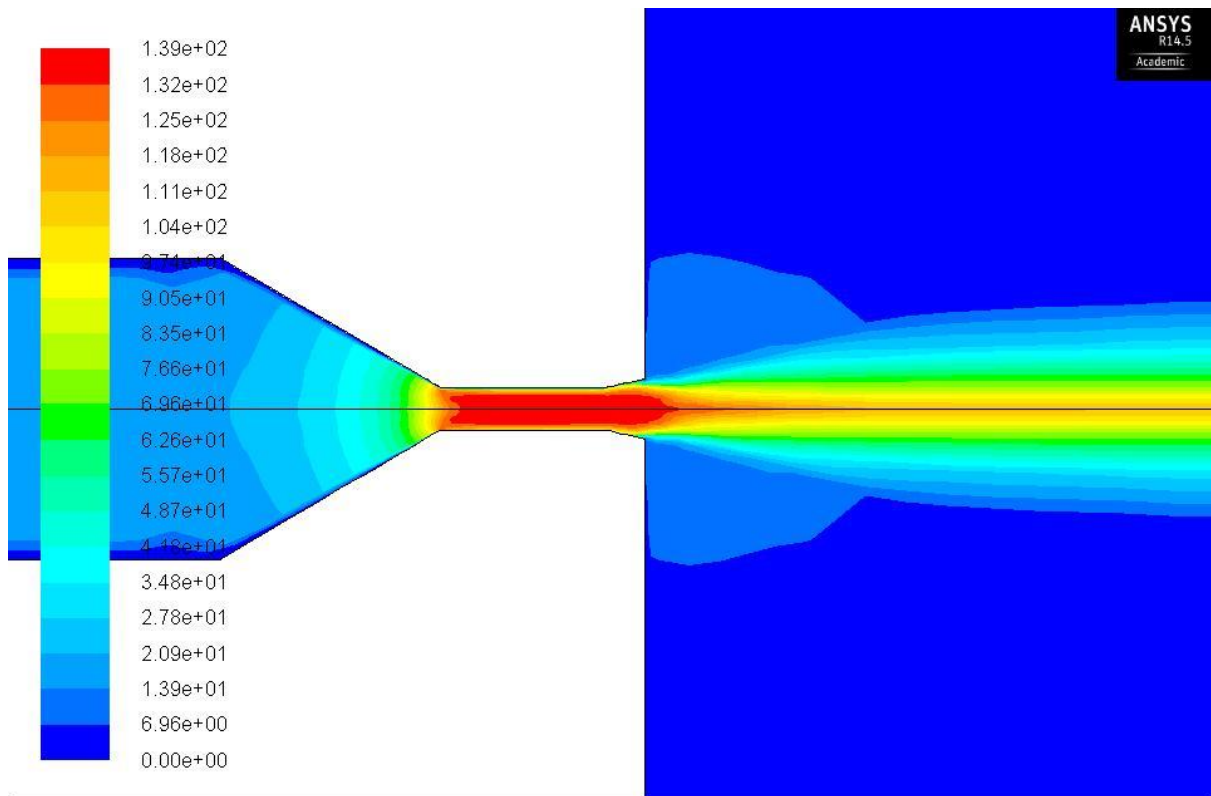
F3: Velocity vectors in flat fan atomizer



Velocity Vectors Colored By Density (mixture) (kg/m3)

Jan 18, 2014
ANSYS Fluent 14.5 (2d, dp, pbns, vof, rke)

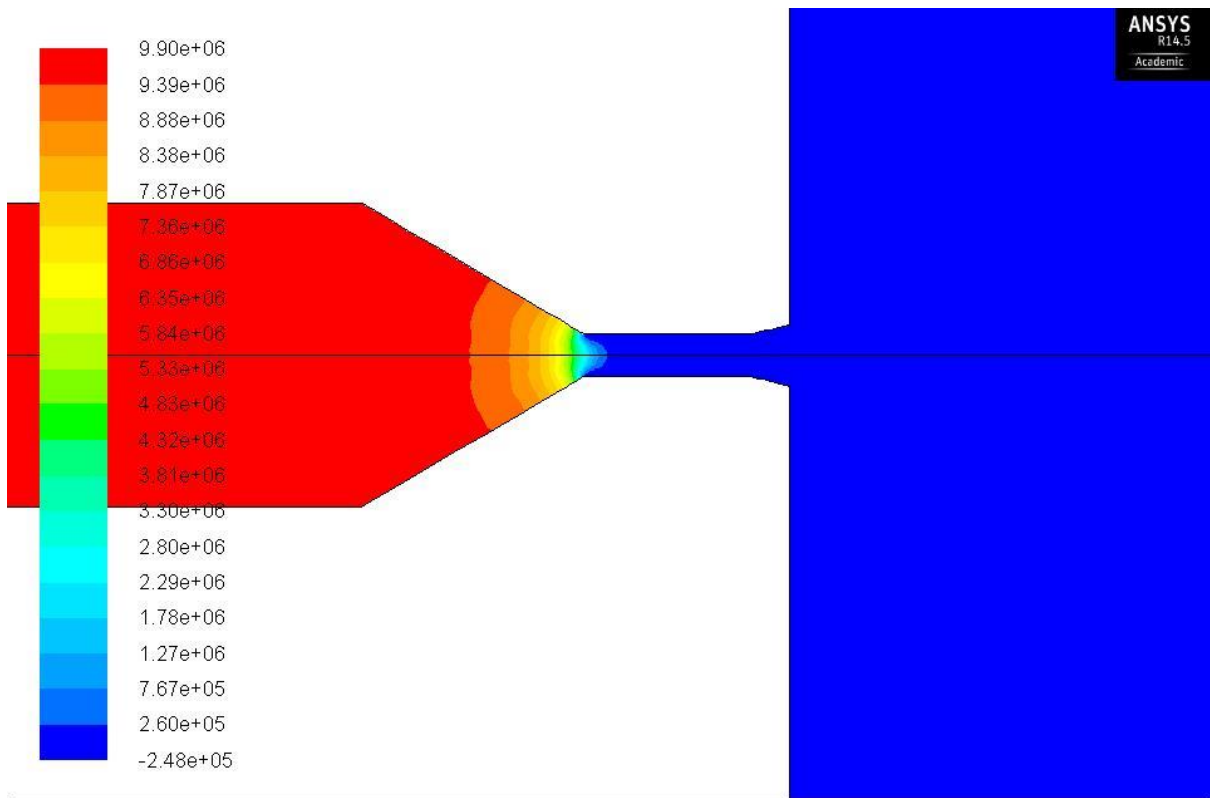
F4: Velocity profile in flat fan atomizer



Contours of Velocity Magnitude (mixture) (m/s)

ANSYS R14.5 Academic
Jan 18, 2014
ANSYS Fluent 14.5 (2d, dp, pbns, mixture, rngke)

F5: Pressure profile in flat fan atomizer



Contours of Static Pressure (mixture) (pascal)

ANSYS R14.5 Academic
Jan 19, 2014
ANSYS Fluent 14.5 (2d, dp, pbns, vof, rke)

Appendix G: Calculations for commercial descaling

G1: Descaling Time for EW 873 field

3150ft		1ft	630min	=10.5hrs
	5ft/min	0.3048m	60	

G2: Mass of Scale removed for EW 873

14706kg	1hr	5min		
10.5hrs	60min		14 Nozzles	

G3: Mass of scale removed for Khuff field

2850kg	1hr	5min		
56hrs	60min		11 Atomizers	

Appendix H: List of Publications